UNIVERSITÀ DEGLI STUDI DELL'AQUILA

Department of Civil, Construction-Architectural and Environmental Engineering

DOCTORAL THESIS

Timber-to-timber, timber-to-steel and timber-to-concrete connections: experimental investigation, analytical and finite element modelling

---

Ph.D Course in Civil, Construction-Architectural and Environmental Engineering

XXXV cycle

Candidate	SSD
Yuri De Santis	**ICAR/09**

Course Coordinator

Prof. Marcello Di Risio

Thesis Tutor	Co-Tutor
Prof. Massimo Fragiacomo	**Ph.D. Martina Sciomenta**

Timber-to-timber, timber-to-steel and timber-to-concrete connections: experimental investigation, analytical and finite element modelling

Yuri De Santis

Prof. Massimo Fragiacomo

Timber-to-timber, timber-to-steel and timber-to-concrete connections: experimental investigation, analytical and finite element modelling

Yuri De Santis
Candidate ID number: 268843

Department of Civil, Construction-Architectural and Environmental Engineering-DICEAA
University of L'Aquila

Website: http://diceaa.univaq.it/

Abstract

Connections can be used to join all kinds of wood products between them or with steel or concrete member to realize composite elements or to join structural elements of a building having different functions. The screws, thanks to their dual resisting mechanism, namely axial and transversal, allow for the realization of high performance shear, bending moment and axial force resisting connections. In determining the most relevant mechanical parameters for connection design, namely slip modulus and failure load, several parameters may have an influence both at the component level and at interaction between components level. Withdrawal, embedment and yielding strengths are currently regarded as influencing parameters. Depending on the angle between connection slip direction and the screw axis, axial, transversal or a combination of axial and transversal screw capacity can be exploited. Slip modulus and strength are found to considerably increase for increasing screw inclination. Interlayers having poor mechanical properties compared to connected members are often used in connections to ensure human comfort in the buildings or because it is required by the structural system. Interlayers were often considered as secondary components, while recent studies testified their influence on the connection mechanical behavior.

In this thesis the influence of soundproofing and OSB interlayer in connections with screws perpendicular or inclined with respect to the sliding plane is experimentally assessed. Analytical models for stiffness prediction are developed, validated and used to derive elementary formulas suitable for design purposes. A novel one-dimensional finite element model is proposed to study the full load-displacement connection behavior, including non-linear effects. Three dimensional models are used to assess interlayer mechanical properties influence, interlayer connection, setup influence and friction contribution on connection strength and stiffness. Empirical models are used to reproduce the constitutive law of a timber-to-steel connection.

Sommario

Le connessioni possono essere utilizzate per unire tra loro o con elementi in acciaio o cemento tutti i tipi di prodotti ingegnerizzati del legno. Le connessioni sono necessarie per realizzare elementi composti o per unire elementi strutturali di un edificio aventi funzioni diverse. Le viti, grazie al loro doppio meccanismo resistente assiale e trasversale, consentono la realizzazione di collegamenti resistenti a taglio, momento flettente e forza assiale ad alte prestazioni. Nel determinare i parametri meccanici più rilevanti per la progettazione della connessione, vale a dire il modulo di scorrimento e il carico di rottura, diversi parametri possono avere un'influenza sia a livello di componente che a livello di interazione tra i componenti. Le resistenze ad estrazione, a rifollamento e la tensione di snervamento sono attualmente considerati parametri influenti. A seconda dell'angolo tra la direzione di scorrimento della connessione e l'asse della vite, è possibile sfruttare la capacità assiale, trasversale o una combinazione di capacità assiale e trasversale della vite. Il modulo di scorrimento e la resistenza aumentano considerevolmente all'aumentare dell'inclinazione della vite. Strati intermedi con proprietà meccaniche scadenti rispetto agli elementi collegati sono spesso inseriti nelle connessioni per garantire il comfort abitativo o perché richiesto dal sistema strutturale. Gli strati intermedi sono stati spesso considerati come componenti secondari, mentre recenti studi hanno testimoniato la loro influenza sul comportamento meccanico della connessione.

In questa tesi si valuta sperimentalmente l'influenza di strati intermedi fonoisolanti o OSB nei collegamenti con viti perpendicolari o inclinate rispetto al piano di scorrimento. Vengono sviluppati modelli analitici per la previsione della rigidità, validati e utilizzati per derivare formule elementari adatte a scopi di progettazione. Viene proposto un nuovo modello a elementi finiti monodimensionali per studiare la relazione che lega il carico allo spostamento relativo della connessione fino a rottura, includendo gli effetti non lineari. Vengono utilizzati modelli tridimensionali per valutare l'influenza delle proprietà meccaniche dello strato intermedio, della connessione tra gli strati, della configurazione di prova e il contributo dell'attrito sulla resistenza e sulla rigidezza della connessione. Si utilizzano modelli empirici per riprodurre la legge costitutiva di una connessione legno-acciaio.

Contents

List of Figures

List of Tables

Chapter 1

Introduction

Connections are necessary to join different structural elements or to realize composite elements. In timber engineering the wide variety of materials and structural typologies reflect on connections also. Connections can be used to join all kinds of engineered wood products including solid timber, glue laminated timber, cross laminated timber, laminated veneer lumber and plywood. Moreover, it is often necessary to join a timber element with a steel or concrete element. Regardless of the connected elements typologies, steel cylindrical shank are the most common fasteners. Nails, screws, dowels and bolts fall into this category.

The screws distinguished for their versatility and efficacy. Screws allow for the realization of shear, bending moment and axial force resisting connections. Depending on the angle between connection slip direction and the screw axis, axial, transversal or a combination of axial and transversal screw capacity can be exploited. Slip modulus and strength are found to considerably increase for increasing screw inclination.

Interlayers having poor mechanical properties compared to connected members are often used in screws connections to ensure human comfort in the buildings or because it is required by the structural system. In cross-laminated timber buildings, soundproofing interlayer can be used in connections between walls or in angle brackets and hold-downs. In light frame buildings the interlayer consist in the OSB sheathing between interstorey steel plates and studs. In retrofitted composite floors interlayer is represented by an existing planking, while in newly build timber-concrete-composite elements the interlayer is often an OSB panel used as a temporary form-work. Few studies focused on interlayer mechanical properties influence on connection behavior.

The slip modulus and strength are commonly regarded as fundamental design parameters. Slip modulus represents a conventional parameter describing the connection stiffness in serviceability range of load. The knowledge of connections stiffness is mandatory in determining structural deformations as interstorey drift and vertical displacements. Moreover, the connection stiffness may influence the share of load between structural elements and the effectiveness of composite elements. The capacity represent the second essential parameter of connections design. Johansen theory is extensively used for the capacity prediction of transversely loaded dowel-type fasteners. However, in connections with inclined fasteners, due to the strong coupling between the fastener axial and transversal behavior, the problem of capacity prediction is non-trivial. Models provided by current standard are not mechanics based.

Models represent a valuable tool to extend the knowledge descending from empirical methods. Analytical and finite element models are the most recurrent approach in literature. They allow to reproduce the overall connection behavior in an approximate way or to deeply study deformation or stress fields depending on the detailing level. Refined models can be used to validate more elementary approaches or to reproduce limit cases difficult to achieve in experimental investigations.

The elements of novelty in the thesis can be itemized as follows:

- The experimental investigation of connections with inclined screws with soundproofing interlayers;

- The development of an analytical model of beam on foundation with coupled axial and transversal behavior for the slip modulus prediction of connections with inclined screws and interlayers;

- The derivation of simplified formulas for the slip modulus prediction of connections with inclined screws and interlayers downstream of the definition of regression formula for model input parameters and variance-based sensitivity analysis;

- The study of non-linearities effects on slip modulus of connections with inclined screws;

- The development of a novel modelling approach based on beam on foundation, able to predict the full non-linear force-displacement response and failure modes of connections with inclined screws and interlayers;

- The derivation of a design model for the capacity prediction of connections with inclined screws and interlayers with improved accuracy compared to the model of the current Eurocode 5 downstream of 500 finite element model simulations;

- The derivation of an hybrid empirical-analytical model for the rocking capacity prediction of CLT wall with openings.

Chapter 2

State of the art

Abstract:
When used as fasteners in connections, self-tapping screws allow for the realization of shear, bending moment and axial force resisting connections. Screws connections can be used to join all kinds of wood product between them or with steel or concrete member to realize composite elements or to join different structural elements of a building having different functions. Interlayers and washers were often considered as secondary components, while recent studies testified their influence on the connection mechanical behavior. Depending on the angle between connection slip direction and the screw axis, axial, transversal or a combination of axial and transversal screw capacity can be exploited. In determining the most relevant mechanical parameters for connection design, namely slip modulus and failure load, several parameters may have an influence. In the following, the parameters that may have an influence on the mechanical behavior of the connections are identified at the component level and at interaction between components level and at connection level. Experimental methods and commonly accepted representative parameters suitable for the mechanical characterization of the screw, of the transversal and axial screw-timber interaction, of the screw head and screw tip-timber interaction, of the member interaction on the sliding plane, are collected and discussed from a modelling point of view. A literature review of the most relevant studies regarding empirical, analytical and finite element modelling of screws connections is carried out.

2.1   Introduction

Applications of self-tapping screws includes reinforcements and connections. When used as fasteners in connections, self-tapping screws allow for the realization of shear, moment and axial force resisting connection. Inclined screws with continuous or double threads leads to connections characterized by high slip modulus and load-carrying capacity and hence more economic connections compared to connections with fasteners perpendicular to the sliding plane. The inclination angle of the axis of the fastener may vary from 0° to 60° with respect to the normal to the sliding plane and for increasing angle of inclination the withdrawal resisting contribution of the screw increases. Then, the ultimate load of joints with highly inclined screws depends primarily on the withdrawal capacity of the fasteners and its tensile strength. For this configuration the screw is mainly loaded in tension and the contact surface between the members in compression and therefore friction develops on the sliding surface between the timber members. For lower angle of inclination the embedding strength of the timber members and the bending capacity also influence the mechanical behavior.

As reinforcing elements screws can be used to improve the compression and tension strength perpendicular to the grain, shear or both shear and tension perpendicular to the grain strengths.

Double threaded screws with differentiated pitch are able to induce a prestress forces in the axial screw direction up to 9 kN [34, 35]. Taking advantage of this ability Giongo et al. [34, 35] had demonstrated the possibility of cambering a timber beam by simply putting another wooden beam on the top of it and inserting screws inclined at 45° relative to the beam axis. In this way sagged timber floors which cannot be buttressed due to heritage issues can be easily retrofitted.

In the following sections, the focus will be on connection applications. The mechanical behavior of each connection component and of each interaction between the components of the connection are characterized by describing how these properties are experimentally assessed and which are the most relevant outcomes of theoretical and experimental studies from literature.
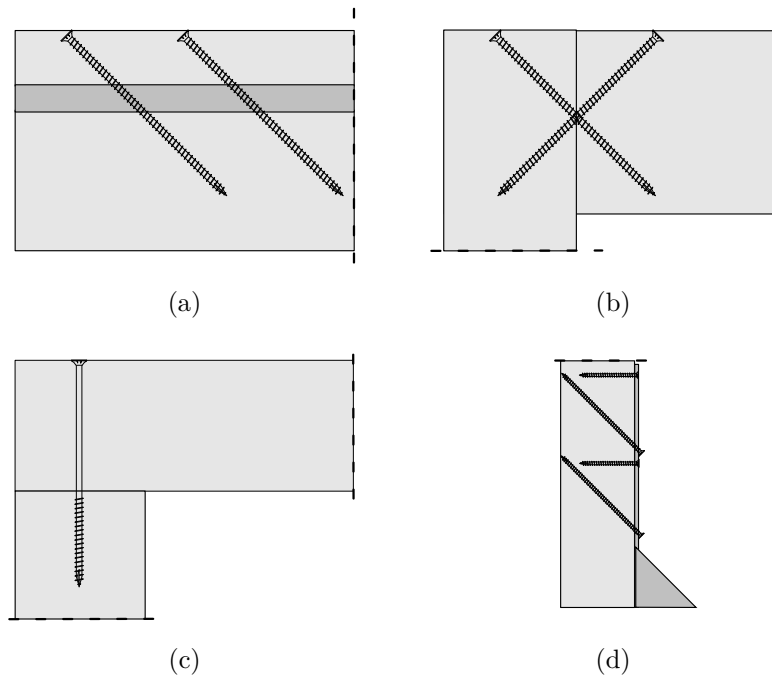
Figure 2.1: Screw connections (a) composite floor (b) beam to column (c) wall to wall (d) hold-down.

2.2 Components of a screw connection

A connection with screws as fasteners includes the screws their-self, the two connected member and eventually a washer and/or an interlayer. The features of this components related to their application in connections are briefly described tn the following.

2.2.1 Screws

Screws are defined as dowel-type fasteners. Screws distinctive properties are the ability to transfer load between members trough their axial capacity, and the possibility of installation without pre-drilling.

The elements of a self-tapping screw are the head, the drive, the shank, the core, the thread and the tip.
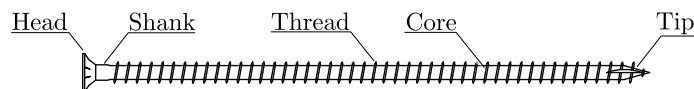
Figure 2.2: Screw elements.

The screw head houses the screw drive and can grant different levels of pull-through capacity depending on its geometry. To minimize the visual impact of the screw for aesthetic reasons, cylindrical head of a diameter approximately equal to the thread outer diameter can be used. In this way the pull-through capacity is minimized and the screw head can be easily incorporated in the timber member without the need of milling the timber member. Conversely when the head capacity is required or it has an appreciable favorable effect on the mechanical behavior, e.g. partially threaded screws, its geometry is optimized to distribute the load over the largest surface possible. In this latter case the head is situated outside the timber member. An intermediate solution is represented by conical screw heads. Conical screw heads allows for installation in-flush with timber member surface and show a certain head pull-through resistance.
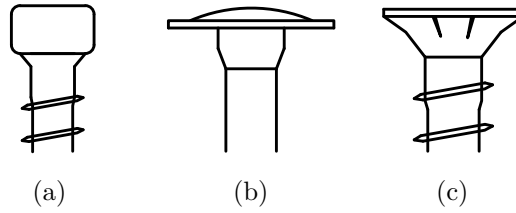
Figure 2.3: Head type: (a) cylindrical (b) flange (c) countersunk.

The drive is the shaped part of the head which allows for torque transfer between the screwdriver and the screw during the installation phase. The most common drive shape in timber screws are "Phillips" and its improved version "Pozidriv" which are both cruciform and "Hex" and "Torx" which belongs to hexalobular drive category.

The shank can be regarded as the portion of the screw comprised between the head and the thread. Its length can be less than a millimeter in case of fully threaded screws or can be most of the screw length in screws for non-structural components fastening. Its diameter is usually equal to the original wire rod diameter and it is therefore comprised between the outer and inner thread diameters.

The core represent the innermost part of the threaded portion of the screw. The core diameter d_c is one of the most influential geometrical parameter as it governs the mechanical behavior of the screw as discussed in Sec. 2.8.

The thread is the components which grants the force transfer between the screw core and the surrounding timber. In self-tapping screws, screw thread generates the thread on timber during the insertion. With regards to the portions of the screw with thread, screws can be divided into: single or partially threaded screws, fully threaded screws and double threaded screws. Double and fully threaded screws are used as inclined fasteners due to their high withdrawal strength from both connected members. Moreover double threaded screws thanks to the differentiated pitch are able to pre-stress members together. Single threaded screws are commonly used perpendicularly to the sliding plane instead.
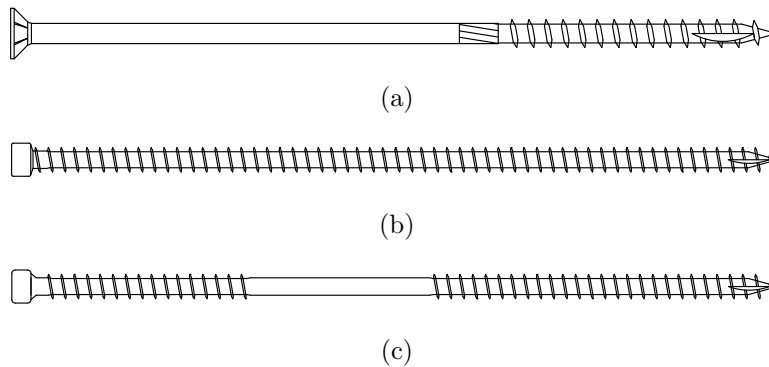
Figure 2.4: Screw type: (a) single threaded (b) fully threaded (c) double threaded.

The screw thread geometry can be mathematically described as a combination of a cone surface and a helicoid function [66] and can be unequivocally described by the following parameters: thread inner diameter or core diameter d_c, η the ratio between d_c and thread outer diameter d that is the nominal diameter (EN 14592 [22]), the pitch p and the thread's flank inclination angle χ.
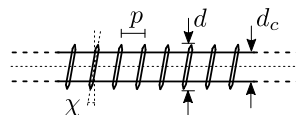
Figure 2.5: Screw parameters.

The range of the values assumed by this parameters in the most recurrent geometries of commercial timber screws are reported in Tab. 2.1. In double threaded screws different parameters can be adopted for each part of the screw. Different pitches and diameters are usually chosen with the aim of inducing a connection pre-stress.

	$d_c{}^*$ (mm)	d^* (mm)	η^*	p (mm)	χ (°)	$l_{thr}{}^*$ (mm)
Min	1.4	2.4	0.6	5	25	$4d$
Max	21.6	24	0.9	6	35	l

Table 2.1: Range of the values assumed by geometrical parameters of threads of commercial timber screws. *According to [22].

The tip ease the screw positioning during the installation and can include a cutter to facilitate the insertion process. In most of the cases the screw tip is threaded.

Screws are made of stainless or carbon hardened steel [17]. The production process begins with the cutting of the necessary wire rods, than the screw head is stamped and finally the thread and tip geometry are made by rolling. The cold-forming of steel leads to an increase of its hardness and strength allowing the reaching of failure stress up to $f_u = 2000\,\mathrm{N/mm^2}$ while reducing its ductility at the same time. After the shape manufacturing several surfaces treatments can be performed. The mechanical properties of the screw surface can be increased by carbonitriding. The process consist in enriching the outer part of the screw with carbon and happens at high temperatures. In this way the torsional resistance can be improved. In order to improve the durability of carbon steel screws a protective coat can be added to the screw surface. In most of the cases the coating consist in a zinc layer added by galvanization. The alternative consist in doing metallurgical modifications like adding chrome which allow for the formation of a passive oxide coating on the exposed surface. To decrease surface friction during the installation process water-based or polymer compounds lubricants can be applied.

2.2.2 Washers

A washer is a disk-shaped metal plate with a hole in its center. The role of the washer is to distribute over a wider area the forces coming from the screw head. Considered the valuable contribution of the rope-effect, even in case of screws perpendicular to the sliding plane, in some cases may be appropriate to increase the head pull-through strength by adding a washer. No specific washers exist for inclined screws with head-side in timber, in this case the withdrawal strength is offered by the threaded part. Some experiments using partially threaded screws and washers inserted in groove cuts have been carried out in [75] and highlighted that the use of single-threaded screws with washers permitted to obtain significantly higher values of capacity than those exhibited by double-threaded screws in similar configurations.

Washers with an insertion angle $\alpha = 45°$ are common for inclined positioned screws in steel-to-timber joints. In this case the washer has the role of replacing the countersunk drill holes in the steel plate by more economically producible slots.

(a)   (b)
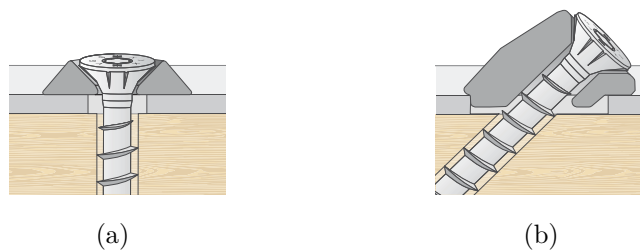
Figure 2.6: Washers (a) perpendicular screws and (b) inclined screws.

2.2.3 Connected members

Connections with inclined screws are used to join two timber members or a timber member with a steel or concrete member. When used in composite floors the connection joins a beam element with a plate element or more rarely a beam element with another beam element used as reinforcement. When used in walls of cross laminated timber buildings screws join two adjoining perpendicular or co-planar plate elements.

All kinds of wood product may potentially be connected by screw connections, from solid timber to glued laminated timber and laminated veneer lumbers for beam elements and from cross laminated timber to oriented strand boards and plywood.

Nowadays timber density is regarded as the major parameter for the design of dowel-type fasteners. Mechanical properties related to both the local and global behavior of a timber elements have a pronounced relationship density.

Although most of the formulas suggested by the standards do not specify timber species, it is known that timber can be divided into three different wood anatomy groups with distinct macroscopic and microscopic differences. The three groups are coniferous, ring porous and diffuse porous deciduous tree. Norway spruce is representative for the coniferous group, black poplar represents the diffuse porous group in the lower density range and oak is the second most common deciduous species in Europe [11].

2.2.4   Interlayers

Main connected members can be separated by intermediate layer having different functions. Typical examples of connections with interlayers can be found in:

- newly built timber-concrete-composite floors (TCC) with wood-based panel acting as a support for the concrete during the construction phases;

- retrofitted existing floor where an additional concrete member (TCC floors) or an additional timber member (TTC floors) is joined to the existing joist and planking;

- joist hanger attached at a shear wall made by wood-based panel and studs [39];

- soundproofed hold-down and angle brackets [52];

- connection between walls or between walls and floors with soundproofing insulation layers [5].

Due to their different functions, interlayers can be made of a wide variety of materials:

- LVL, plywood, and OSB

- particleboards

- MDF

- fibreboards

- plasterboards

- gypsum fibreboards

- cement-bonded particleboards

- softboards

- polyurethane

When used in combination with inclined screws, interlayers may be subjected to compression perpendicularly to their plane and to an embedment action from the fastener. Consequently interlayers can be classified with respect to to their capability of sustaining external forces in:

- interlayers having stiffness and strength perpendicularly to their plane similar to the main timber members;

- interlayers having stiffness and strength perpendicularly to their plane negligible in comparison to the main timber members;

- interlayers having embedment stiffness and strength similar to the main timber members;

- interlayers having embedment stiffness and strength negligible in comparison to the main timber members;

In the following table mechanical properties of the most common interlayer are showed:

Interlayer type	Normal direction	Embedment
LVL, plywood, and OSB	black	black
particleboards	gray	gray
MDF	gray	gray
fibreboards	gray	gray
plasterboards	black	white
gypsum fibreboards	black	gray
cement-bonded particleboards	gray	white
softboards	gray	white
polyurethane	white	white

Table 2.2: Interlayer mechanical properties. Black: properties similar to timber member; White: negligible mechanical properties and Gray: intermediate mechanical properties.

Moreover, interlayers can be divided according to their connection with main timber member in:

- rigidly connected

- weakly connected

- not connected

The interlayer can be considered rigidly connected when it is glued to on of the main timber member. It can be considered weakly connected in most of the cases. The interlayer is weakly connected when the secondary connection between the interlayer and the main timber member has negligible strength and stiffness compared to the main connection. It is the case of staples, nails and small diameter and length screws. Examples of interlayers not connected are soundproofing interlayer.

Depending on the properties needed in the specific connection and depending on the mechanical properties of the interlayer itself and of its connection with the main timber member, from a design point of view they can be defined as:

- structural interlayers;

- non-structural interlayers.

2.3 Mechanical characterization of transversal screw-timber interaction

One of the fundamental load transfer mechanism in a dowel-type connection is the embedment of the connector into the timber which surrounds it. Due to the scale effect, the timber mechanical properties in embedment are significantly different from the mechanical properties that describe the macroscopic behavior of a timber element. Therefore proper tests had to be defined in order to provide suitable parameters for mechanical modelling (Sec. 2.11). Dowel-type connections behave non-linearly even when subjected to service loads. In loading for the first time a connection, initial slip verifies. Reynolds et al. [67] had demonstrated through microscope analysis of specimens before and after testing that initial slip is due to to lack of fit between the screw and the hole and unevenness in the contact surface. Due to transient nature of this behavior, in characterizing the mechanical behavior of transversal screw-timber interaction, initial slip is neglected and the constitutive law is defined as function of the foundation modulus which is a stiffness parameter and the embedding strength which is a strength parameter.

For a dowel-type fastener, the foundation modulus can be experimentally determined via embedding test according to EN 383 [24], ASTM D5764 [3] and ISO/DIS 10984–2 [44]. While the EN 383 standard requires a test on a timber specimen with a full-hole and a dowel loaded on its ends (Fig. 2.7a), the ASTM D5764 regulation prescribes a half-hole test with dowel uniformly loaded along its length in order to eliminate any dowel bending effect (Fig. 2.7b). Despite the differences between the test procedures, a comparison between standards reveals a close agreement in terms of foundation modulus as pointed out by Santos et al. [74]. The ISO/DIS 10984–2 standard is the same as EN 383, except that it allows for both full-hole and half-hole tests.

The loading procedure described in EN 383 [24] consist in a multi-phase tests. First the specimen is loaded until 40% of the estimated maximum load $F_{max,est}$, then after 30 s of holding, a partial unloading until $0.1F_{max,est}$ is performed. The final loading should continue until the reaching of the maximum load or until the displacement is 5 mm.
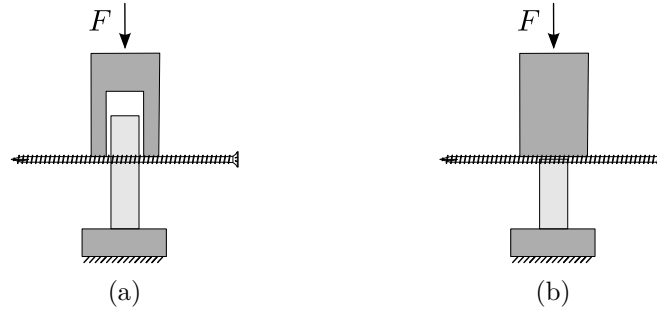
Figure 2.7: Embedment (a) full-hole and (b) half-hole test setups.

According to EN 383 [24] the embedding strength shall be calculated as follows:

$$f_h = \frac{F_{max}}{dt} \tag{2.1}$$

where t is the timber specimen thickness along the screw axis. The initial foundation modulus is defined as:

$$K_s = \frac{0.4f_{h,est}}{w_{i,mod}} \tag{2.2}$$

with $w_{i,mod}$ defined as the modified initial deformation:

$$w_{i,mod} = \frac{4}{3}(w_{04} - w_{01}) \tag{2.3}$$

where w_{04} and w_{01} are the displacements at $0.4f_{h,est}$ and $0.1f_{h,est}$ of the first loading phase. In this way K_s represents the angular coefficient of the secant to the force displacement curve for two reference points in the liner range, thus excluding the initial slip phase. In some cases the authors refers the foundation modulus as $k_s = K_s d$. It is the case of mono-dimensional models where the foundation modulus has the dimension of a stiffness per unit of length $((F/L)/L)$ while K_s is in $((F/L)/L^2)$.

2.3.1 Foundation modulus

On the basis of 400 embedment tests conducted as prescribed by EN 383 Bejtka in [8] proposed an experimental regression formula for the foundation modulus. The nominal diameter the tested fully threaded screws was in the interval $d = 6$ to 12 mm and the angle between the direction of the force and the grain of the timber was varied between $\alpha = 0° \div 90°$.

$$K_{s,m,\alpha} = \frac{0.22\rho d^{-1} + 0.014\rho}{1.17\sin^2\alpha + \cos^2\alpha} \tag{2.4}$$

Embedment tests on screws were conducted also by Reynolds et al. [67]. The tests samples were made of Norway spruce and the nominal screw diameter was $d = 12$ mm. The tests results in an initial foundation modulus $K_s = 65.6$ N/mm^3.

Mirdad et al. [58] derived the following equation by means of non-linear regression analysis of test data that cover Spruce-Pine-Fir and Douglas Fir:

$$K_{s,m,\alpha} = \frac{0.000042\rho^{2.44}d^{-0.96}}{2.89\sin^2\alpha + \cos^2\alpha} \tag{2.5}$$

In the paper included in Sec. 4.9 two experimental regression formula were found by interpolating the results from dowel-type fasteners. A categorization on the basis of the timber product was necessary to achieve reliable predictions.

It is worth noting that both the values from Reynolds et al. [67] and the values from interpolation formulas of Sec. 4.9 provide values significantly higher than those predicted by Eq. 2.4.

No studies were found concerning the influence of thread properties on embedding behavior. Part of the discrepancies between interpolation formulas from literature may come from the different pitch, inner/outer diameter ratio and flank inclination angle.

2.3.2 Embedment strength

According to the Eurocode 5 [29], the characteristic embedment strength for screws with diameters up to 6 mm can be calculated by means of the same expressions provided for nails. In timber and LVL in case of connections without predrilled holes:

$$f_{h,k} = 0.082 \rho_k d_{ef}^{-0.3} \tag{2.6}$$

In case of connections with predrilled holes the expression derived by Ehlbeck in [19] is provided:

$$f_{h,k} = 0.082(1 - 0.01d_{ef})\rho_k \tag{2.7}$$

where ρ_k is the characteristic timber density, in kg/m^3 and d_{ef} is the effective diameter in mm which can be calculated as a function of the thread root diameter d_c ($d_{ef} = 1.1d_c$).

In case of screws with a diameter greater than 6 mm the characteristic embedment strength can be calculated by means of the same expressions provided for bolted connections. In this case the characteristic embedment strength is assumed to be dependent on the angle of the load to the grain α.

$$f_{h,k,\alpha} = \frac{f_{h,0,k}}{k_{90} \sin^2 \alpha + \cos^2 \alpha} \tag{2.8}$$

where $f_{h,0,k}$ should be determined according to Eq. 2.7. Where k_{90} depends on the product and timber type.

$$k_{90} = \begin{cases} 1.35 + 0.015d_{ef} & \text{for softwoods} \\ 1.30 + 0.015d_{ef} & \text{for LVL} \\ 0.90 + 0.015d_{ef} & \text{for hardwoods} \end{cases} \tag{2.9}$$

On the basis of a multiple regression analysis of 733 test results conducted on self-tapping screws with $d = 6$ to 12 mm in solid Norway spruce (Picea abies), Blass et. al [10] proposed the following equations for predicting the mean and characteristic embedment strength:

$$f_{h,\alpha} = \frac{0.022 \rho^{1.24} d^{-0.3}}{2.5 \sin^2 \alpha + \cos^2 \alpha} \tag{2.10}$$

$$f_{h,k,\alpha} = \frac{0.019 \rho_k^{1.24} d^{-0.3}}{2.5 \sin^2 \alpha + \cos^2 \alpha} \tag{2.11}$$

As testified by the empirical expressions, density ρ has a positive effect on embedment strength while for increasing diameter d, f_h decreases due to scale effect. The conventional embedment strength as defined in EN 383 [24] was found to decrease as the angle α between force and timber grain increases. However some authors observed a strong hardening behavior in the direction perpendicular to the grain. Schweigler et al. [76, 78] deeply investigated the embedment behavior of dowel-type fasteners focusing on proposing suitable parameters for definition of a complete constitutive law capable of describing the entire force-slip curve. The authors defined the yielding embedment strength $f_{h,y}$ as the intersection between the tangents defined by the quasi-elastic and elasto-plastic loading stiffness and a second parameter describing the elasto-plastic embedment strength taken at a dowel displacement of two times the dowel diameter, $f_{h,2d}$. It was found that $f_{h,y}$ is similar or slightly lower compared to the conventionally determined embedment strength according to EN 383 [24] (Eq. 2.1), while $f_{h,2d}$ can be significantly higher.

Defining Ψ as the ratio between the yield stress and the conventional embedment strength:

$$\Psi = \frac{f_{h,y}}{f_h} \tag{2.12}$$

and Υ as the ratio between the embedment strength taken at a dowel displacement of two times the dowel diameter and the conventional embedment strength:

$$\Upsilon = \frac{f_{h,2d}}{f_h} \tag{2.13}$$

The research results can be summarized as follows:

- Ψ ranges between 0.85 and 1.02 and no clear influence of angle to the grain or dowel diameter was found;

- Lower diameter dowels showed stronger hardening behavior. Υ is between 1.05 and 1.72 for $d = 12$ mm and Υ is between 1.09 and 1.46 for $d = 16$ mm;

- When loaded perpendicularly to the grain dowels showed considerably stronger hardening behavior. Υ is between 1.46 and 1.72 for $\alpha = 90°$ and Υ is between 1.05 and 1.09 for $\alpha = 0°$.

2.3.3 Viscoelastic behavior

Reynolds et al. [67] presented a study that examines the deformation and energy dissipation of timber in embedment by screw under in-service loads. During the cyclic embedment tests the authors found evidence of a viscoelastic component. In a timescale of 1000 s the rate of creep has found to be decreasing. No further information are provided about the creep evolution for longer time periods. A simple rheological model, combination of Kelvin–Voigt viscoelastic elements, fitted on experimental results, is used to describe the time-dependency and energy dissipation of the timber in embedment by a dowel-type connector. The results showed a stiffness 3.8 times higher under oscillating load than under static loading with the same maximum load.

2.4 Mechanical characterization of axial screw-timber interaction

The mechanical behavior of axially loaded screws, and specifically the withdrawal and the push-in behaviors, depend on the interaction along the axial screw direction between the screw thread and the surrounding timber fibers. The withdrawal failure has to be regarded as a local failure of the timber surrounding the screw. Preliminary studies conducted by Blass et al. [10] had demonstrated that the withdrawal and the push-in behavior of self-tapping screws are similar. Ringhofer [69] accurately described the appearance of a withdrawal failure in different planes with respect to the natural timber reference system. When the screw is inserted parallel to the timber grain ($\alpha = 0°$), the failure affect only the material between the screw shank and the outer thread diameter. As a first approximation a cylinder of diameter d can be regarded as the failure surface. In case of screw inserted perpendicularly to the grain ($\alpha = 90°$) the fracture pattern differs significantly depending on the section plane. In the radial-tangential plane, the failure can be identified again on the cylinder of diameter d, whilst in the radial-longitudinal plane cracks propagates in the longitudinal direction outside the screw outer diameter. Ringhofer [69] suggested also the possible role of the timber shear strengths on different planes on the withdrawal failure. A combination of $f_{v,LR}$ and $f_{v.LT}$ is regarded as the failure stress for $\alpha = 0°$. For $\alpha = 90°$, in the radial-tangential plane the rolling strength $f_{v,RT}$ is identified as the governing parameter whilst in the radial-longitudinal plane the main parameter is identified in $f_{v,RL}$. Despite this elementary schematization of the system, the problem of predicting withdrawal and push-in behavior of screws appears to be non-trivial as testified by the scarce literature source on theoretical modelling. Jensen et al. [48] attempted to relate the timber withdrawal strength to the timber shear strength by means of Volkersen-model and considering a mean stress failure criterion. However this approach requires the knowledge of timber fracture energy and only accounts in an approximate manner the influence of the test configuration. Clauss et al. [13] attempted to clarified the interaction between the screw thread and the surrounding timber by means of an innovative screw sensor with internal fibre Bragg gratings (FBGs) able to measure the forces along the screw axis. The study highlighted that even in the elastic range the axial forces along the screw axis showed a nonlinear distribution and a partial explanation of this phenomena is given in the Chapter 9 of this thesis. However the screw axial deformability can only explain partially the non-linearity of the forces along the screw axis. In fact Clauss et al. [13] have found that both the test setup and the screw-axis to grain angle influences the force distribution. When $\alpha = 90°$ most of the force is transferred from the screw to the timber in the vicinity of the tensile end of the screw, whilst when $\alpha = 0°$ the contribution of the near free-end part increases. Clauss et al. [13] have found also that local peaks of transferred forces change their position for varying support conditions (Fig. 2.8). Volkersen-model has found to be in accordance with experimental results only for $\alpha = 90°$.

According to the investigation conducted by Hoelz et al. [41] the thread pitch p has a significant influence on withdrawal resistance. A smaller pitch results in higher withdrawal strength, while the flank angle χ do not influence significantly the withdrawal performance.

Beyond this literature sources, most of the studies concerning the axial behavior of self-tapping screws are based on experimental results only. The authors determine the withdrawal strength and stiffness of fasteners according to the test methods described in EN 1382 [20] and than formulate a model based on the regression of experimental results.

The EN 1382 [20] describes methods applicable to all types of nails, screws and staples inserted into timber. According to this standard the fastener axis shall be perpendicular to the timber surface. In testing the withdrawal capacity in the direction perpendicular to the grain the width and the depth of the test piece in the direction of insertion of the fastener shall be at least $l_{ef} + 5d$ where l_{ef} is the the penetration depth of the profiled part of the screw. Whereas when the withdrawal capacity in the direction parallel to the grain is tested the length of the test piece in the direction of insertion of the fastener shall be at least $2l_{ef} + 5d$. In both cases the penetration depth should be comprised between $8d$ and $20d$. The transfer of axial force only has to be ensured by the test device and any support of the timber part shall be at least $3d$ from the fastener axis. The test is conducted at a constant rate of loading as to ensure the reaching of F_{max} in $60 \div 120$ s.

According to EN 1382 [20] the withdrawal parameter in N/mm^2 is determined as:

$$f_{ax} = \frac{F_{max}}{dl_{ef}} \tag{2.14}$$

Sometimes the same symbol of the withdrawal parameter is used to indicate the mean stress on the cylindrical surface at failure [11]:

$$f_{ax} = \frac{F_{max}}{\pi dl_{ef}} \tag{2.15}$$

In the following f_{ax} is defined as in Eq. 2.14.

As can be seen from Eq. 2.14 or Eq. 2.15 the withdrawal parameter and the withdrawal failure stress are defined by considering the applied axial force as uniformly distributed along the screw axis. As previously highlighted, this assumption is not true even in the elastic range and thus the withdrawal parameter and the withdrawal failure as defined in Eqs. 2.14 and Eq. 2.15 have to be regarded as a fictitious parameters which multiplied by the screw diameter, the screw length and eventually π give an estimate of the global withdrawal strength of the connections, but that can not be regarded as the actual local interface stress at failure initiation.

The EN 1382 [20] lacks a definition for the withdrawal stiffness. It is usually defined by authors as the slope of the tangent at the origin of the force displacement curve (e.g. Blass et. al [10]) or as the secant secant for the origin and 40% of the maximum load:

$$K_{ax} = \frac{0.4F_{max}}{u_{ax}(0.4F_{max})} \tag{2.16}$$

F_{ax}

α

(a)

F_{ax}

α

(b)
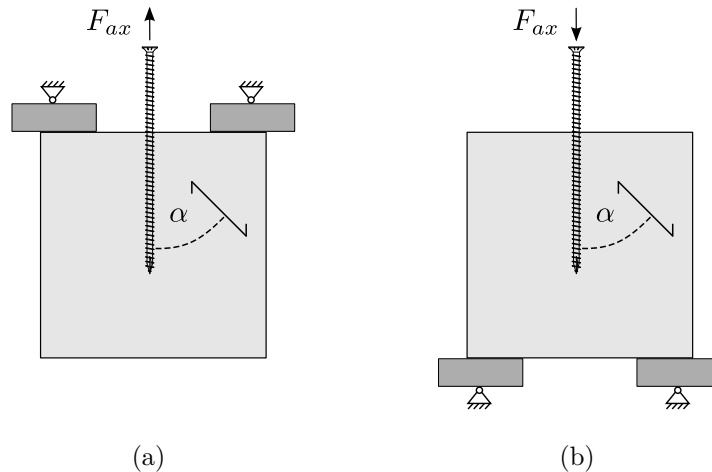
Figure 2.8: Withdrawal (a) and push-in (b) test setups.

The withdrawal behavior of screws in terms of force-displacement curves shows a clear maximum with a subsequent distinct load decrease. In the following a summary and a comparison between the outcomes of the main experimental studies is reported. The influence of the main parameter is discussed.

2.4.1 Withdrawal modulus

On the basis of a multiple regression analysis of 413 withdrawal test results, Blass et. al [10, 8] proposed the following equation for predicting the mean withdrawal modulus in the direction perpendicular to the grain:

$$K_{ax} = 234(\rho d)^{0.2} l_{ef}^{0.4} \qquad (2.17)$$

The tests were conducted on self-tapping screws with outer diameter of the thread $d = 6 \div 12$ in solid Norway spruce (Picea abies) without predrilling. Comparing the test results of Kevarinmäki [50] with the predictions made by Eq. 2.17 the authors observed a large dispersion and a low correlation. The authors concluded that Eq. 2.17 is only valid for the tested screw type and recommend to determine the withdrawal modules for each type of screw by tests.

Ringhofer et al. [71] presented an equation based on 5500 experimental results conducted on laminated product:

$$K_{ax} = 77.6 \rho^{0.75} d^{-0.7} l_{ef}^{0.4} \qquad (2.18)$$

Others expression of K_{ax} can be found in ETAs. In ETA 12/0063 [28] the following expression is proposed:

$$K_{ax} = 25 d l_{ef} \qquad (2.19)$$

while ETA 11/0190 [27] suggest to determine K_{ax} as follows:

$$K_{ax} = 780 d^{0.2} l_{ef}^{0.4} \qquad (2.20)$$

In all three formulations the dependence on diameter and length is considered. Eq. 2.19 is substantially different from the other two, while Eqs. 2.17 and 2.20 coincide when the density is 316 kg/m^3. According to Blass et al. [9] some of the differences between empirical formulas may depend on the experimental setup and measuring point locations.
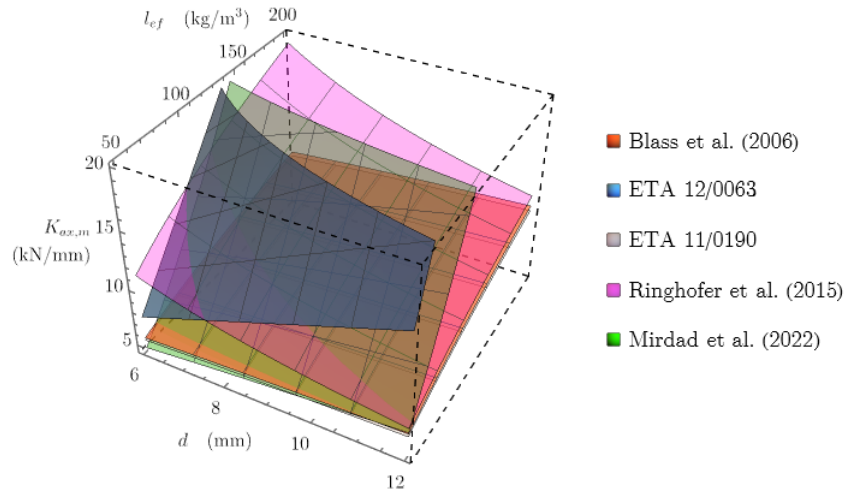
Figure 2.9: Withdrawal stiffness according to literature sources ($\rho = 500 \text{ kg/m}^3$ and $\alpha = 90°$).

In none of the previous formulations a dependence from the angle to the grain is considered, but an influence was found by Ringhofer et al. [71] who proposed the following equation to account for the angle to the grain influence:

$$K_{ax,\alpha} = \begin{cases} K_{ax,m} & \alpha \geq 45° \\ \left(\frac{1}{0.75} + \frac{1 - \frac{1}{0.75}}{45} \alpha \right) K_{ax,m} & 0° \leq \alpha < 45° \end{cases} \qquad (2.21)$$

According to its investigation K_{ax} can be considered approximately constant in case of $45° \leq \alpha \leq 90°$ while it linearly increases for decreasing α for $\alpha \leq 45°$ [69]. The same author observed significantly higher values of K_{ax} in case of non-predrilled specimens due to the material densification.

Mirdad et al. [58] derived the following equation by means of non-linear regression analysis of test data that cover Spruce-Pine-Fir and Douglas Fir:

$$K_{ax} = \frac{0.11 \rho^{0.72} d^{0.49} l_{ef}^{1.41}}{1.25 \sin^2 \alpha + \cos^2 \alpha} \qquad (2.22)$$

Stamatopoulus and Malo [83] proposed the following equation for threaded bars accounting also for the angle to the grain influence:

$$K_{ax} = \frac{50000 \left(\frac{\rho}{470}\right)^2 \left(\frac{d}{20}\right)^2 k_{length,K}}{\sin^{2.3} \alpha + 0.4 \cos^{2.3} \alpha} \tag{2.23}$$

with $k_{length,K} = \min((l/300)^{0.75}, 1)$. It should be noted that Eq. 2.23 is based on the withdrawal test results of a threaded rod with a diameter ranging from 16 to 20 mm and therefore is not suitable for screws with small diameter.

2.4.2 Withdrawal strength

According to the amendment to the Eurocode 5 [30], the characteristic withdrawal strength in the direction perpendicular to the grain is given by the following:

$$f_{ax,k} = 0.52 d^{-0.5} l_{ef}^{-0.1} \rho_k^{0.8} \tag{2.24}$$

$$f_{ax,\alpha,k} = \frac{f_{ax,k}}{\sin^2 \alpha + 1.2 \cos^2 \alpha} \tag{2.25}$$

Whilst according to the previous version of Eurocode 5 [29], the characteristic withdrawal strength in the direction perpendicular to the grain is given by the following:

$$f_{ax,k} = 3.6 \cdot 10^{-3} d^{-0.2} l_{ef}^{-0.2} \rho_k^{1.5} \tag{2.26}$$

$$f_{ax,\alpha,k} = \frac{f_{ax,k}}{\sin^2 \alpha + 1.5 \cos^2 \alpha} \tag{2.27}$$

where ρ_k is the characteristic timber density, in kg/m^3 and α is the angle of the load to the grain.

According to DIN 1052 [15] the screws are divided into capacity classes A, B or C. Depending on the the capacity class the characteristic withdrawal strength in the direction perpendicular to the grain is given by the following:

$$f_{ax,k} = (60 \div 80)10^{-6} \rho_k^2 \tag{2.28}$$

The load to grain angle influence is taken into account in a similar manner to the Eurocode 5. The provided equation is the same of Eq. 2.25 where the coefficient 1.2 is replaced by 4/3.

According to SIA 265 [80], the characteristic withdrawal strength in the direction perpendicular to the grain is given by the following:

$$f_{ax,k} = (30\pi^{-0.2} 10^{-3} d^{-0.2} l_{ef}^{-0.2} \rho_k)\pi \tag{2.29}$$

According to the formulation provided by the standards the density ρ is regarded as the main influencing parameter of the withdrawal parameter f_{ax} and it is the only parameter considered in the DIN 1052. The effective length of penetration l_{ef} has only a marginal influence, since its exponents spans from -0.2 to -0.1. The exponent of the outer thread diameter d varies between -0.5 and -0.2 confirming the presence of a size-effect. Conversely to the withdrawal stiffness, the withdrawal parameter is found to be appreciably dependent on the angle to the the grain α and a modified Hankinson relation is adopted [37].
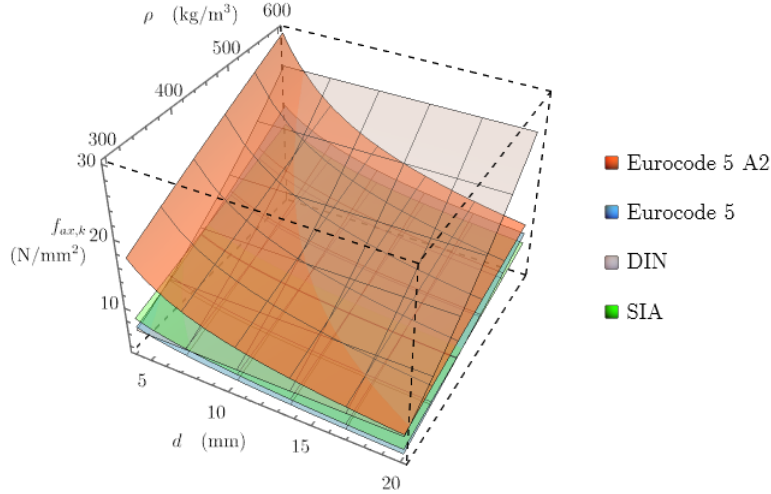
Figure 2.10: Withdrawal parameter according to codes ($l_{ef} = 10d$).

It is worth mentioning that Eq. 2.24 bases on solid timber, but its application is not restricted to it. This equation bases on a multiple regression analysis of 413 test results conducted on self-tapping screws with $d = 6 \div 12$ in solid Norway spruce (Picea abies) without predrilling. The equation descend from the one originally proposed by Blass et. al [10, 8] for predicting the characteristic withdrawal strength:

$$f_{ax,m} = 0.6d^{-0.5}l_{ef}^{-0.1}\rho_m^{0.8} \tag{2.30}$$

$$f_{ax,k} = 0.56d^{-0.5}l_{ef}^{-0.1}\rho_k^{0.8} \tag{2.31}$$

According to Blass et. al [10] the dependence from the angle α is given by:

$$f_{ax,\alpha} = \frac{f_{ax}}{\sin^2\alpha + 1.2\cos^2\alpha} \tag{2.32}$$

The associated ultimate displacement can be calculated with the following regression equation:

$$\delta_{ax} = 0.0016d\sqrt{\rho l_{ef}} \tag{2.33}$$

Pirnbacher et al. [64] conducted an experimental investigation involving 5524 tests. The tests were conducted on solid and glulam Sitka spruce and aimed at identifying the influence of following parameters on the withdrawal parameter: the moisture content, the temperature , the screw diameter, the slenderness, the embedment length of the threaded part, the angle between the screw axis and the grain, the pre-drilling. Conversely to the multiplicative approach proposed by the vast majority of the studies, Pirnbacher et al. suggested the following equation for the mean withdrawal strength in the direction perpendicular to the grain:

$$f_{ax,m} = (0.0135\rho - 0.687d^{0.572} + 2.19)\pi \tag{2.34}$$

The dependence from the angle α is given by:

$$f_{ax,\alpha} = \frac{f_{ax}}{\sin^{2.2}\alpha + 1.3\cos^{2.2}\alpha} \tag{2.35}$$

In the case of screw parallel to the grain:

$$f_{ax,m} = (0.0538\rho - 1.12d^{0.572} + 5.92)\pi \tag{2.36}$$

Temperature has found to have a negligible influence (0.15% of f_{ax} per Celsius degree). While the moisture content influence depends on the considered domain. For u between 0% and 7%, f_{ax} increases with increasing u, whilst from 12% to 20% a linear decrease of f_{ax} with increasing u can be observed.

Frese et al. [33, 32], the mean withdrawal strength in the direction perpendicular to the grain is given by the following:

$$f_{ax,m} = 0.0857\rho d^{-0.342} \tag{2.37}$$

This equation is based on 1847 withdrawal tests conducted in softwood of densities between 325 and $600\,\mathrm{kg/m^3}$. The screw diameters were comprised between 4 and 14 mm and the length of penetration between 20 and 140 mm.

An extended experimental campaign conducted on 3328 test specimens made of hardwood species including European ash, European beech and Black locust was executed by Hubner [42].

$$f_{ax,m} = 2.39 \cdot 10^{-3} \rho_m^{1.6} d^{-0.34} \tag{2.38}$$

$$f_{ax,\alpha} = \begin{cases} f_{ax,m} & \alpha \geq 30° \\ \left(\frac{1}{1.22} + \frac{1-\frac{1}{1.22}}{30}\alpha\right) f_{ax,m} & 0° \leq \alpha < 30° \end{cases} \tag{2.39}$$

Ringhofer et al. [71] presented an equation based on 8000 experimental results conducted on laminated product:

$$f_{ax} = 0.0440\rho^{1.11} d^{-0.33} \tag{2.40}$$

and similarly to Hubner:

$$f_{ax,\alpha} = \begin{cases} f_{ax,m} & \alpha \geq 45° \\ \left(\frac{1}{1.35} + \frac{1-\frac{1}{1.35}}{45}\alpha\right) f_{ax,m} & 0° \leq \alpha < 45° \end{cases} \tag{2.41}$$

The same approach was followed by Brandner et al. [11] for screw applications in hardwood or more general in deciduous timber species:

$$f_{ax} = \begin{cases} 0.01400\rho^{1.10} d^{-0.33} & \text{Coniferous} \\ 0.00310\rho^{1.40} d^{-0.33} & \text{Ring Porous} \\ 0.00042\rho^{1.70} d^{-0.33} & \text{Diffuse Porous} \end{cases} \tag{2.42}$$

As can be observed from Fig. 2.11, despite the differences in the empirical formulations, their results are close together. A good continuity is observed between the formulation provided by Hubner [42] for hardwoods and formulations for softwoods.
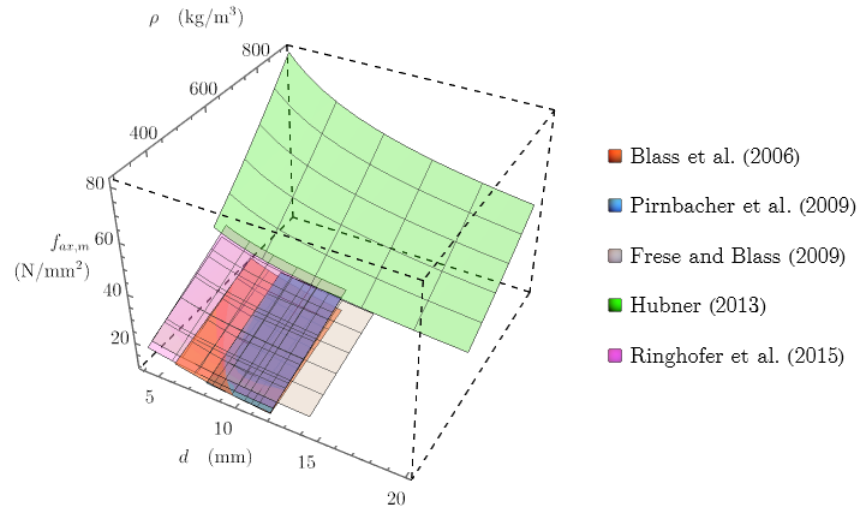
Figure 2.11: Withdrawal parameter according to literature sources in the domain of tested parameters ($l_{ef} = 10d$).

The angle to the grain influence is accounted similarly in the formulation for softwoods, while Eqs. 2.39 significantly differs from the others. The highest reduction (-26%) is predicted by Ringhofer et al. [71].
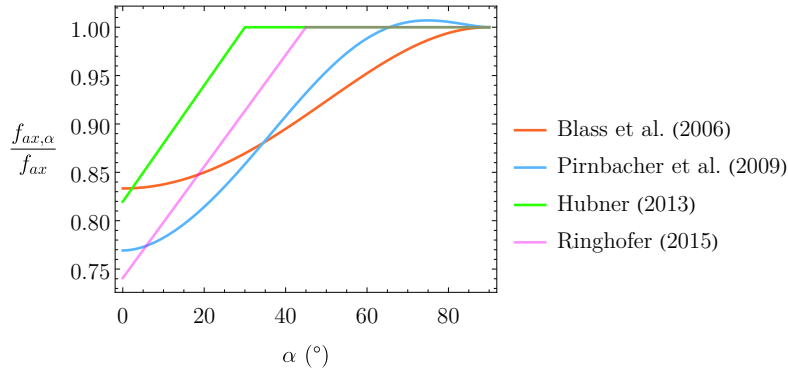
Figure 2.12: Ratio between withdrawal parameter at an angle and perpendicular to the grain according to literature sources.

All the above relations neglects the interrelationship between parameters. The experimental investigation from Ringhofer [69] highlighted a possible interaction between d and α. A more pronounced non-linear decreased of f_{ax} was observed for $\alpha = 0°$ with respect to $\alpha = 90°$.

No significant studies concerning the screw pitch geometrical properties and timber defects influence have been found. Ringhofer [69] an appreciable influence of the annual ring width a_w was found on the withdrawal modulus of screw inserted in the tangential direction. In Ringhofer [69] obtained a novel results. In case of screw inserted parallel to the fibers the dependency of the withdrawal strength on related shear modulus G_{LR} is even higher than that on timber density. A possible explanation is given in Chapter 9 where the proposed analytical model showed that the interface stresses depends on the medium deformability.

2.5 Mechanical characterization of interaction between axial and transversal interactions

A total of 180 wood screws having a diameter of 6 to 12 mm have been tested to withdrawal with different levels of transverse loading by Blass et. al [10]. With a transversal displacement of $\delta_{la} = 5$ mm, the withdrawal parameter has been found reduced to 57.1% of its value without transverse loading. Whilst for a transversal displacement of $\delta_{la} = 2.5$ mm which is near the ultimate displacement of connections with inclined screws, a loss of approximately 11% of the withdrawal strength was observed.

2.6 Mechanical characterization of screw head-timber interaction

Most of the screw applications which involve mainly the screw axial capacity require the use of fully threaded screws in order to achieve satisfactory performance. However, even partially threaded screws posses a certain axial capacity which is limited by the pull-through strength of the screw head since the pull-through is the only resisting mechanism of the non-threaded part of the screw. Despite the pull-through capacity is significantly lower compared to withdrawal strength, the pull-through mechanism can offer a valuable contribution. This mechanism allow for the activation of the rope-effect in connection with screws perpendicular to the sliding plane which commonly use partially threaded screws.

The test methods for determining the resistance of timber to the head pull through of timber fasteners are described in EN 1383 [21]. The test consist in pulling the fastener through the test piece material of thickness $t \leq 7d$ with a continuous movement of the head of the testing machine along the axis of the fastener direction. The pull-through parameter is defined as follows:

$$f_h = \frac{F_{max}}{d_h^2} \tag{2.43}$$

where d_h is the diameter of fastener head.
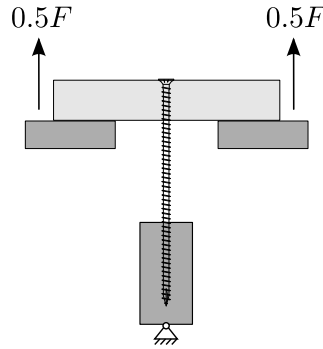
Figure 2.13: Pull-through test setups.

The current design approach consist in adopting the declared values of technical documentation issued by screw producers. Sandhaas and Blass in [73] attempted to derive a general formula for the withdrawal parameter on the basis of 2854 test results from certification test reports. On the basis of a non-linear regression the following expression was derived:

$$f_h = 9.5 \cdot 10^{-4} \rho^{1.67} \tag{2.44}$$

However, the authors underlined the possible influence of some parameters other than the timber density. Head with smaller diameter were found to have higher values of the pull-through diameter. The authors suggested timber densification caused by the absence of pre-milling in smaller head screws as a possible explanation of this trend. Furthermore, due to the high results dispersion, the authors suggested a possible influence of the test setup, namely the support conditions and the thickness of the timber member.

2.7 Mechanical characterization of screw tip-timber interaction

No specific investigation were found in literature concerning the mechanical contribution of the screw-tip. The most recurrent assumption consist in completely neglecting both the tangential and normal interaction.

2.8 Mechanical characterization of the screw

Despite the low dispersion of the mechanical properties of the steel, no general equation for calculating the screw mechanical parameter can be derived. The hardening process can lead to different results depending on the exact procedure followed by each manufacturer. Furthermore the cold forming of the screw thread can cause cracks and notches which may reduce the overall screw strength.

The current approach to the mechanical characterization of the screw requires the determination of yield moment M_y by experimental tests. This values together with tensile failure stress f_u, and the torsional failure stress f_{tor} should be declared in the product technical assessments [22]. However several equations describing the interrelation between parameters have been found in literature and here follow discussed.

2.8.1 Section area and inertia

In the beam-like mono-dimensional models the section area, inertia and torsional inertia becomes relevant parameter in order to properly define the section stiffness.

Approximating the screw geometry as a cylinder of diameter equal to the thread root diameter d_c the geometrical properties of the section can be easily determined by the following:

$$A = \frac{\pi}{4} d_c^2 \tag{2.45}$$

$$I = \frac{\pi}{64} d_c^4 \tag{2.46}$$

$$J = \frac{\pi}{32} d_c^4 \tag{2.47}$$

However this values represent only a lower bound of the actual values due to the neglecting the thread contribution. A recurrent assumption consist in using $1.1d_c$ to account, although in an approximate way, for thread influence [29].

Ringhofer [70] attempted to derive the elastic geometrical properties of the actual section on the basis of the analytical geometrical description of the thread given by Rammer [66]. As underlined by the author himself the expression have been derived under the assumptions of a prismatic beam which is unrealistic due to the discontinuities in the axial direction for a fixed longitudinal-radial plane due to thread.

2.8.2   Tensile failure stress

In order to determine the tensile failure stress the EN 14592 [22] suggest the test methods described in EN 1383 [21] using a steel plate to replace the head side timber member in the test setup described in Sec. 2.6.

There are a few research studies on tensile tests of self-tapping screws. Producers often provide only conservative characteristic values of the tensile failure stress. Ringhofer et al. [68] and Niebuhr et al. [59] both had found that values significantly higher than $1000 \, \text{N/mm}^2$ are possible. In the first study the mean tensile failure stress defined as in the Eq. 2.48 resulted $f_{u,m} = 1482 \, \text{N/mm}^2$ with a $CoV = 0.45\%$ while in the latter the authors reported $f_{u,m} = 1259 \, \text{N/mm}^2$ with a $CoV = 1.36\%$. In both cases carbon steel screws were tested.

$$f_{u,m} = \frac{F_{u,m}}{\pi \frac{d_c^2}{4}} \tag{2.48}$$

Both studies focused on cyclic axial loading. Defining the fatigue failure stress as in Eq. 2.49, Ringhofer suggested a significant notch coefficient, being representative for sensibility against material fatigue, of $k_{SN} = 3.87$.

$$f_{fat,N} = f_{fat,D} \left(\frac{N_D}{N} \right)^{1/k_{SN}} \tag{2.49}$$

Niebuhr et al. [59] compared their results with Ringhofer et al. [68] tests results highlighting that despite the different screw and different stress ratio, the fatigue behavior differs only to a limited extent.

2.8.3   Head tear-off

In order to determine the tensile failure stress the EN 14592 [22] suggest the test methods described in EN 1383 [21] using a steel plate to replace the head side timber member in the test setup described in Sec. 2.6. Niebuhr et al. [59] in testing the fatigue behavior of axially loaded screws have found that a considerable amount of head tear off and therefore concluded that this failure mode cannot be disregarded.

2.8.4   Yielding moment

The test procedure for determining the yield moment of dowel type fasteners are described in EN 409 [26] and in ASTM F1575 [1]. The former standard require a four-point bending tests and the yield moment M_y should be determined for different angle of rotation of the plastic hinges depending on the screw nominal diameter (Fig. 2.14a). The latter require a three-point bending test (Fig. 2.14b).

(a)   (b)
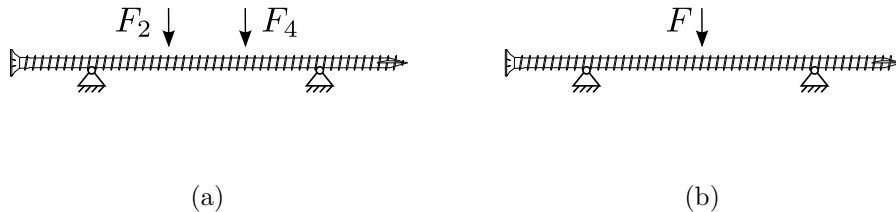
Figure 2.14: EN 409 (a) and ASTM F1575 (b) test setups.

According to Eurocode 5 [29], the characteristic yield moment for screws with diameters up to 6 mm can be calculated by means of the same expressions provided for nails:

$$M_{y,Rk} = \begin{cases} 0.3 f_{u,k} d_{ef}^{2.6} & \text{for round nails} \\ 0.45 f_{u,k} d_{ef}^{2.6} & \text{for square and grooved nails} \end{cases} \tag{2.50}$$

In case of connections with screws with diameters greater than 6 mm:

$$M_{y,Rk} = 0.3 f_{u,k} d_{ef}^{2.6} \tag{2.51}$$

According to DIN 1052 [15], the characteristic yield moment for screws is:

$$M_{y,Rk} = 0.15 f_{u,k} d_{ef}^{2.6} \tag{2.52}$$

Assuming the complete plasticization of the section by bending, so the two part of the section divided by the plastic neutral axis are subjected to constant and equal compressive and tensile yielding stress, the yield moment is given by the following:

$$M_{y,Rk} = \frac{\pi}{6} f_{y,k} d_c^3 \tag{2.53}$$

Assuming the incipient plasticization of the section circumference by bending, the yield moment is given by the following:

$$M_{y,Rk} = \frac{\pi}{32} f_{y,k} d_c^3 \tag{2.54}$$

2.9 Mechanical characterization of the interaction between timber members

In connections with inclined screws in tension a compression in the direction perpendicular to the sliding plane develops. This compression force generates a friction force parallel to the sliding surface. According to literature this contribution leads to an increase in slip modulus and strength.

The surface roughness has the highest influence on the coefficient of friction. A rough-cut is characterized by a friction coefficient higher than planed surfaces and planed surface are characterized by a friction coefficient higher than treated surfaces. In timber-to-steel connection rusted and sandblasted surfaces have higher friction coefficient compared to polished surfaces.

According to the literature review done in [4] the coefficient of friction of softwood on softwood has a mean value of $\mu = 0.48$ and confirmed the suitability of $\mu = 0.25$ as characteristic value. This latter value is also prescribed by Eurocode 5 [29] for rope effect contribution in Johansenn formulas.

The coefficient of friction can be increased by treating the surface adequately as done in [4] where two different bonding agents were used to coat the specimen either with quartz sand or with grit.

2.10 Experimental studies

Research studies on connections with screws showed that the load-slip behavior mainly depends on the following parameters:

- angle between the external load and the axis of the screw

- angle between the axis of the screw and the timber grain orientation

- diameter of the screw

- length of penetration of the screw in each member

- timber density

- coupled materials

- friction on sliding plane

- interlayers

- screw type

- pre-drill

In the following the influence of each one of this parameters on the slip modulus, strength and ductility is discussed on the basis of the most significant outcomes of research studies from literature.

While the failure of connection with screws perpendicular to the sliding plane (PS) are related to hinge formation in the fastener and timber embedment, the failure of connection with inclined screws (IS) is often governed by the reaching of the withdrawal capacity. Stiffness and strength of IS can be 5 to 10 times the stiffness and strength of PS. While for PS the ultimate force is usually reached at the conventional displacement of 15 mm with a ductile behavior, for IS the failure displacement is between 1 mm and 5 mm depending mainly on the inclination angle of the screw. In IS after the reaching of the maximum force a markedly softening behaviors follows with a residual strength due to dowel-contribution [39, 50, 10, 85, 46, 75, 9, 86].

For timber-to-timber connections with screw in tension (TS) both stiffness and strength increase for increasing angle of inclination of the fasteners with respect to the sliding plane whilst for connections with screw in compression (CS) the load-bearing capacity and the slip modulus remain approximately unvaried for varying angles of inclination [85, 86]. In connections with inclined screws in compression stiffness is approximately equal to the stiffness of connection with screws perpendicular to the sliding plane. Connections with crossed screws (XS) shows a similar qualitative behavior to connection with screws in tension [85]. Similar results were found by Du et al. [16] for timber-to-concrete connections. XS exhibited lower load bearing capacities compared to TS and CS exhibited lower slip modulus compared to both XS and TS. Connections with $\theta = 60°$ showed 54.6% more slip modulus and 31.9% more strength compared to connections with $\theta = 30°$.

The tests from Kevarinmaki [50] showed that tension screw joints have $25 \div 30\%$ higher load carrying capacity per screw than the cross screw joints due to the friction between timber members.

Jockwer et al. [65] tested connection with inclined screw in shear and in pull with respect to plane between members and observed a more pronounced dependence of the load-carrying capacity from the angle between screw axis and the sliding plane when the connection is subjected to shearing compared to pulling.

Blass and Laskewitz in [39] tested timber-to-timber connections with nails and OSB interlayer connected to the timber member by staples. The authors observed double-hinge in the nails and plastic deformation of the staples. The relative displacement between the OSB and the member connected with it through staples was found to be small compared to the relative displacement between the OSB and the other timber member. Blass and Laskewitz in [39] tested also timber-to-steel connections with nails and OSB interlayer considering both the case of interlayer stapled to the timber member and interlayer glued to the timber member. The role of this secondary connection has proved to be crucial in determining the failure mode of the main connection. A more stiff behavior of the connection with glued interlayer was found. The failure mode in this case was a single plastic hinge whilst in the case of a stapled interlayer two plastic hinges occurred in every nail.

Regarding the screw type, Schiro et al. had found in [75] that double threaded screws (DT) exhibit higher stiffness than single threaded (ST) screws, despite having a smaller diameter. The authors also underlined the appreciable contribution of washers when using ST screws. Using washers increase both the head push-in stiffness and strength. The increased push-in stiffness resulted in an increased compression perpendicular to the sliding plane and therefore to an increase of friction. Consequently the ultimate load increase of 24% and the slip modulus of 22%. When using washers with hardwood, the benefits in terms of capacity are lower (6%) while the slip modulus increases consistently (34%).

In timber-to-timber connection failure load and stiffness both depends on the weak side. As observed by Schiro et al. in [75] the reduced penetration length of fully threaded screws or double threaded screws in one of the timber member could be compensated by using hardwood. In case of single threaded screws the author suggest the use of wide washers. Alternatively, to reinforce the weak side of a timber-to-timber connection, the screw can be embedded in cementitious or epoxy pockets [12]. In this way withdrawal from smaller thickness member could be prevented.

In connections with inclined screw and interlayer it was observed that a mechanical behavior similar to connections without interlayer can be achieved by using longer screw to compensate for the loss of withdrawal contribution in the interlayer [75].

Jacquier et al. [46] tested combined screw-punched metal plate joints. According to this study the stiffness and the strength of combined connection are 3.6 and 4.2 times of the analogous connection with screws inclined at 45° only. The author also suggest to optimize this kind of connection by varying the inclination of the screw to make additive the strength contribution of the plate and of the screws.

In connections with CS or XS the restraint between connected members has an influence. When the relative displacement between connected members perpendicularly to the sliding plane is not restrained members tends to separate and the friction contribution is lost [86].

For the cases studied by Tomasi et al. no-group effect was observed [85], while in Blass et al. [10] an appreciable group effect is observed in some of the tested configuration for both IS and XS. This study showed that group effect increases for decreasing screw diameter while maintaining the spacing to 4d. No significant group effect was observed for spacing equal to 30d. Liu et al. [56] investigated the spacing effect on slip modulus and strength of connection with inclined screws. For spacing greater than 8d no change in the maximum load was observed while slip modulus increases for increasing spacing up to 16d.

A quasi-linear relationship can be found between the slip modulus of inclined screws and the length of penetration of the threaded part in timber members, while a quadratic relationship exist between the slip modulus and the diameter of the screw [9]. Also in timber-to concrete connection the same linear relationship can be found and the diameter has an influence. Increasing the diameter by 40% results in a 38.7% and 25.7% increase in terms of slip modulus and load capacities were obtained [16].

The stiffness of IS with $\theta = 75°$ resulted up to 3.7 times the stiffness with $\theta = 15°$ [9]. According to Blass and Steige [9] the pre-drill reduces the stiffness of a connection with IS of 29.2% on average. The authors noticed that due to the small diameter of the drill bit a deviation of the trajectory of the hole and consequently of the screw axis could happen. According to Blass and Steige [9] an increase up to 20% of the moisture content has no significant effect on the axial stiffness.

For timber-to-concrete connections concrete strength has an influence on both stiffness and strength. Increasing the concrete strength by 50% resulted in an increase of 8% and 24% in terms of stiffness and strength respectively [16]. In Appavuravther [2] it was demonstrated that even with lightweight concrete of strength equal to 14.5 N/mm^{2}effective connection between members and consequently composite action can be obtained.

For timber-to-concrete connections, concrete failure in embedment and cone expulsion of concrete ahead of the shear-compression loaded screw should be considered in determining the load-bearing capacity [16, 2].

Moderate to high ductility ratios can be obtained by combining PS to IS. In Krauss et al. [51] it was shown that the highest ductility can be achieved combining IS and PS in a 1 : 2.5 ratio.

None of the previously cited studies investigated the interlayer mechanical properties influence on the connection mechanical behavior. The wide variety of interlayers described in Sec. 2.2.4 may led to different mechanical performances. Another aspect that has never fully been addressed by scholars is related to members interaction. No experimental campaign was found to investigate the influence of connection type between interlayer and main members on the strength and stiffness of the resulting connection. Moreover, no systematic work has been done to assess if the installation procedures type could affect the development of friction on the sliding planes.

2.11   Modelling

Models can predict the connection behavior by defining the causal relationship between some input parameters regarded as significant and some output parameters of interest. The output of the model can be represented by synthetic parameters of engineering interest like service slip modulus K_s and connection strength R_v or R_n or can be the overall non-linear load-slip curve. Models can reduce the number of experimental tests needed to characterize a specific class of problems. As the predictability of the model increases the number of necessary input parameters decreases.

The relationship between input and output can be defined by means of different methods:

- analytical;

- finite element;

- empirical.

Analytical models describe the problem with equations derived by defining kinematic, equilibrium and constitutive relationship for the components of the system. The resulting equations can have closed form solution or may require numerical methods to be solved.

In finite element modelling the problem is discretized by dividing the geometric domain of the problem in multiple sub-domain whose analytical definition is easier.

Empirical models are directly based on observations. In their most-trivial form they consist in an interpolation of the outcomes of experimental test. It is assumed that for intermediate configuration between those tested, the system behaves as described by the regression.

While analytical models are more computationally efficient and able the researcher to directly understand the response of the system by studying the closed form solution or by means of parametric analyses, finite element models

allow for more detailed investigations. Analytical and empirical models are usually more suitable for practitioners reducing their effort to the implementation of a formula and thus reducing also the probability of errors.

The input parameters may change depending on the chosen methods and on the desired output. Less inputs are usually required for models for stiffness prediction compared to models able to describe the full-non linear behavior until failure. In the first case it is assumed that the connection is in the elastic range. In the following, a literature review of existing model for stiffness and strength prediction is presented.

2.11.1 Stiffness prediction

While the stiffness of laterally loaded screws is mostly governed by the embedment behavior of the timber and by the bending behavior of the screw, joints with inclined screws have a more complex behavior due to the combined transversal and axial action on the screw already at small displacements. A wide literature on the stiffness of laterally loaded fasteners exist as testified by the presence of formulations in standards [29], while only a few researchers focused on the problem of inclined screws. In the following some models suitable for inclined screws are described and compared.

Empirical

The case of inclined screw connections is not explicitly threaded in Eurocode 5 [29]. Consequently the slip modulus should be determined according to the same formula of connections with dowel-type fasteners perpendicular to the sliding plane:

$$K_{v,ser} = \frac{1}{23}\rho^{1.5}d \tag{2.55}$$

This model derives from [18]. The instantaneous slip modulus to be used for ultimate limit state design checks is defined as follows in Eurocode 5 [29].

$$K_{v,u} = \frac{2}{3}K_{v,ser} \tag{2.56}$$

Although withdrawal tests described in Subsec. 2.4.2 are primarily used to determine withdrawal parameter f_{ax} which is to be intended as local property, in reality the tests involve a full-scale specimen with a screw subjected to axial forces only, where the axial deformability of the screw makes the withdrawal parameter and the withdrawal stiffness per unit of length not completely geometry-independent as discussed in the Chapter 9. Therefore the formulas discussed in Subsec. 2.4.2 can be regarded both as mechanical-properties characterizing formulas with a certain degree of approximation and as empirical models for pure-axial stressed screws.

Semi-empirical

Blass in [10] presented a semi-empirical model for the slip modulus of joints with inclined screws. The model is capable of accounting of interface friction. Neglecting the transversal contribution, the stiffness of a timber-to-timber connection is expressed as follows:

$$K_v = \frac{1 + \mu\tan(90° - \theta)}{\frac{1}{K_{ax,1}} + \frac{1}{K_{ax,2}}} \tag{2.57}$$

where μ is the friction coefficient and $K_{ax,i}$ are the axial stiffness of each part of the screw whose value it is suggested to be calculated on the basis of the regression of withdrawal test.

The stiffness of timber-to-timber connections with inclined screws loaded in direction parallel to the shear plane was also studied by Tomasi et al. [85]. The screw is considered linear-elastic. In this case both the transversal and the axial contribution are considered, but no coupling is assumed between transversal and axial behavior. Imposing the kinematic compatibility and the equilibrium the following equation is derived:

$$K_v = K_{tr}\cos\theta\,(\cos\theta - \mu\sin\theta) + K_{ax}\sin\theta\,(\sin\theta + \mu\cos\theta) \tag{2.58}$$

where K_v is the ratio between the force and the slip in the direction parallel to the shear plane, K_{tr} is the transversal stiffness of a connection with a fastener perpendicular to the sliding plane, K_{ax} is the axial stiffness of a connection with an axially loaded fastener, θ is the angle between the axis of the fastener and the normal to the sliding plane and μ is the friction coefficient on the sliding plane. Also in this case experimentally derived or producer declared expression are suggested for K_{ax} while the authors suggest the use of Eq. 2.55 for K_{tr}.

The stiffness of timber-to-timber connections with inclined screws loaded in direction perpendicular to the plane between members was studied by Jockwer et al. [65].

$$\frac{1}{K_n} = \frac{1}{K_{ax}} + \frac{1}{K_{v,pulling}} \tag{2.59}$$

Jockwer et al. [65] assumes that the timber layer perpendicular to the screw axis near the timber surface is too thin to resist the loading from embedment, therefore the authors propose an equation that considers the axial stiffness of the screw in series with the stiffness of the free part of the screw which is in the outermost zone. The corresponding structural system is a cantilever beam with elastic clamping, whose stiffness is approximated by the authors assuming fixed clamping:

$$K_{v,pulling} = \frac{3E\pi d_c^4}{64x_1^3} \tag{2.60}$$

where the length of the zone of reduced embedment is assumed as:

$$x_1 = \frac{f_h d_{ef}}{2\tan(90° - \theta)f_{v,RT}} \tag{2.61}$$

Analytical

More complex analytical models based on beam on elastic foundation have been derived by Symons et al. [84] and Di Nino et al. [14]. These two models are suitable for timber-to-concrete connections with inclined screws. Both considered the concrete acting as an encastre for the screw. In [14] the model from Symons et al. [84] was extended to account also for the presence of interlayer.

While in the models of Blass [10], Tomasi et al. [85] and Jockwer et al. [65] the model inputs are themselves stiffness of connection, although of more elementary cases, in the models of Symons et al. [84], Girhammar et al. [36] and Di Nino et al. [14], the required inputs are foundation modules. In the first and in the last model only embedment modules are necessary, whilst in the model from Girhammar et al. [36] the interaction between the timber and the screw is represented by axial and transversal springs thus requiring also the knowledge of axial properties. Being the springs oriented in the direction parallel and perpendicularly to the grain in the models from Symons et al. [84] and Di Nino et al. [14] the orthotropic behavior of timber is accounted by the analytical model itself whilst in the model from Girhammar et al. [36] the orthotropic behavior of timber should be accounted in the inputs.

With the schematization adopted by Symons et al. [84] and Di Nino et al. [14] the screw-timber relative displacement in axial direction is considered to be null that is reasonable in serviceability conditions.

Although the model from Girhammar et al. [36] considers the screw as a rigid body, flexibility and extensibility of the screw are taken into account by theoretically derived correction factor.

Further discussions on analytical models can be found in Sec. 4.9 and 4.10.

Compared to empirical and semi-empirical models these analytical models allow for the slip modulus calculation of connection with screws of any length and diameter being the model itself rather than the empirically determined input to account for these parameters.

Numerical

No numerical studies explicitly focusing on slip modulus prediction of connections with inclined screws were found in literature.

2.11.2 Strength prediction

The main load resisting mechanisms of connection with inclined screws are related to the axial and bending capacity of the screw, to the embedment and withdrawal strength of the screw into the timber, to the friction between the timber elements as well as to the screw inclination. In the following analytical, numerical and experimental models from literature that consider some or all of this parameters are described and compared.

Analytical

The load carrying capacity of joints with transversely loaded dowel-type fasteners can be determined by means of Johansen's yield theory [49]. Johansen's yield theory assumes an ideal rigid-plastic material behavior of the timber in embedding and of the fastener in bending. According to this theory three different failure modes can be considered:

- embedment in one or multiple timber members

- one plastic hinge in one or multiple timber members

- two plastic hinges in one or multiple timber members

The load carrying capacity of fasteners in single shear of timber-to-timber connections associated with each failure mode can be predicted by the following formulas:

$$R_v = \min \begin{cases} f_{h,1}t_1 d & (a) \\ f_{h,2}t_2 d & (b) \\ \frac{f_{h,1}t_1 d}{1+\beta}\left[\sqrt{\beta + 2\beta^2\left[1 + \frac{t_2}{t_1} + \left(\frac{t_2}{t_1}\right)^2\right] + \beta^3\left(\frac{t_2}{t_1}\right)^2} - \beta\left(1 + \frac{t_2}{t_1}\right)\right] + \mu R_{ax} & (c) \\ 1.05\frac{f_{h,1}t_1 d}{2+\beta}\left[\sqrt{2\beta(1+\beta) + \frac{4\beta(2+\beta)M_y}{f_{h,1}t_1^2 d}} - \beta\right] + \mu R_{ax} & (d) \\ 1.05\frac{f_{h,1}t_2 d}{1+2\beta}\left[\sqrt{2\beta^2(1+\beta) + \frac{4\beta(1+2\beta)M_y}{f_{h,1}t_2^2 d}} - \beta\right] + \mu R_{ax} & (e) \\ 1.15\sqrt{\frac{2\beta}{1+\beta}}\sqrt{2M_y f_{h,1} d} + \mu F_{ax,R} & (f) \end{cases} \tag{2.62}$$

The load carrying capacity of fasteners in double shear of timber-to-timber connections associated with each failure mode can be predicted by the following formulas:

$$R_v = \min \begin{cases} f_{h,1}t_1 d & (g) \\ 0.5f_{h,2}t_2 d & (h) \\ 1.05\frac{f_{h,1}t_1 d}{2+\beta}\left[\sqrt{2\beta(1+\beta) + \frac{4\beta(2+\beta)M_y}{f_{h,1}t_1^2 d}} - \beta\right] + \mu R_{ax} & (j) \\ 1.15\sqrt{\frac{2\beta}{1+\beta}}\sqrt{2M_y f_{h,1} d} + \mu F_{ax,R} & (k) \end{cases} \tag{2.63}$$

where $f_{h,i}$ is the embedment strength in timber member, $\beta = f_{h,2}/f_{h,1}$, t_i is the timber thickness or penetration depth, d is the fastener diameter, M_y the fastener yield moment, μ is the friction coefficient, R_{ax} the axial connection capacity and R_v the connection capacity in the direction parallel to the sliding plane.
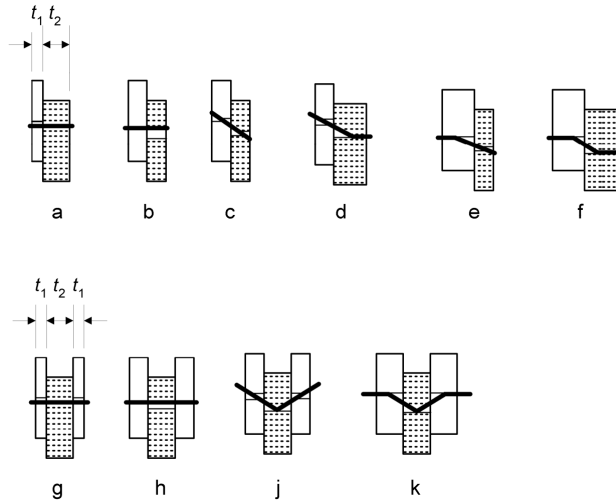
Figure 2.15: Timber-to-timber connections failure modes.

The load carrying capacity associated with each failure mode of a fasteners in single shear of timber-to-steel connections with thin plate can be predicted by the following formulas:

$$R_v = \min \begin{cases} 0.4f_{h,1}t_1 d & (a) \\ 1.15\sqrt{2M_y f_{h,1} d} + \mu R_{ax} & (b) \end{cases} \tag{2.64}$$

The load carrying capacity associated with each failure mode of a fasteners in single shear of timber-to-steel connections with thick plate can be predicted by the following formulas:

$$R_v = \min \begin{cases} f_{h,1}t_1d & (e) \\ f_{h,1}t_1d\left[\sqrt{2 + \frac{4M_y}{f_{h,1}t_1^2d}} - 1\right] + \mu R_{ax} & (c) \\ 2.3\sqrt{2M_y f_{h,1}d} + \mu F_{ax,R} & (d) \end{cases} \tag{2.65}$$

The load carrying capacity associated with each failure mode of a fasteners in single shear of timber-to-steel connections with steel plate as central member can be predicted by the following formulas:

$$R_v = \min \begin{cases} f_{h,1}t_1d & (f) \\ f_{h,1}t_1d\left[\sqrt{2 + \frac{4M_y}{f_{h,1}t_1^2d}} - 1\right] + \mu R_{ax} & (g) \\ 2.3\sqrt{2M_y f_{h,1}d} + \mu F_{ax,R} & (h) \end{cases} \tag{2.66}$$

The load carrying capacity associated with each failure mode of a fasteners in single shear of timber-to-steel connections with thin plate as the outer member can be predicted by the following formulas:

$$R_v = \min \begin{cases} 0.5 f_{h,2}t_2d & (j) \\ 1.15\sqrt{2M_y f_{h,2}d} + \mu R_{ax} & (k) \end{cases} \tag{2.67}$$

The load carrying capacity associated with each failure mode of a fasteners in single shear of timber-to-steel connections with thick plate as the outer member can be predicted by the following formulas:

$$R_v = \min \begin{cases} 0.5 f_{h,2}t_2d & (l) \\ 2.3\sqrt{M_y f_{h,2}d} + \mu R_{ax} & (m) \end{cases} \tag{2.68}$$

where t_1 is the smaller of the thickness of the timber side member or the penetration depth and t_2 is the thickness of the timber middle member;
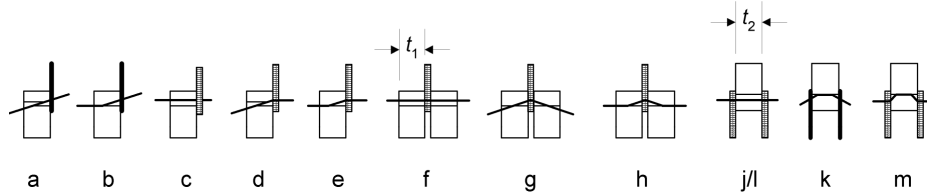
Figure 2.16: Timber-to-steel connections failure modes.

In Bejtka et al. [43] an extension of Johansen's yield theory to the case of inclined screws was proposed. The proposed equation are based on the equilibrium in undeformed configuration assuming that withdrawal failure only occurs in one timber member and neglecting the elongation of the screw. On the basis of experimental test results the authors affirm that the withdrawal capacity per unit length increases from the interface between the members towards the plastic hinge. To account for the interaction between embedment and withdrawal, an averaged reduced withdrawal parameter is introduced ($f_{w,mod} = 0.7 f_w$). Still in this model the pronounced hardening behavior of timber in embedment perpendicular to the grain is neglected. Moreover no interaction is considered between the tension and bending in the fastener in determining the yield moment M_y. The Eqs. 2.62 modified by Bejtka are the following:

$$R_v = \min \begin{cases} f_{h,1}ds_1\cos\theta + R_{ax,1a1}\sin\theta & (a) \\ f_{h,2}ds_2\cos\theta + R_{ax,1a2}\sin\theta & (b) \\ (1 - \mu\tan\theta)\frac{f_{h,1}s_1d}{1+\beta}\left[\sqrt{\beta + 2\beta^2\left[1 + \frac{s_2}{s_1} + \left(\frac{s_2}{s_1}\right)^2\right] + \beta^3\left(\frac{s_2}{s_1}\right)^2} - \beta\left(1 + \frac{s_2}{s_1}\right)\right] + R_{ax,1b}(\mu\cos\theta + \sin\theta) & (c) \\ (1 - \mu\tan\theta)\frac{f_{h,1}s_1d}{2+\beta}\left[\sqrt{2\beta(1+\beta) + \frac{4\beta(2+\beta)M_y\cos^2\theta}{f_{h,1}s_1^2d}} - \beta\right] + R_{ax,2a}(\mu\cos\theta + \sin\theta) & (d) \\ (1 - \mu\tan\theta)\frac{f_{h,1}s_2d}{1+2\beta}\left[\sqrt{2\beta^2(1+\beta) + \frac{4\beta(1+2\beta)M_y\cos^2\theta}{f_{h,1}s_2^2d}} - \beta\right] + R_{ax,2b}(\mu\cos\theta + \sin\theta) & (e) \end{cases} \tag{2.69}$$

where s_i is the length of the projection of the axis of the fastener over the normal to the sliding plane and θ is the angle between the axis of the fastener and the normal to the sliding plane and $R_{ax,i}$ is the modified axial capacity for each failure mode.

An extension of Johansenn theory to the case of timber-to-concrete connections with inclined screws has been performed by Marchi et al. in [57].

Jockwer et al. [65] described the mechanical behavior of connections with inclined screws loaded in direction perpendicular to the plane between members by modifying the EYM. They assume that at the very surface the resisting timber layer in the transversal direction of the screw has zero thickness and consequently no embedment stresses can be balanced by this layer. The full embedment strength f_h is considered fully available at a distance x_1 from the surface (Eq. 2.61). In axial direction of the screw, the effective length l_{ef} is reduced by x_1, assuming no load transfer in that zone.

The resulting load-carrying capacity of the connection with an inclined screw loaded perpendicular to the sliding plane can be determined as:

$$R_n = R_{ax} \sin(90° - \theta) + R_{tr,pulling} \cos(90° - \theta) \tag{2.70}$$

where R_{ax} and $R_{v,pulling}$ are the reduced screw axial and transversal capacities respectively.

$$R_{v,pulling} = -f_h x_1 d_{ef} + \sqrt{(2M_y + f_h x_1^2 d_{ef}) f_h d_{ef}} \tag{2.71}$$

Eurocode 5 [29] prescribes the use of a quadratic combination formula of the screw transversal and axial strengths for the definition of the load-bearing capacity of screws simultaneously subjected to shear and axial forces, as in the case of inclined screws.

$$\left(\frac{F_{tr}}{R_{tr}}\right)^2 + \left(\frac{F_{ax}}{R_{ax}}\right)^2 \leq 1 \tag{2.72}$$

where F_{tr} is the design transversal force, R_{tr} is the design transversal strength, F_{ax} is the design axial force, R_{ax} is the design axial strength. Eq. 2.72 can be rewritten solving the associated equality at failure:

$$R_v = \frac{1}{\sqrt{\left(\frac{\cos\theta}{R_{tr}}\right)^2 + \left(\frac{\sin\theta}{R_{ax}}\right)^2}} \tag{2.73}$$

According to Tomasi et al. [85] this calculation method underestimates the strength of inclined screws connections.

Blass and Laskewitz in [39] derived the load-carrying capacity of timber-to-timber and timber-to-steel connections with an interlayer according to Johansenn theory [49]. The fastener is assumed perpendicular to the sliding plane and both the case of interlayer rigidly connected and unconnected to main timber members have been considered.

A wide literature on analytical models for transversely loaded dowel-type fasteners exist whilst less more research have been done on analytical modelling of axially loaded screws. Jensen et al. in [48] applied a mean stress failure criterion to the Volkersen model deriving expression for both pull-pull as well as pull-push loading conditions. According to this model withdrawal failure occurs on a cylindrical surface of diameter equal to the thread outer diameter d. It is assumed that all shear deformations occurs on an infinitely thin shear layer with finite stiffness. It was also concluded that for the lag-screw-bolts used in the experiments, the difference between mean stress failure criterion and a maximum stress failure criterion is insignificant. When the maximum stress failure criterion is used the ultimate load can be expressed as follows for pull-pull and pull-push respectively:

$$R_n = \pi d l (f_v - \tau_{m,i}) \left(1 + \frac{2t}{d_c}\right)(1 + \alpha)\frac{\sinh\omega}{\omega} \min \begin{cases} \frac{1}{1+\alpha\cosh\omega} \\ \frac{1}{\alpha+\cosh\omega} \end{cases} \tag{2.74}$$

$$R_n = \pi d l (f_v - \tau_{m,i}) \left(1 + \frac{2t}{d_c}\right)(1 + \alpha)\frac{\sinh\omega}{\omega} \min \begin{cases} \frac{1}{1+\alpha\cosh\omega} \\ \frac{1}{\alpha+\cosh\omega} \end{cases} \tag{2.75}$$

where ω depends on the ratio between the axial stiffness of the timber cylinder and the axial stiffness of screw, on the core diameter d_c, on the thread depth t, on the shear stiffness of the shear layer, on the screw length and on the steel moduli elasticity. The stiffness of the shear layer is related to the timber shear strength f_v and fracture energy G_f.

Numerical

In recent years, several advanced three-dimensional numerical models have been proposed to study the behavior of connections made of threaded fasteners embedded in timber. The complex screw-timber interaction, due to the presence of thread, has been modeled using various techniques ranging from the reproduction of the actual thread geometry [82] to the use of cohesive contact with damage evolution in conjunction with a fictitious material that wraps the screw and models a complex medium where steel and timber interact [6, 7]. In order to avoid the detailed three-dimensional modelling of the screw using solid elements, some authors developed an approach based on beam to-solid coupling [61].

Another approach to the problem is represented by Beam-On-Foundation (BOF) modelling. According to this method fasteners are numerically modeled as elasto-plastic beams on a nonlinear foundation. BOF modelling has been used to reproduce the hysteretic behavior and failure mechanisms of timber joints with dowel-type fasteners perpendicular to the sliding plane [53, 54, 55, 45, 38].

BOF models have proven to be accurate in describing the macroscopic behavior in terms of failure load and failure modes of fasteners perpendicular to the sliding plane. The idea of using BOF non-linear modelling of inclined screw connections have been proposed in [40], but the model has not been defined nor in analytical form nor in finite element form. Constitutive laws for components have not been defined. Not even the model has been validated or used to predict the force-slip behavior of a single case.

The possibility of using the beam on springs non-linear model as a design tool for dowel type fasteners has been proposed by some scholars. Although possible, the implementation of a black-box model in a commercial software makes the user completely unaware of the relationship between capacity and input parameters. Moreover, the computational cost resulting by the analysis of a structure with thousand of fasteners may be unbearable for the practitioners.

Three-dimensional finite element models allow for the investigation of the stress distribution in the components and on the sliding planes, thus enabling for more in-depth studies. In [72] a constitutive model for timber, based on continuum damage mechanics, was developed and implemented via a subroutine into a FE solver. The model is able to account both ductile and brittle failures. The model include element deletion techniques and is capable of predicting the mechanical behavior of embedment test specimens.

Empirical

No specific empirical models for inclined screws were found in literature. For the same reasons discussed in the previous Subsection, empirical formulas for the withdrawal parameter f_{ax} in Subsec. 2.4.2 can be intended also as empirical models for pure-axially stressed screws connections. Examples of empirical models for dowel-type fasteners subjected to transversal loads are presented by Hassanieh et al. in [38] and Schweigler et al. in [77].

In Schweigler et al. a multi-step approach for the parametrization of the connection non-linear slip behavior is presented. First, exponential or polynomial regression functions are used to fit the single experimentally determined load-slip curves, then, regression analysis was applied to introduce the coefficients dependency on the load-to-grain angle α. More importantly, it was shown that the regression coefficients assume a physical meaning when the load-slip curve is parameterized with exponential functions. They coincides with synthetic conventional parameters determined in experiments (e.g. K_s, K_u and R_v) [31]. In this way it can be possible to define the constitutive law of a connection to be used by practitioners or researchers in structural models by knowing only a small number of parameters for which predictive models often exist.

Hassanieh et al. in [38] proposed a model which describes the load-slip behavior of a steel-CLT joints with screws. Three asymptotic lines defined by seven-parameter are used to approximate the load-slip curve. The parameters have been found by non-linear regression based on the least squares method with trust-region algorithm and bi-square robustness.

Chapter 3

Timber-to-timber and timber-to-steel screw connections with interlayers: experimental investigation

Abstract: Interlayers having poor mechanical properties compared to connected members are often used in connections to ensure human comfort in the buildings or because it is required by the structural system. In cross-laminated timber buildings, soundproofing interlayer can be used in connections between walls or in angle brackets and hold-downs. In light frame buildings the interlayer consist in the OSB sheathing between interstorey steel plates and studs. Interlayer may affects the mechanical behavior of connections with inclined screws. Few studies focused on interlayer mechanical properties influence on the slip modulus and strength. No studies investigating the behavior of timber-to-steel screws connections with interlayers were found. In this chapter the influence of soundproofing and OSB interlayer is assessed in connections with screws perpendicular or inclined with respect to the sliding plane.

3.1   Introduction

As described in the state of the art section, only a few experimental tests have been performed on connections with inclined screws and interlayers. Current literature completely lacks experimental results about timber-to-timber connections with soundproofing interlayers and the only existing tests of timber-to-steel connections involve the entire connection assembly, e.g. hold-down, making difficult to isolate the screwed connection behavior. In the tests carried out by Kržan and Azinović [52] the behavior of a commercial steel angle brackets with two different screw configuration and interlayer stratigraphy on each side has been assessed. The particular configuration tested makes it difficult to evaluate the impact of the interlayer on the mechanical performance of each of the two steel-to-timber sub-connections.

The aim of the experimental campaign is twofold, to evaluate the mechanical behavior of the connection as each of the significant parameters varies and to validate the modeling approaches of Chapters 4, 5 and 6. The experimental configurations have been chosen with respect to these needs: perpendicular screws configurations have been tested to validate the model when the transversal behavior is prevalent; inclined screws configuration have been tested to assess the ability of the model to predict tensile-bending combined screw failure mode; reduced length configuration have been used to verify the withdrawal predicted failure load.

3.2   Configuration description

The experimental configurations have been carefully chosen to confirm the most relevant results derived from the existing literature, but above all from analytical models and numerical simulations.

For the timber-to-timber connections, the configurations have been chosen to evaluate the impact of the insertion of a soundproofing interlayer of two different types on the mechanical performance of connection with a partially threaded screw perpendicular to the sliding plane and of connection with a fully threaded screw inclined with respect to the sliding plane. Influence of test setup was assessed by comparing classical push-out configuration (Fig. 3.1) with inclined shear configuration (Fig. 3.2). The materials used and the geometries of the configurations are shown in Tab. 3.1 and in Fig. 3.1.

Name	Description	Screw	ϑ (°)	Interlayer	d(mm)	l (mm)
TT 0 8 200 R	Reference 0°	HBS 8x200	0	-	8	200
TT 0 8 200 S35	Soft interlayer 0°	HBS 8x200	0	XYL35100	8	200
TT 0 8 200 S90	Stiff interlayer 0°	HBS 8x200	0	XYL90100	8	200
TT 45 7 300 R	Reference 45°	VGZ 7x300	45	-	7	300
TT 45 7 300 S35	Soft interlayer 45°	VGZ 7x300	45	XYL35100	7	300
TT 45 7 300 S90	Stiff interlayer 45°	VGZ 7x300	45	XYL90100	7	300
TT 30 7 300 S35	Soft interlayer 30°	VGZ 7x300	30	XYL35100	7	300
TT 0 8 200 IS	Inclined shear 0°	HBS 8x200	0	-	8	200
TT 45 7 300 IS	Inclined shear 45°	VGZ 7x300	45	-	7	300

Table 3.1: Timber-to-timber configurations.
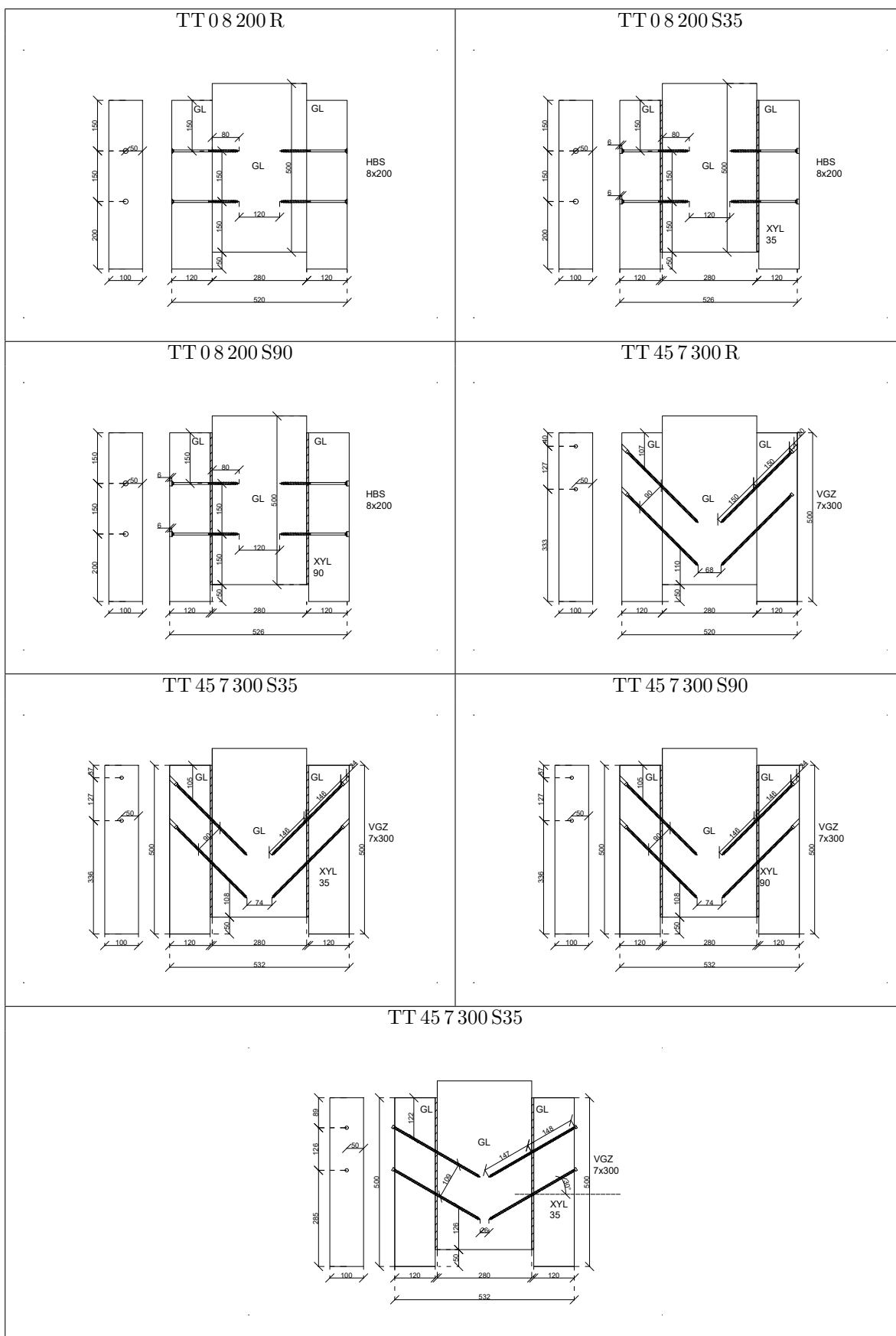
Figure 3.1: Design drawings of timber-to-timber configurations
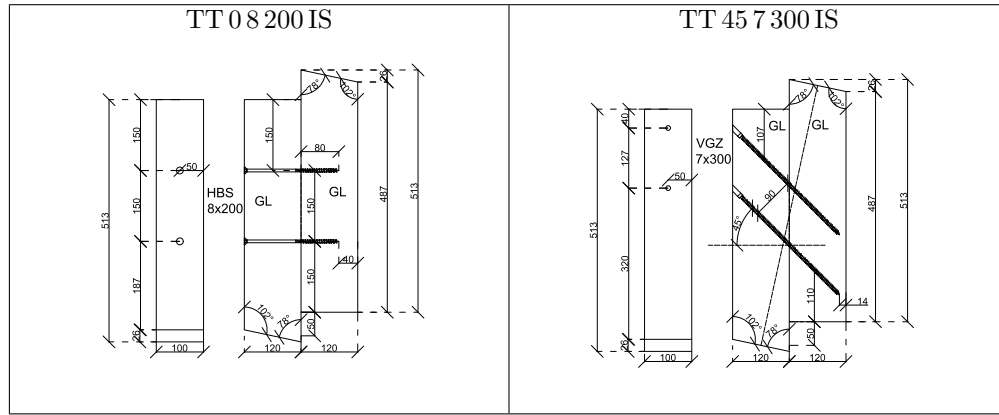
Figure 3.2: Design drawings of timber-to-timber configurations in inclined shear

In the case of timber-to-steel connections, e.g. angle-brackets, hold-down, plates, there is no significant force perpendicular to the sliding plane and consequently for the soundproofing layer to be effective, it must be sufficiently deformable Kržan and Azinović [52]. Because of this, the configurations have been chosen to evaluate the impact of the insertion of a soft soundproofing interlayer on the mechanical performance of connection with a partially threaded screw perpendicular to the sliding plane and of connection with a fully threaded screw inclined with respect to the sliding plane.

As can be seen from Fig. 3.3 (TS 0 9 140 S35), By using a single soundproofing layer, the contact surface between steel and timber is insulated on the sliding surface, but vibrations can still propagate from one member to another through the screw head and washer. To prevent this from happening, some manufacturers like Pitzl and Getzner have proposed to use a second steel plate and a second soundproofing layer so that the screw head is also decoupled from the main steel member. To reproduce this decoupling scheme, a configuration with the same stratigraphy was proposed and is showed in Fig. 3.3 (TS 45 9 240 DS35).

Also a configuration with an OSB (Oriented strand board)-type interlayer, representative of the panel attached to the frame of LTF (Light-timber-frame) buildings that is interposed between the metal plate of the connection and the elements of the frame was considered.

In order to have a configuration in which the failure would have occurred by withdrawal of the screw, a configuration with a very short screw length was added.

The materials used and the geometries of the configurations are shown in Tab. 3.2 and in Fig. 3.3.

Name	Description	Screw	ϑ (°)	Interlayer	d (mm)	l (mm)
TS 0 9 140 R	Reference 0°	VGS 9x140	0	-	9	140
TS 0 9 140 S35	Soft interlayer 0°	VGS 9x140	0	XYL35100	9	140
TS 45 9 240 R	Reference 45°	VGS 9x240	45	-	9	240
TS 45 9 240 S35	Soft interlayer 45°	VGS 9x240	45	XYL35100	9	240
TS 45 9 240 O	OSB Interlayer 45°	VGS 9x240	45	OSB	9	240
TS 45 9 140 RL	Reduced length 45°	VGS 9x140	45	-	9	140
TS 45 9 240 DS35	Double soft interlayer 45°	VGS 9x240	45	Double XYL35100	9	240

Table 3.2: Timber-to-steel configurations.
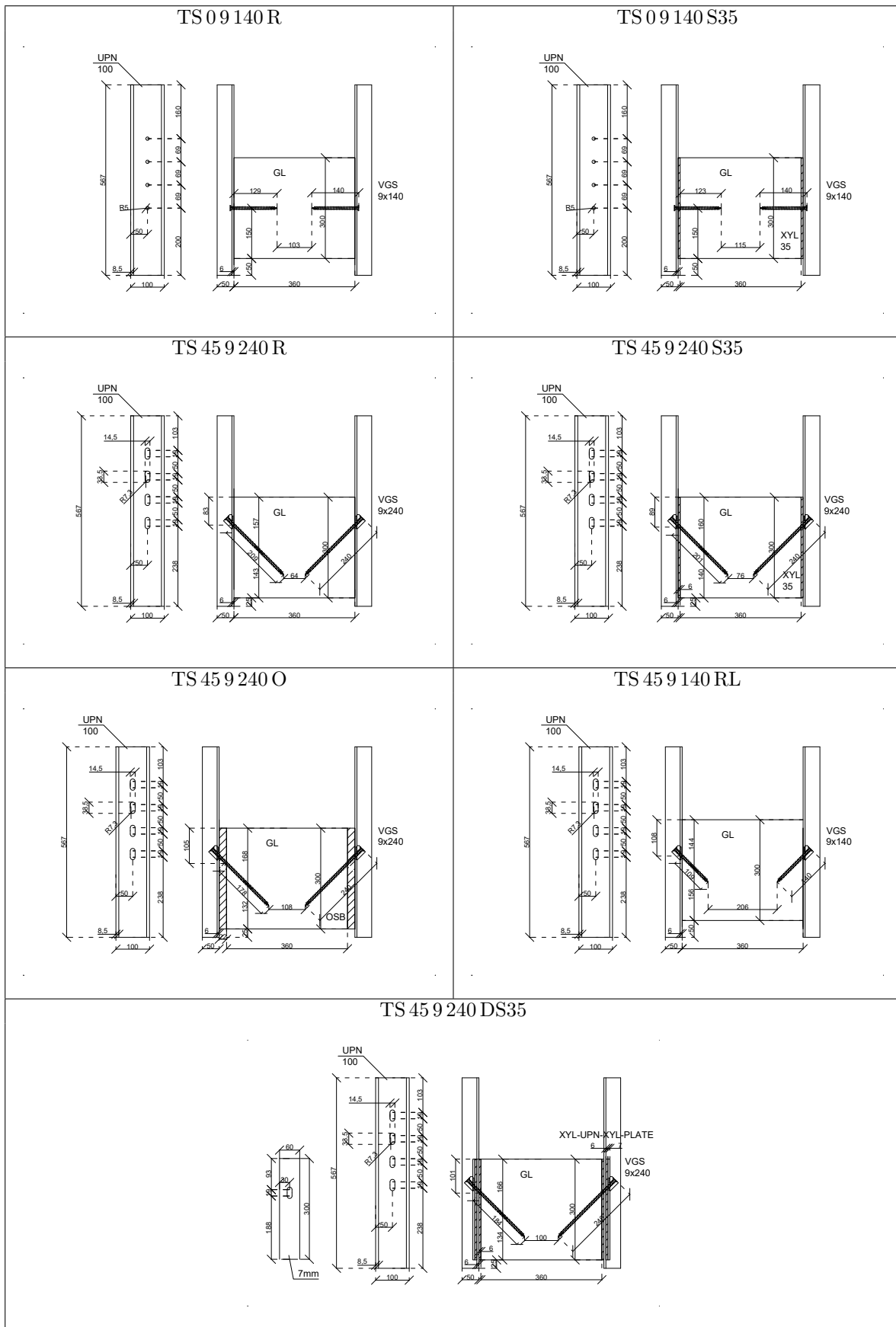
Figure 3.3: Design drawings of timber-to-steel configurations

3.2.1 Materials

The timber elements of the entire experimental campaign are made of glulam GL24h with 40 mm lamellas. Each specimen was weighed and the density of the timber is reported in Tab. 3.8 and Tab. 3.11.

The steel elements of the steel-to-timber configurations are made of UPN100 profiles with laser-cutted holes for washers. The web thickness is 6 mm.

The soundproofing interlayers are Rothoblaas XYLOFON with 35 and 90 shore, 6 mm thick and 100 mm wide (Tab. 3.3 and Fig. 3.4).

		Standard	**35 shore**	**90 shore**
Elastic modulus at 10% (compression)	(N/mm^2)	ISO 604	2,74	43,5
Dynamic stiffness s'	(MN/m^3)	ISO 9052	1262	>2200
Creep	(%)	EN 1606	< 0,5	< 0,5
Compression deformation DVR	(%)	ISO 1856	1,5	3,7
Dynamic elastic modulus E', 10 Hz (DMTA)	(N/mm^2)	ISO 4664	2,16	43
Dynamic shear modulus G', 10 Hz (DMTA)	(N/mm^2)	ISO 4664	1,13	16,7
Damping factor $\tan\delta$		ISO 4664	0,177	0,230
Max processing temperature (TGA)	(°C)	-	200	> 200
Reaction to fire		EN 13501-1	class E	class E
Thermal conductivity λ	(W/mK)	-	0,2	0,2

Table 3.3: Technical specification of soundproofing interlayers.
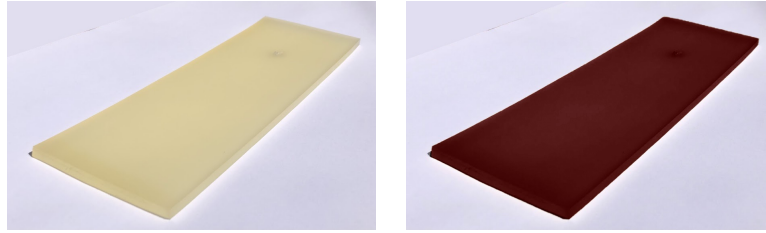
Figure 3.4: Soundproofing interlayers: 35 and 90 shore

The properties of the self-tapping screws are shown in Tab. 3.4 and Fig. 3.5.

			VGZ 7x300	**HBS 8x200**	**VGS 9x240**	**VGS 9x140**
Nominal diameter	d	(mm)	7	8	9	9
Head diameter	d_h	(mm)	9.5	14.5	16	16
Core diameter	d_c	(mm)	4.6	5.4	5.9	5.9
Shank diameter	d_s	(mm)		5.8		
Head thickness	t_1	(mm)		4.5	6.5	6.5
Pre-drilling hole diameter	d_p	(mm)	4	5	5	5
Length	l	(mm)	300	200	240	240
Characteristic yield moment	$M_{y,k}$	(Nm)	14.2	20.1	27.2	27.2
Characteristic withdrawal resistance	$f_{ax,k}$	(N/mm^2)	11.7	11.7	11.7	11.7
Associated density	ρ_a	(kg/m^3)	350	350	350	350
Characteristic withdrawal resistance	$f_{ax,k}$	(N/mm^2)	15	15		
Associated density	ρ_a	(kg/m^3)	500	500		
Characteristic head-pull-through	$f_{head,k}$	(N/mm^2)		10.5		
Associated density	ρ_a	(kg/m^3)		350		
Characteristic head-pull-through	$f_{head,k}$	(N/mm^2)		20		
Associated density	ρ_a	(kg/m^3)		500		
Characteristic tensile strength	$f_{tens,k}$	(kN)	15.4	20.1	25.4	25.4
Characteristic yield strength	$f_{y,k}$	(N/mm^2)	1000		1000	1000

Table 3.4: Technical specification of screws.
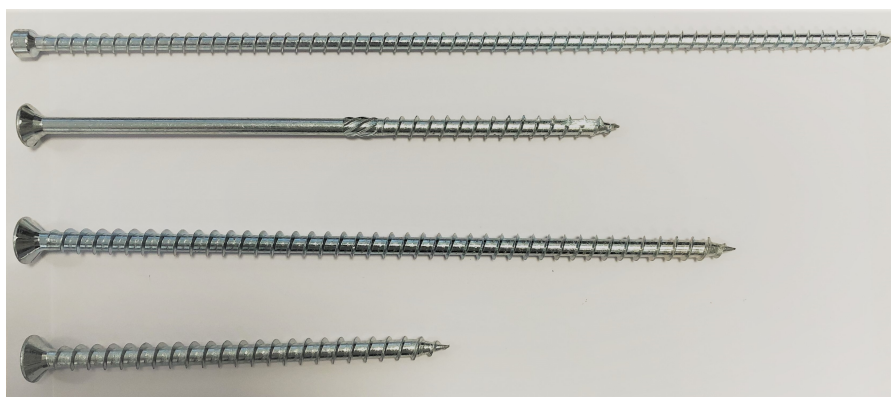
Figure 3.5: Screws, from the top down: VGZ 7x300, HBS 8x200, VGS 9x240 and VGS 9x140.

The properties of the washers are shown in Tab. 3.5 and Fig. 3.6.

VGS screw diameter	d	(mm)	9,0
VGS screw pre-drilling hole diameter	d_p	(mm)	5,0
Internal diameter	D_1	(mm)	9,7
External diameter	D_2	(mm)	19,0
Base length	L	(mm)	31,8
Base height	h	(mm)	3,0
Global height	H	(mm)	23,0
Slotted-hole length	L_F	(mm)	min. 33.0 max. 34.0
Slotted-hole width	B_F	(mm)	min. 14.0 max. 15.0
Steel plate thickness	S_{PLATE}	(mm)	min. 3.0 max. 12,0

Table 3.5: Technical specification of washer.

Figure 3.6: VGU washer.

3.3 Assembly and test procedure

To prevent the side elements to separate from the central element during the assembly process, a clamping has been used. Considering the chosen timber species and distances from the edges, in no case was it necessary to pre-drill the specimen. The screw was inserted until it was level with the lateral face of the specimen.

The typical test consisted in a standard push-out test. The specimen, consisting of 3 members and therefore 2 shear planes, is brought to failure by pushing the central member. The relative displacement between the central member and the side members has been measured through a LVDT (Linear Variable Differential Transformer). Due to the eccentricity between the load applied to the central member and the reaction that the test plane exerts on the lateral members, in the standard configuration for push-out tests the members tend to separate during the test. For this reason, a crossbar screwed to the side members and not able to induce pre-stress was used.
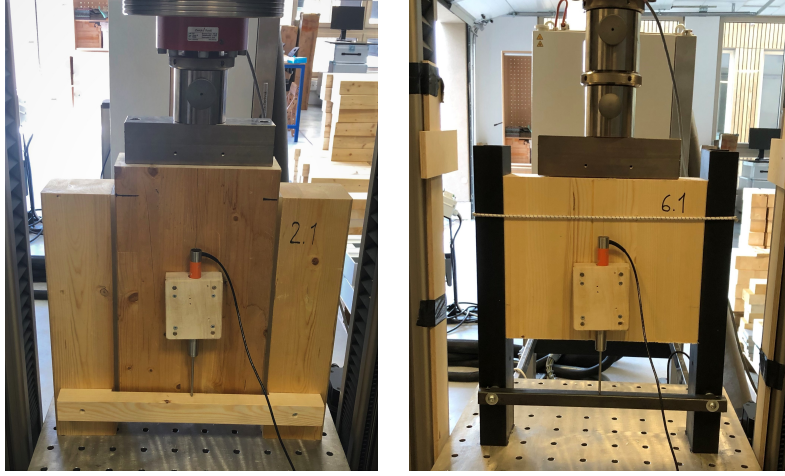
Figure 3.7: Timber-to-timber and steel-to-timber setups.

The general principles for the determination of strength and deformation characteristics of joints made with mechanical fasteners are described in the European standard EN-26891 [23]. The procedure requires the knowledge of an estimated maximum load F_{est} to be determined on the basis of experience, calculation or preliminary tests, and should be adjusted if, during the execution of the tests, the mean value of the maximum load of the tests already carried out deviates by more than 20% from the estimated value.

The chosen loading procedure is divided in the following phases:

1. force controlled loading from $0.0F_{est}$ to $0.4F_{est}$

2. force controlled holding at $0.4F_{est}$ for 30 s

3. force controlled unloading from $0.4F_{est}$ to $0.1F_{est}$

4. force controlled holding at $0.1F_{est}$ for 30 s

5. force controlled loading from $0.1F_{est}$ to $0.7F_{est}$

6. displacement controlled until failure or 45 mm

The speed in the displacement controlled phase has been set equal to 0.058 mm/s and the loading speed in all other phases has been calculated in order to achieve 15 mm of relative displacement in 11.5 min resulting in a loading speed comprised between 0.03 kN/s and 0.23 kN/s depending on the estimated maximum load.

Each of the timber-to-timber configurations was repeated on 3 different specimens, for a total of 12 screws tested in the same configuration. For the timber-to-steel configurations, the tests were repeated on 4 specimens, each equipped with 2 screws.

Due to the reduced number of specimens for each of the configurations, it was decided to repeat the test keeping the estimated maximum load constant, even in cases where the experimental maximum load differed by more than 20 from that initially assumed. In this way, the consistency of the tests was favored in compliance with the condition imposed by the standard.

3.4 Results

From the recorded measurements, the initial slip modulus, the slip modulus, the ultimate slip modulus and the maximum load have been determined.

In order to calculate the stiffness and ultimate displacement values net of displacement components related to local crushing at the member ends, in the post-processing of the experimental data the LVDT displacement measurements were used instead of the upper crossbar displacement of the press.

The initial slip modulus has been determined with the following definition:

$$k_i = \frac{\min(0.4F_{est}, 0.4F_{max})}{\nu_{04}} \tag{3.1}$$

Where F_{max} is the maximum force measured up to a relative slip of 15 mm and ν_{04} is the relative slip in the first loading phase corresponding to the considered load. The definition provided by EN-26891 [23] was revised as a consequence of the choice not to update the estimated value of the maximum load F_{est} in the event of a difference between estimated maximum load F_{est} and the experimental maximum load F_{max} greater than 20. Substituting $\min(0.4F_{est}, 0.4F_{max})$ to $0.4F_{est}$, in case of connections with $F_{max} < F_{est}$, the stiffness is still determined in the elastic range.

The slip modulus has been determined with the following definition:

$$k_s = \frac{\min(0.4F_{est}, 0.4F_{max}) - 0.1F_{max}}{\nu_{04} - \nu_{01}} \tag{3.2}$$

Where ν_{04} and ν_{01} are the relative slip in the loading phase corresponding to the considered loads. Substituting $0.1F_{max}$ to $0.1F_{est}$, in case of connections with $F_{max} > F_{est}$, the stiffness is still determined after the initial slip phase.

The ultimate slip modulus has been determined with the following definition:

$$k_u = \frac{2}{3}k_s \tag{3.3}$$

The definition of k_u is given in Eurocode 5. An alternative definition based on the effective force-displacement curve shape near failure has been proposed:

$$k_{up} = \frac{F_{max} - 0.6F_{max}}{\nu_u - \nu_{26}} \tag{3.4}$$

Where ν_u and ν_{26} are the relative slip in the reloading phase corresponding to F_{max} and $0.6F_{max}$.

3.4.1 Timber-to-timber

The failure modes, the initial slip modulus, the slip modulus, the ultimate slip modulus and the maximum load and its corresponding displacement have been determined and reported in the following Tab. 3.8.

All the configurations with inclined screws showed a failure due to withdrawal of the screw from the central member (Fig. 3.12e, f and g). It was not possible to extract the screws from the specimens with screws perpendicular to the sliding plane and consequently it was not possible to assess whether the failure occurred with one or two plastic hinges.

The insertion of the soft interlayer in the perpendicular screw connection led to an 8% reduction in strength. A significantly greater reduction was found in the case of the stiff interlayer. In this last case the reduction was 24%. Significantly greater deformation of the soft interlayer was observed compared to the deformation of the stiff interlayer Fig. 3.11d, b and c. Probably due to the greater friction timber-soft interlayer coefficient compared to the timber-stiff interlayer coefficient, in the first case the relative sliding between timber and soundproofing interlayer is lower than in the second case causing the deformation of the interlayer itself.

The insertion of the soft interlayer in the configuration with 45° screws led to a reduction of 28% and 33% in strength in the cases of soft interlayer and stiff interlayer respectively.

The reduction in terms of slip modulus is particularly high for connections with perpendicular screw, 43% and 50% for soft and stiff interlayer respectively. Also in the case of inclined screws, the reduction is significant: 34% and 29% for soft and stiff interlayer respectively.

The configuration with screws inclined at 30° and soft soundproofing layer has a slip modulus 30% lower than that of the connection with a screw at 45° and the same strength.

Inclined shear configurations showed similar results compared to classical push-out configurations in terms of strength (Fig. 3.13). An increase of the strength equal to 13% and 2% for perpendicular and inclined screws configuration has been found. A decrease of 9% in terms of stiffness was observed for inclined screws configuration. Due to the high dispersion of stiffness values of perpendicular screws in inclined screws, no reliable comparison can be done.

In conclusion, the insertion of an interlayer always leads to a reduction of the mechanical properties of the connection. The reduction is more pronounced for stiffness than for strength. The mechanical properties of the interlayer influence mostly the strength reduction.
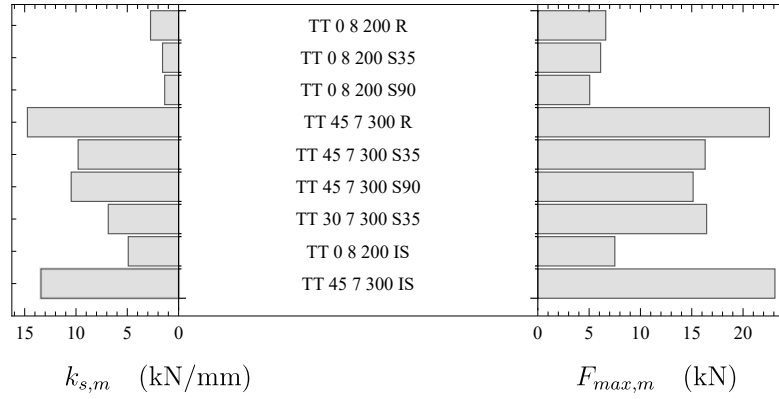
Figure 3.8: Timber-to-timber slip modulus and failure load referred to a single screw.

Name	$k_{i,m}$ (kN/mm)	CoV (%)	$k_{s,m}$ (kN/mm)	CoV (%)	$F_{max,m}$ (kN/mm)	CoV (%)	$v_m(F_{max})$ (mm)	CoV (%)
TT 0 8 200 R	5,75	47%	2,74	23%	6,62	9%	14,9	0%
TT 0 8 200 S35	2,08	5%	1,57	7%	6,12	3%	15,0	0%
TT 0 8 200 S90	2,10	6%	1,36	8%	5,06	2%	15,0	0%
TT 45 7 300 R	15,05	8%	14,73	6%	22,57	20%	1,9	26%
TT 45 7 300 S35	11,11	6%	9,79	7%	16,31	4%	2,1	13%
TT 45 7 300 S90	13,45	58%	10,47	24%	15,14	9%	2,3	17%
TT 30 7 300 S35	7,31	26%	6,86	24%	16,45	6%	5,1	6%
TT 0 8 200 IS	7,37	81%	4,91	80%	7,51	11%	15,0	0%
TT 45 7 300 IS	13,24	17%	13,42	19%	23,11	14%	3,3	7%

Table 3.6: Results of of timber-to-steel configurations referred to a single screw.

Tab. 3.7 compares the results of the conventional definition of k_u given by the Eq. 3.3 with the proposed definition given by the Eq. 3.4. It can be observed that the reduction of stiffness between in service and ultimate condition is more evident for screws perpendicular to the sliding plane, that are characterized by ductile failures. Therefore, the fixed ratio of 0,67 between the slip modulus and the ultimate slip modulus defined by the Eurocode 5, is unsuitable for representing the actual stiffness at failure of connections with screws perpendicular to the sliding plane.

Name	$k_{u,m}$ (kN/mm)	$k_{u,m}/k_{s,m}$	$k_{up,m}$ (kN/mm)	$k_{up,m}/k_{s,m}$
TT 0 8 200 R	1,82	0,67	0,19	0,07
TT 0 8 200 S35	1,04	0,67	0,18	0,12
TT 0 8 200 S90	0,91	0,67	0,12	0,09
TT 45 7 300 R	9,82	0,67	7,15	0,48
TT 45 7 300 S35	6,53	0,67	5,80	0,59
TT 45 7 300 S90	6,98	0,67	4,53	0,43
TT 30 7 300 S35	4,57	0,67	1,92	0,28
TT 0 8 200 IS	3,27	0,67	0,19	0,04
TT 45 7 300 IS	8,94	0,67	4,51	0,34

Table 3.7: Comparison between ultimate slip modulus and proposed definition of ultimate slip modulus.

Name	ρ (kg/m³)	Failure mode	k_i (kN/mm)	k_s (kN/mm)	$k_{s,m}$ (kN/mm)	k_u (kN/mm)	F_{max} (kN)	$F_{max,m}$ (kN)	$v(F_{max})$ (mm)
	425	-	10.6	7.4		4.9	23.1		15.0
TT 0 8 200 R	411	-	21.4	12.9	10.9	8.6	28.2	26.5	14.9
	419	-	36.9	12.5		8.3	28.2		15.0
	463	-	8.3	6.6		4.4	24.3		15.0
TT 0 8 200 S35	446	-	7.8	5.7	6.3	3.8	25.4	24.5	15.0
	454	-	8.9	6.6		4.4	23.7		15.0
	444	-	7.8	5.1		3.4	20.7		15.0
TT 0 8 200 S90	433	-	8.5	5.2	5.4	3.5	20.0	20.2	15.0
	449	-	8.9	6.1		4.0	20.0		15.0
	431	W	64.9	63.4		42.2	53.0*		1.3
TT 45 7 300 R	418	W	53.8	54.3	58.9	36.2	85.4	90.3	2.5
	414	W	61.8	59.1		39.4	95.2		2.0
	458	W	44.4	35.2		23.5	68.6		2.5
TT 45 7 300 S35	445	W	41.4	42.1	39.2	28.1	62.4	65.2	1.9
	449	W	47.6	40.1		26.8	64.8		1.9
	433	W	97.8	55.9		37.3	63.9		1.9
TT 45 7 300 S90	441	W	31.4	34.8	41.9	23.2	64.8	60.5	2.2
	440	W	32.2	34.9		23.3	52.9		2.8
	443	W	18.5	18.2		12.1	60.8		4.7
TT 30 7 300 S35	450	W	33.2	30.1	27.4	20.1	69.8	65.8	5.2
	442	W	35.9	33.9		22.6	66.8		5.4
	-	-	2.4	1.8		1.2	12.3		15.0
TT 0 8 200 IS	-	-	34.4	22.9	9.8	15.3	16.5	15.0	15.0
	-	-	10.4	7.2		4.8	15.0		15.0
	-	-	11.8	7.4		4.9	16.3		15.0
	-	W	31.5	29.5		19.7	56.9		3.2
TT 45 7 300 IS	-	W	26.5	25.8	26.8	17.2	42.7	46.2	3.1
	-	W	19.1	19.2		12.8	39.5		3.7
	-	W	28.8	32.8		21.9	45.8		3.2

W: screw withdrawal, S: screw tension failure, DH: screw double hinge, E: timber embedment

Table 3.8: Results of of timber-to-timber configurations.
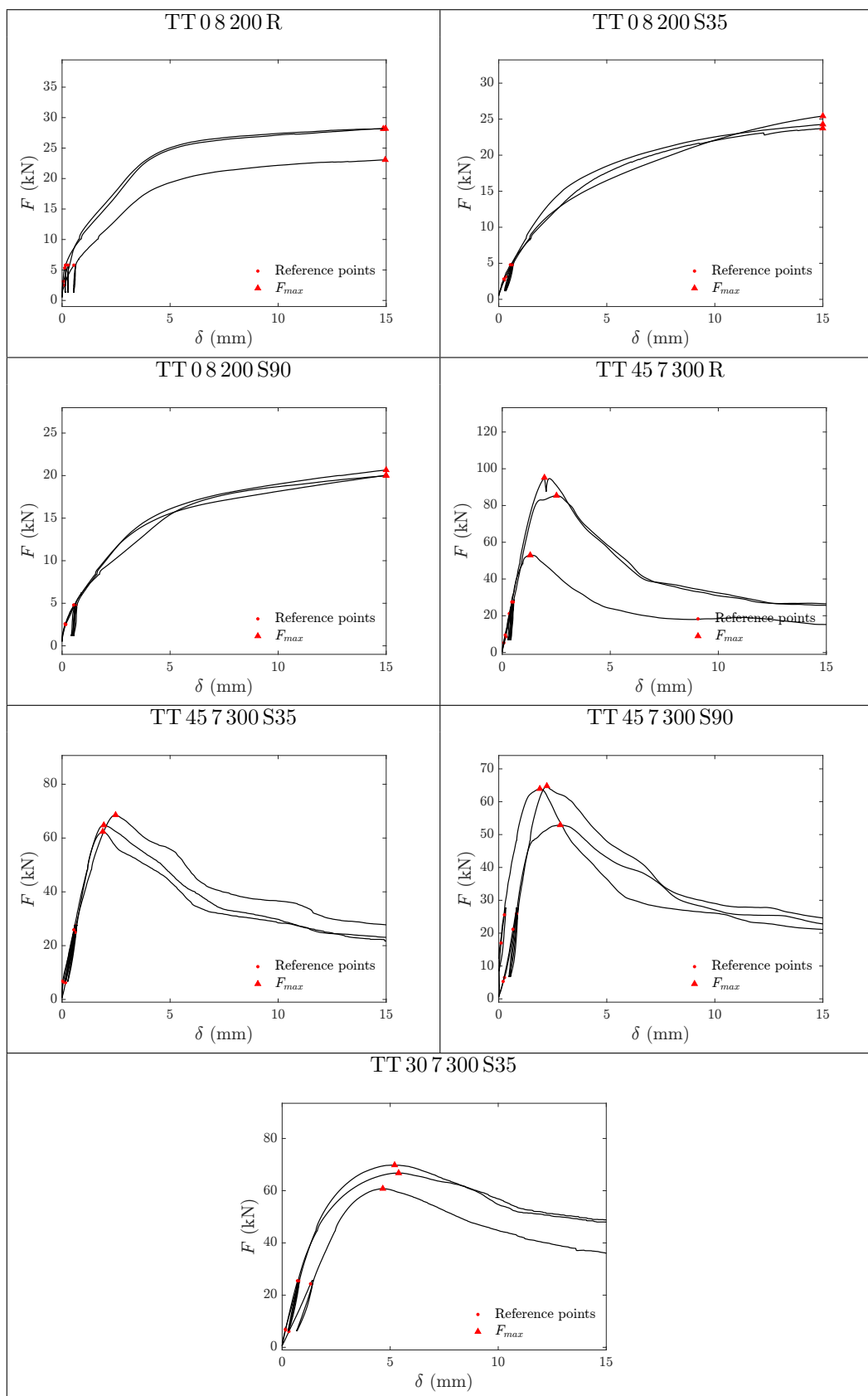
Figure 3.9: Force-displacement curves of timber-to-timber configurations
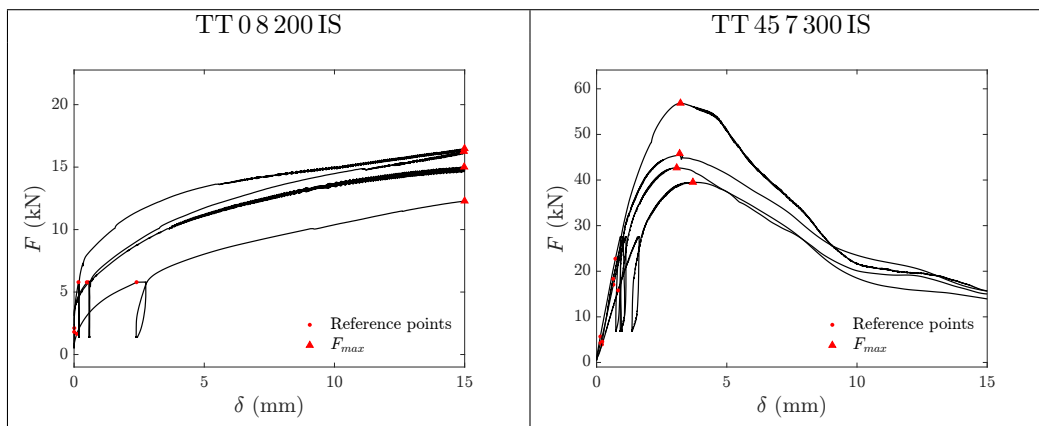
Figure 3.10: Force-displacement curves of timber-to-timber configurations in inclined shear

(a)

(b)

(c)

(d)

Figure 3.11: Timber-to-timber failure modes.

(e)

(f)

(g)

Figure 3.12: Timber-to-timber failure modes.

(a)   (b)
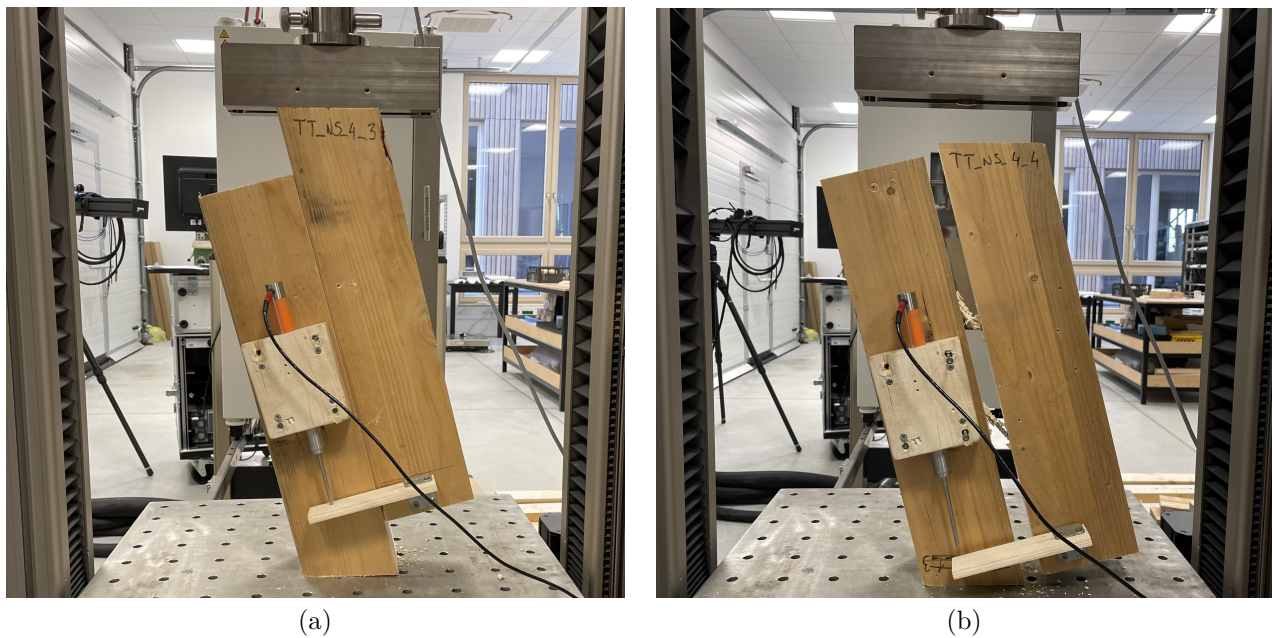
Figure 3.13: Inclined shear timber-to-timber: (a) setup and (b) failure mode.

3.4.2   Timber-to-steel

The failure modes, the initial slip modulus, the slip modulus, the ultimate slip modulus and the maximum load and its corresponding displacement have been determined and reported in the following Tab. 3.11.

All the configurations with perpendicular screws showed a failure due to timber embedment and double hinge of the screw (Fig. 3.16a and b). The reference configuration for screws inclined to 45°, the configuration with single soundproofing interlayer and the configuration with an OSB interlayer showed a failure due to the screw tensile failure or due to screw withdrawal with one hinge (Fig. 3.16c and Fig. 3.17g and l). The configuration with screws inclined to 45° and reduced length showed in all specimens a failure due to the screw withdrawal (Fig. 3.16d). The configuration with screws inclined to 45° and double soundproofing interlayer showed in all specimens a failure due to the screw tensile failure. Contrary to the other cases (Fig. 3.16e), damage to the UPN profile was found due to contact with the screw shank (Fig. 3.16f).

The insertion of the soft interlayer in the perpendicular screw connection led to a 5% increase in strength.

The insertion of the soft interlayer in the configuration with 45° screws led to a reduction of 10%, 17% and 23% in strength in the cases of soft interlayer, OSB interlayer and double soundproofing interlayer respectively.

In the case of perpendicular screw there is no variation in terms of slip modulus with the interlayer insertion (-1%). In the case of inclined screws, the reduction is significant: 23%, 45% and 84% in the cases of soft interlayer, OSB interlayer and double soundproofing interlayer respectively.

The configuration with screws inclined at 45° and reduced length has a slip modulus 38% higher than that of the reference connection and the 51% less strength.

It is worth noting that the coefficient of variation of the slip modulus of configurations with OSB interlayer, screw with reduced length and double interlayer is 42% or higher. Part of the scatter can be explained by having only two screws per specimen making the test samples extremely sensible to installation modes.

In conclusion, the insertion of an interlayer always leads to a reduction of the mechanical properties of the connection also for timber-to-steel configurations. The reduction is more pronounced for stiffness than for strength.
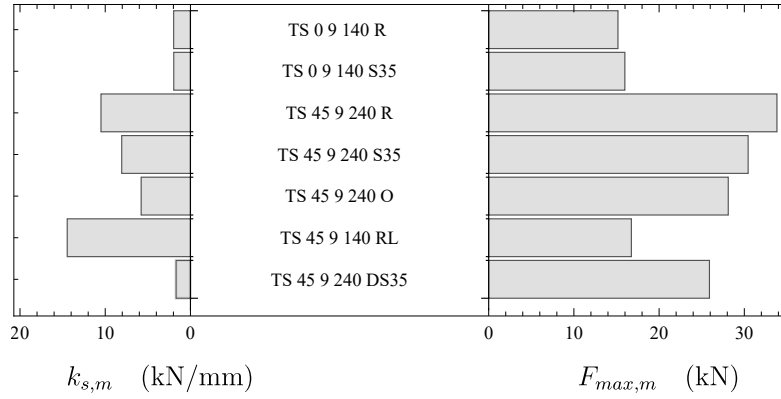
Figure 3.14: Timber-to-steel slip modulus and failure load referred to a single screw.

Name	$k_{i,m}$ (kN/mm)	CoV (%)	$k_{s,m}$ (kN/mm)	CoV (%)	$F_{max,m}$ (kN/mm)	CoV (%)	$v_m(F_{max})$ (mm)	CoV (%)
TS 0 9 140 R	2,40	19%	1,97	25%	15,17	14%	15,00	0%
TS 0 9 140 S35	3,20	12%	1,96	15%	15,98	3%	15,00	0%
TS 45 9 240 R	9,12	33%	10,50	24%	33,83	12%	6,08	30%
TS 45 9 240 S35	9,07	12%	8,07	10%	30,45	4%	5,50	19%
TS 45 9 240 O	4,55	51%	5,78	42%	28,12	12%	6,84	50%
TS 45 9 140 RL	20,61	32%	14,46	48%	16,74	10%	3,00	39%
TS 45 9 240 DS35	1,18	24%	1,69	44%	25,91	7%	15,00	0%

Table 3.9: Results of of timber-to-steel configurations referred to a single screw.

Tab. 3.10 compares the results of the conventional definition of k_u given by the Eq. 3.3 with the proposed definition given by the Eq. 3.4. It can be observed that the reduction of stiffness between in service and ultimate condition is more evident for screws perpendicular to the sliding plane, that are characterized by ductile failures. Therefore, the fixed ratio of 0,67 between the slip modulus and the ultimate slip modulus defined by the Eurocode 5, is unsuitable for representing the actual stiffness at failure of connections with screws perpendicular to the sliding plane. It is worth noting that the configuration TS 45 9 140 RL that exhibit considerable initial stiffness is characterized by the higher decay in ultimate conditions.

Name	$k_{u,m}$ (kN/mm)	$k_{u,m}/k_{s,m}$	$k_{up,m}$ (kN/mm)	$k_{up,m}/k_{s,m}$
TS 0 9 140 R	1,32	0,67	0,41	0,21
TS 0 9 140 S35	1,31	0,67	0,37	0,19
TS 45 9 240 R	7,00	0,67	3,34	0,32
TS 45 9 240 S35	5,38	0,67	4,35	0,54
TS 45 9 240 O	3,86	0,67	2,10	0,36
TS 45 9 140 RL	9,64	0,67	0,77	0,05
TS 45 9 240 DS35	1,12	0,67	0,70	0,42

Table 3.10: Comparison between ultimate slip modulus and proposed definition of ultimate slip modulus.

Name	ρ (kg/m³)	Failure mode	k_i (kN/mm)	k_s (kN/mm)	$k_{s,m}$ (kN/mm)	k_u (kN/mm)	F_{max} (kN)	$F_{max,m}$ (kN)	$v(F_{max})$ (mm)
	446	E, DH	5,5	4,4		17,3	35,9		14,9
	450	E, DH	3,9	2,9		83,3	32,3		15,0
TS 0 9 140 R		E, DH	5,9	2,9	3.9	2,0	27,5*	30.3	12,3
		E, DH	13,3*	5,6		3,7	29,0		15,0
		E, DH	3,9	3,9		2,6	24,2		15,0
	449	E, DH	6,7	4,3		2,9	32,8		15,0
TS 0 9 140 S35	436	E, DH	7,1	4,1	3.9	2,7	30,7	32.0	14,9
	444	E, DH	6,7	4,4		2,9	31,6		14,9
	452	E, DH	5,1	2,9		1,9	32,8		14,8
	456	S	12,2	25,4		17,0	75,9		5,1
	453	S	26,7	26,4		17,6	75,4		4,5
	447	W, H	23,1	25,5		17,0	76,2		4,4
TS 45 9 240 R	430	W, H	19,3	16,3	21.0	10,9	63,8	67.7	5,5
		S	7,7*	5,0*		3,4	54,6		7,3
		W, H	8,9	13,9		9,2	69,0		6,8
		S	6,9*	6,7*		4,5	57,8		10,1
		W, H	19,2	18,5		12,3	68,5		4,8
	466	S	18,4	17,5		11,7	61,1		4,1
TS 45 9 240 S35	444	S	21,4	16,1	16.1	10,7	58,1	60.9	6,6
	444	W, H	15,4	13,4		8,9	59,9		6,4
	457	S	17,3	17,6		11,7	64,5		5,0
	459	S	5,5	5,6		3,7	61,3		9,9
	463	S	11,7	17,4		11,6	62,9		4,5
TS 45 9 240 O	445	W, H	3,9	6,0	11.6	4,0	45,9	56.2	11,9
		W, H	15,3	14,0		9,3	51,1		4,2
		W, H	41,4*	14,8		9,9	60,0		3,6
	452	W	51,1	47,5		31,6	31,2		2,1
	447	W	29,4	27,4		18,2	34,9		2,1
TS 45 9 140 RL	448	W	60,7	28,6	28.9	19,1	29,8	33.5	2,4
	463	W	24,7	18,8		12,5	31,8		2,2
		W	40,2	44,3		29,5	32,8		4,1
		W	8,7	7,0		4,7	40,5		5,0
	457	S	3,3	4,7		3,1	51,6		15,0
TS 45 9 240 DS35	439	S	1,9	4,9	3.4	3,3	56,0	51.8	15,0
	463	S	2,0	2,6		1,7	53,3		15,0
	450	S	2,2	1,3		0,9	46,3		15,0

W: screw withdrawal, S: screw tension failure, H: screw single hinge, DH: screw double hinge, E: timber embedment

Table 3.11: Results of of timber-to-steel configurations.
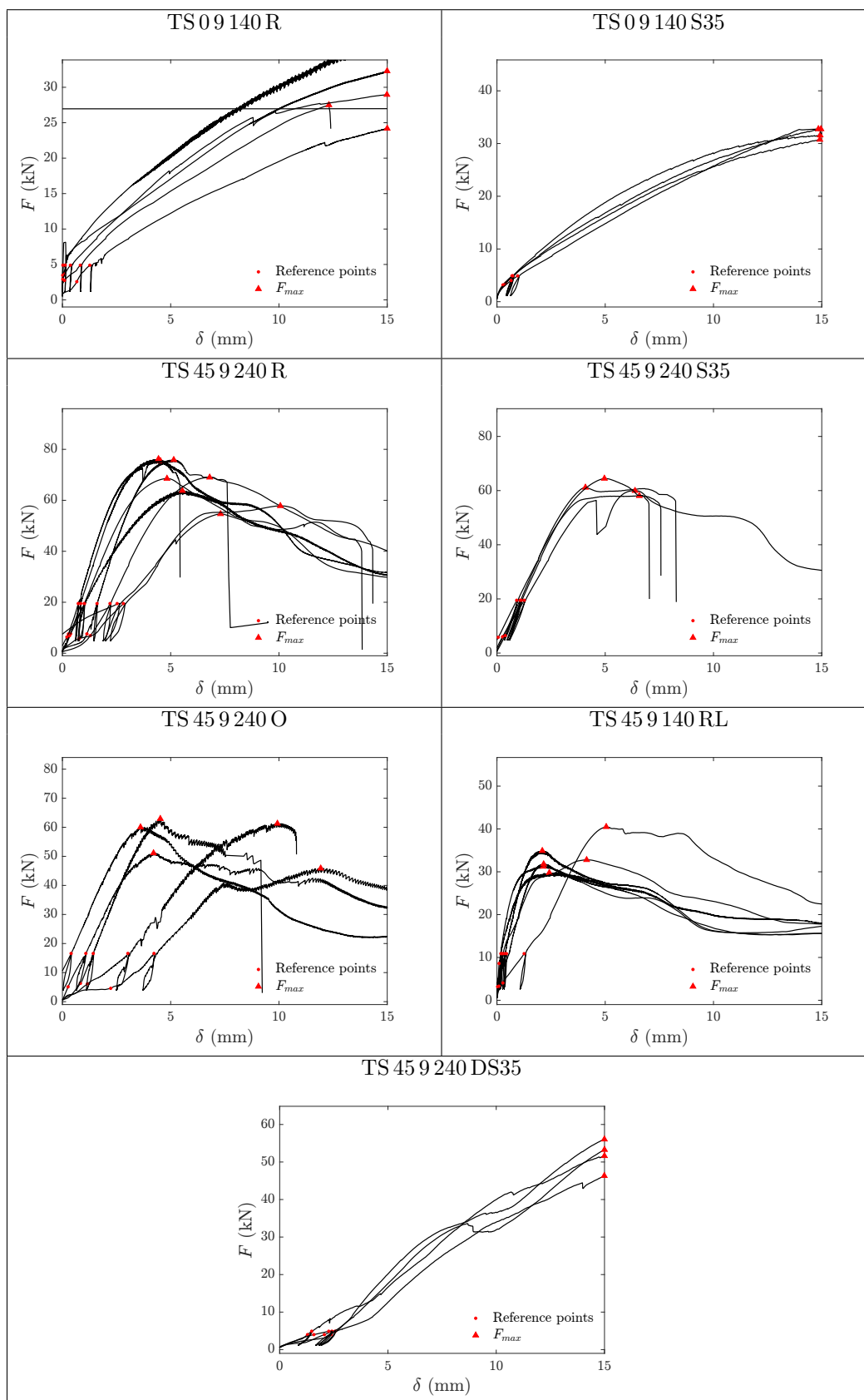
Figure 3.15: Force-displacement curves of timber-to-steel configurations

(a)
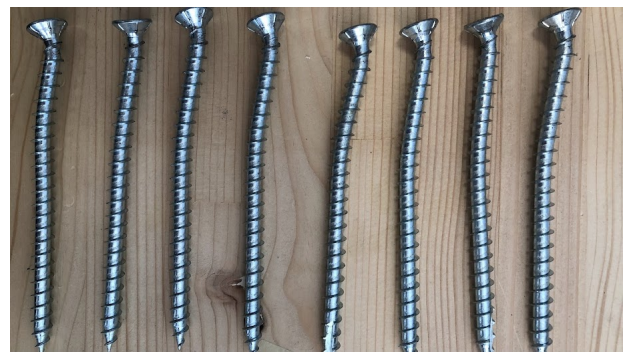
(b)

(c)

(d)

(e)

(f)

Figure 3.16: Timber-to-steel failure modes.

(g)

(h)

(i)

(l)

Figure 3.17: Timber-to-steel failure modes.

3.5 Conclusions

The main results of the experimental investigation consisting in push-out tests of screws connections with interlayers can be itemized as follows:

- the interlayer reduces more the slip modulus than the capacity;

- in timber-to-timber configurations, the slip modulus reduction caused by the interlayer is more pronounced for screws perpendicular to the sliding plane than for inclined screws;

- in timber-to-steel configurations, the slip modulus reduction caused by the interlayer is more pronounced for inclined screws than for screws perpendicular to the sliding plane;

- the capacity reduction caused by the interlayer is more pronounced for inclined screws than for screws perpendicular to the sliding plane;

- softer soundproofing interlayers may have higher friction coefficients;

- inclined shear test configuration lead to an increase in connections capacity.

Chapter 4

Slip modulus prediction of timber-to-timber and timber-to-steel screw connections: one-dimensional analytical models

Abstract: Slip modulus represents a conventional parameter describing the connection stiffness in serviceability range of load. The knowledge of connections stiffness is mandatory in determining structural deformations as inter-storey drift and vertical displacements. Moreover, the connection stiffness may influence the share of load between structural elements and the effectiveness of composite elements. Beam on elastic foundation modelling can be used to tackle with this linear problem. Different boundary conditions can be used to reproduce timber-to-timber and timber-to-steel connections behavior. Being the density universally regarded as the parameter having the major impact on mechanical behavior, foundation modulus can be related to density to make the model predictive. In the following chapter this approach is extensively validated. Different methods of solution are presented for the differential equations that describe the problem. One-variable-at-time and variance-based sensitivity analysis are performed. Elementary formulas, suitable for code implementation, are derived by the regression of the numerical solution.

4.1 Introduction

This chapter presents a one-dimensional analytical model of a beam on elastic foundation for the slip modulus prediction of timber-to-timber, timber-to-steel and timber-to-concrete connections with inclined screws. The cases of connections without interlayer, with non-structural interlayer and with structural interlayer are considered.

The aim is to define a unitary approach to the problem of the prediction of the slip modulus. The same analytical model is used to solve the problem of prediction of the slip modulus in all configurations of greatest interest in engineering practice.

A model simple enough to be used for the derivation of simplified formulas and suitable to be implemented in the standards and codes and at the same time rigorous and accurate is proposed. The proposed model guarantees kinematic compatibility, equilibrium and uses constitutive law deriving from data of experimental campaigns from literature.

The problem is faced with a linear model of a beam on elastic foundation which in its simplest version was initially proposed by Winkler [87].

The model is defined in such a way as to make possible to use the results deriving from canonical embedment test parallel and perpendicular to the grain as input parameters.

The followed approach is similar to that proposed by Symons et al. [84] and Di Nino et al. [14] for the derivation of the slip modulus of timber-to-concrete connections without interlayer and with non-structural interlayer respectively.

The screw is represented by an inclined beam with respect to the normal to the sliding plane and the interaction between the timber and the screw is modeled by means of two orders of independent springs directed in the direction parallel and perpendicular to the timber grain.

According to this approach the three-dimensional problem is reduced to a one-dimensional problem. Reducing the size of the problem requires some assumptions including assuming an independent behavior of each layer of the springs distributed along the screw. The springs that belongs to different planes parallel to the sliding plane are independent, thus implicitly neglecting the shear deformability in the plane containing the screw and the normal to the sliding plane. In the planes parallel to the sliding plane, shear deformability is implicitly considered in the foundation modulus that is experimentally assessed. Another assumption regards the absence of relative slip between screw and timber in the axial direction of the screw and therefore the nature of the screw-timber interaction depends on the underlying timber deformability only and not on the timber-screw relative slip. In the transverse direction of the screw, it is implicitly assumed that the screw can only be in contact with the timber on one of its two sides, considering linear symmetrical elastic springs. The deformability of timber members themselves is neglected. This assumption is coherent with the experimental definition of the slip modulus that requires the relative slip to be measured on the center line of the specimens, thus being net of the deformability of members.

This schematization, unlike those proposed by other authors, e.g. Girhammar et al. [36], allows the direct use of the mechanical properties that characterize the orthotropic behavior of timber in its natural reference system, which are well known from experimental tests. Moreover, this model accounts for the coupled axial-transversal behavior of the fastener.

In the following paragraphs the field equations of the described problem are derived, and the boundary conditions relative to all cases of practical interest are provided.

The analytical model is governed by two coupled differential equations for which approximate analytical solutions, exact numerical solutions and interpolating functions valid in the domains of the parameters chosen with reference to the application needs are reported.

In the following the discussion will be mixed. Reference will be made to the published research papers for most of the results, but the salient aspects of the model will be introduced in the dedicated paragraphs together with in-depth analysis and further results.

4.2   Derivation of the field equations

In accordance with the current standards EN 26891 [23], the so called slip modulus or stiffness of the connection is evaluated between 10 % and 40 % of the connection strength. A relative slip, known as initial slip of the assembly, is excluded from the evaluation of the so-called k_{ser} [23]. Consequently, in the serviceability range of load, a linear elastic behavior of the connection and therefore of the materials of which it is made can be assumed with a good degree of approximation. The problem can be treated as linear from the mechanical point of view.

It is experimentally observed that the relative displacement between the members of a connection in service condition is between 0.2 mm and 5 mm for the connections with screws inclined and perpendicular to the sliding plane respectively. Consequently, it is also legitimate to treat the problem as linear from the geometric point of view.

The field equations are derived below by referring to a beam segment of infinitesimal length dx inclined of an angle θ with respect to the normal to the sliding plane.

(a)   (b)
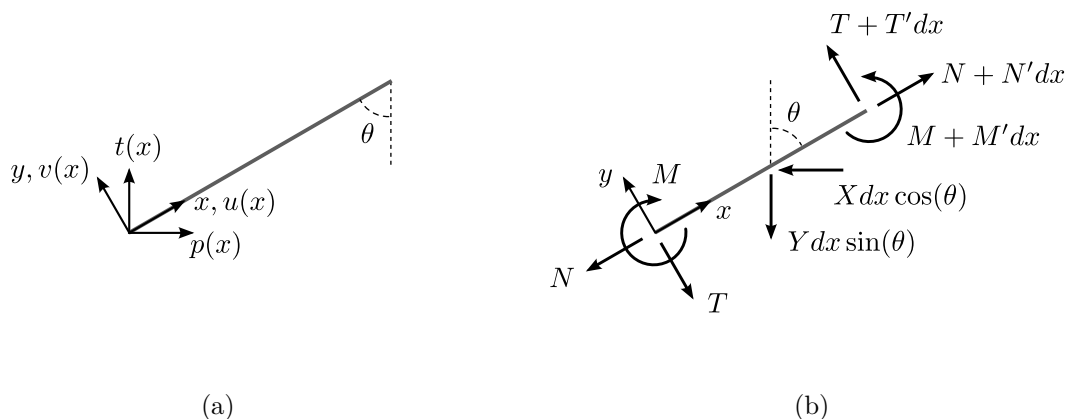
Figure 4.1: Scheme of beam on elastic foundation model: (a) Kinematic; (b) Equilibrium.

Naming $u(x)$ and $v(x)$ the axial and the transversal displacements respectively, and $p(x)$ and $t(x)$ the displacements parallel and perpendicular to the sliding plane (Fig.4.1a), under the hypothesis of small displacements and small deformations the linear kinematic equations are the following:

$$\begin{aligned}
\epsilon &= u' \\
\gamma &= v' - \phi \\
\kappa &= \phi' \\
p &= u\sin(\theta) - v\cos(\theta) \\
t &= u\cos(\theta) + v\sin(\theta)
\end{aligned} \tag{4.1}$$

where ϵ is the beam axial elongation, γ is the shear deformation and κ is the bending curvature.

Naming E and G the Young's modulus and shear modulus respectively, K_p and K_t the stiffness of the distributed springs per unit of length in the direction parallel and perpendicular to the sliding plane and A, A_t and I, the area, the shear area and the moment of inertia of the section of the beam, the constitutive law equations are:

$$\begin{aligned}
N &= EA\epsilon \\
T &= GA_t\gamma \\
M &= EI\kappa \\
X &= K_p p \\
Y &= K_t t
\end{aligned} \tag{4.2}$$

where N, T and M are the axial force, shear force and bending moment respectively and X and Y are the distributed springs reaction forces.

The equilibrium of the forces and of the moments on the segment of infinitesimal dimensions can be written starting from the forces indicated in Fig.4.1b.

$$\begin{aligned}
\sum F_x = 0 \quad & -N + N + N'dx - Y\,dx\sin(\theta)\cos(\theta) - X\,dx\sin(\theta)\cos(\theta) = 0 \\
\sum F_y = 0 \quad & -T + T + T'dx - Y\,dx\sin^2(\theta) + X\,dx\cos^2(\theta) = 0 \\
\sum M = 0 \quad & -M + M + M'dx + T\frac{dx}{2} + T\frac{dx}{2} + T'dx\frac{dx}{2} = 0
\end{aligned} \tag{4.3}$$

Simplifying equilibrium and ignoring superior order:

$$\begin{aligned}
N' - Y\sin(\theta)\cos(\theta) - X\sin(\theta)\cos(\theta) &= 0 \\
T' - Y\sin^2(\theta) + X\cos^2(\theta) &= 0 \\
M' + T &= 0
\end{aligned} \tag{4.4}$$

Rewriting shear force in terms of bending moments the equilibrium equations can be rewritten:

$$\begin{aligned}
T &= -M' \\
N' - Y\sin(\theta)\cos(\theta) - X\sin(\theta)\cos(\theta) &= 0 \\
-M'' - Y\sin^2(\theta) + X\cos^2(\theta) &= 0
\end{aligned} \tag{4.5}$$

Introducing the hypothesis of shear rigid beam, the kinematic Eqs.4.1 reduce to Eqs.4.6.

$$\begin{aligned}
\epsilon &= u' \\
\phi &= v' \\
\kappa &= v'' \\
p &= u\sin(\theta) - v\cos(\theta) \\
t &= u\cos(\theta) + v\sin(\theta)
\end{aligned} \tag{4.6}$$

Substituting kinematic Eqs.4.6 in constitutive Eqs.4.2:

$$\begin{aligned}
N &= EAu' \\
M &= EIv'' \\
X &= K_p(u\sin(\theta) - v\cos(\theta)) \\
Y &= K_t(u\cos(\theta) + v\sin(\theta))
\end{aligned} \tag{4.7}$$

Substituting Eqs.4.7 in equilibrium and changing signs

$$T = -EIv'''$$
$$-EAu'' + K_t(u\cos^2(\theta)\sin(\theta) + v\sin^2(\theta)\cos(\theta)) + K_p(u\sin^2(\theta)\cos(\theta) - v\cos^2(\theta)\sin(\theta)) = 0 \tag{4.8}$$
$$EIv'''' + K_t(u\cos(\theta)\sin^2(\theta) - v\sin^3(\theta)) - K_p(u\sin(\theta)\cos^2(\theta) - v\cos^3(\theta)) = 0$$

With the following positions:

$$\begin{aligned}
K_{xx} &= K_t\cos^2(\theta)\sin(\theta) + K_p\sin^2(\theta)\cos(\theta) \\
K_{yy} &= K_t\sin^3(\theta) + K_p\cos^3(\theta) \\
K_{xy} &= K_t\sin^2(\theta)\cos(\theta) - K_p\cos^2(\theta)\sin(\theta) \\
K_{yx} &= K_{xy}
\end{aligned} \tag{4.9}$$

The coupled sixth-order system of differential equations of an inclined beam on elastic foundation can be rewritten in the following form:

$$\begin{aligned}
K_{xx}u + K_{xy}v - EAu'' &= 0 \\
K_{yx}u + K_{yy}v + EIv'''' &= 0
\end{aligned} \tag{4.10}$$

4.3 BCs equations

In all the cases analyzed below, the part of the screw inserted in the timber member of length l_1 can be modeled as a beam on elastic foundation, free on the tip side ($x = 0$).

The part of the screw of length l_2 inserted in any interlayer is represented by a second domain to allow the assignment of different properties to the distributed springs, and consequently the continuity of displacements and internal forces between the domain schematizing the part of the screw on the tip side member and the domain schematizing the part of the screw inserted in the interlayer must be granted.

The screw head side member is schematized in a different way according to the type of member.

The stiffness of the system is determined by assigning an imposed displacement at an external or internal constraint located on the sliding plane and determining the components parallel to the sliding plane of the internal forces associated with it. The stiffness or slip modules can be determined as the ratio between these components and the imposed displacement. Alternatively, it is possible to assign a force to the boundary of a domain and determine the corresponding displacement.

4.3.1 Timber to timber

The case of timber-to-timber connections with interlayer has been extensively dealt with in the research paper in Sec. 4.9. It is assumed that the relative sliding between the main members occurs on the contact surface between the interlayer and the head side member. Preliminary sensitivity studies have shown that the choice of the sliding plane has limited influence on the resulting stiffness. Assuming the sliding plane between the interlayer and the head-side member is the most realistic assumption since, albeit weakly, the interlayer is usually bound to the point side member.

It should be noted that according to the adopted schematization, imposing a relative displacement δ between the head-side member and the tip-side member with interlayer, in a direction parallel to the sliding plane, is equivalent to considering the same relative displacement between the two screw portions on the sliding plane (Fig. 4.2).
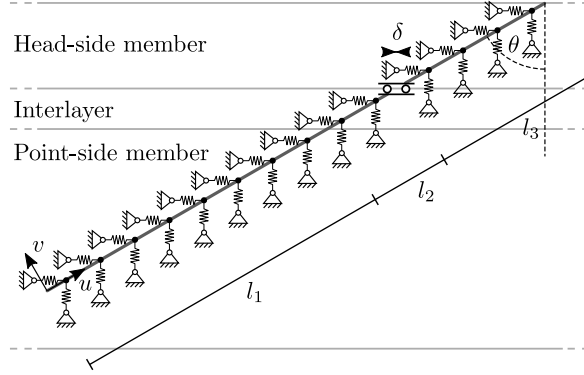
Figure 4.2: Timber-to-timber connection with interlayer model.

$$EAu_1'(0) = 0$$
$$EIv_1''(0) = 0$$
$$-EIv_1'''(0) = 0$$

$$EAu_1'(l_1) = EAu_2'(l_1)$$
$$EIv_1''(l_1) = EIv_2''(l_1)$$
$$-EIv_1'''(l_1) = -EIv_2'''(l_1)$$
$$u_1(l_1) = u_2(l_1)$$
$$v_1(l_1) = v_2(l_1)$$
$$v_1'(l_1) = v_2'(l_1)$$

$$\text{(4.11)}$$

$$EAu_2'(l_1 + l_2) = EAu_3'(l_1 + l_2)$$
$$EIv_2''(l_1 + l_2) = EIv_3''(l_1 + l_2)$$
$$-EIv_2'''(l_1 + l_2) = -EIv_3'''(l_1 + l_2)$$
$$u_2(l_1 + l_2) - \delta\sin(\theta) = u_3(l_1 + l_2)$$
$$v_2(l_1 + l_2) + \delta\cos(\theta) = v_3(l_1 + l_2)$$
$$v_2'(l_1 + l_2) = v_3'(l_1 + l_2)$$

$$EAu_3'(l_1 + l_2 + l_3) = 0$$
$$EIv_3''(l_1 + l_2 + l_3) = 0$$
$$-EIv_3'''(l_1 + l_2 + l_3) = 0$$

The case of timber-to-timber connections without interlayer is similar to the previous and has been extensively studied in the conference paper (Sec. 4.10), the corresponding boundary conditions are reported here for completeness:
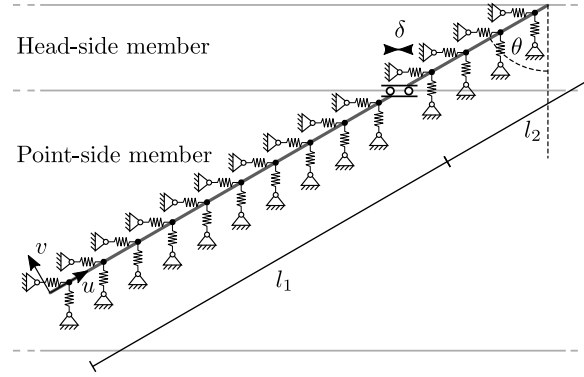
Figure 4.3: Timber-to-timber connection model.

$$EAu_1'(0) = 0$$
$$EIv_1''(0) = 0$$
$$-EIv_1'''(0) = 0$$

$$EAu_1'(l_1) = EAu_2'(l_1)$$
$$EIv_1''(l_1) = EIv_2''(l_1)$$
$$-EIv_1'''(l_1) = -EIv_2'''(l_1)$$
$$u_1(l_1) - \delta\sin(\theta) = u_2(l_1) \qquad\qquad (4.12)$$
$$v_1(l_1) + \delta\cos(\theta) = v_2(l_1)$$
$$v_1'(l_1) = v_2'(l_1)$$

$$EAu_2'(l_1 + l_2) = 0$$
$$EIv_2''(l_1 + l_2) = 0$$
$$-EIv_2'''(l_1 + l_2) = 0$$

4.3.2 Steel to timber

The case of timber-to-steel connections with interlayer has been extensively dealt in the journal paper (Sec. 4.9). It is assumed that the plate is sufficiently thin not to be able to prevent rotation of the end of the screw on the head-side, or that the gap between the screw shank and the hole in the plate is such as to allow the screw end free rotation for the displacements associated with the service conditions. It is also assumed that the steel plate is sufficiently wide to distribute the force perpendicular to the sliding plane over a large surface, i.e. the plate prevents the screw head from moving in the direction of the normal to the sliding plane (Fig. 4.4).
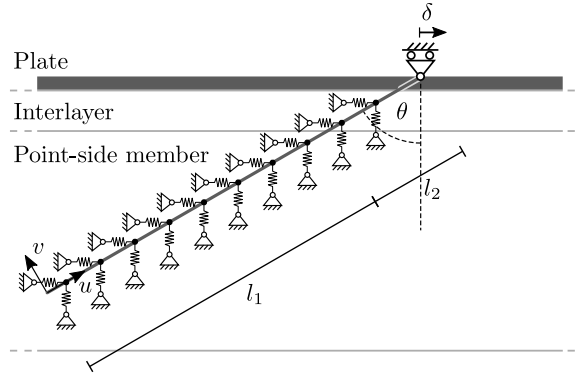
Figure 4.4: Timber-to-steel connection with interlayer model.

$$
\begin{aligned}
&EAu_1'(0) = 0 \\
&EIv_1''(0) = 0 \\
&-EIv_1'''(0) = 0 \\[8pt]
&EAu_1'(l_1) = EAu_2'(l_1) \\
&EIv_1''(l_1) = EIv_2''(l_1) \\
&-EIv_1'''(l_1) = -EIv_2'''(l_1) \\
&u_1(l_1) = u_2(l_1) \\
&v_1(l_1) = v_2(l_1) \\
&v_1'(l_1) = v_2'(l_1) \\[8pt]
&EIv_2''(l_1 + l_2) = 0 \\
&u_2(l_1 + l_2) = \delta \sin(\theta) \\
&v_2(l_1 + l_2) = -\delta \cos(\theta)
\end{aligned}
\tag{4.13}
$$

In the case of timber-to-steel connections with a deformable interlayer in the direction perpendicular to the sliding plane (e.g. soundproofing interlayers or small plates) the system may be schematized as beam with a spring of stiffness K_m at the head-side end. To find the lower bound of connection slip modulus K_m can be assumed null as done in Sec. 6.2. Assuming the spring reaction force as $R = K_m(u_2(l_1 + l_2)\cos(\theta) + v_2(l_1 + l_2)\sin(\theta))$, the boundary conditions can be written as follows:
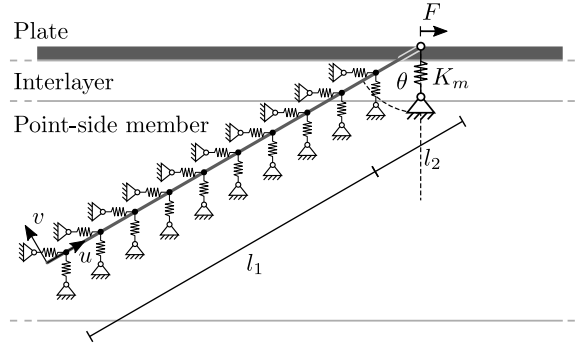
Figure 4.5: Timber-to-steel connection with deformable interlayer model.

$$EAu'_1(0) = 0$$
$$EIv''_1(0) = 0$$
$$- EIv'''_1(0) = 0$$

$$EAu'_1(l_1) = EAu'_2(l_1)$$
$$EIv''_1(l_1) = EIv''_2(l_1)$$
$$- EIv'''_1(l_1) = -EIv'''_2(l_1)$$
$$u_1(l_1) = u_2(l_1)$$
$$v_1(l_1) = v_2(l_1)$$
$$v'_1(l_1) = v'_2(l_1)$$

$$EIv''_2(l_1 + l_2) = 0$$
$$EAu'_2(l_1 + l_2) = F\sin(\theta) - R\cos(\theta)$$
$$- EIv'''_2(l_1 + l_2) = -F\cos(\theta) - R\sin(\theta)$$

(4.14)

In the case of timber-to-steel connections with thin steel plate and without interlayer the boundary condition can be written as follows:
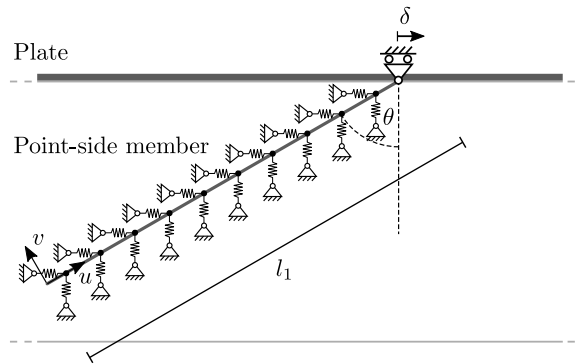
Figure 4.6: Timber-to-steel connection model.

$$EAu_1'(0) = 0$$
$$EIv_1''(0) = 0$$
$$-EIv_1'''(0) = 0$$

$$(4.15)$$

$$EIv_1''(l_1) = 0$$
$$u_1(l_1) = \delta \sin(\theta)$$
$$v_1(l_1) = -\delta \cos(\theta)$$

4.3.3 Concrete to timber

When the connection is composed of a concrete slab, a common assumption in the literature is to consider the screw embedded in the slab as rotationally restrained and traslationally restrained in the direction perpendicular to the sliding plane (Di Nino et al. [14]).

The following equations are equivalent to those described in Di Nino et al. [14] and are suitable for describing the case of timber-to-concrete connections with interlayers:
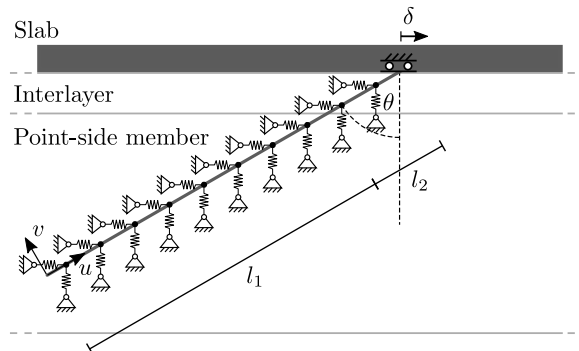
Figure 4.7: Timber-to-concrete connection with interlayer model.

$$EAu_1'(0) = 0$$
$$EIv_1''(0) = 0$$
$$-\,EIv_1'''(0) = 0$$

$$EAu_1'(l_1) = EAu_2'(l_1)$$
$$EIv_1''(l_1) = EIv_2''(l_1)$$
$$-\,EIv_1'''(l_1) = -EIv_2'''(l_1)$$
$$u_1(l_1) = u_2(l_1)$$
$$v_1(l_1) = v_2(l_1)$$
$$v_1'(l_1) = v_2'(l_1)$$

$$\tag{4.16}$$

$$v_2'(l_1 + l_2) = 0$$
$$u_2(l_1 + l_2) = \delta \sin(\theta)$$
$$v_2(l_1 + l_2) = -\delta \cos(\theta)$$

The following equations are equivalent to those described in Symons et al. [84] and are suitable for describing the case of timber-to-concrete connections without interlayers:
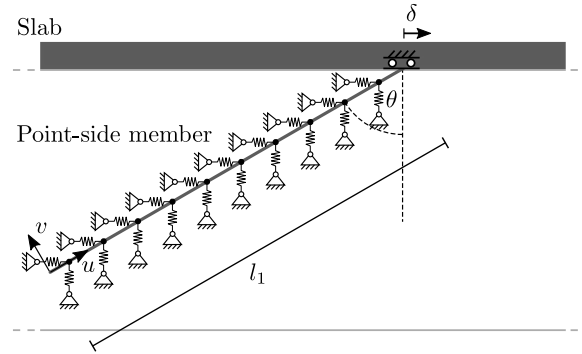
Figure 4.8: Timber-to-concrete connection model.

$$EAu_1'(0) = 0$$
$$EIv_1''(0) = 0$$
$$-\,EIv_1'''(0) = 0$$

$$\tag{4.17}$$

$$v_1'(l_1) = 0$$
$$u_1(l_1) = \delta \sin(\theta)$$
$$v_1(l_1) = -\delta \cos(\theta)$$

4.4   Perturbation method solution

Perturbation method is an analytical techniques for determining approximate solution of equations for which closed form exact solutions are not known. The approximate solution is given as a perturbation of a known solution of a similar, simpler problem. According to this approach the solution can be written as a power series of a small

parameter ϵ. The main advantage of perturbation method consist in providing closed formulas which allow to identify the influence of the system parameters on its response [79].

The problem of an inclined beam on elastic foundation is governed by a coupled sixth-order system of differential equations (Eqs. 4.10) in the unknown field displacement function $u(x)$ and $v(x)$. Introducing the dimensionless parameters defined in Eqs. 4.18, the system of Eqs. 4.10 can be rewritten as Eqs. 4.19.

$$
\begin{aligned}
\kappa_{xx} &= \sqrt{\frac{K_{xx}}{EA}} \\
\kappa_{yy} &= \sqrt[4]{\frac{K_{yy}}{4EI}} \\
\kappa_{xy} &= \sqrt{\frac{K_{xy}}{EA}} \\
\kappa_{yx} &= \sqrt[4]{\frac{K_{yx}}{4EI}}
\end{aligned}
\tag{4.18}
$$

$$
\begin{aligned}
\kappa_{xx}^2 u + \kappa_{xy}^2 v - u'' &= 0 \\
4\kappa_{yx}^4 u + 4\kappa_{yy}^4 v + v'''' &= 0
\end{aligned}
\tag{4.19}
$$

When the coupling terms coefficients κ_{xy}^2 and $4\kappa_{yx}^4$ in Eqs. 4.19 are null, the system of coupled differential equations reduce to the equations of a rod and a beam on elastic foundation for which the closed form solution is known. Therefore is convenient to solve this problem using perturbation approach.

4.4.1 Steel to timber

In this paragraph a solution with the perturbation method is derived for the case of timber-to-steel connection without inter-layer. In this case the problem is described by the field equation of Eqs. 4.19 and by the following boundary conditions:

$$
\begin{aligned}
u'(0) &= 0 \\
v''(0) &= 0 \\
v'''(0) &= 0 \\
\\
u(l) - \delta \sin(\theta) &= 0 \\
v(l) + \delta \cos(\theta) &= 0 \\
v''(l) &= 0
\end{aligned}
\tag{4.20}
$$

Assuming the coefficients κ_{xy}^2 and κ_{yx}^4 small of order ϵ as in Eqs. 4.21 and substituting the field displacement function $u(x)$ and $v(x)$ with their first order series power expansion (Eqs. 4.22 with $n = 1$), the system (Eqs. 4.19) and the boundary conditions (Eqs. 4.20) can be rewritten as Eqs. 4.23 and Eqs. 4.24 respectively.

$$
\begin{aligned}
\kappa_{xy}^2 &= \epsilon \hat{\kappa}_{xy}^2 \\
\kappa_{yx}^2 &= \epsilon \hat{\kappa}_{yx}^2
\end{aligned}
\tag{4.21}
$$

$$
\begin{aligned}
u &= \sum_{i=1}^{n} \epsilon^i u_i \\
v &= \sum_{i=1}^{n} \epsilon^i v_i
\end{aligned}
\tag{4.22}
$$

$$
\begin{aligned}
\kappa_{xx}^2 \left(u_0 + \epsilon u_1\right) - \left(u_0 + \epsilon u_1\right)'' &= -\hat{\kappa}_{xy}^2 v_0 \\
4\kappa_{yy}^4 \left(v_0 + \epsilon v_1\right) + \left(v_0 + \epsilon v_1\right)'''' &= -4\hat{\kappa}_{yx}^2 u_0
\end{aligned}
\tag{4.23}
$$

$$
\begin{aligned}
(u_0(0) + \epsilon u_1(0))' &= 0 \\
(v_0(0) + \epsilon v_1(0))'' &= 0 \\
(v_0(0) + \epsilon v_1(0))''' &= 0 \\
u_0(l) + \epsilon u_1(l) - \delta \sin(\theta) &= 0 \\
v_0(l) + \epsilon v_1(l) + \delta \cos(\theta) &= 0 \\
(v_0(l) + \epsilon v_1(l))'' &= 0
\end{aligned}
\tag{4.24}
$$

The Eqs. 4.23 and Eqs. 4.24 should be valid for every ϵ and consequently both the zero order (Eqs. 4.25 and 4.26) and first order equations (Eqs. 4.28 and 4.29) must be verified.

$$
\begin{aligned}
\kappa_{xx}^2 u_0 - u_0'' &= 0 \\
\kappa_{yx}^4 u_0 + v_0'''' &= 0
\end{aligned}
\tag{4.25}
$$

$$
\begin{aligned}
u_0'(0) &= 0 \\
v_0''(0) &= 0 \\
v_0'''(0) &= 0 \\
u_0(l) - \delta \sin(\theta) &= 0 \\
v_0(l) + \delta \cos(\theta) &= 0 \\
v_0''(l) &= 0
\end{aligned}
\tag{4.26}
$$

The zero order equations lead to the following solution:

$$
\begin{aligned}
u_0 &= \delta \sin(\theta)\mathrm{sech}(\kappa_{xx}l)\cosh(\kappa_{xx}x) \\
v_0 &= \frac{\delta \cos(\theta)e^{(-1-i)\kappa_{yy}(l+x)}}{4(\sin(2\kappa_{yy}l)-\sinh(2\kappa_{yy}l))} \left(-ie^{2\kappa_{yy}l} - e^{2i\kappa_{yy}l} + (1+i)e^{(2+2i)\kappa_{yy}l} + (1-i)\left(-e^{2\kappa_{yy}(x+il)}\right) + (1-i)e^{2\kappa_{yy}(l+ix)} \right. \\
&\quad \left. + e^{2\kappa_{yy}(x+(1+i)l)} + e^{2\kappa_{yy}(l+(1+i)x)} + ie^{(2+2i)\kappa_{yy}l+2i\kappa_{yy}x} + ie^{2i\kappa_{yy}l+(2+2i)\kappa_{yy}x} - ie^{2\kappa_{yy}x} - e^{2i\kappa_{yy}x} - (1+i)e^{(2+2i)\kappa_{yy}x} \right)
\end{aligned}
\tag{4.27}
$$

$$
\begin{aligned}
\kappa_{xx}^2 u_1 - u_1'' &= -\hat{\kappa}_{xy}^2 v_0 \\
\kappa_{yx}^4 u_1 + v_1'''' &= -4\hat{\kappa}_{yx}^2 u_0
\end{aligned}
\tag{4.28}
$$

$$
\begin{aligned}
u_1'(0) &= 0 \\
v_1''(0) &= 0 \\
v_1'''(0) &= 0 \\
u_1(l) - \delta \sin(\theta) &= 0 \\
v_1(l) + \delta \cos(\theta) &= 0 \\
v_1''(l) &= 0
\end{aligned}
\tag{4.29}
$$

By solving the non-homogeneous first order problem and with the following positions:

$$
\begin{aligned}
\gamma &= A + I\kappa_{xy}^2 \\
\zeta &= \kappa_{xx}^4 + 4\kappa_{yy}^4
\end{aligned}
\tag{4.30}
$$

$$
\begin{aligned}
S_\theta &= \sin(\theta) \\
C_\theta &= \cos(\theta) \\
S_y &= \sin(l\kappa_{yy}) \\
C_y &= \cos(l\kappa_{yy}) \\
S_{hx} &= \sinh(l\kappa_{xx}) \\
C_{hx} &= \cosh(l\kappa_{xx}) \\
S_{hy} &= \sinh(l\kappa_{yy}) \\
C_{hy} &= \cosh(l\kappa_{yy})
\end{aligned}
\tag{4.31}
$$

The stiffness of the connection given by the ratio between boundary forces and imposed displacement (Eq. 4.32) is given in its explicit form in Eq. 4.33.

$$k_{ser} = \frac{EAu'(l) + EIv'''(l)}{\delta} \tag{4.32}$$

$$k_{ser} = \frac{E}{\zeta C_{hx}(C_{hy}S_{hy} - C_y S_y)} \left\{ S_\theta \left[2\gamma C_{hx} \kappa_{xy}^2 \kappa_{yy}^3 S_y^2 C_\theta + A\zeta \kappa_{xx} S_{hx} S_\theta (C_{hy}S_{hy} - C_y S_y) \right] + 2I\zeta C_{hx}\kappa_{yy}^3 C_\theta^2 \left(S_{hy}^2 - S_y^2 \right) + \right.$$
$$\left. + \gamma \kappa_{xy}^2 S_\theta C_\theta \left[\kappa_{yy}\kappa_{xx}^2 C_{hx} \left(S_{hy}^2 - 2\left(\frac{\kappa_{yy}}{\kappa_{xx}}\right)^2 S_{hy}^2 + S_y^2 - 2\frac{S_{hy}S_y}{C_{hx}}\right) - \kappa_{xx}^3 S_{hx} \left(C_{hy}S_{hy} - C_y S_y \right)\right] \right\} \tag{4.33}$$

The percentage scatters distribution between the perturbation method solution and exact numerical solution in term of k_{ser} is reported in Fig. 4.9 for 875 configurations in the domain of practical interest.

It is worth noting that despite the equation 4.33 is more complex than those derived by interpolation of the numerical solution, this formula is valid for every angle of screw inclination and it has significantly lower percentage deviations compared to the previous case. When the problem is naturally decoupled as in the case of screw perpendicular to the sliding plane ($\theta = 0°$), the perturbation method solution and the exact solution coincide. Also in the case of screw mainly stressed in the axial direction the solutions are really close together ($\theta \geq 60°$)
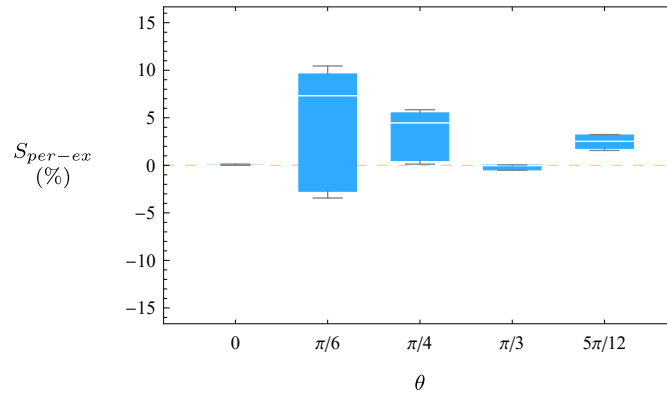
Figure 4.9: Maximum, 95th percentiles, median, 5th percentiles and minimum values of the scatters between perturbation method solution and exact solution in terms of k_{ser} for 175 configurations for each θ.

4.5   Foundation modulus

Foundation modulus may be termed also sub-grade modulus. In timber engineering, foundation values are used to predict the failure load of connections with dowel type connectors using models based on limit analysis as in the European yielding model (Eurocode 5 [29]). The foundation strength is also called embedment strength and it is determined through embedment test. The embedment test consist in loading the fastener perpendicular to its axis through a steel loading apparatus and measuring the load and the corresponding displacement due to the fastener indentation (Fig. 2.7, EN-383 [25]). The dimension of the specimen are defined by standards and they are such as to avoid the bending of the fastener.

The embedment test allow also to identify the foundation modulus which is determined in the elastic range.

An accurate description of how the foundation modulus is defined and how it is used in this model is provided in the research paper in Sec. 4.9.

4.6   Validation on experimental data

Current literature is rich in experimental data of timber-to-timber connections without interlayer. The experimental tests consist of symmetrical push-out tests, push-out tests with symmetry constraints (teflon surface), or inclined shear tests. The reference standard is EN-26891 [23]. A large number of results have been collected and used for the validation of the timber-to-timber model and are reported in the research paper of Sec. 4.9. Only a few of the collected tests refer to connections with interlayer and none of them concerns connections with soundproofing

interlayers. To compensate for the lack of these data and allow the validation of the timber-to-timber model with interlayers, the tests described in Chap. 3 were performed and a comparison with predicted values is reported in the following tables.

The timber-to-timber model was found to be overall accurate, with a weak tendency to overestimate the slip modulus in interlayer configurations (Tab. 4.1). In the analytical model, the interlayer has been assumed capable of maintaining constants the distance between main timber members (Fig. 4.2 and Eqs. 4.11). This assumption can be considered valid when the interlayer possess an appreciable stiffness in the direction of the normal to the sliding plane. The soundproofing interlayers have elastic modulus considerably lower than the elastic modulus of timber in the direction perpendicular to the grain of timber. While the mean elastic modulus of the timber used in the test series is $E_{90} = 300\,\text{N/mm}^2$, the elastic modules of the soundproofing interlayers are $E_{S35} = 2.74\,\text{N/mm}^2$ and $E_{S90} = 43.5\,\text{N/mm}^2$ (Tab. 3.3). Being the elastic modules of soundproofing interlayers about 1/110 and 1/7 times the elastic modulus of timber in the direction perpendicular to the grain, this assumption strictly holds only for higher shore soundproofing interlayers. Similar comparisons are made for timber-to-steel test series in Sec. 6.2.

Name	Description	$\rho_1 = \rho_3$ (kg/m^3)	ϕ (mm)	l_1 (mm)	l_2 (mm)	l_3 (mm)	$k_{s,exp}$ (kN/mm)	$k_{s,pred}$ (kN/mm)	$S_{pred-exp}$ (%)
TT 0 8 200 R	Reference 0°	440	8	80	0	120	2.74	3.07	12
TT 0 8 200 S35	Soft int. 0°	440	8	74	6	120	1.57	1.99	27
TT 0 8 200 S90	Stiff int. 0°	440	8	74	6	120	1.36	1.99	46
TT 45 7 300 R	Reference 45°	440	7	130	0	170	14.73	12.94	-12
TT 45 7 300 S35	Soft int. 45°	440	7	122	8	170	9.79	12.04	23
TT 45 7 300 S90	Stiff int. 45°	440	7	122	8	170	10.47	12.04	15
TT 30 7 300 S35	Soft int. 30°	440	7	155	7	139	6.86	5.66	-17

Table 4.1: Timber-to-timber configurations parameters, prediction and results.

4.7 Variance-based sensitivity analysis

The models described so far can be solved analytically only in some particular cases and the analytical solutions, even the approximate ones, are too complex to perform a function study that allows us to understand the role of the variables.

To increase understanding of the relationships between geometrical and mechanical input variables and the model output in terms of connection slip modulus, a variance-based sensitivity analysis was carried out.

The results of the analyses in the following paragraphs have had a crucial role to simplify the search for interpolating formulas of the exact solution.

Sensitivity analysis method can be classified as local or global. Local SA calculates the effect of small perturbations of a parameters around a chosen value and approximate the first-order partial derivative of the model perturbing one parameter at time. Global SA aims at exploring the whole domain of the input parameters.

Despite the higher computational effort required, a global sensitivity method was chosen.

According to the Sobol method by Sobol [81], the variance of the output of the model is decomposed into fractions which can be attributed to inputs. The so-called Sobol indices measure sensitivity across the whole input space.

The computation of Sobol integrals, have been performed performed through a Monte Carlo simulation. Latin hyper-cube sampling has been used to generate a near-random sample of parameter values from a multidimensional distribution. In the first step, a matrix of $N = 10000$ randomly sampled input combinations is generated, each one made up of M components, where M is the number of model inputs.

Both the Sobol index S_1 and the total sensitivity index S_T are computed for the examined models. While S_1 measures the effect of varying a single parameter alone averaged over variations in other input parameters, S_T measures the contribution to the output variance of the selected parameter, including all variance caused by its interactions. In other words, the more different the ranking generated by the two indices, the more complex the interaction between the parameters.

According to Sobol [81] given a model in the form of $Y = f(X)$, where X is a vector of d inputs and Y is the model output and assuming that the inputs are independently and uniformly distributed within the unit hyper-cube, first-order sensitivity index can be written as follows:

$$S_{1i} = \frac{V_i}{Var(Y)} \tag{4.34}$$

where $V_i = Var_{X_i}(E_{X\sim i}(Y|X_i))$.

The total-effect index is given by:

$$S_{Ti} = 1 - \frac{V_{Ti}}{Var(Y)} \tag{4.35}$$

where $V_{Ti} = Var_{X\sim i}(E_{Xi}(Y|X_{\sim i}))$.

The generation of the configurations necessary for the calculation of the indices and the post processing of the results were carried out using the SAFE toolbox by Pianosi et al. [62] and Pianosi et al. [63].

The sensitivity analyses were performed on timber-to-timber and timber-to-steel models with interlayer and repeated considering both the case of screw perpendicular to the sliding plane $\theta = 0°$ and inclined to $\theta = 45°$.

4.7.1 Timber to timber

The sensitivity analysis highlighted that the thickness of the interlayer and the diameter of the screw are the most significant parameters for the slip modulus of screws perpendicular to the shear plane (Tab. 4.2 and Fig. 4.10, 4.11). For inclined screws the diameter and length of the screw sections in the main members are the main variables (Tab. 4.3 and Fig. 4.12 and 4.13).

In both cases the limited differences between the first-order indices and the total-effect indices suggests a limited interaction between parameters.

Parameter	S_1	S_T
ρ_1	0.02	-0.01
ρ_3	0.01	0.01
ϕ	0.38	0.49
l_1	0.01	-0.01
l_2	0.47	0.56
l_3	0.02	0.04
Sum	0.91	1.07

Table 4.2: Sensitivity indices: timber-to-timber model with $\theta = 0°$.
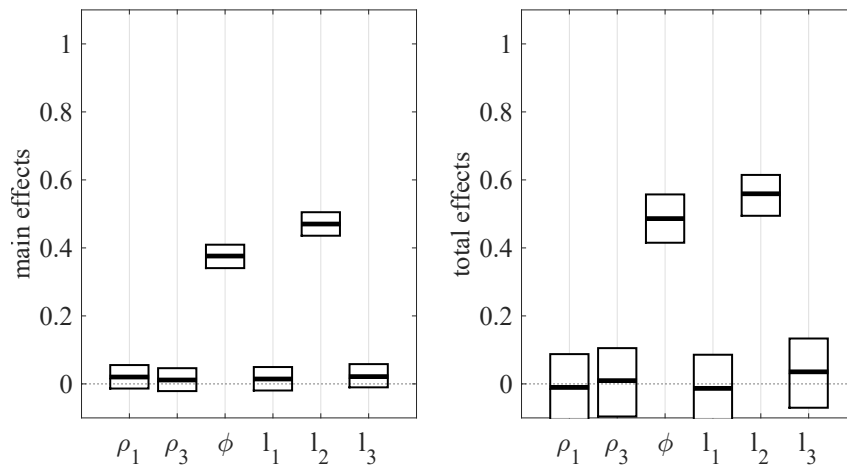
Figure 4.10: Sensitivity indices: timber-to-timber model with $\theta = 0°$.
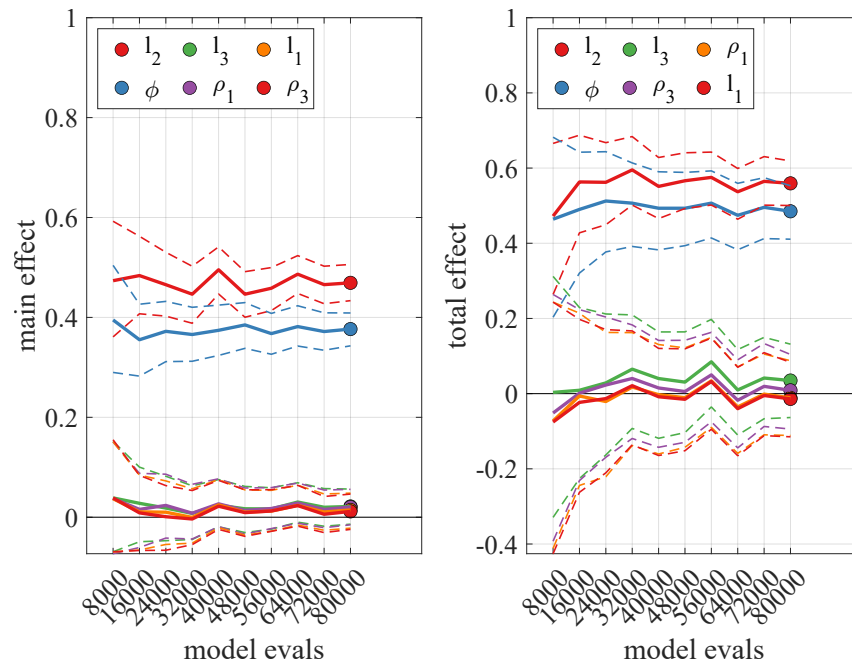
Figure 4.11: Convergence of sensitivity indices: timber-to-timber model with $\theta = 0°$.

Parameter	S_1	S_T
ρ_1	0.09	0.02
ρ_3	0.05	0.09
ϕ	0.38	0.37
l_1	0.21	0.18
l_2	0.04	-0.03
l_3	0.25	0.11
Sum	1.02	0.73

Table 4.3: Sensitivity indices: timber-to-timber model with $\theta = 45°$.
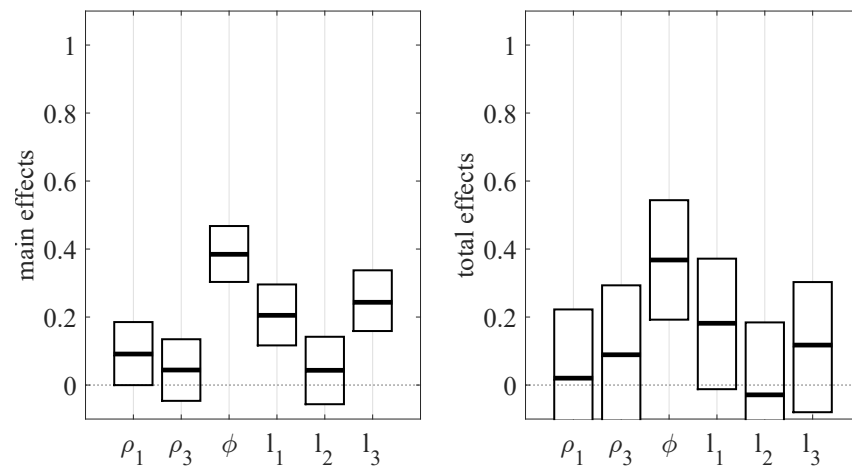
Figure 4.12: Sensitivity indices: timber-to-timber model with $\theta = 45°$.
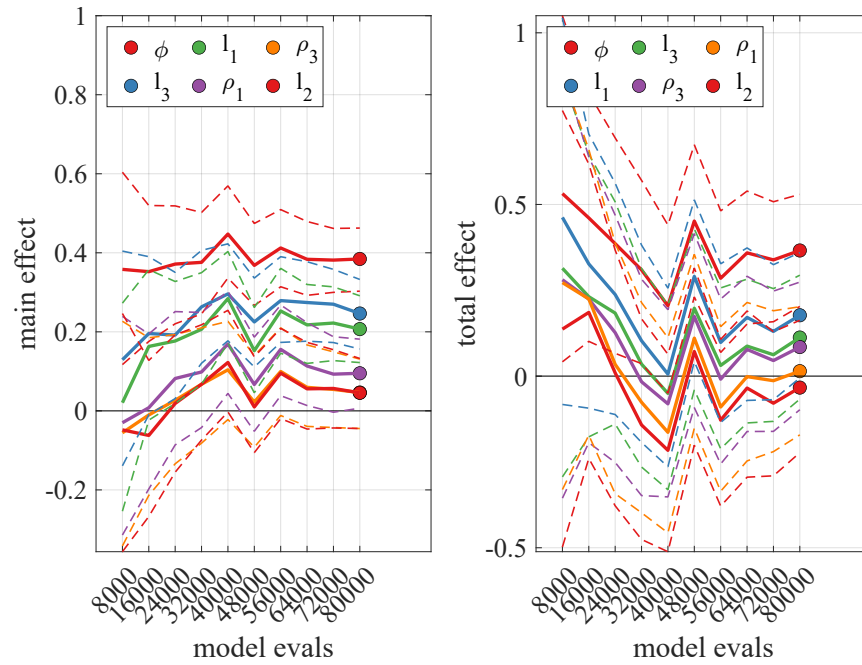
Figure 4.13: Convergence of sensitivity indices: timber-to-timber model with $\theta = 45°$.

4.7.2   Steel to timber

The sensitivity analysis highlighted that the thickness of the interlayer and the diameter of the screw are the most significant parameters for the slip modulus of screws perpendicular to the shear plane (Tab. 4.4 and Fig. 4.14 and 4.15). For inclined screws the diameter and length of the screw sections in the main member are the main variables (Tab. 4.5 and Fig.4.16 and 4.17).

In both cases the limited differences between the first-order indices and the total-effect indices suggests a limited interaction between parameters.

Parameter	S_1	S_T
ρ_1	-0.02	-0.03
ϕ	0.14	0.25
l_1	-0.02	-0.06
l_2	0.67	0.85
Sum	0.77	1.01

Table 4.4: Sensitivity indices: timber-to-steel model with $\theta = 0°$.
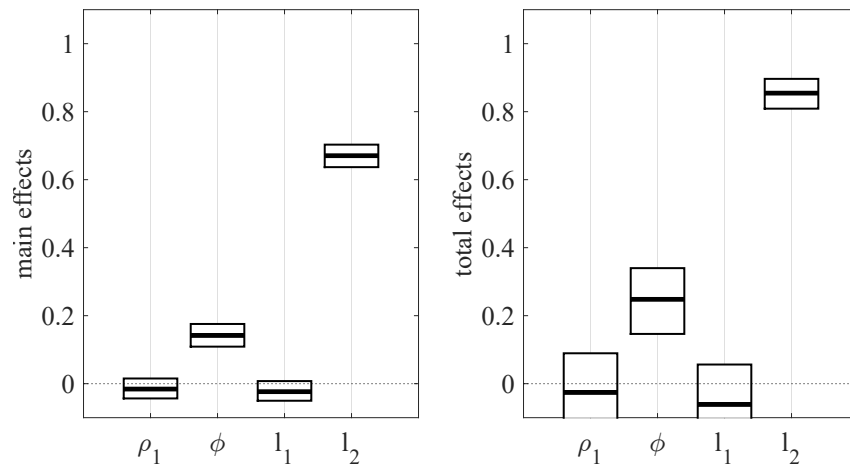
Figure 4.14: Sensitivity indices: timber-to-steel model with $\theta = 0°$.
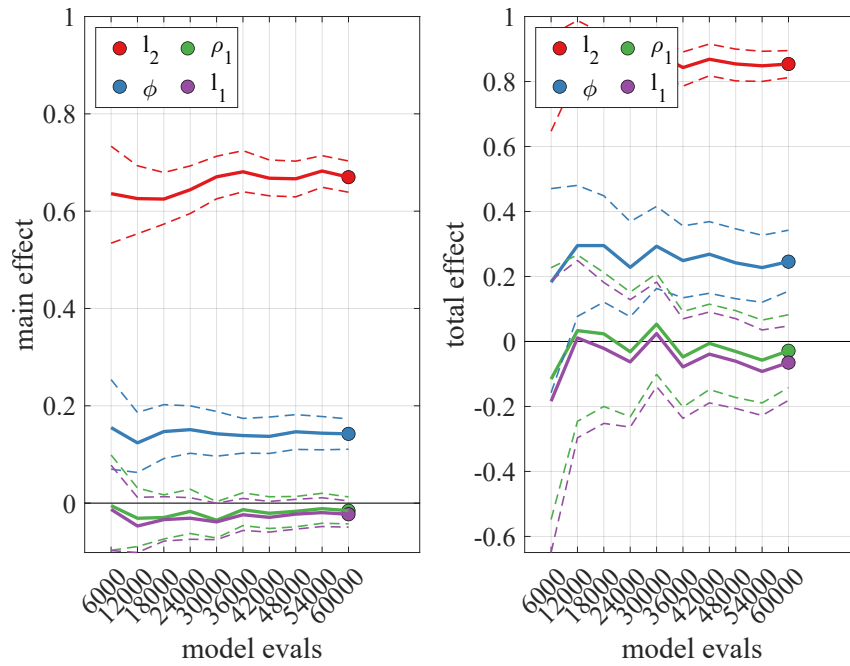
Figure 4.15: Convergence of sensitivity indices: timber-to-steel model with $\theta = 0°$.

Parameter	S_1	S_T
ρ_1	0.18	0.17
ϕ	0.31	0.36
l_1	0.40	0.42
l_2	0.05	0.01
Sum	0.94	0.96

Table 4.5: Sensitivity indices: timber-to-steel model with $\theta = 45°$.
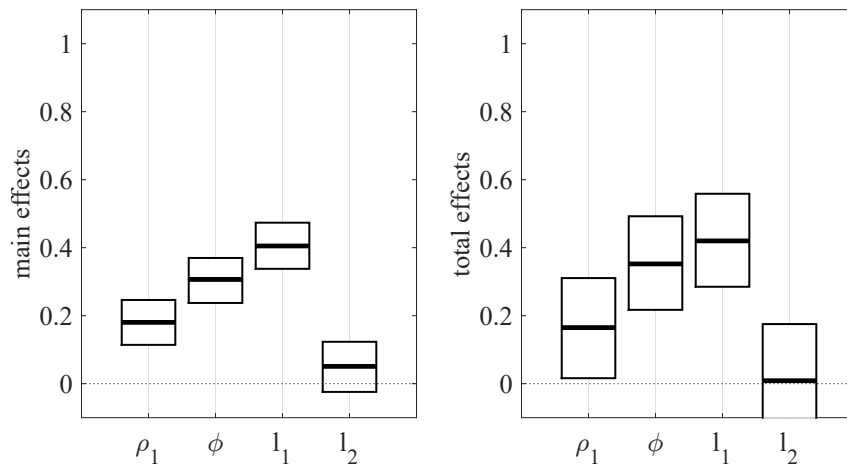
Figure 4.16: Sensitivity indices: timber-to-steel model with $\theta = 45°$.
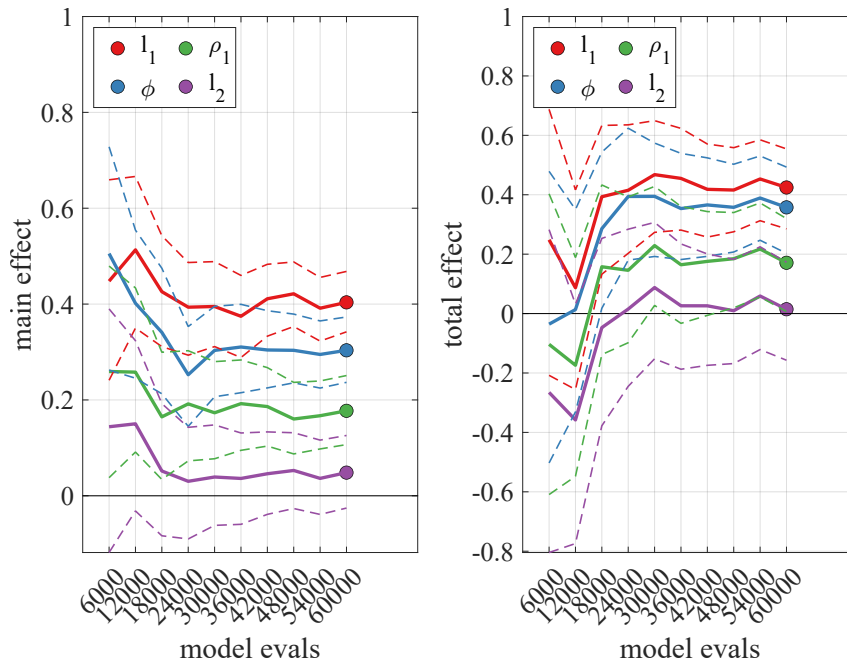
Figure 4.17: Convergence of sensitivity indices: timber-to-steel model with $\theta = 45°$.

4.8 Simplified formulas

The problem of an inclined beam on elastic foundation as defined in this chapter is governed by a coupled sixth-order system of differential equations. The system of differential equation does not admit exact closed form solutions. As discussed in Subs. 4.4.1, an analytical approximate solution can be found through perturbation method, but even in the simplest case of timber-to-steel connections without interlayer, the solution it is not simple enough to be used by practitioners or to be implemented in codes.

Simpler formulas were obtained by interpolation of the numerical solution of the problem. The choice of the structure of the interpolation formulas was guided by the results of the variance-based sensitivity analysis.

In the following discussion, distinction between non load-bearing and load-bearing interlayer is made. Both interlayer type are assumed to be able to prevent the relative displacement of the main members in the direction perpendicular to the shear plane. The distinction between the two interlayer type lies in their foundation modulus and connection with main member.

4.8.1 Non load-bearing interlayer

Discontinuous interlayers like existing planking of timber floors, or oriented strand boards weakly connected to the main timber members are assumed as non load-bearing in this discussion. This kind of interlayer is considered in the model as a portions of the beam without distributed springs.

Simplified formulas for timber-to-timber and steel-to-timber connections with non load-bearing interlayers are presented in the research paper of Sec. 4.9.

4.8.2 Load-bearing interlayer

The simplified formulas for the slip modulus prediction of connections with load-bearing interlayer have been obtained with the same methodology used for the case of connections with non load-bearing interlayer.

The following hypotheses have been added with respect to the non load-bearing interlayer case:

- the interlayer is considered to be rigidly connected to one of the main timber members;

- the foundation modulus of the interlayer can be correlated to its density with the same interpolation formulas used for the main members.

The first hypothesis allows identifying a single sliding plane and to remove the dependence of the slip modulus on the stiffness of the connection between the interlayer and the main member.

In order to understand whether specific formulations should be derived for the case of load-bearing interlayer, the slip modulus increment predicted by the analytical model moving from a non-load-bearing interlayer to a load-bearing interlayer with the same configuration is assessed. The following methodology has been used:

- slip modulus calculation for a series of configurations with non-load-bearing interlayer;

- slip modulus calculation for a series of similar configurations, but with load-bearing interlayer of different densities;

- evaluation of the quartiles of the ratios between the slip modulus of configurations with load-bearing interlayer and the slip modulus of the corresponding configurations with non-load-bearing interlayer.

For timber-to-timber connections with screws perpendicular to the sliding plane, even for weak interlayers ($\rho = 350 kg/m^3$), 75% of the configurations with load-bearing interlayer have a sliding modulus at least 2.3 times the sliding modulus of the corresponding configuration with a non-load-bearing interlayer.
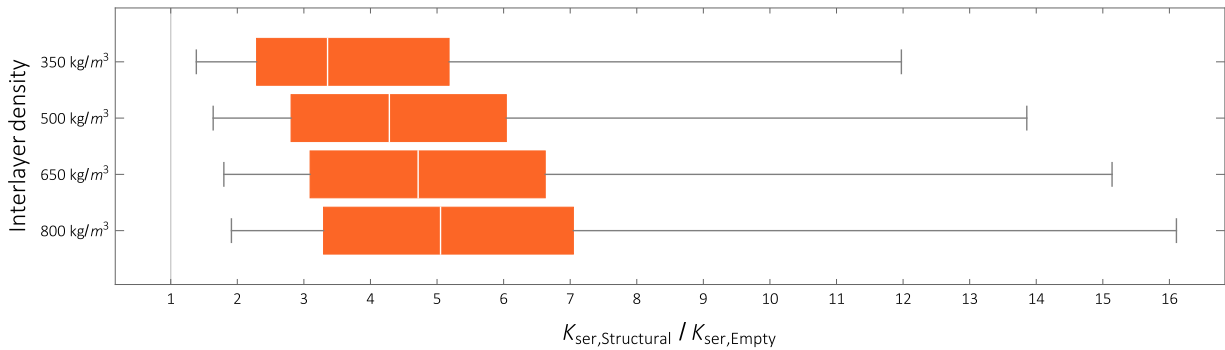
Figure 4.18: Timber to timber connections with screws perpendicular to the sliding plane: ratios between the slip modulus of configurations with load-bearing interlayer and the slip modulus of the corresponding configurations with non-load-bearing interlayer.

For timber-to-timber connections with inclined screws, the benefit is appreciable only for strong interlayers ($\rho = 800$ kg/m^3). Only 25% of the configurations with 800 kg/m^3 density load-bearing interlayer have a sliding modulus at least equal to 1.5 times the sliding modulus of the corresponding configuration with a non-load-bearing interlayer.
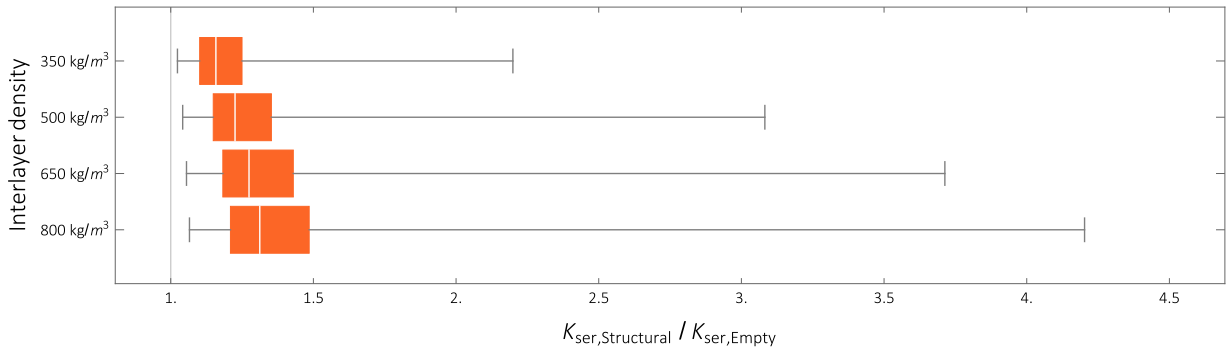
Figure 4.19: Timber to timber connections with 45° screws: ratios between the slip modulus of configurations with load-bearing interlayer and the slip modulus of the corresponding configurations with non-load-bearing interlayer.

For steel-to-timber connections with screws perpendicular to the sliding plane, even for weak interlayers ($\rho = 350$ kg/m^3), 75% of the configurations with load-bearing interlayer have a sliding modulus at least 4.7 times the sliding modulus of the corresponding configuration with a non-load-bearing interlayer.
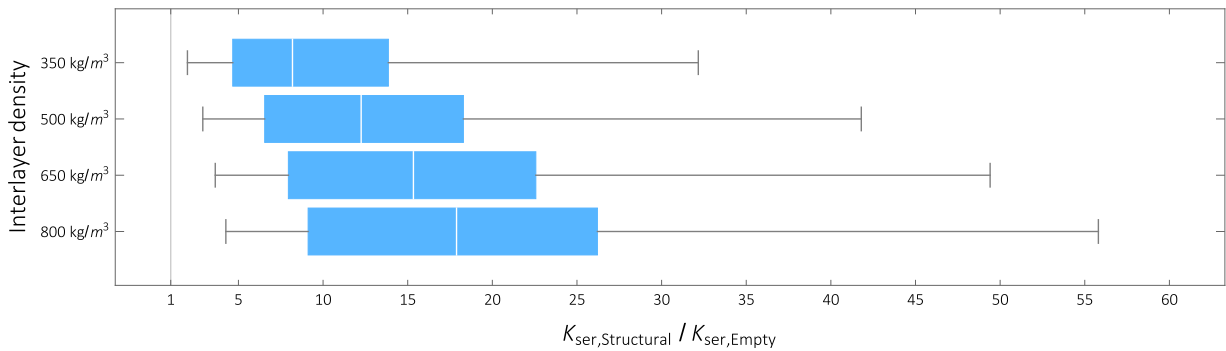
Figure 4.20: Timber to steel connections with screws perpendicular to the sliding plane: ratios between the slip modulus of configurations with load-bearing interlayer and the slip modulus of the corresponding configurations with non-load-bearing interlayer.

For steel-to-timber connections with inclined screws, the benefit is appreciable only for strong interlayers ($\rho = 800$ kg/m^3). 75% of the configurations with load-bearing interlayer of density 800 kg/m^3 have a sliding modulus at least equal to 1.4 times the sliding modulus of the corresponding configuration with a non-load-bearing interlayer.
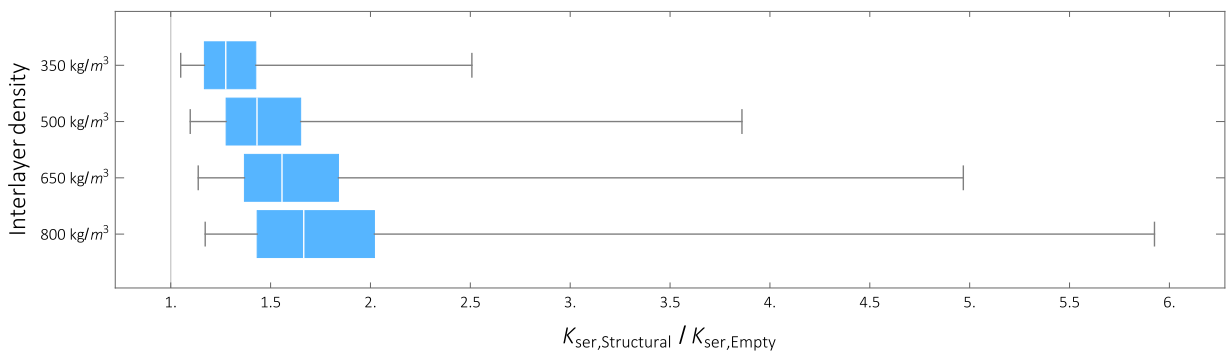
Figure 4.21: Timber to steel connections with 45° screws: ratios between the slip modulus of configurations with load-bearing interlayer and the slip modulus of the corresponding configurations with non-load-bearing interlayer.

The derived simplified formulas are valid only for interlayers with thickness $\geq 9mm$.

For timber-to-timber connections with screws perpendicular to the sliding plane, the model responds as a system of 3 springs in parallel.

$$k_{ser} = \quad 0.12(\rho_1 l_1^{0.1} + \rho_2^{1.1} + \rho_3 l_3^{0.1})\phi^{1.1} \tag{4.36}$$

For timber-to-timber connections with inclined screws, the model responds as a system of 3 springs in series where the stiffness of the spring schematizing the structural layer glued to the interlayer counts twice.

$$k_{ser} = \quad \frac{0.5\phi^{0.7}}{\frac{0.48}{\rho_1 l_1^{0.62}} + \frac{1}{\rho_2^{1.6} l_2^{0.4}} + \frac{1}{\rho_3 l_3^{0.62}}} \tag{4.37}$$

For steel-to-timber connections with screws perpendicular to the sliding plane, the model responds as a system of 2 springs in parallel.

$$k_{ser} = \quad 0.9(\rho_1^{0.8} l_1^{0.1}\phi^{0.4} + \rho_2\phi^{1.23}) \tag{4.38}$$

$$k_{ser} = \quad 0.48(\rho_1^{0.9} l_1^{0.6}\phi + \rho_2^{1.2} l_2^{0.4}\phi^{0.4}) \tag{4.39}$$

The differences between exact analytical solutions and simplified formulas solutions were evaluated on 31000 configurations with parameters chosen in the domain of practical interest for each case shown in the following box-plot.
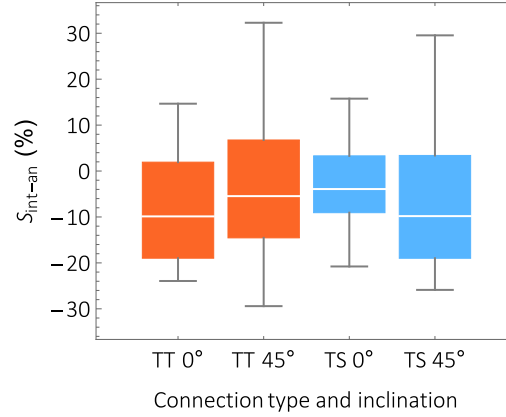
Figure 4.22: Maximum, 95th percentiles, median, 5th percentiles and minimum values of the scatters between interpolating formulas and exact solution

4.9 Paper: *Timber-to-timber and steel-to-timber screw connections: Derivation of the slip modulus via beam on elastic foundation model*

The following paper deal with timber-to-timber and steel-to-timber screw connections with non-structural interlayers. The models are described by equations Eqs. 4.10, 4.11 and 4.13.
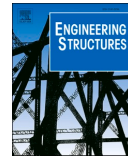
Timber-to-timber and steel-to-timber screw connections: Derivation of the slip modulus via beam on elastic foundation model

Yuri De Santis [*], Massimo Fragiacomo

Department of Civil, Building-Construction and Environmental Engineering, University of L'Aquila, 67100 L'Aquila, Italy

ABSTRACT

The aim of this paper is to propose formulations for the slip modulus prediction of timber-to-timber connections (TTC) and steel-to-timber connections (STC) with inclined screws and possible interlayers. The beam on elastic foundation model, previously developed for timber-to-concrete connections, was extended to consider the flexibility of both media where the screw is inserted. Since a significant influence of the fastener diameter on the foundation modulus was observed in tests, an interpolating formula correlating the foundation modulus with timber density and the fastener diameter was derived. The exact solution of the timber-to-timber analytical model was found to agree well with experimental results for total and double thread screws. A parametric study was undertaken to prove that connections with inclined screws have significantly higher slip modulus and lower degradation of performance as the diameter decreases or the thickness of the intermediate layer increases compared to connections with screws perpendicular to the sliding plane. Furthermore, the slip modulus of inclined screws was found to be limited by the weakest timber layer. Closed form expressions for the prediction of the slip modulus were derived by interpolation for the most important cases of technical interest. These formulas can be proposed for the implementations in codes of practice such as the Eurocode 5, since simplified formulas of the slip modulus are currently missing for connections with inclined fasteners and interlayers.

1. Introduction

Timber connections with inclined self-tapping screws are characterized by high slip modulus values, and can be effectively used in composite beams. The most common uses include the construction of new timber floors, the upgrade of existing timber floors, and the upgrade of deteriorated beams. The possibility of joining together different materials such as sawn timber, engineered wood products [1], concrete [2] and steel [3] leads to a combination of aesthetic and functional advantages. In many cases of retrofit, the existing timber flooring usually made of planks is left in place between the existing timber joist or beam and the new added upper member (Fig. 1) [4]. The intermediate layer may also be made by an OSB panel loosely bound to one of the two timber members.

Self-tapping screws can also be used for connecting timber with steel members, for instance the plates used in beam-to-beam and beam-to-pillar joints and the plates used as inter-story connections (Fig. 1) or the hold downs of XLAM [5] or LTF buildings.

The performance in terms of strength and stiffness of a composite beam markedly depends on the strength and stiffness properties of the shear connection between the members. The current Eurocode 5 [6] only contains an empirical formulation to predict the slip modulus of connections with screws perpendicular to the sliding plane and without an interlayer. As highlighted by Tomasi et al. [7] and Girhammar et al. [8], the overall slip modulus of a connection with inclined screw is given by the sum of two contributions: (i) one linked to the flexural behavior of the screw, which decreases as the angle of inclination with respect to the normal to the sliding plane increases, and (ii) another one linked to the axial behavior of the screw, which increases for increasing angle. The withdrawal properties of axially loaded self-tapping screws are affected by several parameters, including the effective thread length, the shank diameter, the thread geometry, the axis to grain angle, and timber stiffness [9].

The aim of this paper is to present a mathematical model suitable for prediction of the slip modulus of timber-to-timber (TTC) and steel-to-timber connections (STC) with inclined screws. The model is capable to take into account all the aforementioned parameters affecting the system behavior.

---

* Corresponding author.
E-mail address: yuri.desantis@graduate.univaq.it (Y. De Santis).
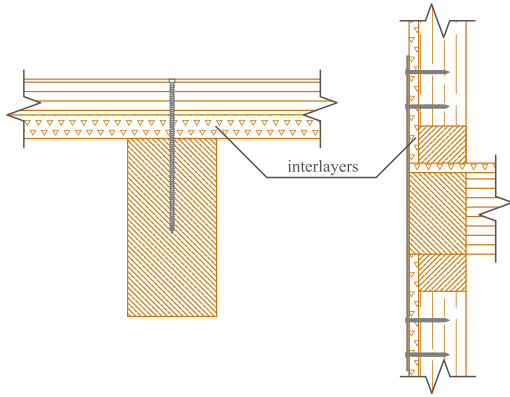
Fig. 1. Examples of use of self-tapping screws: upgrade of existing floor and inter-story connections of LTF building.

2. Mechanical model for slip modulus derivation

Inclined elastic beam on an elastic foundation model was previously used by Di Nino et al. [10] to predict the slip modulus of timber-to-concrete connections with interlayer. A similar approach is proposed in this paper to extend the model to timber-to-timber and steel-to-timber connections. In the model, the elastic beam represents the screw, and the surrounding timber is modelled through two sets of independent springs. One set of springs, characterized by stiffness k_p, is parallel to the shear plane of the connection, whilst another set of springs, characterized by stiffness k_t, is perpendicular to the shear plane. The use of two set of springs allows the user to account for the timber anisotropy (Fig. 2 (a) and (b)).

Due to the complex geometry of the screws, it is not easy to identify the diameter to be used for calculating the axial (*EA*) and flexural stiffness (*EI*) of the beam. Commons assumptions are to use either the outer thread diameter of the screw ϕ as done by Di Nino et al. [10] or the inner thread diameter [11]. Preliminary studies have shown that in the cases of parallel or slightly inclined screw with respect to the normal to the sliding plane, i.e. when the flexural stiffness contribution is prevalent, the aforementioned model overestimates the experimental results when the outer thread diameter is adopted. This behavior could indicate that the transition zone between the screw shank and the surrounding undistorted timber fibres consisting of the screw thread and the disturbed timber fibres, only contributes to increasing the axial stiffness of the shank. Consequently, from now on the axial stiffness is assumed to be $EA = E\pi\phi^2/4$ and flexural stiffness $EI = E\pi(\alpha\phi)^4/64$, where E is the

steel Young's modulus, ϕ is the outer thread diameter and α the ratio between the inner thread diameter and the outer thread diameter.

2.1. General field equations

By assuming small strains and small displacements and by adopting linear kinematics, the elastic problem of an inclined beam on elastic foundation is governed by Eqs. (1) for the *i*-th domain. The beam, schematizing the screw of a timber-to-timber connection, can be divided into three domains ($i = 1, 2, 3$) characterized by same axial and flexural stiffness, but different length and spring stiffness (Fig. 2 (a)). In the case of a steel-to-timber connection, the screw can be divided into only two domains ($i = 1, 2$) (Fig. 2 (b)).

Eqs. (1) consists of a system of sixth-order differential equations. $u_i(x)$ and $v_i(x)$ denote the displacement of fields in axial and transverse direction respectively for the *i*-th domain, θ is the angle between the normal of the sliding plane and the fastener (Fig. 2 (a), Fig. 2 (b)) and $K_{xx_i}, K_{xy_i}, K_{yx_i}, K_{yy_i}$ are defined by Eqs. (2).

$$K_{xx_i}(\theta)u_i(x) + K_{xy_i}(\theta)v_i(x) - EA\ddot{u}_i(x) = 0$$

$$K_{yx_i}(\theta)u_i(x) + K_{yy_i}(\theta)v_i(x) + EI\ddddot{v}_i(x) = 0 \qquad (1)$$

$$K_{xx_i}(\theta) = \cos\theta\sin\theta(k_{t_i}\cos\theta + k_{p_i}\sin\theta)$$

$$K_{yy_i}(\theta) = k_{p_i}\cos^3\theta + k_{t_i}\sin^3\theta$$

$$K_{xy_i}(\theta) = \cos\theta\sin\theta(-k_{p_i}\cos\theta + k_{p_i}\sin\theta)$$

$$K_{yx_i}(\theta) = K_{xy_i}(\theta) \qquad (2)$$

2.2. Boundary conditions for timber-to-timber connections

In a three-layer composite system (Fig. 3), the slip modulus on plane 2–3 is defined as the ratio between the resultant of the components
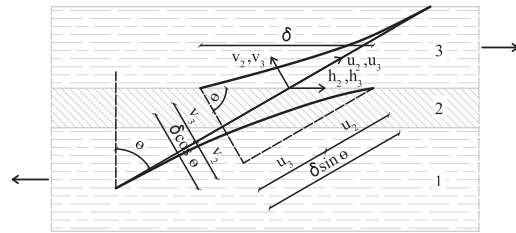
Fig. 3. Initial and deformed configurations of the beam representing the fastener of a three-layer composite system.

(a)

(b)
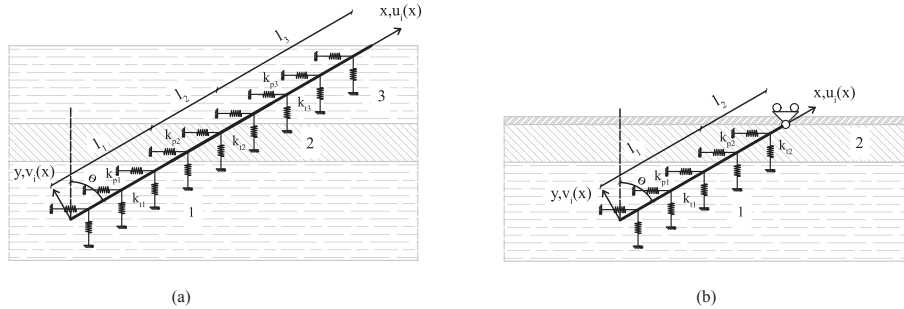
Fig. 2. (a) Timber-to-timber connection model (b) Steel-to-timber connection model.

parallel to the sliding plane of the forces reciprocally exchanged by the members and the relative sliding of the members 2 and 3 on the shear plane 2–3.

The relative sliding of the member 2 with respect to the member 3 on the shear plane 2–3 (δ) corresponds to the sum of the embedment depths of the fastener in member 2 (h_2) and in member 3 ($-h_3$) in the sliding plane direction (total indentation of fastener) (Fig. 3). Consequently, the slip modulus of the connection can be calculated by imposing an internal distortion δ parallel to the sliding plane to the beam at $x = l_1 + l_2$. The slip modulus of the connection is given by the ratio between the component parallel to the sliding plane of the internal forces of the beam and the internal distortion δ (Eq. (3)). The first term of Eq. (3) k_{ax}, represents the axial stiffness contribution or withdrawal stiffness, while k_{fl} represent the flexural stiffness contribution or embedment stiffness.

$$k_{s,an} = \frac{N_2\sin(\theta) - T_2\cos(\theta)}{\delta} = +\frac{EAu_2'(l_1+l_2)\sin(\theta)}{\delta} + \frac{EIv_2'''(l_1+l_2)\cos(\theta)}{\delta}$$
$$= k_{ax} + k_{fl}$$

(3)

It is worth noting that Eq. (3) is true when the forces reciprocally exchanged by members on the sliding plane are only the axial $N_2(l_1+l_2) = N_3(l_1+l_2)$ and shear forces $T_2(l_1+l_2) = T_3(l_1+l_2)$ of the fastener. This assumption corresponds to neglecting the contribution offered by the friction on the sliding plane.

Solving Eqs. (1) require six boundary conditions for each domain leading to a total of eighteen boundary conditions for the timber-to-timber connection case (Eqs. (4)). At free ends of the beam ($x = 0$ and $x = l_1 + l_2 + l_3$) the forces and bending moments shall be equal to zero (Eqs. (4.1) and Eqs. (4.4)). At $x = l_1$, boundary conditions grant continuity of the internal forces and moments and of the displacement fields between the two contiguous domains (Eqs. (4.2)). At the sliding plane ($x = l_1 + l_2$) it is necessary to impose, in addition to the internal distortion, the continuity of the internal forces, bending moments and of the rotation of the sections (Eqs. (4.3)). Fig. 3 shows the case in which h_2, the component parallel to the sliding plane of the displacement of member 2 in $x = l_1 + l_2$, is greater than h_3, the component parallel to the sliding plane of the displacement of member 3 in $x = l_1 + l_2$, i.e. the case of a fastener subject to traction.

$$EAu_1'(0) = 0$$

$$EIv_1''(0) = 0$$

$$-EIv_1'''(0) = 0$$

(4.1)

$$EAu_1'(l_1) = EAu_2'(l_1)$$

$$EIv_1''(l_1) = EIv_2''(l_1)$$

$$-EIv_1'''(l_1) = -EIv_2'''(l_1)$$

$$u_1(l_1) = u_2(l_1)$$

$$v_1(l_1) = v_2(l_1)$$

$$v_1'(l_1) = v_2'(l_1)$$

(4.2)

$$EAu_2'(l_1+l_2) = EAu_3'(l_1+l_2)$$

$$EIv_2''(l_1+l_2) = EIv_3''(l_1+l_2)$$

$$-EIv_2'''(l_1+l_2) = -EIv_3'''(l_1+l_2)$$

$$u_2(l_1+l_2) - \delta\sin\theta = u_3(l_1+l_2)$$

$$v_2(l_1+l_2) + \delta\cos\theta = v_3(l_1+l_2)$$

$$v_2'(l_1+l_2) = v_3'(l_1+l_2)$$

(4.3)

$$EAu_3'(l_1+l_2+l_3) = 0$$

$$EIv_3''(l_1+l_2+l_3) = 0$$

$$-EIv_3'''(l_1+l_2+l_3) = 0$$

(4.4)

2.3. Boundary conditions for steel-to-timber connections

In the case of steel-to-timber connections with an intermediate layer, since the withdrawal and the embedment of the screw in the steel plate are negligible, the third domain of the beam on elastic foundation can be reduced to an external restraints. The plate can be regarded as a restraints which prevents displacements of the beam perpendicular to the sliding plane at $x = l_1 + l_2$ (Fig. 4).

If the plate is thin enough or the hole in it is large enough to allow free rotation of the screw end, in $x = l_1 + l_2$ the bending moment of the beam should be zero and the axial and transverse displacement of the beam should be the same as the corresponding δ projections (Eqs. (5.3)). The remaining boundary conditions are the same as those for the timber-to-timber case, and the slip modulus of the connection is given by Eq. (3).

$$EAu_1'(0) = 0$$

(5.1)

$$EIv_1''(0) = 0$$

$$-EIv_1'''(0) = 0$$

$$EAu_1'(l_1) = EAu_2'(l_1)$$

(5.2)

$$EIv_1''(l_1) = EIv_2''(l_1)$$

$$-EIv_1'''(l_1) = -EIv_2'''(l_1)$$

$$u_1(l_1) = u_2(l_1)$$

$$v_1(l_1) = v_2(l_1)$$

$$v_1'(l_1) = v_2'(l_1)$$

$$EIv_2''(l_1+l_2) = 0$$

(5.3)

$$u_2(l_1+l_2) = \delta\sin\theta$$

$$v_2(l_1+l_2) = -\delta\cos\theta$$
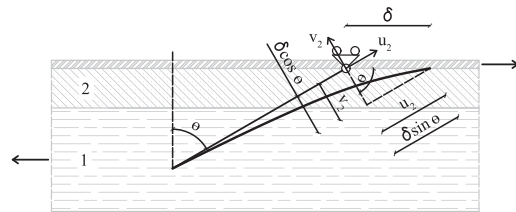
Fig. 4. Initial and deformed configurations of the beam representing the fastener of a two-layer composite system with a steel plate on the top.

2.4. Interpolation formulas for the foundation modulus of the main timber members

In the proposed model the timber is modelled by two orders of elastic springs, this simplification, which is valid in the serviceability operation range, allows to determine directly from experimental tests the only timber stiffnesses parameters to be included in the model without introducing further parameters as it happens in the case of numerical models in which complex contact algorithms and soft layers are used and whose properties must be carefully evaluated [12,13].

For a dowel-type fastener, the foundation modulus can be experimentally determined via embedding test according to EN 383 [14], ASTM D5764 [15] and ISO/DIS 10984–2 [16]. While the EN 383 standard requires a test on a timber specimen with a full-hole and a dowel loaded on its ends, the ASTM D5764 regulation prescribes a half-hole test with dowel uniformly loaded along its length in order to eliminate any dowel bending effect. Despite the differences between the test procedures, a comparison between standards reveals a close agreement in terms of foundation modulus as pointed out by Santos et al. [17]. The ISO/DIS 10984–2 standard is the same as EN 383, except that it allows for both full-hole and half-hole tests.

The experimental foundation modulus $K_f(\text{N/mm}^3)$ can be derived, accordingly to EN 383 [14], from the secant stiffness of first loading phase $k_f(\text{N/mm}) = 0.4F_{h,est}/[4/3(w_{04} - w_{01})] = (0.4F_{h,est} - 0.1F_{h,est})/(w_{04} - w_{01})$:

$$K_f\left(\frac{\text{N}}{\text{mm}^3}\right) = \frac{k_f\left(\frac{\text{N}}{\text{mm}}\right)}{t\phi(\text{mm}^2)} \qquad (6)$$

where ϕ is the fastener diameter and t the thickness of the timber member.

The analytical model developed in this paper requires the knowledge of the stiffness of parallel and perpendicular springs with respect to the sliding plane (Eqs. (2)). In the most common application, the grain direction of main timber members (1 and 3) coincides with the sliding direction and consequently the foundation modulus $K_p(\text{N/mm}^3)$ to be used to calculate the stiffness of the springs parallel to the sliding plane $k_p(\text{N/mm}^2) = K_p\phi$ can be obtained from embedding tests performed parallel to the grain $K_p = K_{f0}$. On the basis of the results of embedment tests performed in the orthogonal direction with respect to the grain ([17,19,20,21,26;23]) and as also done in [10] and [11], perpendicular spring stiffness can be taken as $k_t(\text{N/mm}^2) = \beta k_p$ with $\beta = 0.5$.

The consistency between the two test procedures allowed the results of thirty-eight embedding tests to be gathered from the literature (Table 1). The foundation modulus K_f was found to be dependent upon the direction with respect to the timber grain, the timber density ρ and, as also highlighted in [18], the dowel diameter ϕ as the foundation modulus decreases for increasing diameters.

As can be seen from Fig. 5 (a) and (b), sawn timber (ST), glued laminated timber (GL) and cross laminated timber (CLT) have significantly higher foundation modulus parallel to the grain K_{f0} than laminated veneer lumber (LVL), parallel strand lumber (PSL), laminated strand lumber (LSL) and plywood (PLY). From this categorization of timber products the two interpolation laws Eq. (7) (ST, GL and XLAM) and Eq. (8) (LVL, PSL, LSL and PLY) can be derived. The goodness of fit statistics for Eq. (7) and Eq. (8) are respectively: $R^2 = 0.79$, $RMSE = 20.1 \text{ N/mm}^3$ and $R^2 = 0.74$, $RMSE = 15.9 \text{ N/mm}^3$.

Table 1
Foundation modulus parallel to timber grain.

Authors and [reference]	Materials	Standard	(mm)	(kg/m³)	(kg/m³)
Gattesco [19]	(GL) Eastern Alps spruce	EN 383	16	468	75.55
Gattesco [20]	(GL) Eastern Alps red spruce	EN 383	16	440	82.50
Santos [17]	(ST) Pinus pinaster	EN 383	14	560	113.3
Santos [17]	(ST) Pinus pinaster	ASTM D5764	14	600	120.9
Karagiannis [21]	(GL) Scandinavian spruce	EN 383	12	430	31.33
Karagiannis [21]	(GL) Scandinavian spruce	EN 383	16	430	64.62
Tuhkanen [22]	(GL) Norway spruce	EN 383	20	459	44.87
Tuhkanen [22]	(CLT) Norway spruce	EN 383	20	456	41.43
Franke [23]	(ST) Beech	ISO/DIS 10984–2	6	734	193.0
Franke [23]	(ST) Beech	ISO/DIS 10984–2	12	734	137.0
Franke [23]	(ST) Beech	ISO/DIS 10984–2	20	734	96.00
Lederer [24]	(ST) Norway spruce	EN 383	12	450	61.11
Lederer [25]	(ST) Norway spruce	ASTM D5764	12	422	45.95
Schweigler [26]	(LVL) Spruce	EN 383	12	510	29.80
Schweigler [26]	(LVL) Spruce	EN 383	16	502	38.30
Hwang [18]	(LVL) Radiata pine	ASTM D5764	6	491	58.60
Hwang [18]	(LVL) Radiata pine	ASTM D5764	6	508	70.30
Hwang [18]	(PSL) Douglas Fir	ASTM D5764	6	657	117.9
Hwang [18]	(LSL) Douglas Fir	ASTM D5764	6	619	84.60
Hwang [18]	(LVL) Radiata pine	ASTM D5764	8	491	54.80
Hwang [18]	(LVL) Radiata pine	ASTM D5764	8	508	64.70
Hwang [18]	(PSL) Douglas Fir	ASTM D5764	8	657	107.1
Hwang [18]	(LSL) Douglas Fir	ASTM D5764	8	619	77.60
Hwang [18]	(LVL) Radiata pine	ASTM D5764	10	491	51.00
Hwang [18]	(LVL) Radiata pine	ASTM D5764	10	508	59.10
Hwang [18]	(PSL) Douglas Fir	ASTM D5764	10	657	96.30
Hwang [18]	(LSL) Douglas Fir	ASTM D5764	10	619	70.60
Hwang [18]	(LVL) Radiata pine	ASTM D5764	12	491	47.20
Hwang [18]	(LVL) Radiata pine	ASTM D5764	12	508	53.50
Hwang [18]	(PSL) Douglas Fir	ASTM D5764	12	657	85.50
Hwang [18]	(LSL) Douglas Fir	ASTM D5764	12	619	63.60
Lemaitre [27]	(PLY) Pine	EN 383	12	673	155.6
Lemaitre [27]	(PLY) Pine	EN 383	16	679	77.85
Lemaitre [27]	(PLY) Poplar	EN 383	12	496	53.46
Lemaitre [27]	(PLY) Poplar	EN 383	16	483	28.89
Lemaitre [27]	(LVL) Spruce	EN 383	16	498	30.97
Schweigler [27]	(LVL) Spruce	EN 383	12	518	27.63
Schweigler [27]	(LVL) Spruce	EN 383	16	509	17.24
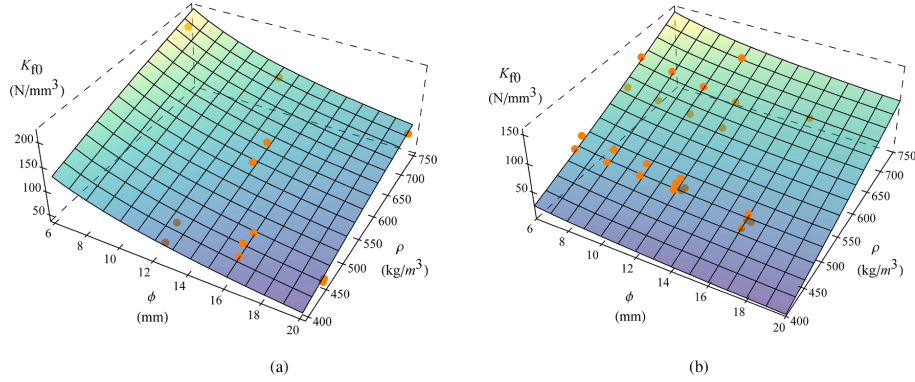
Fig. 5. Experimental data and interpolating functions of the foundation modulus for (a) ST, GL and XLAM and (b) LVL, PSL, LSL and PLY.
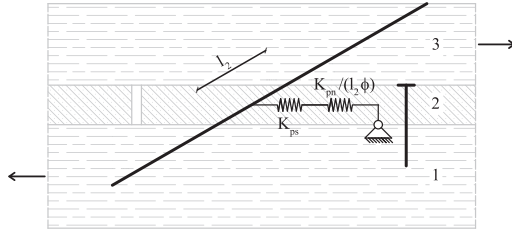
Fig. 6. Three layers composite system with timber planks interlayer connected to the timber member 1 by a nailed secondary connection.

$$K_{f0}(\rho, \phi) = -147.8 + \frac{30.9\rho^{0.46}}{\phi^{0.32}} \tag{7}$$

$$K_{f0}(\rho, \phi) = -62.3 + \frac{0.0282\rho^{1.41}}{\phi^{0.23}} \tag{8}$$

2.5. Foundation modulus of the interlayer

The intermediate layer, in the most common applications, consists of a flooring made of planks arranged perpendicularly to the beam (Fig. 6) or made of an oriented strand board (OSB) panel (Fig. 7) loosely bound
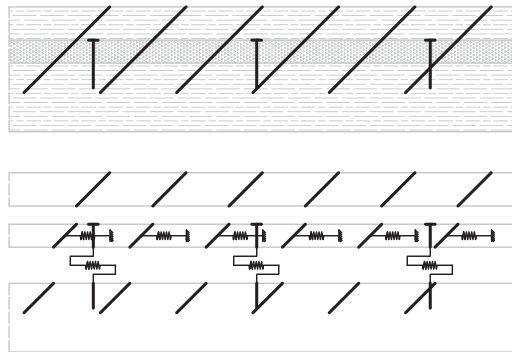
Fig. 7. Three layers composite system with OSB panel interlayer connected to the timber member 1 by a nailed secondary connection.

to one of the two timber members through a secondary connection (e.g. nailed connection between member 1 and 2).

With reference to the first case (Fig. 6) it can be observed that the timber plank (member 2) is not free to slide due to the secondary connection of diameter ϕ_s with the lower timber member (member 1). The beam schematizing the inclined screw will have, along the length l_2, a fictitious foundation modulus K_{p2} dependent upon the foundation modulus of the plank in perpendicular direction with respect to grain K_{ps} and the stiffness of the secondary connection K_{pn}.

To determine the order of magnitude of K_{p2}, two limit cases can be considered:

- *Rigid secondary connection and deformable screw-plank contact:*

$K_{p2} = K_{ps} = K_{f90} = \beta K_{f0}(\rho, \phi) \cong 15$ to 60 N/mm³ according to literature data (Table 1).

- *Deformable secondary connection and rigid screw-plank contact:*

$K_{p2} = K_{pn}/(\phi l_2) = \rho_m^{1.5}\phi_s^{0.9}/(30 \cdot \phi l_2) \cong 420^{1.5}3^{0.9}/(30 \cdot 8 \cdot 28) \cong 3.4$ N/mm³ from EN1995-1–1 [6] formulation for the slip modulus of timber to timber connection with vertical fasteners.

In the real connection:

- *Deformable secondary connection and deformable screw-plank contact:*

$$K_{p2} = \frac{1}{\frac{1}{K_{ps}} + \frac{1}{K_{pn}/(\phi l_2)}} \cong 3 \text{ N}\Big/\text{mm}^3 \tag{9}$$

As can be seen, the estimated values of fictitious foundation modulus of the intermediate layer (K_{p2}), are 10 to 40 times lower than foundation modulus of main timber members (K_{p1} and K_{p3}). It should be also noted that the obtained values are valid in the hypothesis that each plank where a screw is inserted also has a secondary connection with the lower timber element. If this secondary connection is not present and there is also a gap between adjacent planks, K_{p2} must be assumed null.

When the interlayer consists of an OSB panel (Fig. 7), the fictitious foundation modulus K_{p2} depends upon the ratio between the number of inclined screws per panel n_s and the number of nails per panel n_n. For a ratio of 2 (Fig. 7) and assuming a rigid screw-to-panel contact: $K_{p2} \cong (n_n/n_s) [K_{pn}/(\phi l_2)] = (n_n/n_s)[\rho_m^{1.5}\phi_s^{0.9}/(30 \cdot \phi l_2)] \cong (3/6) \cdot [420^{1.5}3^{0.9}/(30 \cdot 8 \cdot 28)] \cong 1.7$ N/mm³.

In both cases described before the fictitious foundation modulus of the intermediate layer assumes values at most equal to $1/10$ of those
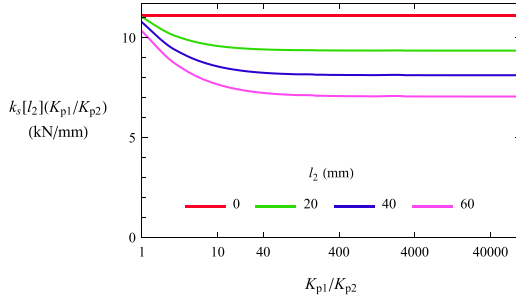
Fig. 8. Slip modulus variation on K_{p1}/K_{p2} for interlayer length of penetration ranging from 0 to 60 mm for $\theta = \pi/4$ with constant K_{p1} and screw length.

expected for the other members. Preliminary studies (Fig. 8) have also shown that as K_{p2} decreases the predicted slip modulus of the connection converges to the value calculated assuming $K_{p2} = 0$ already for $K_{p1}/K_{p2} = 10$, consequently it is possible to neglect the stiffness of the intermediate layer.

3. Model validation on experimental data

The exact solutions of the analytical model developed for the timber-to-timber connections were compared with the experimental results carried out on 50 different configurations.

The test procedures of joints made with mechanical fasteners are described in EN 26891 [28]. This standard requires the user to perform a push-out test divided into a first phase carried out in load or slip control and a second phase carried out in slip control. By denoting with F_{est} the estimated maximum load, during the first phase the load is increased up to $0.4F_{est}$ and then is kept constant for $30s$. Subsequently, the load is reduced to $0.1F_{est}$, maintained for $30s$ and again increased up to failure. The slip modulus $k_{s,exp}$ can be determined using Eq. (10):

$$k_{s,exp} = \frac{0.4F_{est} - 0.1F_{est}}{\nu_{0.4} - \nu_{0.1}} \tag{10}$$

where $\nu_{0.4}$ and $\nu_{0.1}$ are the connection slips of first loading phase corresponding to a shear load of $0.4F_{est}$ and $0.1F_{est}$, respectively. If the mean value of the maximum load of the tests deviates by more than 20% from F_{est}, F_{est} has to be replaced by F_{max}, i.e. the value derived from the test, and $\nu_{0.4}$ and $\nu_{0.1}$ are assumed as the connection slips corresponding to a shear load of $0.4F_{max}$ and $0.1F_{max}$, respectively.

The experimental slip modulus $k_{s,exp}$ reported in Table 2 and Fig. 10 derive from push-out, half push-out and diagonal shear tests performed according to EN 26891 on test specimens with double threaded (Dt) or total threaded (Tt) screws, inclined (shear-tension) or crossed (X) (shear-tension and shear-compression). The analytical predicted values $k_{s,an}$ were obtained by numerically solving Eqs. (1) and Eqs. (4) with Mathematica software [29]. The ratio between the inner thread diameter and the outer thread diameter was assumed $\alpha = 0.66$ based on the most common geometries among a sample of 80 screw types from different manufacturers. In the case of double threaded screws , the outer thread diameter ϕ was assumed the same as the average value of the outer threads diameters. The foundation modulus used were determined in accordance with Eq. (7) and Eq. (8). The correspondence between the analytical and experimental values was evaluated by calculating the percentage error as: $S_{an-exp} = (k_{s,an} - k_{s,exp})/k_{s,exp} \cdot 100\%$.

The values predicted by the analytical model are in good agreement with the experimental data. For 38 of the 50 configurations analyzed the error is less than 25% with an average of $S_{an-exp,m} = -7.6\%$ (Table 2). The analytical model tends to slightly underestimate the experimental results and a possible reason is the friction generated by the forces acting

perpendicularly to the sliding plane. These forces, which are not taken into account by the analytical model, are the timber member reactions to the internal forces induced in the fastener by the relative sliding of the members and by the screwing of the fasteners themselves in the case of double treaded screws. As highlighted by Giongo et al. [34], double threaded screws can introduce prestressing forces of 3 to 7 kN and the corresponding friction force, assuming a friction coefficient $\mu = 0.25$, is of the same order of magnitude as the $0.4F_{est}$ and therefore it might affect the experimentally measured slip modulus.

4. Derivation of simplified formulas

The analytical model, due to its complexity, does not directly provide a simple equation for the slip modulus of timber-to-timber and steel-to-timber connections. In order to obtain closed form expressions for use from the profession and possible implementation in codes of practice such as the Eurocode 5 [6], configurations of practical interest were selected and suitable interpolating functions were found.

4.1. Methods

First, the ranges of technical interest were identified for each of the 7 or 5 model parameters affecting the timber-to-timber and steel-to-timber connections, respectively. Datasets composed by the parameter values and the corresponding slip modulus values calculated by numerically solving the equations of the proposed analytical model were then generated.

Due to the complex dependence of the slip modulus on the fastener inclination, and in order to obtain interpolating formulas both simple and accurate, different interpolating formulas were sought for perpendicular and inclined fasteners with respect to the sliding plane. Datasets values were interpolated and best fit coefficients were found for the given type of function.

4.2. Results

Eqs. (11), (12), (13) and (14) provides the connection slip modulus in N/mm when the timber density ρ_i is measured in kg/m^3, the length of penetration in the timber member l_i is measured in mm and the external diameter of the screw ϕ is measured in mm. The formulations are valid when the timber members belong to the first category of products as defined in paragraph 2.4. Eqs. (11) and (12) are valid for timber-to-timber connections with inclined and perpendicular screws with respect to the shear plane, respectively, and the corresponding coefficients are reported in Table 3.

Eqs. (11) and (12) can be used when the timber member densities ρ_i belong to the 400–750 kg/m^3 range and the external diameter is included between 6 and 18 mm. Eq. (11) is valid when the lengths of penetration in the main timber members is in the range 50–200 mm and the length of penetration in the interlayer, if present, is no more than 60 mm. Eq. (12) allows for lengths of penetration in the main members belonging to the 60–150 mm range and a maximum interlayer thickness of 40 mm. Eq. (11) has the basic structure of the resultant stiffness formula of two springs arranged in series.

$$k_{s,int} = \frac{ee\phi^{cc}}{\frac{1}{\rho_1^{aa}l_1^{bb}} + \frac{1}{\rho_3^{aa}l_3^{bb}}} dd^{\left(\frac{l_2}{\phi^{0.55}}\right)} \tag{11}$$

$$k_{s,int} = ee(\rho_1^{aa-0.0186l_2}l_1^{bb-0.0015l_2} + \rho_3^{aa-0.0186l_2}l_3^{bb-0.0015l_2})\phi^{cc-0.0316l_2} + ddl_2 \tag{12}$$

Eqs. (13) and (14) are valid for steel-to-timber connections with inclined and perpendicular screws with respect to the shear plane respectively. The corresponding coefficients are reported in Table 4.

Eqs. (13) and (14) can be used when the timber member densities ρ_i range between 400 and 750 kg/m^3, length of penetration in the main

Table 2
Comparison between experimental mean and analytically predicted stiffness values.

Authors and [reference]	Member1	Member3	ϕ (mm)	ρ_{1m} $\left(\frac{kg}{m^3}\right)$	ρ_{3m} $\left(\frac{kg}{m^3}\right)$	l_1 (mm)	l_2 (mm)	l_3 (mm)	Screw type and layout	θ (°)	$k_{s,exp}$ $\left(\frac{N}{mm}\right)$	$k_{s,an}$ $\left(\frac{N}{mm}\right)$	S_{an-exp} (%)
Schiro et al. [30] PA	Beech LVL	CLT	8.3	796	465	69	0	81	Dt	45	13,234	11,031	−17
Schiro et al. [30] PH	Spruce solid C24	Beech LVL GL70	8.3	460	846	91	28	71	Dt	45	13,468	10,660	−21
Schiro et al. [30] PI	Spruce solid C24	CLT	8.3	460	465	69	0	81	Dt	45	9773	9783	0
Schiro et al. [30] PM	Spruce solid C24	CLT	8.6	460	465	81	28	81	Dt	45	7835	9369	20
Wang et al.[31]	Douglas Fir LVL	Douglas Fir LVL	5.3	560	560	39	0	61	Tt	45	3647	2984	−18
Wang et al. [31]	Douglas Fir LVL	Douglas Fir LVL	5.3	560	560	50	0	50	Tt	30	2457	1831	−25
Wang et al. [31]	Douglas Fir LVL	Douglas Fir LVL	5.3	560	560	55	0	45	Tt	15	1557	1230	−21
Wang et al. [31]	Douglas Fir LVL	Douglas Fir LVL	5.3	560	560	57	0	43	Tt	0	954	1167	22
Ringhofer [32]	Spruce solid T24	Spruce solid T24	8.0	408	408	113	0	113	Tt	45	12,100	11,501	−5
Ringhofer [32]	Spruce solid T24	Spruce solid T24	8.0	410	408	130	0	130	Tt	60	16,200	14,705	−9
Jacquier et al. [33] S1	Spruce GL32	CLT C24	6.5	456	471	75	0	85	Dt	45	9700	9024	−7
Jacquier et al. [33] S2	Spruce GL32	CLT C24	8.2	462	459	75	0	85	Dt	45	12,700	10,222	−20
Blaß et al. [9] 1	Spruce solid T28	Spruce solid T28	8.0	409	409	113	0	113	Tt	45	12,100	11,528	−5
Blaß et al. [9] 2	Spruce solid T28	Spruce solid T28	8.0	412	412	130	0	130	Tt	60	16,500	14,799	−10
Blaß et al. [9] 3	Spruce solid T28	Spruce solid T28	8.0	412	412	113	0	113	Tt X	45	11,150	11,607	4
Blaß et al. [9] 4	Spruce solid T28	Spruce solid T28	8.0	407	407	130	0	130	Tt X	60	17,500	14,631	−16
Blaß et al. [9] 6	Spruce solid T28	Spruce solid T28	8.0	421	421	130	0	130	Tt	60	13,300	15,097	14
Blaß et al. [9] 8	Spruce solid T28	Spruce solid T28	8.0	427	427	130	0	130	Tt X	60	11,975	15,292	28
Blaß et al. [9] 9	Spruce solid T28	Spruce solid T28	8.0	475	475	113	0	113	Tt	45	12,950	13,159	2
Blaß et al. [9] 10	Spruce solid T28	Spruce solid T28	8.0	438	438	130	0	130	Tt	60	19,250	15,645	−19
Blaß et al. [9] 11	Spruce solid T28	Spruce solid T28	8.0	482	482	113	0	113	Tt X	45	11,750	13,321	13
Blaß et al. [9] 12	Spruce solid T28	Spruce solid T28	8.0	456	456	130	0	130	Tt X	60	17,100	16,205	−5
Blaß et al. [9] 15	Spruce solid T28	Spruce solid T28	6.0	424	424	85	0	85	Tt	45	9050	8343	−8
Blaß et al. [9] 16	Spruce solid T28	Spruce solid T28	6.0	416	416	85	0	85	Tt X	45	6825	8213	20
Blaß et al. [9] 17	Spruce solid T28	Spruce solid T28	10	411	411	141	0	141	Tt	45	18,450	15,007	−19
Blaß et al. [9] 18	Spruce solid T28	Spruce solid T28	10	414	414	141	0	141	Tt X	45	13,950	15,120	8
Blaß et al. [9] 21	Spruce solid T28	Spruce solid T28	8.0	426	426	130	0	130	Tt	30	7600	6684	−12
Blaß et al. [9] 22	Spruce solid T28	Spruce solid T28	8.0	424	424	130	0	130	Tt X	30	7075	6656	−6
Blaß et al. [9] 23	Spruce solid T28	Spruce solid T28	8.0	433	433	130	0	130	Tt	50	17,500	14,892	−15
Blaß et al. [9] 24	Spruce solid T28	Spruce solid T28	8.0	429	429	130	0	130	Tt X	50	11,950	14,773	24
Blaß et al. [9] 25	Spruce solid T28	Spruce solid T28	8.0	428	428	130	0	130	Tt	60	24,650	15,325	−38
Blaß et al. [9] 27	Spruce solid T28	Spruce solid T28	8.0	426	426	130	0	130	Tt	70	22,000	12,263	−44
Blaß et al. [9] 28	Spruce solid T28	Spruce solid T28	8.0	430	430	130	0	130	Tt X	70	26,250	12,373	−53
Blaß et al. [9] 29	Spruce solid T28	Spruce solid T28	8.0	442	442	40	0	40	Tt	45	6400	5640	−12
Blaß et al. [9] 30	Spruce solid T28	Spruce solid T28	8.0	417	417	40	0	40	Tt X	45	5100	5315	4
Blaß et al. [9] 31	Spruce solid T28	Spruce solid T28	8.0	420	420	80	0	80	Tt	45	10,300	9276	−10

Table 2 (*continued*)

Authors and [reference]	Member1	Member3	ϕ (mm)	ρ_{1m} $\left(\frac{kg}{m^3}\right)$	ρ_{3m} $\left(\frac{kg}{m^3}\right)$	l_1 (mm)	l_2 (mm)	l_3 (mm)	Screw type andlayout	θ (°)	$k_{s,exp}$ $\left(\frac{N}{mm}\right)$	$k_{s,an}$ $\left(\frac{N}{mm}\right)$	S_{an-exp} (%)
Blaß et al. [9] 32	Spruce solid T28	Spruce solid T28	8.0	434	434	80	0	80	Tt X	45	10,525	9575	−9
Blaß et al. [9] 33	Spruce solid T28	Spruce solid T28	8.0	443	443	113	0	113	Tt	45	12,600	12,394	−2
Blaß et al. [9] 34	Spruce solid T28	Spruce solid T28	8.0	455	455	113	0	113	Tt X	45	13,075	12,686	−3
Blaß et al. [9] 35	Spruce solid T28	Spruce solid T28	8.0	413	413	160	0	160	Tt	45	14,900	14,169	−5
Blaß et al. [9] 36	Spruce solid T28	Spruce solid T28	8.0	427	427	160	0	160	Tt X	45	11,650	14,562	25
Blaß et al. [9] 37	Spruce solid T28	Spruce solid T28	8.0	433	433	200	0	200	Tt	45	14,000	16,097	15
Blaß et al. [9] 38	Spruce solid T28	Spruce solid T28	8.0	446	446	200	0	200	Tt X	45	14,575	16,444	13
Tomasi et al. [7]	Spruce GL24h	Spruce GL24h	8.6	426	426	79	0	141	Dt	45	15,959	11,428	−28
Tomasi et al. [7]	Spruce GL24h	Spruce GL24h	8.6	426	426	105	0	115	Dt	30	9321	6443	−31
Tomasi et al. [7]	Spruce GL24h	Spruce GL24h	8.6	426	426	86	0	104	Dt	15	6321	3523	−44
Tomasi et al. [7]	Spruce GL24h	Spruce GL24h	8.6	426	426	90	0	100	Dt	0	2112	3237	53
Tomasi et al. [7] X	Spruce GL24h	Spruce GL24h	8.6	426	426	79	0	141	Dt X	45	14,372	11,428	−20
Tomasi et al. [7] X	Spruce GL24h	Spruce GL24h	8.6	426	426	105	0	115	Dt X	30	10,544	6443	−39
Tomasi et al. [7] X	Spruce GL24h	Spruce GL24h	8.6	426	426	86	0	104	Dt X	15	7166	3523	−51
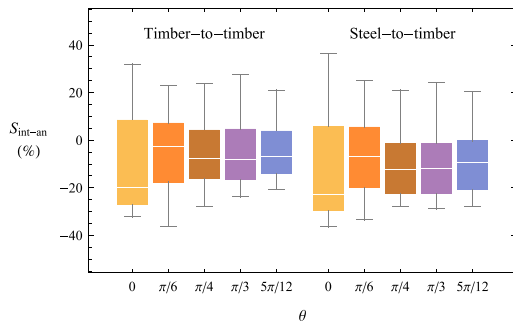
Fig. 9. Maximum, 95th percentiles, median, 5th percentiles and minimum values of the scatters between interpolating formulas and exact solution for 10,000 configurations.

timber member is in the range 75 to 175 mm, and the external diameter lays in the 6 to 18 mm interval. Eq. (13) is valid when the length of penetration in the interlayer, if present, is no more than 60 mm. Eq. (14) can be used when the interlayer thickness is not greater than 40 mm.

$$k_{s,int} = hh\rho_1^{aa} l_1^{bb} \phi^{cc} dd^{\left(\frac{ccl_2}{ddl}\right)} + ggl_2 \tag{13}$$

$$k_{s,int} = hh\rho_1^{aa-ddl_2} l_1^{bb-eel_2} \phi^{cc-ffl_2} \left(1 + 1.1^{-l_2}\right) + ggl_2 \tag{14}$$

Fig. 9 displays statistical data of the scatters between the simplified formulas and the exact solution of the analytical model for 10,000 cases with parameters randomly chosen in the domain of practical interest. The scatters are defined as: $S_{int-an} = (k_{s,int} - k_{s,an})/k_{s,an} \cdot 100\%$.

Fig. 10 shows the slip modulus predicted by the interpolation formulas in comparison to the exact solution of the analytical model and the experimental results of Table 2.

5. Parametric studies

Parametric studies were carried out using the exact solutions of developed analytical model to identify the dependence of the connection slip modulus on the system parameters. The studies are denoted as $k[discreteparameter](continuousparameter)$ and displayed in the form of

two-dimensional multi-curve graphs where one parameter is continuously varied and the other assumes some discrete values. The graphs allow the reader to investigate the dependence of the slip modulus on two parameters by arbitrarily fixing all the others. In the following graphs, together with the exact solution (solid line), the solutions of interpolating formulas (filled diamond) are reported for comparison. The values chosen for the basic parameters, unless otherwise specified, are the following: $E = 200000$ N/mm², $\phi = 8$ mm, $\rho_1 = \rho_3 = 430$ kg/m³, $\alpha = 0.66$, $\beta = 0.5$, $l_1 + l_2 + l_3 = 200$ mmfor timber-to-timber connections or $l_1 + l_2 = 100$ mmfor steel-to-timber connections, $l_1 = l_3$ and $l_2 = 40$ mm.

5.1. Timber-to-timber connections

5.1.1. $k[\phi](\theta)$ and $k[\phi](l_2)$: slip modulus variation on fastener inclination and interlayer length of penetration for divers diameters

The slip modulus is markedly affected by the screw inclination. Consistently with what was experimentally found, the highest value of slip modulus for varying θ is reached for $\theta \in [\pi/4, \pi/3]$. The fasteners with larger diameter reach the maximum value of the slip modulus for lower θ compared to those of smaller diameter (Fig. 11 (a)). The parametric studies carried out show that joints made with small diameter screws lose almost all of their stiffness when the fastener approaches the orthogonal position with respect to the sliding plane (e.g. red line of Fig. 11 (a)). However, when $\theta = \pi/4$ (e.g. red line of Fig. 11 (b)), these joints are also characterized by a lower loss of stiffness as the thickness of the intermediate layer increases compared to joints with greater screws diameters.

5.1.2. $k[l_1/l_3](\theta)$ and $k[l_2](\theta)$: slip modulus variation on fastener inclination for divers length of penetration ratio and interlayer length of penetration

The parametric study displayed in Fig. 12 (a) shows that with constant screw length and interlayer penetration length, the best performance with inclined fastener is obtained with the same screw penetration lengths. As l_1/l_3 becomes greater than 2 or smaller than 0.5, the slip modulus quickly decreases. In the $\theta \in [0, \pi/12]$ region, i.e. when the flexural behavior of the screws prevails, the slip modulus is constant with l_1/l_3.

Despite the presence of an intermediate layer that makes the arrangement of the layers not symmetrical with respect to the sliding plane, the system has a similar behavior, showing no appreciable difference when the ratio l_1/l_3 is inverted. For smaller angles of inclination,
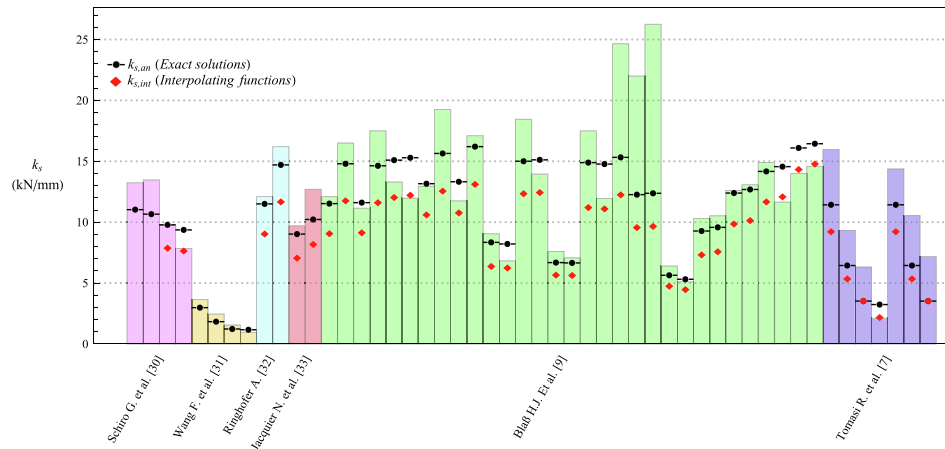
Fig. 10. Comparison between experimental mean (bars) and predicted stiffness values.

Table 3

Coefficients of interpolating formulas for timber-to-timber connections.

θ	aa	bb	cc	dd	ee
0	1.11	0.103	1.10	0.852	0.0814
$\pi/6$	1.04	0.598	0.676	0.965	0.274
$\pi/4$	1.05	0.695	0.657	0.988	0.325
$\pi/3$	1.07	0.755	0.608	0.993	0.266
$5\pi/12$	1.13	0.846	0.489	0.996	0.106

the slip modulus decreases much faster than for inclined fasteners as the length of penetration in the intermediate layer increases (Fig. 12 (b)).

5.1.3. $k[\rho_1/\rho_3](\theta)$: slip modulus variation on fastener inclination for divers pairs of densities

In both the case of a connection with and without an intermediate layer (Fig. 13 (a)) and with $l_1 = l_3$, the parametric studies show that by doubling the density of any of the two members leads to the same increase in slip modulus. Conversely it should be noted that assuming $l_3 > l_1$, the greatest benefit is obtained by increasing the density of the member with lower penetration length (Fig. 13 (b)).

Table 4

Coefficient of interpolating formulas for steel-to-timber connections.

θ	aa	bb	cc	dd	ee	ff	gg	hh
0	1.02	0.0748	1.24	−0.0259	−0.00220	0.0467	0.623	0.220
$\pi/6$	1.14	0.622	0.790	0.870	0.201	0.266	36.2	0.0886
$\pi/4$	1.14	0.710	0.621	0.192	0.0716	1.08	84.5	0.172
$\pi/3$	1.17	0.773	0.549	0.610	0.413	1.44	108	0.145
$5\pi/12$	1.20	0.857	0.449	0.9996	541	1.75	46.4	0.0656
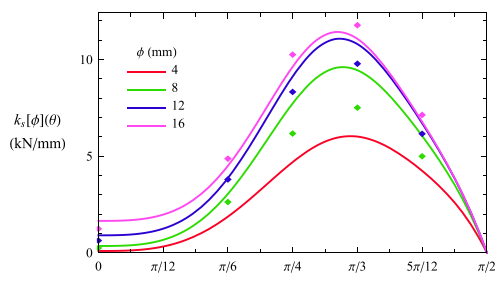
(a)
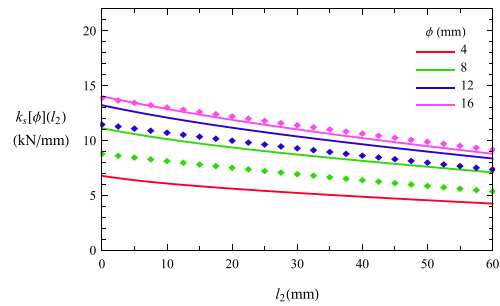
(b)

Fig. 11. Timber-to-timber connections: (a) Slip modulus variation on fastener inclination for diameters ranging from 4 to 16 mm with 4 mm steps; (b) Slip modulus variation on interlayer length of penetration for $\theta = \pi/4$ with constant screw length and $l_1 = l_3$.
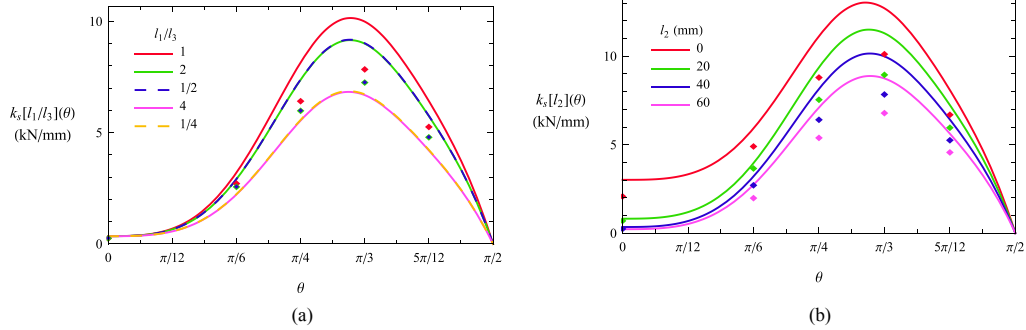
Fig. 12. Timber-to-timber connections: (a) Slip modulus variation on fastener inclination for length of penetration ratio l_1/l_3 ranging from $1/4$ to 4 with constant screw length and interlayer length of penetration; (b) Slip modulus variation on fastener inclination for interlayer length of penetration ranging from 0 to 60 mm with constant screw length and $l_1 = l_3$.

5.2. Steel-to-timber connections

5.2.1. $k[\phi](\theta)$ and $k[\phi](l_2)$: slip modulus variation on fastener inclination and interlayer length of penetration for divers diameters

The parametric studies displayed in Fig. 14 are similar to those in Fig. 11 for timber-to-timber connections. An even stronger dependence of the slip modulus on the θ parameter is highlighted. Due to the lack of a constraint preventing the rotation of the fastener in $x = l_1 + l_2$, steel-to-timber connections demonstrate lower slip modulus than the corresponding timber-to-timber connections in the region where the flexural stiffness contribution (k_{fl} in Eq. (3)) prevails (i.e. $\theta \in [0, \pi/12]$). For higher inclination values, despite the higher l_2/l, steel-to-timber connections show greater slip modulus than the corresponding timber-to-timber joints.

5.2.2. $k[l_2](\theta)$: slip modulus variation on fastener inclination for divers interlayer length of penetration

Performance degradation for increasing l_2 occurs faster than for the corresponding timber-to-timber connections (Fig. 15 and Fig. 14 (b)). It is worth noting that in the particular case of connections without an interlayer (e.g. red line of Fig. 15), in the region of $\theta \in [0, \pi/12]$ the slip modulus is higher than the slip modulus of a similar timber-to-timber connection.

6. Comparisons with other simplified models for timber-to-timber connections

The equation provided by EN 1995–1-1 [6] in Table 7.1, Eq. (15),

relates the slip modulus to the average density of the timber members and the screw outer thread diameter. There is no dependence on the penetration length of the fastener.

$$k_{s,EC5} = \frac{\rho_m^{1.5}\phi}{23} \tag{15}$$

By comparing Eq. (15) with Eq. (12), it can be observed that although the penetration length appears in the proposed simplified formula, there is only a weak dependence on it for screws perpendicular to the sliding plane (i.e. l_1 and l_3 have exponent $bb = 0.103$ in Eq. (12)). The diameter dependence is also similar in the two formulations (i.e. ϕ has exponent $cc = 1.11$ in Eq. (12)).

Eq. (15) returns value in excellent agreement with the exact solution of the proposed analytical model for the configuration with screws perpendicular to the sliding plane tested by Tomasi ($k_{s,EC5} = 3269$ N/mm and $k_{s,an} = 3237$ N/mm), but both are distant from the experimental results (Table 2). The proposed analytical model returns rather accurate results for the tests performed by Wang ($+22\%$) (Table 2), while the Eurocode formulation provides values 220% higher ($k_{s,EC5} = 3054$ N/mm) than the corresponding experimental data.

Tomasi et al. [7] proposed the formulation of Eq. (16). $K_\perp$ is given by Eq. (15) assuming $\phi = 1.1\phi_{core}$ and $K_\parallel$ must be determined experimentally or in accordance with formulation provided by the producer of the screws in the corresponding European Technical Approval Guideline (ETAG).

$$k_{s,Tom} = K_\perp \cos\theta(\cos\theta - \mu\sin\theta) + K_\parallel \sin\theta(\sin\theta + \mu\cos\theta) \tag{16}$$

The authors state that strictly speaking $K_\parallel$ is given by the resulting

Fig. 13. Timber-to-timber connections: (a) Slip modulus variation on fastener inclination for divers pairs of values of ρ_1 and ρ_3 with a base density of ρ_0, and $l_1 = l_3$ and (b) with $l_1/l_3 = 0.6$.
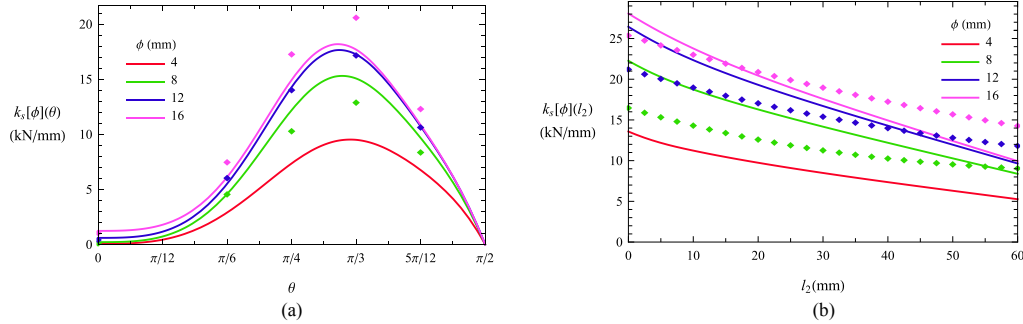
Fig. 14. Steel-to-timber connections: (a) Slip modulus variation on fastener inclination for diameters ranging from 4 to 16 mm with 4 mm steps; (b) Slip modulus variation on interlayer thickness for $\theta = \pi/4$ with constant screw length.
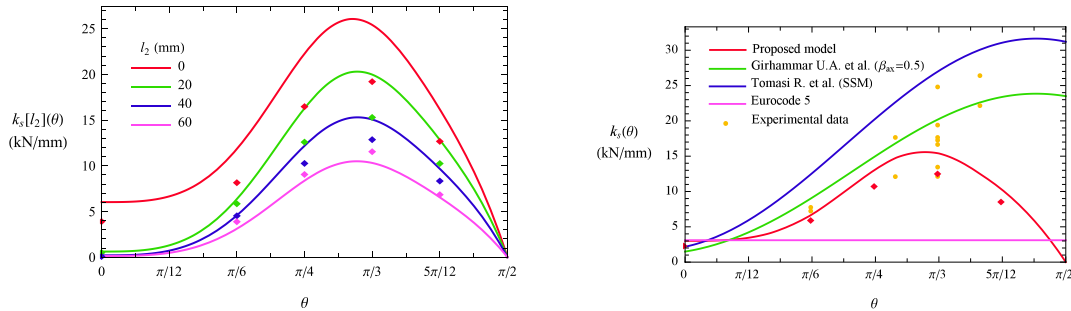
Fig. 15. Steel-to-timber connections: Slip modulus variation on fastener inclination for interlayer length of penetration ranging from 0 to 60 mm with constant screw length.

Fig. 16. Comparison between experimental mean (points) and predicted (solid line: exact solution, filled diamond: interpolating formulas) stiffness values for Blaß et al. [9] test n°: 2, 4, 6, 8, 10, 12, 21, 22, 23, 24, 25, 27, 28.

stiffness of two springs in series representing the axial slip modulus of each threaded part anchored into each timber element ("DSM - double stiffness model"). Nevertheless, a good correspondence with experimental results is obtained considering that the pullout of the screw takes place only in the timber element on the side of the screw head ("SSM - single stiffness model").

Compared to Eq. (16), the proposed beam on elastic foundation model returns values in between those of the double stiffness model and those of the single stiffness model for the shear-tension screw connections tested by Tomasi. It is worth nothing that Eq. (16) allows for the influence of friction on the sliding plane, but does not directly consider the dependence of $K_\perp$ and $K\|$ on the inclination of the fastener and, consequently, the anisotropy of the timber.

Girhammar et al. [8] also developed an analytical model that considers both the axial and transverse contribution of stiffness, as well as the friction on the sliding plane. Compared to the analytical model presented herein, Girhammar's et al. model is simplified as it considers a uniformly distributed withdrawal stress over the fastener length and takes into account the bending and axial flexibility of the screw only through a correction factor.

Fig. 16 shows a comparison between the proposed model and the others, together with the results of those experimental tests of Table 2 having approximately the same density and the same penetration lengths. In order to make the results comparable with all the mentioned models, the chosen configurations are all characterized by $l_1 = l_3$, $l_2 = 0$, $\rho_1 = \rho_3$. The models of Tomasi and Girhammar have been applied consistently with what the authors themselves did in the experimental comparisons of [7] and [8]. For both models $\mu = 0.25$ was adopted.

For $\theta \in [0, \pi/3]$ the proposed model and the model of Girhammar return slip modulus values which, with a good approximation, are in agreement with each other and with the experimental results, while the model of Tomasi overstimates the slip moduli. For $\theta > \pi/3$ the results of the proposed model differ qualitatively from those of the other two models. While for the proposed model when $\theta \to \pi/2$, $k_s \to 0$ (the thickness of the members $\to 0$ for constant screw length), for the models of Tomasi and Girhammar this limit case, which is far outside the applications range of interest, is characterized by the maximum value of slip modulus.

7. Conclusions

Two analytical models based on the theory of the beam on elastic foundation were developed for the calculation of the slip modulus of timber-to-timber and steel-to-timber connections. The foundation modulus was correlated to the density of the timber members and to the diameter of the screw. As a result, the dependence of the slip modulus on the diameter is not only linked to the axial and flexural stiffness of the fastener itself, but also to the timber-fastener interaction.

The model for timber-to-timber connection was validated on the results of push-out tests. The wide range of variation of the geometric and mechanical parameters of the configurations tested ensures the reliability of the analytical model for almost all cases of technical interest.

The parametric studies carried out confirmed that the use of inclined screws leads to significant increases in stiffness (an order of magnitude). Compared to screws perpendicular to the sliding plane, inclined screws

are characterized by a lower degradation of performance as the diameter decreases or the thickness of the interlayer increases. The slip modulus of TTC with inclined screws is limited by the weakest timber layer, i.e. the layer characterized by the smallest product between the density and penetration length of the screw with the appropriate power coefficients (Eq. (11)). Conversely, the slip modulus of screws perpendicular to the sliding plane depends upon the sum of the products between the density and penetration length of the screw with the appropriate power co-efficients of both timber members (Eq. (12)).

Simplified formulas were derived by interpolating the solutions of the analytical model calculated over a wide range of parameters of technical interest. These formulas were found to be sufficiently accurate to reflect the dependence of the slip modulus on the main parameters of the systems, namely: timber member densities, lengths of penetration in the timber members and external diameter of the screw. This proposal may be implemented in codes of practice such as the Eurocode 5 where no formula is currently given for connections with inclined screws and connections with interlayers.

Further experimental tests and studies are necessary for the validation of the proposed analytical model for steel-to-timber connections and to evaluate and predict with advanced models [35] the cyclical behavior of inclined screws. Further experimental tests and numerical simulations are also needed to better understand when the friction on the sliding surface offers a significant and reliable contribution to the slip modulus of the connection and the influence of thicker interlayers.

Funding

CRediT authorship contribution statement

Yuri De Santis: Methodology, Software, Validation, Formal analysis, Investigation, Data curation, Writing - original draft, Writing - review & editing, Visualization. **Massimo Fragiacomo:** Conceptualization, Methodology, Resources, Writing - original draft, Writing - review & editing, Supervision.

Declaration of Competing Interest

The authors declare that they have no known competing financial interests or personal relationships that could have appeared to influence the work reported in this paper.

References

[1] Giongo I, Piazza M, Tomasi R. Out of plane refurbishment techniques of existing timber floors by means of timber to timber composite structures. Proceedings of WCTE 2012 – World Conference on Timber Engineering, Auckland, Canada, July 16-19; 2012.

[2] Yeoh D, Fragiacomo M, De Franceschi M, Heng Boon K. State of the art on timber-concrete composite structures: literature review. J Struct Eng 2010;137(10): 1085–95. https://doi.org/10.1061/(ASCE)ST.1943-541X.0000353.

[3] Hassanieh A, Valipour HR, Bradford MA. Experimental and numerical study of steel-timber composite (STC) beams. J Constr Steel Res 2016;122:367–78. https://doi.org/10.1016/j.jcsr.2016.04.005.

[4] Turrini G, Piazza M. Una tecnica di recupero statico dei solai in legno. Rivista tecnica. Recuperare no. 5, 6, 7; 1983.

[5] Benedetti F, Rosales V, Opazo Vega A, Norambuena Contreras J, Jara Cisterna A. Experimental and numerical evaluation of hold-down connections on radiata pine Cross-Laminated-Timber shear walls: a case study in Chile. Eur J Wood Wood Prod 2019;77:79–92. https://doi.org/10.1007/s00107-018-1365-1.

[6] European Committee for Standardization (CEN). EN 1995-1-1:2004 (E). Eurocode 5 Design of timber structures: CEN; 2004.

[7] Tomasi R, Crosatti A, Piazza M. Theoretical and experimental analysis of timber-to-timber joints connected with inclined screws. Constr Build Mater 2010;24(9): 1560–71. https://doi.org/10.1016/j.conbuildmat.2010.03.007.

[8] Girhammar UA, Jacquier N. Källsner, Stiffness model for inclined screws in shear-tension mode in timber-to-timber joints. Eng Struct 2017;136:580–95. https://doi.org/10.1016/j.engstruct.2017.01.022.

[9] Blaß HJ, Steige Y. Steifigkeit axial beanspruchter Vollgewindeschrauben. Karlsruhe: KIT Scientific Publishing; 2018. https://doi.org/10.5445/KSP/1 000085040.

[10] Di Nino S, Gregori A, Fragiacomo M. Experimental and numerical investigations on timber-concrete connections with inclined screws. Eng Struct 2020;209. https://doi.org/10.1016/j.engstruct.2019.109993.

[11] Symons D, Persaud R, Stanislaus H. Slip modulus of inclined screws in timber–concrete floors. Proc Instit Civ Engineers – Struct Build 2010;163(4): 245–55. https://doi.org/10.1680/stbu.2010.163.4.245.

[12] Iraola B, Cabrero JM, Basterrechea-Arévalo M, Gracia J. A geometrically defined stiffness contact for finite element models of wood joints. Eng Struct 2021;235: 112062. https://doi.org/10.1016/j.engstruct.2021.112062.

[13] Avez C, Descamps T, Serrano E, Léoskool L. Finite element modelling of inclined screwed timber to timber connections with a large gap between the elements. Eur J Wood Prod 2016;74:467–71. https://doi.org/10.1007/s00107-015-1002-1.

[14] European Committe for Standardization (CEN). SS-EN 383:2007 - Timber Structures - Test methods - Determination of embedding strength and foundation values for dowel type fasteners; 2007.

[15] ASTM International. ASTM D5764-97a Standard Test Method for Evaluating Dowel-Bearing Strength of Wood and Wood-Based Products (Reapproved 2007).

[16] ISO/TC 165. ISO 10984-2:2009 - Timber structures - Dowel-type fasteners - Part 2: Determination of embedding strength; 2009.

[17] Santos CL, De Jesus AMP, Morais JJL, Lousada JLPC. A comparison between the EN 383 and ASTM D5764 test methods for dowel-bearing strength assessment of wood: experimental and numerical investigations. Strain 2010;46:159–74. https://doi.org/10.1111/j.1475-1305.2008.00570.x.

[18] Hwang K, Komatsu K. Bearing properties of engineered wood products I: effects of dowel diameter and loading direction. J Wood Sci 2002;48:295–301. https://doi.org/10.1007/BF00831350.

[19] Gattesco N. Strength and local deformability of wood beneath bolted connectors. J Struct Eng 1998;124(2):195–202.

[20] Gattesco N, Toffolo I. Experimental study on multiple-bolt steel-to-timber tension joints. Mater Struct 2004;37(2):129–38. https://doi.org/10.1007/BF02486609.

[21] Karagiannis V, Málaga-Chuquitaype C, Elghazouli AY. Modified foundation modelling of dowel embedment in glulam connections. Constr Build Mater 2016; 102:1168–79. https://doi.org/10.1016/j.conbuildmat.2015.09.021.

[22] Tuhkanen E, Mölder J, Schickhofer G. Influence of number of layers on embedment strength of dowel-type connections for glulam and cross-laminated timber. Eng Struct 2018;176:361–8. https://doi.org/10.1016/j.engstruct.2018.09.005.

[23] Franke S, Magnière N. The embedment failure of european beech compared to spruce wood and standards. In: Aicher S., Reinhardt HW, Garrecht H, editors. Materials and Joints in Timber Structures. RILEM Bookseries, vol 9. Dordrecht: Springer; 2014, p. 221–29. https://doi.org/10.1007/978-94-007-7811-5_21.

[24] Lederer W, Bader TK, Muszyński L, Eberhardsteiner J. Exploring a multi-modal experimental approach to investigation of local embedment behaviour of wood under steel dowels. Strain 2016;52:531–47. https://doi.org/10.1111/str.12199.

[25] Lederer W, Bader TK, Unger G, Eberhardsteiner J. Influence of different types of reinforcements on the embedment behavior of steel dowels in wood. Eur J Wood Prod 2016;74:793–807. https://doi.org/10.1007/s00107-016-1058-6.

[26] Schweigler M, Bader TK, Hochreiner G, Unger G, Eberhardsteiner E. Load-to-grain angle dependence of the embedment behavior of dowel-type fasteners in laminated veneer lumber. Constr Build Mater 2016;126:1020–33. https://doi.org/10.1016/j.conbuildmat.2016.09.051.

[27] Schweigler M, Bader TK, Bocquet JF, Lemaitre R, Sandhaas C. Database of embedment parameters from soft- and hardwoods. Växjö, Sweden: Linnaeus University; 2019. http://urn.kb.se/resolve?urn=urn:nbn:se:lnu:diva-87945.

[28] UNI EN 26891. Timber structure – Joints made with mechanical fasteners – General principles for the determination of strength and deformation characteristic. CEN; 1991.

[29] Wolfram Mathematica computer software, v.10.0, Wolfram Research.

[30] Schiro G, Giongo I, Sebastian W, Riccadonna D, Piazza M. Testing of timber-to-timber screw-connections in hybrid configurations. Constr Build Mater 2018;171: 170–86. https://doi.org/10.1016/j.conbuildmat.2018.03.078.

[31] Wang F, Wang X, Cai W, Chang C, Que Z. Effect of inclined self-tapping screws connecting laminated veneer lumber on the shear resistance. BioResources 2019; 14(2):4006–21. https://doi.org/10.15376/biores.14.2.4006-4021.

[32] Ringhofer A. Stiffness Properties of Axially Loaded Self-Tapping Screws. COST-STSM-FP1402-30283. Graz; 2016.

[33] Jacquier N, Girhammar UA. Tests on glulam–CLT shear connections with double-sided punched metal plate fasteners and inclined screws. Constr Build Mater 2014; 72:444–57. https://doi.org/10.1016/j.conbuildmat.2014.08.095.

[34] Giongo I, Piazza M, Tomasi R. Investigation on the self tapping screws capability to induce internal stress in timber elements. Adv Mater Res 2013;778:604–11. https://doi.org/10.4028/www.scientific.net/AMR.778.604.

[35] Aloisio A, Alaggio R, Köhler J, Fragiacomo M. Extension of generalized Bouc-Wen hysteresis modeling of wood joints and structural systems. J Eng Mech 2020;146 (3):04020001. https://doi.org/10.1061/(ASCE)EM.1943-7889.0001722.

4.10 Paper: *Slip modulus formulas for timber-to-timber inclined screw connections – Comparison with other simplified models*

The following paper deal with timber-to-timber screw connections without interlayers and focus on comparing the proposed model with existing models from literature. The proposed model is described by equations Eqs. 4.10 and 4.12.

Slip modulus formulas for timber-to-timber inclined screw connections – Comparison with other simplified models

Yuri De Santis, Department of Civil, Building-Construction and Environmental Engineering, University of L'Aquila, 67100 L'Aquila, Italy

Massimo Fragiacomo, Department of Civil, Building-Construction and Environmental Engineering, University of L'Aquila, 67100 L'Aquila, Italy

1 Introduction

Joints made with dowel-type fasteners are among the most commonly used types of connections in timber engineering. In particular the self-tapping screws, thanks to the speed and ease of installation and the possibility of arranging them in various geometric configurations, are well suited for use in composite floors and beams. The high values of withdrawal stiffness of the screws and the possibility of arranging them inclined with respect to the sliding plane lead to connections with high slip modulus and consequently high performance of the composite element in terms of strength and stiffness.

According to the current *Eurocode 5* (2004) the slip modulus k_{ser} per shear plane per fastener under service load for joints made with dowel-type fasteners is related to the mean density ρ_m (2) and the diameter d by (1).

$$K_{ser,EC5} = \rho_m^{1.5}d/23 \qquad (1)$$

$$\rho_m = \sqrt{\rho_{m,1}\rho_{m,2}} \qquad (2)$$

The current formulation lacks parameters such as the length of penetration of the screw into the timber members and the angle of inclination with respect to the sliding plane which numerous studies have shown to be closely related to the slip modulus of connections with inclined screws, e.g. *Tomasi et al.*(2010), *Girhammar et al.*(2017) and *Blass & Steige* (2018).

According to the formulation (3) proposed by *Tomasi et al.*(2010), the sliding modulus of a joint with inclined screw can be determined starting from the lateral stiffness defined for the orthogonal screws in *Eurocode 5* (2004) $K_\perp$ (1) where the effective screw diameter is used $d_{ef}=1.1d_{core}$ and the withdrawal stiffness $K_\parallel$ calculated using experimentally derived interpolation laws, e.g. *Blass et al.*(2006), *Ringhofer et al.*(2015), and *Blass & Steige* (2018). The authors suggest the expression given in the technical approval of the SFS-Intec WT-T screws (4) for the calculation of $K_\parallel$ where s_g is the embedment length of the threaded segment of the screw, and d is the outer diameter of the screws thread (*Allgemeine baufsichliche Zulassung*, 2006).

$$k_{ser,Tom}=K_\perp \cos\vartheta \left(\cos\vartheta -\mu \sin\vartheta\right)+K_\parallel \sin\vartheta \left(\sin\vartheta +\mu \cos\vartheta\right) \tag{3}$$

$$K_\parallel=30s_g d \tag{4}$$

An analytical formulation for the calculation of withdrawal stiffness that still requires a regression analysis on the experimental results, was proposed by *Stamatopoulos et al.*(2016). An alternative approach to the problem was proposed by *Girhammar et al.*(2017), in this case the formulation (5) for the slip modulus was derived from an analytical model that considers the screw as a rigid body on elastic springs.

$$k_{ser,Gir}=\frac{1}{2}K_{h,1}d_h l_1 \frac{2-\dfrac{s_1}{x_1}}{1+\dfrac{x_2}{x_1}} \cos\vartheta \left(\cos\vartheta -\mu \sin\vartheta\right)+ \tag{5}$$

$$+K_{ax,eff,1}\pi d_{ax} l_{thr,1} \frac{1}{1+(1/\beta_{ax})(l_{thr,1}/l_{thr,2})} \sin\vartheta \left(\sin\vartheta +\mu \cos\vartheta\right)$$

Where the embedment stiffness of the timber per unit area $K_{h,1}$ must be determined experimentally via embedment test and effective axial withdrawal stiffness per unit area $K_{ax,eff,1}$ can be determined from (4). The authors, to account for the flexibility and extensibility of the screw in approximate manner, suggest expressions of corrective coefficients to be applied to $K_{h,1}$ and $K_{ax,eff,1}$ depending on the geometry and mechanical properties of the system.

The final draft revision of the connections chapter of Eurocode 5 (*Revision of Eurocode 5*, 2021) suggests the formulation (6) analogous to the one proposed by *Tomasi et al.*(2010) (3). The mean slip modulus per fastener in lateral direction $K_{ser,v}$ is given by (1) and should be reduced by 50% for connection members loaded perpendicular to grain. As discussed by *Tomasi et al.*(2010), from a theorical point of view, the withdrawal contribution $K_{ser,ax}$ should be determined by considering the simultaneous pull-out of the two threaded portions of the screw from both timber members (DSM: Double-Stiffness-Model) and therefore $K_{ser,ax}$ of (6) is the resulting withdrawal stiffness of two springs placed in series each of stiffness calculated according to the experimentally derived interpolation law (7) found by *Blass H.J. & Steige Y.* (2018) where d is the outer diameter of the screws thread. The same authors, due to a better correspondence between experimental results and model predictions, suggest to

consider only the withdrawal stiffness of the portion of the screw inserted in the member on the head side (SSM: Single-Stiffness-Model). In this work DSM is considered for the EC5 proposal, while SSM is considered for Tomasi et al. model.

$$k_{ser,EC5P}=K_{ser,v} \cos \vartheta \, (\cos \vartheta - \mu \sin \vartheta) + K_{ser,ax} \sin \vartheta \, (\sin \vartheta + \mu \cos \vartheta) \qquad (6)$$

$$K_{ser,ax}=2d^{0.6} l_w^{0.6} \rho_m^{0.9} \qquad (7)$$

The aim of the work presented herein is to propose simplified but more accurate formulas to predict the sliding modulus starting from the geometric characteristics and timber member densities of the connection. These formulas, based on an analytical model taking into account the timber anisotropy and the axial and flexural stiffness of the screws, are then compared with current literature proposals. A modification of the new formulation proposed in the revision of EN 1995-1-1 is then suggested.

2 Proposed formulas derivation

The model used for the derivation of the proposed simplified formulas consist of a beam on two layers of continuous elastic springs, one parallel and the other perpendicular to the sliding plane. The beam on elastic foundation model has been previously applied by *Symons et al.*(2010) and *Di Nino et al.*(2020) for the slip modulus prediction of timber-concrete connections. The model has been extended to the case of timber-timber connections.
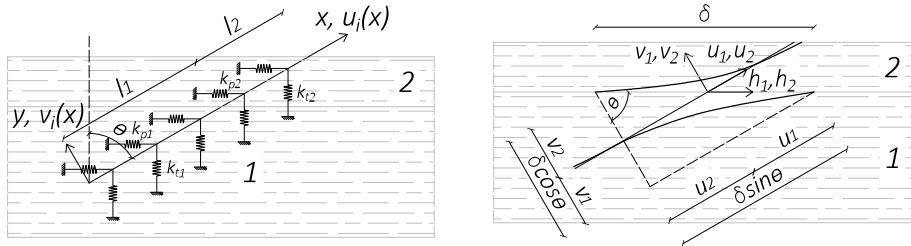
Figure 1 Analytical model representation. (a) Division into domains; (b) Initial and deformed configuration of the beam representing the screw

By assuming small strains and small displacements and by adopting linear kinematics, the elastic problem of an inclined beam on elastic foundation is governed by Eqs. (8) for the *i*-th domain. $u_i(x)$ and $v_i(x)$ denote the displacement of fields in axial and transverse direction respectively for the *i*-th domain, ϑ is the angle between the normal of the sliding plane and the fastener (Figure 1) and K_{xxi}, K_{xyi}, K_{yxi}, K_{yyi} are defined by Eqs. (9).

$$K_{xx_i}(\vartheta)u_i(x)+K_{xy_i}(\vartheta)v_i(x)-EAu_i''(x)=0$$

$$K_{yx_i}(\vartheta)u_i(x)+K_{yy_i}(\vartheta)\,v_i(x)+EIv_i''''(x)=0 \tag{8}$$

$$K_{xx_i}(\vartheta)=\cos\vartheta\sin\vartheta\,(k_{t_i}\cos\vartheta+k_{p_i}\sin\vartheta)$$

$$K_{yyi}(\vartheta)=k_{p_i}\cos^3\vartheta+k_{t_i}\sin^3\vartheta$$

$$K_{xy_i}(\vartheta)=\cos\vartheta\sin\vartheta\,(-k_{p_i}\cos\vartheta+k_{p_i}\sin\vartheta)$$

$$K_{yx_i}(\vartheta)=K_{xy_i}(\vartheta) \tag{9}$$

EA and EI represent the axial and flexural stiffness of the beam respectively. E is the elastic modulus of the steel, A is the section area and I is the second moment of area. It should be noted that due to the complex geometry of the screws whose central section is often of reduced crossed section due to the lack of thread, it is not easy to identify the diameters to be used for the calculation of the axial and bending stiffness. Preliminary studies have shown a good correspondence with the experimental results when the external diameter of the thread is adopted for the axial stiffness calculation, while the internal diameter of the thread is adopted for the bending stiffness calculation ($A = \pi\phi^2/4$ and $I = \pi\phi_{inn}^4/64$).

k_{pi} and k_{ti} in Eqs. (9) represent the stiffnesses of the two layers of springs (Figure 1). The stiffness of the springs parallel to the sliding plane can be determined starting from the experimental foundation modulus deriving from embedment tests carried out parallel to the grain: $k_{pi}=Kf_0\phi$. On the basis of the results of embedment tests performed in the orthogonal direction with respect to the grain and as also done in by *Symons et al.*(2010) and *Di Nino et al.*(2020), perpendicular spring stiffness can be taken as $k_{ti}= \beta k_{pi}$ with $\beta= 0.5$. Interpolation laws Eq. (10) for sawn timber (ST), glued laminated timber (GL) and cross laminated timber (CLT) and Eq. (11) for laminated veneer lumber (LVL), parallel strand lumber (PSL), laminated strand lumber (LSL) and plywood (PLY) was found based on thirty-eight embedment tests results. The interpolated data come from the following experimental campaigns (Figure 2): *Gattesco* (1998), *Gattesco and Toffolo* (2004), *Santos et al.*(2010), *Karagiannis et al.*(2016), *Tuhkanen et al.*(2018), *Franke et al.*(2014), *Lederer et al.*(2016), *Schweigler et al.*(2016), *Hwang et al.*(2002), *Lemaitre et al.*(2019) and *Schweigler et al.*(2019).

$$K_{f0}(\rho,\phi)=-147.8+\frac{30.9\,\rho^{0.46}}{\phi^{0.32}} \tag{10}$$

$$K_{f0}(\rho,\phi)=-62.3+\frac{0.0282\,\rho^{1.41}}{\phi^{0.23}} \tag{11}$$
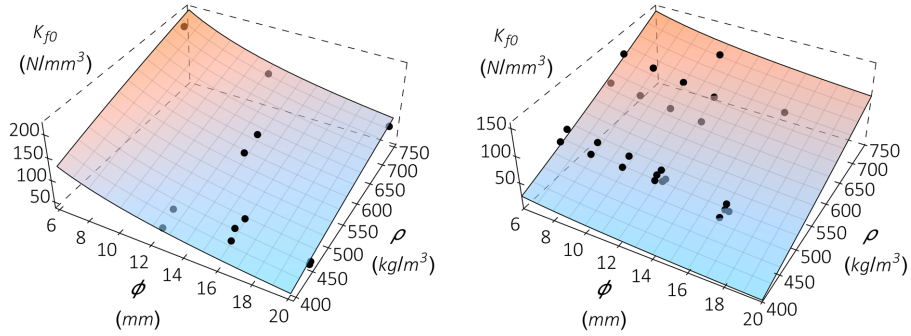
Figure 2 Experimental data and interpolating functions of the foundation modulus for (a) ST, GL and XLAM and (b) LVL, PSL, LSL and PLY.

The slip modulus of the connection is given by the ratio between the component parallel to the sliding plane of the internal forces of the beam and the internal distortion δ (*Figure 1*).

$$k_{ser,An} = \frac{N_1 \sin(\vartheta) - T_1 \cos(\vartheta)}{\delta} = \frac{EA \, u_1'(l_1) \sin(\vartheta)}{\delta} + \frac{EI \, v_1'''(l_1) \cos(\vartheta)}{\delta} \tag{12}$$

The boundary conditions of described model are expressed by Eqs. (13).

$$EA \, u_1'(0) = 0$$
$$EI \, v_1''(0) = 0$$
$$-EI \, v_1'''(0) = 0 \tag{13.1}$$

$$EA \, u_1'(l_1) = EA \, u_2'(l_1)$$
$$EI \, v_1''(l_1) = EI \, v_2''(l_1)$$
$$-EI \, v_1'''(l_1) = -EI \, v_2'''(l_1)$$
$$u_1(l_1) - \delta \sin \vartheta = u_2(l_1)$$
$$v_1(l_1) + \delta \cos \vartheta = v_2(l_1)$$
$$v_1'(l_1) = v_2'(l_1) \tag{13.2}$$

$$EA \, u_2'(l_1 + l_2) = 0$$
$$EI \, v_2''(l_1 + l_2) = 0$$
$$-EI \, v_2'''(l_1 + l_2) = 0 \tag{13.3}$$

The exact solution of the analytical model was interpolated by means of the Eqs. (14) ($\vartheta=0°$ and $\vartheta=15°$) and (15) ($\vartheta\geq30°$) whose coefficients for various screw inclinations are contained in *Table 1*.

$$k_{ser,Int}= dd(\rho_1^{aa} l_1^{bb}+\rho_2^{aa} l_2^{bb}) \phi^{cc} \tag{14}$$

$$k_{ser,Int}=\frac{dd\ \phi^{cc}}{\dfrac{1}{\rho_1^{aa} l_1^{bb}} + \dfrac{1}{\rho_2^{aa} l_2^{bb}}} \tag{15}$$

Table 1. Coefficient of interpolating formulas.

ϑ (°)	aa	bb	cc	dd
0	1.04	0.056	1.11	0.18
15*	1.04	0.056	1.11	0.18
30	1.07	0.51	0.76	0.31
45	1.07	0.68	0.65	0.29
60	1.09	0.77	0.58	0.23
75	1.14	0.86	0.47	0.095

* The formula found for orthogonal screws is used.
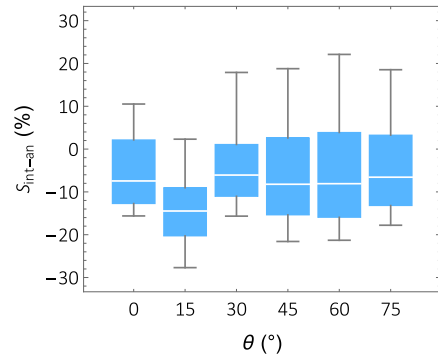
Figure 3 Figure 4 Maximum, 95th percentiles, median, 5th percentiles and minimum values of the scatters between interpolating formulas and exact solution for 3000 configurations.

The formulas has been tested for random configurations of diameters ϕ 6÷18 mm, ρ 400÷750 kg/m³, l 50÷200 mm excepts for Eqs. *(14)* for which l was limited to the interval 60÷150 mm. The scatters between the exact solution of the analytical model and simplified interpolating law are given in Figure 3.

3 Experimental verification

The slip modulus of joints made with mechanical connections can be experimentally evaluated according to the procedure described in *UNI EN 26891* (1991). The push-out test consists of a partial loading and unloading cycle followed by a second phase carried out in displacement control that ends with the reaching of ultimate load or of a sliding of 15 mm. The slip modulus is given by the slope of the secant to the first load branch of the force-slip curve for the points corresponding to 40% and 10% of the estimated maximum load (Eq. (16)).

$$k_{ser,Exp}=\frac{0.4F_{est}-0.1F_{est}}{v_{0.4}-v_{0.1}} \tag{16}$$

The reliability of the proposed model and simplified formulas was quantified and compared with the reliability of other formulations based on the results of extensive

experimental push-out test programmes. The push-out tests taken as reference were performed on connection specimens with double threaded screws and fully treaded screws placed in shear-tension or crossed configurations (Table 2).

The external thread diameter ϕ assumed in the calculations is shown in Table 2. In the case of double-threaded screws, ϕ corresponds to the average value of the two threaded sections. The inner thread diameter has been assumed: ϕ_{inn}=0.66ϕ.

The anchorage lengths used in the calculation of the withdrawal stiffness were obtained subtracting from the penetration lengths $(l_1$ and $l_2)$ of Table 2 the tip length $(l_p$=1.1$\phi)$ and, in the case of double threaded screws, the length of the central smooth section.

The friction coefficients considered for the inclined screws in shear-tension and for the crossed-screws configurations are μ=0.25 and μ=0 respectively.

In the models in which withdrawal from only one of the two members is assumed, this were considered to happen in the screw-head side (*Tomasi et al.*, 2010).

Table 2. Experimental setups description for reference experimental data.

Authors	Member 1	Member 2	ϕ (mm)	ρ_1 (kg/m^3)	ρ_2 (kg/m^3)	l_1 (mm)	l_2 (mm)	Screw type and layout	ϑ (°)
Schiro G. et al. (2018)	Beech LVL	CLT	8.3	796	465	69	81	Dt	45
	Spruce solid C24	Beech LVL GL70	8.3	460	846	91	71	Dt I	45
	Spruce solid C24	CLT	8.3	460	465	69	81	Dt	45
	Spruce solid C24	CLT	8.6	460	465	81	81	Dt I	45
Wang F. et al. (2019)	Douglas Fir LVL	Douglas Fir LVL	5.3	560	560	39	61	Tt	45
	Douglas Fir LVL	Douglas Fir LVL	5.3	560	560	50	50	Tt	30
	Douglas Fir LVL	Douglas Fir LVL	5.3	560	560	55	45	Tt	15
	Douglas Fir LVL	Douglas Fir LVL	5.3	560	560	57	43	Tt	0
Ringhofer A. (2016)	Spruce solid T24		8.0	408	408	113	113	Tt	45
			8.0	410	408	130	130	Tt	60
Jacquier N. (2014)	Spruce GL32	CLT C24	6.5	456	471	75	85	Dt	45
	Spruce GL32	CLT C24	8.2	462	459	75	85	Dt	45
Blaß H.J. et al. (2018)	Spruce solid T28		8.0	409	409	113	113	Tt	45
			8.0	412	412	130	130	Tt	60
			8.0	412	412	113	113	Tt X	45
			8.0	407	407	130	130	Tt X	60
			8.0	421	421	130	130	Tt	60
			8.0	427	427	130	130	Tt X	60
			8.0	475	475	113	113	Tt	45
			8.0	438	438	130	130	Tt	60

	8.0	482	482	113	113	Tt X	45
	8.0	456	456	130	130	Tt X	60
	6.0	424	424	85	85	Tt	45
	6.0	416	416	85	85	Tt X	45
	10.0	411	411	141	141	Tt	45
	10.0	414	414	141	141	Tt X	45
	8.0	426	426	130	130	Tt	30
	8.0	424	424	130	130	Tt X	30
	8.0	433	433	130	130	Tt	50
	8.0	429	429	130	130	Tt X	50
	8.0	428	428	130	130	Tt	60
	8.0	426	426	130	130	Tt	70
	8.0	430	430	130	130	Tt X	70
	8.0	442	442	40	40	Tt	45
	8.0	417	417	40	40	Tt X	45
	8.0	420	420	80	80	Tt	45
	8.0	434	434	80	80	Tt X	45
	8.0	443	443	113	113	Tt	45
	8.0	455	455	113	113	Tt X	45
	8.0	413	413	160	160	Tt	45
	8.0	427	427	160	160	Tt X	45
	8.0	433	433	200	200	Tt	45
	8.0	446	446	200	200	Tt X	45
	8.6	426	426	79	141	Dt	45
	8.6	426	426	105	115	Dt	30
Tomasi R. et al. (2010)	8.6	426	426	86	104	Dt	15
Spruce GL24h	8.6	426	426	90	100	Dt	0
	8.6	426	426	79	141	Dt X	45
	8.6	426	426	105	115	Dt X	30
	8.6	426	426	86	104	Dt X	15

* Tt: total thread screws, Dt: double thread screw, X: crossed screws, I: interlayer.

The slip modulus values predicted by the proposed analytical model have a good correspondence with the experimental results, both in terms of determination coefficient (Table 3) and in terms of percentage deviations (Figure 5). The slight tendency of the model to underestimate the predicted values could result from neglecting the friction on the sliding plane. The analytical model proposed by *Girhammar et al.*(2017) is characterized by a distribution of percentage deviations similar to that of the proposed model.

Although the coefficient of determination of the proposed simplified formulas is the same of that of the model of the final draft revision of Eurocode 5, proposed formu-

las have a lower 95th percentile and a lower maximum value of the percentage devia-
tions as well as a 50th percentile closer to zero. The Tomasi et al. model strongly
overestimate the slip modulus in the vast majority of cases. On the contrary, the cur-
rent formulation of the *Eurocode 5* (2004) underestimates the slip modulus in almost
all cases.
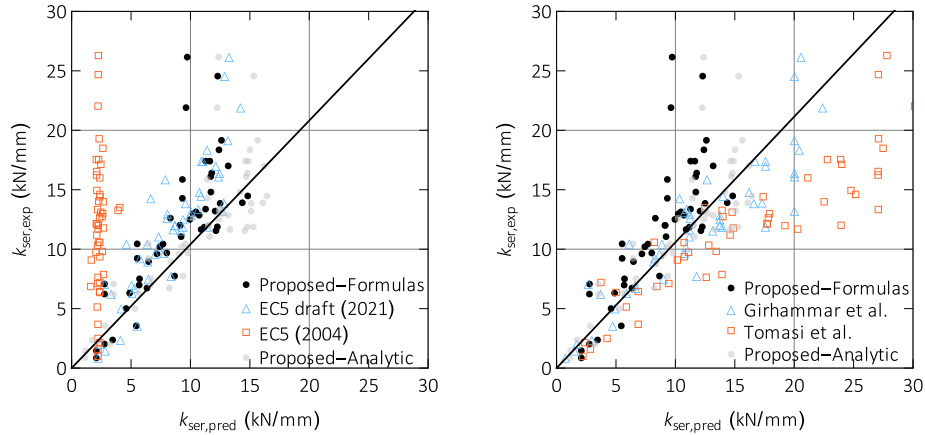
Figure 4 The observed slip modulus versus the estimated slip modulus

Table 3. Coefficient of determination.

Models	Proposed-Analytic	Proposed-Formulas	EC5 draft (2021)	EC5 (2004)	Girhammar et al.	Tomasi et al.
R^2	0.62	0.28	0.28	-3.03	0.79	-0.29
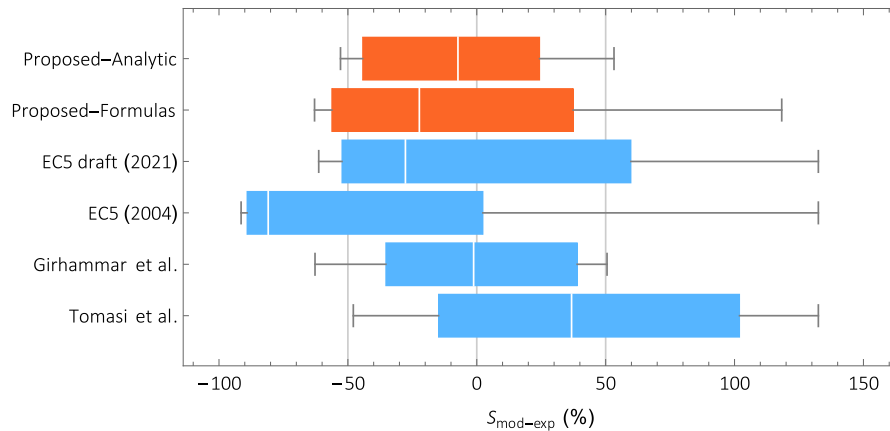
Figure 5 Maximum, 95th percentiles, median, 5th percentiles and minimum values of the scatters
between models and experimental slip modulus.

9

4   Comparison with other models through parametric studies

The qualitative and quantitative differences between the proposed analytical model and simplified formulas and the other models from literature including the new formulation in the revised EN 1995-1-1 have been studied by varying each of the significant parameters of the system such as the inclination of the screw, the diameter of the screw, the lengths of penetration and the densities of the members.

The first parametric study was performed with the aim of investigating the dependence of the slip modulus on the screw diameter (Figure 6). A symmetrical connection was considered, i.e., with member density $\rho_1=\rho_2=430$ kg/m^3 and penetration lengths $l_1=l_2=100$ mm. It is worth noting that the dependence of the slip modulus on the screw diameter is very similar between the proposed formulas and the model of *Revision of Eurocode 5* (2021). The predicted slip modulus of all other models increases, for increasing diameter, much faster than the slip modus predicted by proposed formulas and analytical model. It is also noted that the proposed formulas return values in good agreement with those of the current EC5 for orthogonal screws of diameters up to 12 mm.
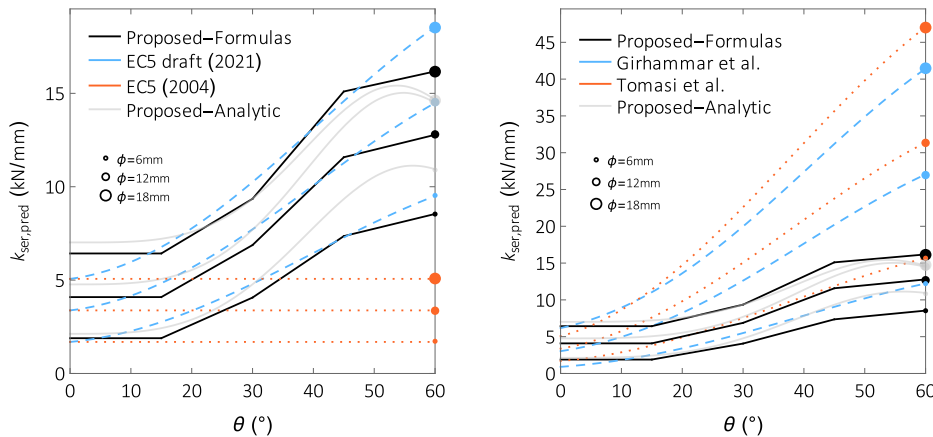
Figure 6 Models predictions for varying diameters (6, 12 and 18 mm). (a) Comparison of proposed formulas and model with standards proposal and current standard; (b) Comparison of proposed simplified formulas with exact solution of analytical model and other models.

The second parametric study aims to highlight how the expected values of the slip modulus vary when the penetration lengths in the timber members on the screw head side or tip side are doubled (Figure 7). The analyzed configuration is characterized by $\rho_1=\rho_2=430$ kg/m^3 and $\phi=8$ mm. According to the proposed model and the model of *Revision of Eurocode 5* (2021), the sliding modulus increases by the same amount by doubling the length of penetration in one or the other member. According

to the Tomasi et al. model the slip modulus increases only when the penetration length on the head side member is increased. In the Girhammar et al. model, the greatest increase is obtained by doubling the length of penetration into the member on the screw head side for which a halved withdrawal stiffness is assumed as suggested by the author.
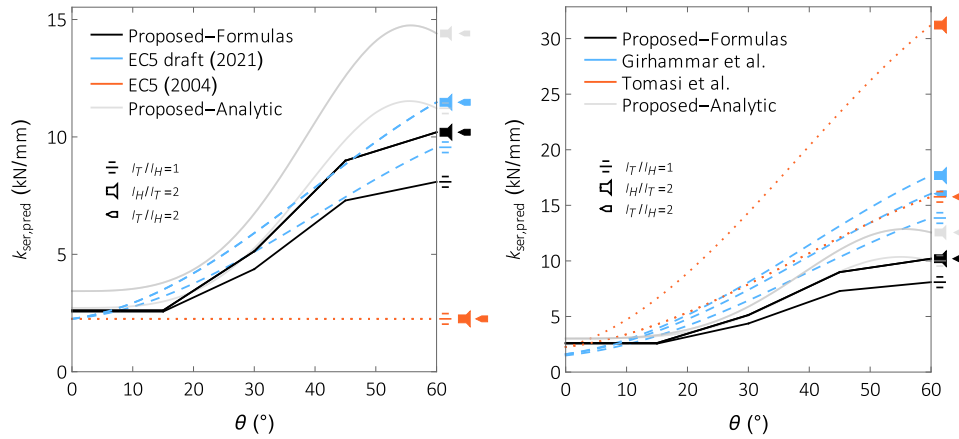
Figure 7 Models predictions for varying length penetration (l_T= l_H=75 mm, l_T=75 mm and l_H=150 mm and l_T=150 mm and l_H=75 mm). (a) Comparison of proposed formulas and model with standards proposal and current standard; (b) Comparison of proposed simplified formulas with exact solution of analytical model and other models.

The third parametric study aims to highlight how the expected values of the slip modulus vary when the density of the timber members on the screw head side or tip side are doubled (Figure 8). The analyzed configuration is characterized by l_1=l_2=100 mm and ϕ=8 mm. According to the proposed model and to the model of *Revision of Eurocode 5* (2021), the sliding modulus increases by the same amount by doubling the density of one or the other member. According to the Tomasi et al. model, the density affects only the lateral contribution, therefore doubling the density of any timber member produces the same limited increase of the slip modulus. In the Girhammar et al. model, as presented and applied by the author, the dependence of the slip modulus on density is not explicit, as the author considers experimentally derived embedment and withdrawal stiffnesses.
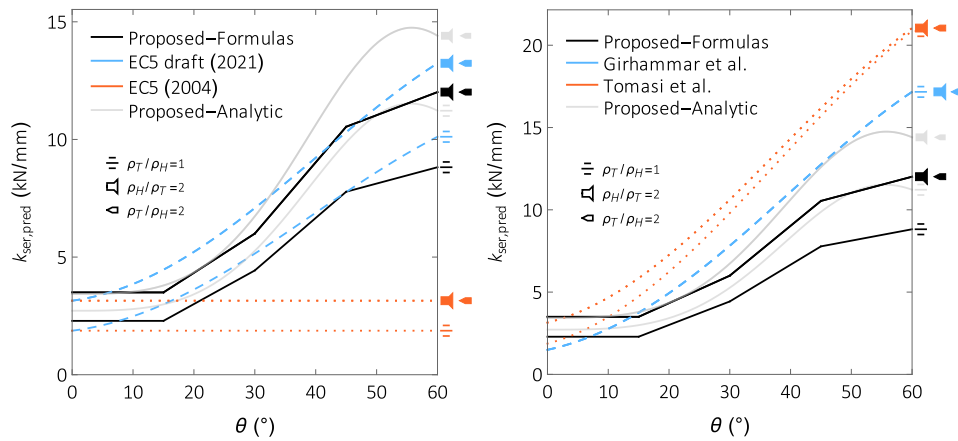
Figure 8 Models predictions for varying member densities ($\rho_1 = \rho_2 = 380$ kg/m^3, $\rho_1 = 380$ kg/m^3 and $\rho_2 = 760$ kg/m^3 and $\rho_1 = 760$ kg/m^3 and $\rho_2 = 380$ kg/m^3). (a) Comparison of proposed formulas and model with standards proposal and current standard; (b) Comparison of proposed simplified formulas with exact solution of analytical model and other models.

5   Conclusions

The derived analytical model for calculating the slip modulus of screw connections proved effective. The proposed model allows to consider the effective flexural and axial stiffness of the screw, the orthotropic behavior of the timber and the geometric and mechanical characteristics of the connection.

The interpolation functions found for the foundation elastic modulus make the model completely predictive without the need to perform withdrawal tests. Therefore, the model allows to predict the sliding modulus when the external diameter of the thread, the density of the members, the penetration lengths and the angle of inclination are known.

The reliability of the proposed analytical model is similar to that of Girhammar et al. model, but both, due to their complexity, cannot be directly implemented in standards. Simplified formulas have been obtained from the proposed analytical model. Although the expression proposed in the revision drafts of Eurocode 5 (2021) for withdrawal stiffness was derived by interpolation of the results of withdrawal tests performed on specimens with the same screws and timber as many of the push-out tests taken as a reference for the validation of the models (*Blass & Steige*, 2018), the proposed simplified formulas are more accurate than the model of *Revision of Eurocode 5* (2021).

The proposed model allows to consider the withdrawal of the screw from both members resulting more accurate than Tomasi et al. model for those configurations in which the withdrawal stiffness of the tip-side cannot be considered infinitely greater

than that on the head-side, i.e. those cases in which the density and/or the length of penetration on the tip side are significantly lower than those on the head-side.

The proposed approach may be proposed for implementation in the revised EN 1995-1-1. Furthermore, an extension of this formula could also be proposed in an Annex of EN 1995-1-1 for the prediction of the slip modulus of connections with an interlayer.

6 References

Eurocode 5 (2004): Design of timber structures - Part 1-1: General and rules for buildings. CEN. (EN 1995-1-1).

Tomasi R., Crosatti A., Piazza M. (2010): Theoretical and experimental analysis of timber-to-timber joints connected with inclined screws. Constr. Build. Mater. 24, 1560–1571.

Girhammar U.A., Jacquier N., Källsner B. (2017): Stiffness model for inclined screws in shear-tension mode in timber-to-timber joints. Eng. Struct. 136, 580–595.

Blass H.J. & Steige Y. (2018): Steifigkeit axial beanspruchter Vollgewindeschrauben. KIT Scientific Publicing, Karlsruhe.

Blass H.J., Bejtka I., Uibel T. (2006): Trägfähigkeit von Verbindung mit selbst bohrenden Holzschrauben mit Vollgewinde. Karlsruher Berichte zum Ingenieurholzbau.

Ringhofer A., Brandner R., Schickhofer G. (2015): A Universal Approach for Withdrawal Properties of Self-Tapping Screws in Solid Timber and Laminated Timber Products. INTER, Sibenik (Croatia).

Allgemeine baufsichliche Zulassung (2006): SFS Befestiger WT-T-6,5, WT-T-8,2

und WR-T-8,9 als Holzverbindungsmittel. Deutsches Institut für Bautechnik (DIBt),

Z-9.1-472, Berlin (Germany).

Stamatopoulos H., Malo K. (2016): Withdrawal Stiffness of Threaded Rods Embedded in Timber Elements. Constr. Build. Mater. 116, 263–72.

Revision of Eurocode 5 (2021): Final draft revision of chapter connections. CEN/TC 250/SC 5 N 1339. (prEN 1995-1-1).

Symons D., Persaud R., Stanislaus H. (2010): Slip modulus of inclined screws in timber–concrete floors. Proc Instit Civ Engineers – Struct Build 163(4), 245–55.

Di Nino S., Gregori A., Fragiacomo M. (2020): Experimental and numerical investigations on timber-concrete connections with inclined screws. Eng. Struct. 209.

Gattesco N. (1998): Strength and local deformability of wood beneath bolted connectors. J. Struct. Eng. 124(2), 195–202.

Gattesco N., Toffolo I. (2004): Experimental study on multiple-bolt steel-to-timber tension joints. Mater. Struct. Constr. 37(2), 129–38.

Santos C.L., De Jesus A.M.P., Morais J.J.L., Lousada J.L.P.C. (2010): A Comparison Between the EN 383 and ASTM D5764 Test Methods for Dowel-Bearing Strength Assessment of Wood: Experimental and Numerical Investigations. Strain 46, 159-174.

Karagiannis V., Málaga-Chuquitaype C., Elghazouli AY. (2016): Modified foundation modelling of dowel embedment in glulam connections. Constr. Build. Mater.102, 1168–1179.

Tuhkanen E., Mölder J., Schickhofer G. (2018): Influence of number of layers on embedment strength of dowel-type connections for glulam and cross-laminated timber. Eng. Struct. 176, 361–368.

Franke S., Magnière N. (2014): The Embedment Failure of European Beech Compared to Spruce Wood and Standards. In: Aicher S., Reinhardt HW, Garrecht H (eds) Mater. Struct. Constr. RILEM Bookseries, vol 9. Dordrecht: Springer; 221-229.

Lederer W., Bader T.K., Muszyński L., Eberhardsteiner J. (2016): Exploring a Multi-modal Experimental Approach to Investigation of Local Embedment Behaviour of Wood under Steel Dowels. Strain 52, 531-547.

Lederer W., Bader T.K., Unger G., Eberhardsteiner J. (2016): Influence of different types of reinforcements on the embedment behavior of steel dowels in wood. Eur. J. Wood Prod. 74, 793–807.

Schweigler M., Bader T.K., Hochreiner G., Unger G., Eberhardsteiner E. (2016): Load-to-grain angle dependence of the embedment behavior of dowel-type fasteners in laminated veneer lumber. Constr. Build. Mater. 126, 1020–1033.

Hwang K., Komatsu K. (2002): Bearing properties of engineered wood products I: effects of dowel diameter and loading direction. J. Wood Sci. 48, 295-301.

Schweigler M., Bader T.K., Bocquet J.F., Lemaitre R., Sandhaas C. (2019): Database of embedment parameters from soft and hardwoods. Linnaeus University, Växjö, Sweden.

UNI EN 26891 (1991): Timber structure – Joints made with mechanical fasteners – General principles for the determination of strength and deformation characteristic. CEN.

Schiro G., Giongo I., Sebastian W., Riccadonna D., Piazza M. (2018): Testing of timber-to-timber screw-connections in hybrid configurations. Constr. Build. Mater. 171, 170–186.

Wang F., Wang X., Cai W., Chang C., Que Z. (2019): Effect of Inclined Self-tapping Screws Connecting Laminated Veneer Lumber on the Shear Resistance. BioResources 14(2), 4006-4021.

Ringhofer A. (2016): Stiffness Properties of Axially Loaded Self-Tapping Screws. COST-STSM-FP1402-536 30283, Graz.

Jacquier N., Girhammar U.A. (2014): Tests on glulam–CLT shear connections with double-sided punched metal plate fasteners and inclined screws. Constr. Build. Mater. 72, 444–457.

4.11   Simplified formulas for Eurocodes

The following excerpt is taken from the draft revision of Eurocode 5. The annex proposes the adoption of the simplified formulas determined as illustrated in this Chapter. In some cases, the formulas have been slightly modified with the aim of making them more readable than those originally proposed in the research papers and in the previous Sections. Here follow, for the sake of clarity the origin of each formula is explained.

Equations EC. 1, 2, 5 and 6 descend from Eq. 12, 11, 14 and 13 of the journal paper of Section 4.9 respectively. In this cases the simplifications were made by removing the less significant terms, rounding the terms closest to the decimal and recalculating the remaining coefficients and then minimizing the mean squared error on the same dataset used in the paper.

Equations EC. 3, 4, 7 and 8 are the same of Eqs. 4.36, 4.37, 4.38 and 4.39 respectively.

The results of timber-to-timber experimental test of Chapt. 3 are compared with predicted values in Tab. 4.6. Similar comparisons are made for timber-to-steel test series in Sec. 6.2.

Name	Description	$\rho_1 = \rho_3$ (kg/m^3)	ϕ (mm)	l_1 (mm)	l_2 (mm)	l_3 (mm)	$k_{s,exp}$ (kN/mm)	$k_{s,pred}$ (kN/mm)	$S_{pred-exp}$ (%)
TT 0 8 200 R	Reference 0°	440	8	80	0	120	2.74	2.27	-17%
TT 0 8 200 S35	Soft int. 0°	440	8	74	6	120	1.57	1.62	3%
TT 0 8 200 S90	Stiff int. 0°	440	8	74	6	120	1.36	1.62	19%
TT 45 7 300 R	Reference 45°	440	7	130	0	170	14.73	9.36	-36%
TT 45 7 300 S35	Soft int. 45°	440	7	122	8	170	9.79	9.04	-8%
TT 45 7 300 S90	Stiff int. 45°	440	7	122	8	170	10.47	9.04	-14%
TT 30 7 300 S35	Soft int. 30°	440	7	155	7	139	6.86	-	-

Table 4.6: Timber-to-timber configurations parameters, prediction and experimental results.

Eurocode 5 draft revision excerpt: Annex B (normative) - Timber to timber connections

No connection between interlayer and timber

For connections made with screws and $\epsilon = 90°$, see Fig. EC.1a, the mean slip modulus per fastener $K_{\text{SLS,mean}}$ may be taken from the following expression:

$$K_{SLS,mean} = 0.09(\rho_{mean,1}^{1.1-0.02t_{h,i}} t_{h,1}^{0.1} + \rho_{mean,2}^{1.1-0.02t_{h,i}} t_{h,2}^{0.1})d^{1.1+0.032t_{h,i}} \qquad \text{(EC.1)}$$

For connections made with double or fully threaded screws and $\epsilon = 45°$, see Fig. EC.1b and c, the mean slip modulus per fastener $K_{\text{SLS,mean}}$ may be taken from the following expression:

$$K_{SLS,mean} = \frac{0.33d^{0.7}}{\frac{1}{\rho_{mean,1}t_{h,1}^{0.7}} + \frac{1}{\rho_{mean,2}t_{h,2}^{0.7}}} 0.9^{\left(\frac{t_{h,i}}{d^{2.4}}\right)} \qquad \text{(EC.2)}$$

Connection between interlayer and timber

For connections made with screws and $\epsilon = 90°$, see Fig. EC.1a, the mean slip modulus per fastener $K_{\text{SLS,mean}}$ may be taken from the following expression:

$$K_{SLS,mean} = 0.12(\rho_{mean,1}t_{h,1}^{0.1} + \rho_{mean,i}^{1.1} + \rho_{mean,2}t_{h,2}^{0.1})d^{1.1} \qquad \text{(EC.3)}$$

For connections made with fully threaded screws and $\epsilon = 45°$, see Fig. EC.1c, the mean slip modulus per fastener $K_{\text{SLS,mean}}$ may be taken from the following expression:

$$K_{SLS,mean} = \frac{0.5d^{0.7}}{\frac{0.48}{\rho_{mean,1}t_{h,1}^{0.62}} + \frac{1}{\rho_{mean,i}^{1.6}t_{h,i}^{0.4}} + \frac{1}{\rho_{mean,2}t_{h,2}^{0.62}}} \qquad \text{(EC.4)}$$
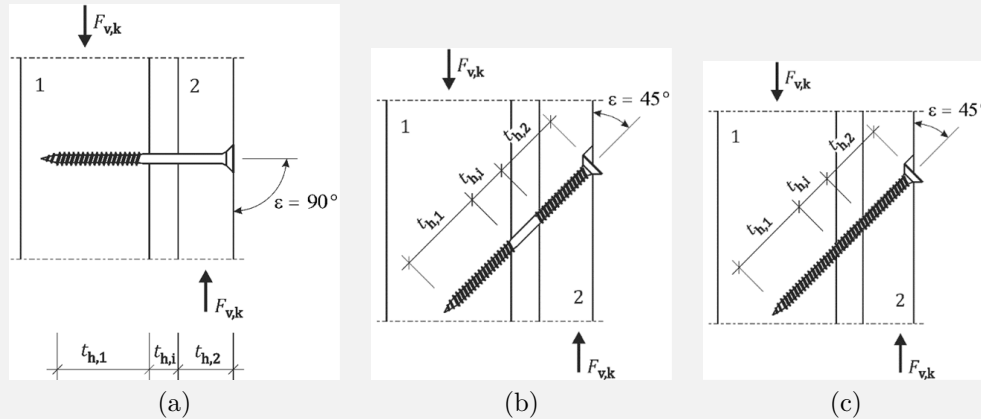
Figure EC.1: Screwed timber to timber connection.

Eurocode 5 draft revision excerpt: Annex B (normative) - Steel to timber connections

No connection between interlayer and timber

For connections made with screws and $\epsilon = 90°$, see Fig. EC.2a, the mean slip modulus per fastener $K_{\text{SLS,mean}}$ may be taken from the following expression:

$$K_{SLS,mean} = 0.27\rho_{mean,1}^{1.1-0.027t_{h,i}}t_{h,1}^{0.073-0.0026t_{h,i}}d^{1.22+0.05t_{h,i}}(1+1.1^{-t_{h,i}})+0.86t_{h,i} \tag{EC.5}$$

For connections made with partially or fully threaded screws and $\epsilon = 45°$, see Fig. EC.2b and c, the mean slip modulus per fastener $K_{\text{SLS,mean}}$ may be taken from the following expression:

$$K_{SLS,mean} = 0.25\rho_{mean,1}^{1.1}t_{h,1}^{0.7}d^{0.6}0.2^{(\frac{0.07t_{h,i}}{d^{1.1}})}+85t_{h,i} \tag{EC.6}$$

Connection between interlayer and timber

For connections made with screws and $\epsilon = 90°$, see Fig. EC.2a, the mean slip modulus per fastener $K_{\text{SLS,mean}}$ may be taken from the following expression:

$$K_{SLS,mean} = 0.9(\rho_{mean,1}^{0.8}t_{h,1}^{0.1}d^{0.4}+\rho_{mean,i}d^{1.23}) \tag{EC.7}$$

For connections made with fully threaded screws and $\epsilon = 45°$, see Fig. EC.2c, the mean slip modulus per fastener $K_{\text{SLS,mean}}$ may be taken from the following expression:

$$K_{SLS,mean} = 0.48(\rho_{mean,1}^{0.9}t_{h,1}^{0.6}d+\rho_{mean,i}^{1.2}t_{h,i}^{0.4}d^{0.4}) \tag{EC.8}$$

(a)   (b)   (c)
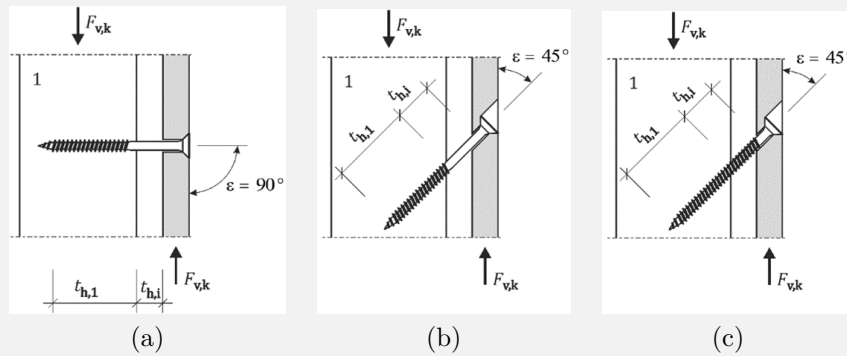
Figure EC.2: Screwed steel to timber connection.

Chapter 5

Non-linear effects on slip modulus of timber-to-timber connections: one-dimensional finite element models

Abstract: As the relative slip between the members of a connection increases, the screw deforms and the screw axis moves away from the initial undeformed configuration. As a consequence, the internal forces of the screw, namely axial and shear forces, change their direction. In most of simplified models from literature as well as in the model proposed in the previous Chapter, to simplify the problem, geometric linearity is assumed. In this Chapter, the limits of this assumption are studied. Moreover, friction on sliding plane may influence the connection behavior, even in serviceability condition. However, friction contribution is hard to be considered in a rigorous manner by analytical models. Therefore, mechanical non-linearity assumption is also verified. Lastly the influence of load application position may have an influence on the connection behavior. Push-out tests are characterized by load-reaction eccentricity while direct-shear tests not. All these aspects are investigated by a finite element method implementation of a beam on elastic foundation analogous to the model presented in the previous Chapter. Moreover, a cross-validation between analytical and finite element model is carried out.

5.1 Introduction

In this chapter a Finite Element Model for the stiffness prediction of connections with inclined screws is presented. The proposed model is similar to the analytical model presented in Sec. 4.9, but its solution is determined via Finite Element Method. The solution from the Finite Element method is first compared to the exact solution of the analytical model, then the model is improved with the aim of overcoming some limitations of the analytical one clarifying the influence of the:

- load application position;

- friction on the sliding plane;

- geometric non-linearity.

Finally the results of the improved model are compared with experimental results from literature and tests from the experimental campaign described in Chapter 3.

The improved model turned out to be more accurate than the analytical one while maintaining low the computational effort and thus resulting suitable for accurate parametric analyses.

5.2 Model definition

The problem of the determination of the slip modulus of connection with inclined screws is reduced from the point of view of mathematical dimensions by assuming a beam behavior for the screw and describing its interaction with timber by 2-node connector elements (Fig. 5.1).
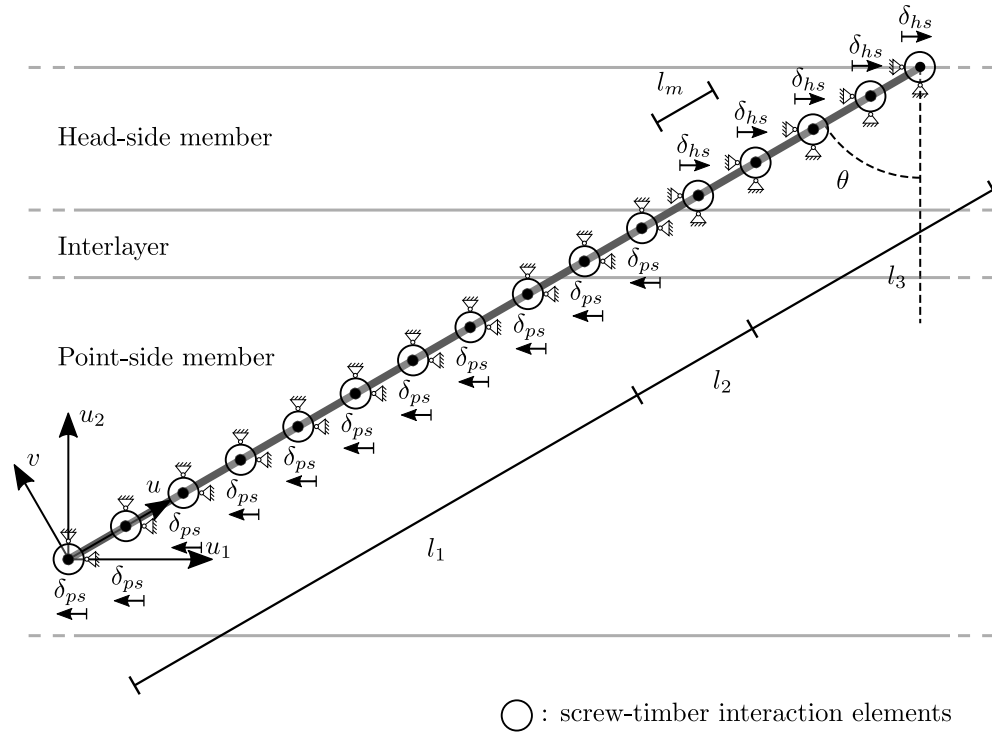
Figure 5.1: Timber-to-timber connection model.

A beam, in finite element method, is an element in which assumptions are made so that the problem is reduced to one dimension. In this way the primary solution are functions of position along the beam axis only. The fundamental assumption in the beam theory is the indeformability of the cross-section. As a first approximation the cross-section of the screw can be regarded as a solid circular section neglecting the thread contribution. Circular section belongs to the category of compact sections and therefore they are not prone to in-plane section deformation making valid the fundamental assumption.

The beam theory can provide a good approximation of a three-dimensional continuum when the axial dimension noticeably prevails on the transversal section dimensions. In general the axial dimension should be interpreted as the distance between significant discontinuities in cross-section or distance between restraints. Common screw types have negligible section variations over screw length. The small section increments are usually made in areas without threads thus causing a partial compensation of the geometric properties.

One of the most common approach to beam theory consist in assuming that plane cross-sections initially normal to the beam's axis remain plane, normal to the beam axis, and undistorted. This approach is commonly known as Euler-Bernoulli beam. For thicker beams, Timoshenko beam theory is usually implied as it considers the transverse shear strain also. As the beam slenderness increases the Euler-Bernoulli beam becomes more accurate. A typical threshold for the slenderness is $l/h = 15$, where l is the axial dimension and h is the transverse section dimension.

In finite element method Euler-Bernoulli beam elements use cubic interpolation functions (Fig. 5.2b) whilst Timoshenko beam elements use linear or quadratic interpolation (Fig. 5.2a). In the following paragraph both hypotheses are considered.
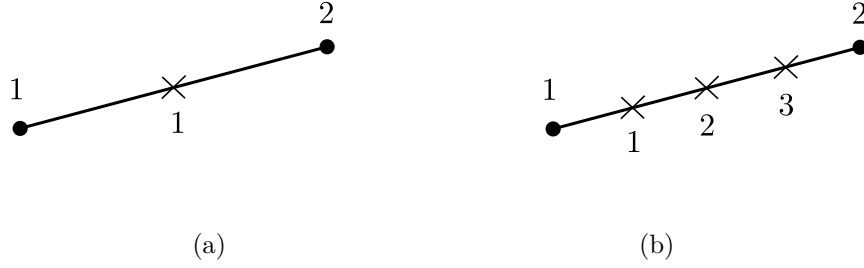
Figure 5.2: Nodes and integration points position: (a) linear elements and (b) cubic elements.

Screw steel has been schematized as a homogeneous and isotropic material with a linear elastic constitutive behavior ($E = 210000 \text{ N/mm}^2$). The screw section has been assumed circular of diameter equal to inner thread diameter ($d = d_c$).
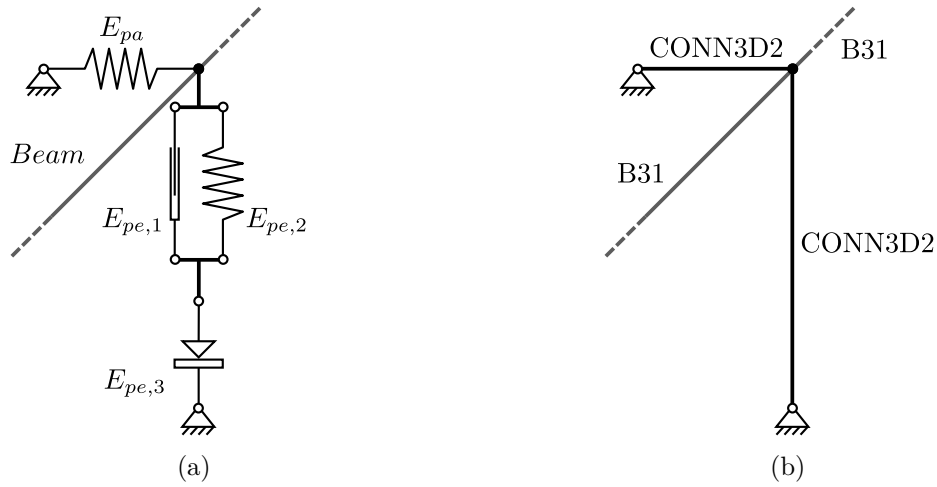
Figure 5.3: Scheme of screw-timber interaction: (a) Elements; (b) Connectors.

The interaction between the screw and the surrounding timber is modeled through discrete connectors. Connector elements in Abaqus/Standard do not eliminate degrees of freedom. The kinematic constraints are enforced with Lagrange multipliers which are additional solution variables. In the following paragraphs different assumptions are considered for the connectors (Fig. 5.3). First, as in the analytical model, a linear elastic behavior of parallel and perpendicular springs has been assumed, then a more complex interaction involving the friction on the sliding plane has been implemented. Fig. 5.3a shows the elementary elements that form the connectors in the latter case. The element E_{pa} is an elastic spring which schematize the interaction in the grain direction. In the direction perpendicular to the grain, the timber deformability is accounted via the analogous elastic spring $E_{pe,2}$.

The stiffness of E_{pa} and $E_{pe,2}$ have been assumed as:

$$K_{pa} = K_{f0}(\rho, d)dl_m \tag{5.1}$$

$$K_{pe} = \beta K_{f0}(\rho, d)dl_m \tag{5.2}$$

where $K_{f0}(\rho, d)$ is determined according to Eqs. 7 and 8 of the paper in Sec. 4.9, ϕ_{out} is the outer thread diameter and l_m is the connector spacing. According to this schematization it is assumed that no relative slip occurs on the screw-timber contact surface and therefore the interaction between the two components is reduced to the elastic deformability of timber only. This hypothesis can be considered valid in the serviceability conditions where the connection exhibit mainly an elastic behavior and therefore is valid in the context in the definition of a model for determining the connection stiffness.

The friction on the sliding plane is considered via the combination of $E_{pe,1}$ and $E_{pe,3}$. $E_{pe,1}$ represents a transversely rigid and axially free element. The role of $E_{pe,1}$ is to transmit forces parallel to the sliding plane between the sliding plane and the screw. $E_{pe,3}$ is a friction element; It provides a reaction parallel to the sliding plane proportional to the force acting perpendicular to it, only when it is axially compressed ($F_{\parallel} = \mu F_{\perp}$). It should be noted that according to this schematization which considers the connectors perpendicular to the sliding plane independent of each other, the timber members are implicitly considered infinitely shear-deformable in the plane of the inclined screw. In this way the equilibrium of each portion of the contact surface between timber members is independent of the others. In case some of the connectors perpendicular to the slip plane are in tension (u_y opposite with respect to the sliding plane, see Fig. 5.1), the connectors do not contribute to the equilibrium in the horizontal direction in terms of friction. Strictly speaking, considering that the timber member is only partially shear-deformable, the forces applied by the screw on the timber member and directed in the opposite direction to the sliding plane should contribute to the global equilibrium of the timber member by reducing the resultant of the forces perpendicular to the sliding plane and consequently reducing the overall frictional contribution. However, preliminary parametric studies have demonstrated that this condition does not occurs even for diameters of the screw, much smaller than those of practical interest. As can be seen from Fig. 5.11d and 5.12d the displacement perpendicular to the sliding plane is always directed to the sliding plane, even for screws with $d_c = 1\,\mathrm{mm}$.

In Fig. 5.4 the axial and transversal qualitative behavior of each element is described.
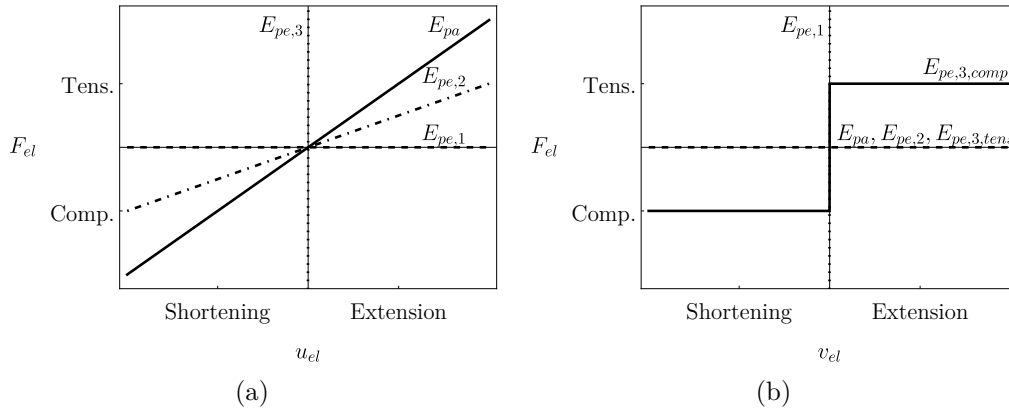
Figure 5.4: Constitutive law of elements: (a) axial behavior; (b) transversal behavior.

The connectors are restrained to external hinges capable of blocking translational degree of freedom only. In the analytical model of beam on elastic foundation the relative displacement between members was reproduced by an imposed relative displacement on the shear plane between the two contiguous beam domain. Since in finite element method this is not possible, two alternative strategies were considered. In the first case equal and opposite displacements are imposed to the external hinges of point-side member and head-side member (Fig. 5.1), thus reproducing a push-out test where the applied external forces are baricentric with respect to the section of the members. In this case the slip modulus can be calculated as the ratio between the reaction forces of the hinges of the springs parallel to the sliding plane and the imposed displacement. Whilst in the second case equal and opposite forces are applied on the screw on the sliding plane, thus reproducing a direct shear test where the members are loaded on the sliding plane and therefore there is no eccentricity between external forces. In order to make the assignment possible, a special connector is inserted on the sliding plane (Fig. 5.5). This connector restrain the translation degree of freedom u_2 and the rotational degree of freedom ϕ of the end nodes. In this latter case the slip modulus has been determined as the ratio between the sum of applied force and horizontal reaction of the connector perpendicular to the sliding plane (friction contribution) and the relative displacement on the sliding plane.
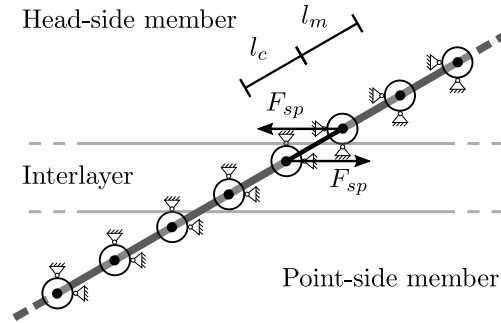
Figure 5.5: Timber-to-timber connection model.

In the following sections several sensitivity analyses results are reported. Unless otherwise specified the adopted base parameters are those reported in Tab. 5.1.

$K_{f0,1}$ (N/mm^3)	$K_{f0,3}$ (N/mm^3)	β	l_1 (mm)	l_2 (mm)	l_3 (mm)	d_c (mm)	θ (°)	μ	l_m (mm)	Elements	Geometric non-linearities
82.5	82.5	0.5	100	0	100	8	60	0	1	linear 2-node	No

Table 5.1: Base parameters for sensitivity analyses.

5.3   Numerical parameters sensitivity studies

The discretization of the problem requires the choice of the number of beam elements in which the screw is divided. Only one beam element was used between two connector elements. In the parametric study of Fig. 5.6 the total number of beam elements and therefore the connector spacing is changed while maintaining constant the spring stiffness per unit-length of screw. Increasing the number of elements, the slip modulus slightly decreases. Even with only 10 elements the approximation is reasonable. In the following studies a mesh length of $l_m = 1$ mm is adopted, in this way, even for the shortest screws, 100 elements are used.
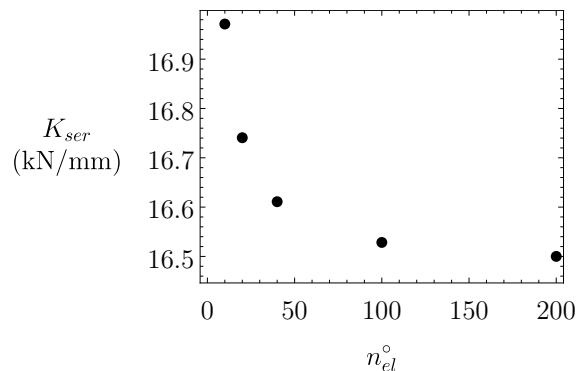
Figure 5.6: Mesh sensitivity of the connection slip modulus.

The analytical model described in Sec. 4.9 clarified the role of the screw bending and axial stiffness. To understand if also the shear deformability of the screw affect the slip modulus two different finite elements have been tested. A linear 2-node, 1-integration point element (B31, Fig. 5.2a) which is able to account for shear deformability (Timoshenko theory) and a cubic 2-node, 3-integration point element (B33, Fig. 5.2b) which consider

the beam as shear rigid (Eulero-Bernoulli theory). The influence of the shear deformability appear to be negligible even for the squattest screws (Fig. 5.7), nonetheless B31 elements are used for the following analyses.
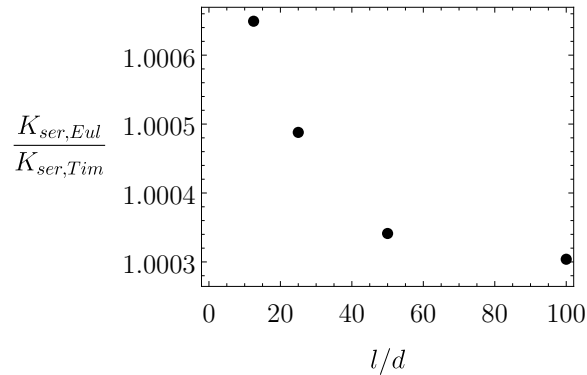
Figure 5.7: Connection slip modulus sensitivity to the element type for varying screw slenderness.

5.4   Cross-validation

The finite element models reproducing the push-out and direct-shear test configuration are here follow validated on the analytical model results in term of internal forces (N: axial force, T: shear force and M: bending moment) and displacements (u: axial displacement, v: transversal displacement, u_x: displacement parallel to the sliding plane and u_y: displacement perpendicular to the sliding plane). For validation purposes only elements E_{pa} and $E_{pe,2}$ have been considered, therefore the friction on the sliding plane has been neglected as done in the analytical model.

A small scatter between the bending moment diagram of direct-shear and the bending moment diagram of finite element model in push-out configuration and analytical model was observed. This was caused by the finite dimensions of the internal connector whose length is $l_c = 1$ mm (Fig. 5.5). The eccentricity of the forces on the sliding plane induce a concentrated moment. No significant differences were observed in term of other internal forces or displacement.

N
(kN)

(a)

T
(kN)

(b)

M
(kNmm)

(c)
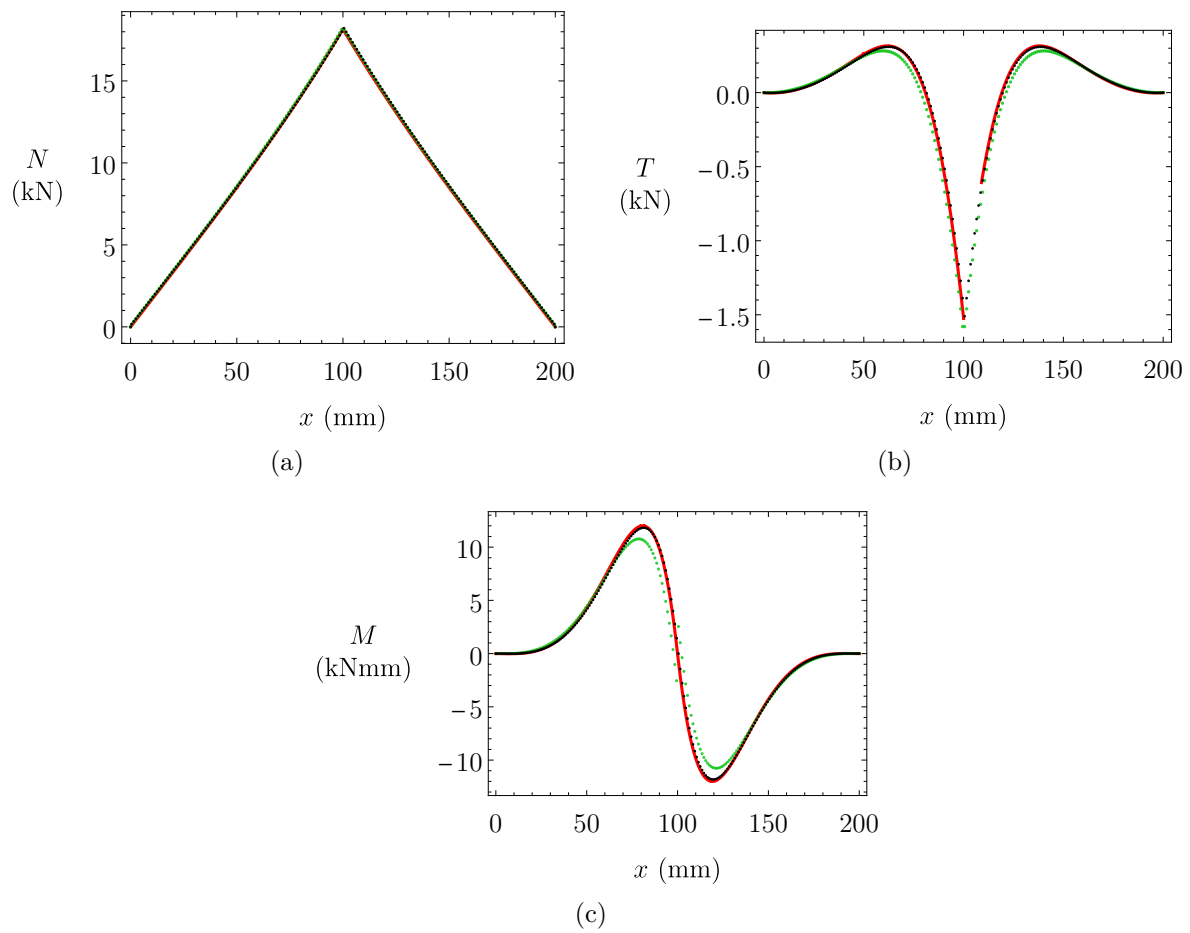
Figure 5.8: Analytical model (red), finite element model direct shear (green) and finite element model push-out (black) results in terms of internal forces: (a) axial force, (b) shear force, (c) bending moment.
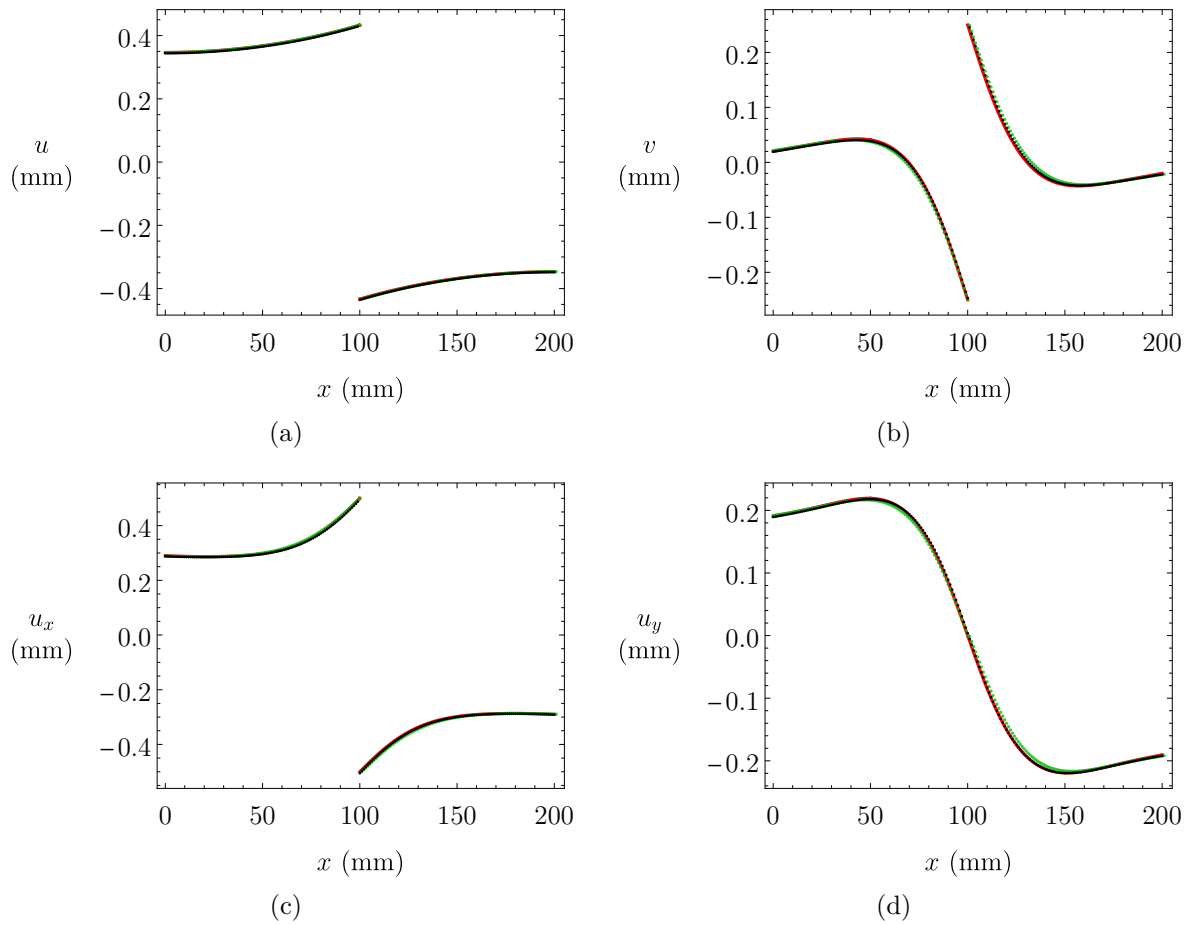
Figure 5.9: Analytical model (red), finite element model direct shear (green) and finite element model push-out (black) results in terms of displacements: (a) axial, (b) transversal, (c) parallel to the sliding plane and (d) perpendicular to the sliding plane.

In the following plot the slip modulus of the three models is compared for varying screw inclination angle θ.

(a)
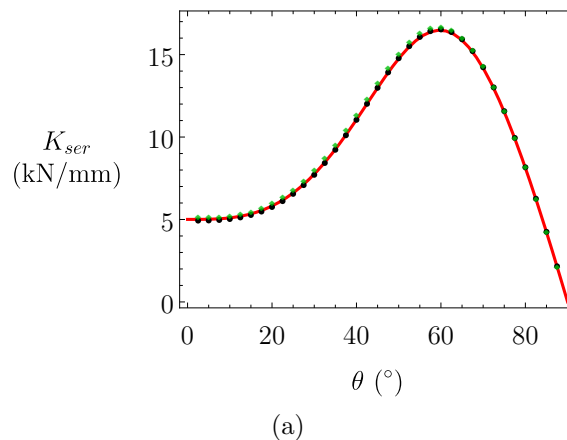
Figure 5.10: Analytical model (red), finite element model direct shear (green) and finite element model push-out (black) results in terms of slip modulus.

5.5 Screw stiffness

Just as in the classical theory of the beam on elastic foundation (transverse springs only), it has been demonstrated that also for the inclined beam model on the elastic foundation, the ratio between the screw stiffness and the springs stiffness is a significant parameter in determining the qualitative behavior of the model. In this section, the results of the finite element model in terms of displacements are reported for varying screw diameter while maintaining the springs stiffness constant. When the diameter is $d_c = 18$ mm, in both $\theta = 60°$ and $\theta = 30°$ cases the screw behaves approximately like a rigid body as demonstrated by the linearity of the displacements. When the diameter $d_c = 8$ mm the screw deformability is significant and small changes of the first derivative of the displacements happens. When considering the limit case of $d_c = 1$ mm, the qualitative behavior changes significantly leading to a quasi-local response of the model.
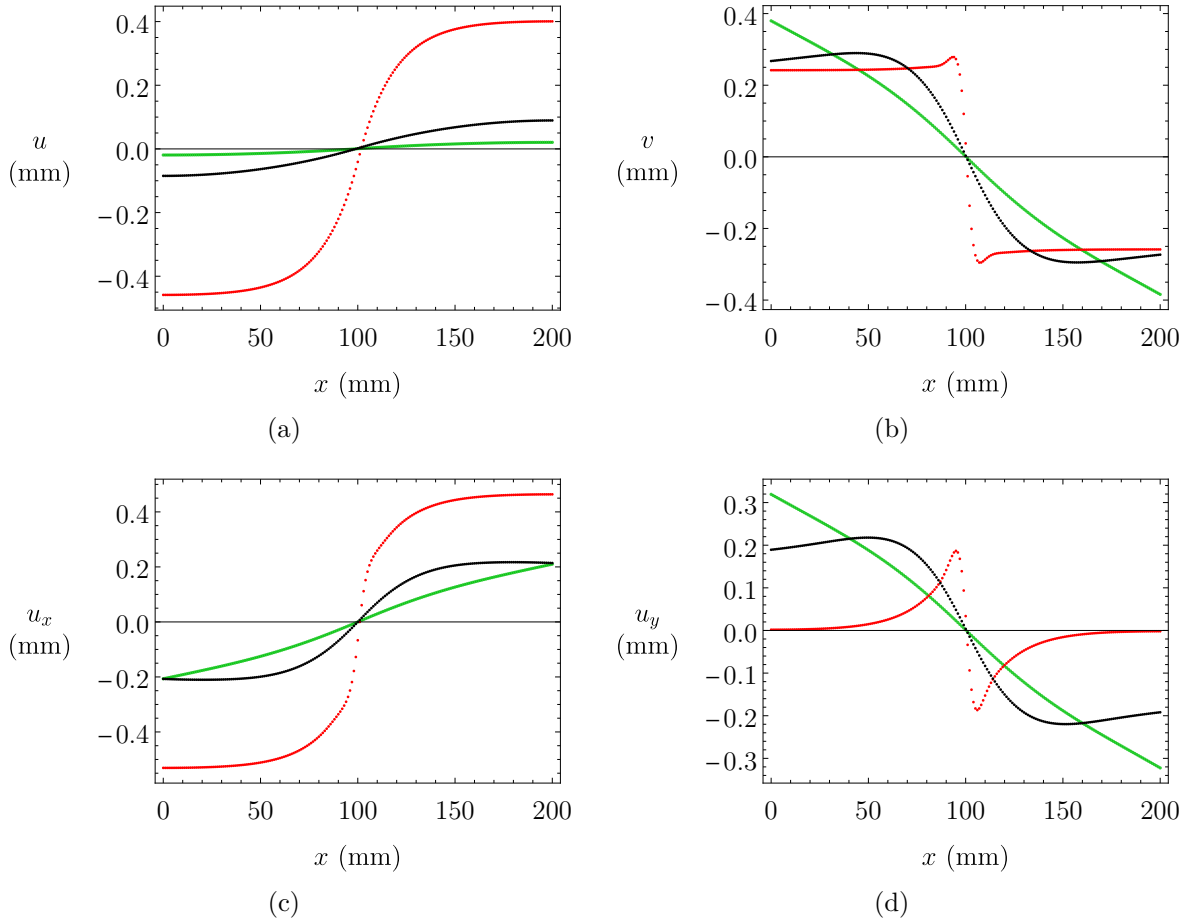
Figure 5.11: Inclined screw with $\theta = 60°$. $d_c = 1$ mm (red), $d_c = 18$ mm (green) and $d_c = 8$ mm (black) results in terms of displacements: (a) axial, (b) transversal, (c) parallel to the sliding plane and (d) perpendicular to the sliding plane.
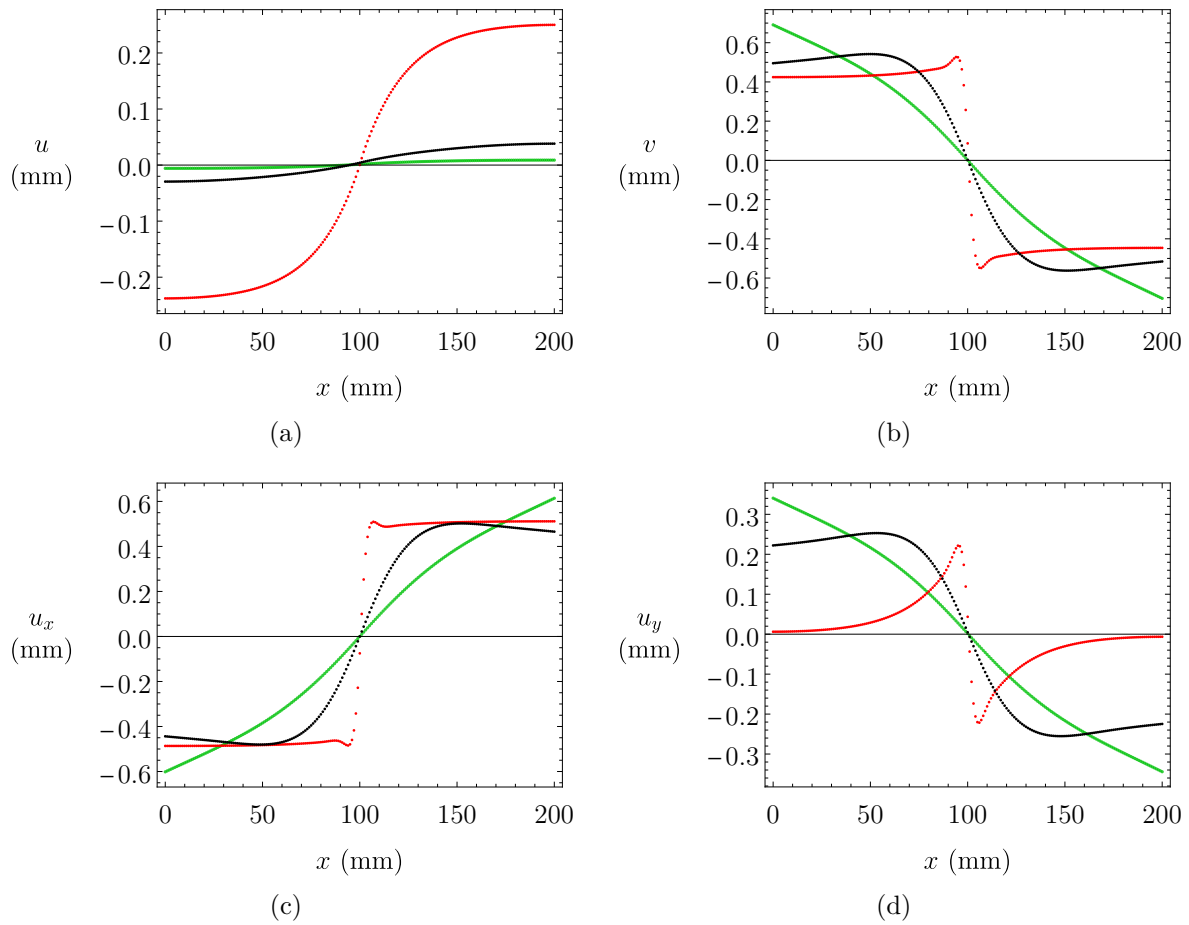
Figure 5.12: Inclined screw $\theta = 30°$. $d_c = 1\,\mathrm{mm}$ (red), $d_c = 18\,\mathrm{mm}$ (green) and $d_c = 8\,\mathrm{mm}$ (black) results in terms of displacements: (a) axial, (b) transversal, (c) parallel to the sliding plane and (d) perpendicular to the sliding plane.

5.6   Friction influence

Minor differences can be found in terms of internal forces distribution and displacements between friction and friction-less cases (Fig. 5.13 and 5.14). A significant difference can be found in terms of slip modulus (Fig. 5.15a). Increments up to 20% and 40% have been observed for $\mu = 0.25$ and $\mu = 0.50$ respectively (Fig. 5.15b). The largest increase happens when $\theta = 37.5°$ for the studied case.
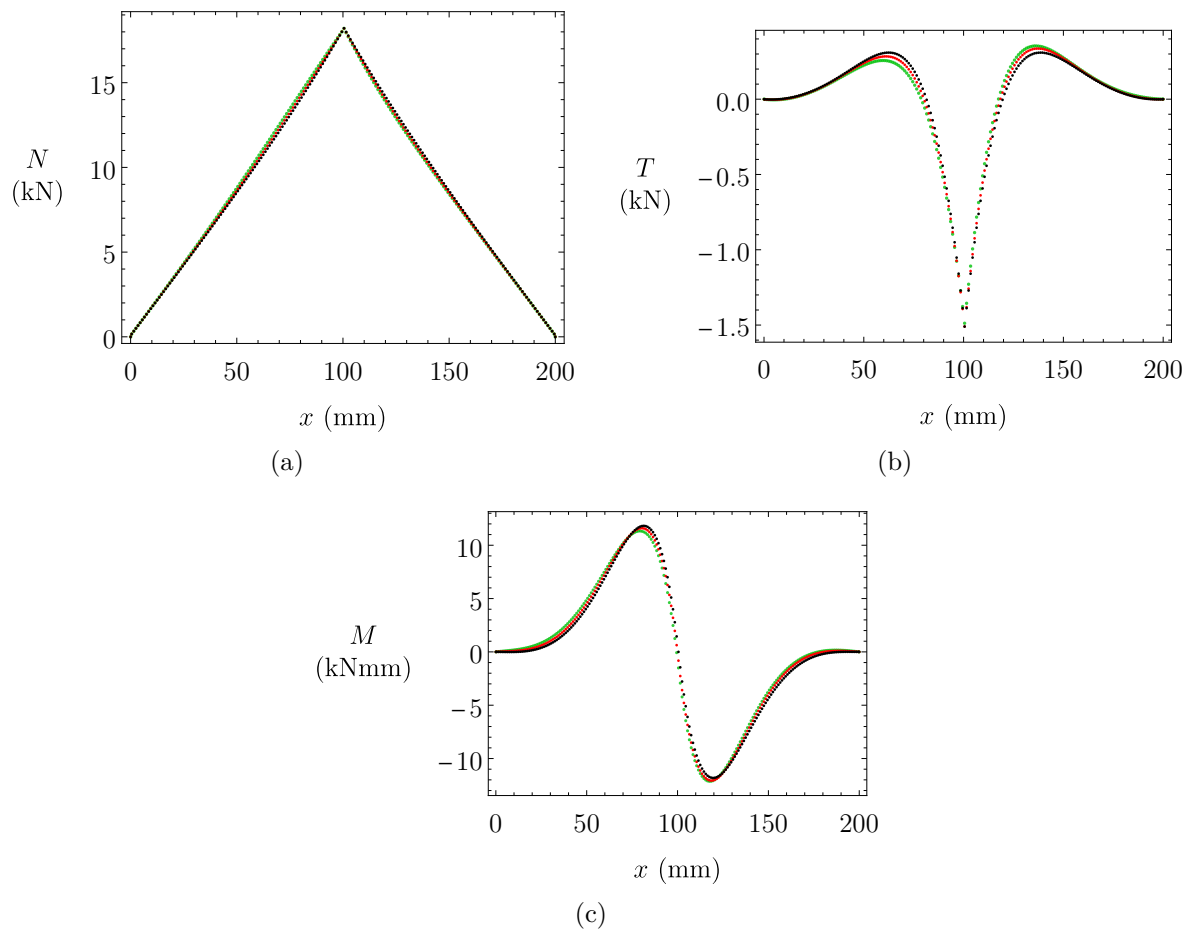
Figure 5.13: $\mu = 0$ (black), $\mu = 0.25$ (red) and $\mu = 0.50$ (green) results in terms of internal forces: (a) axial force, (b) shear force, (c) bending moment.
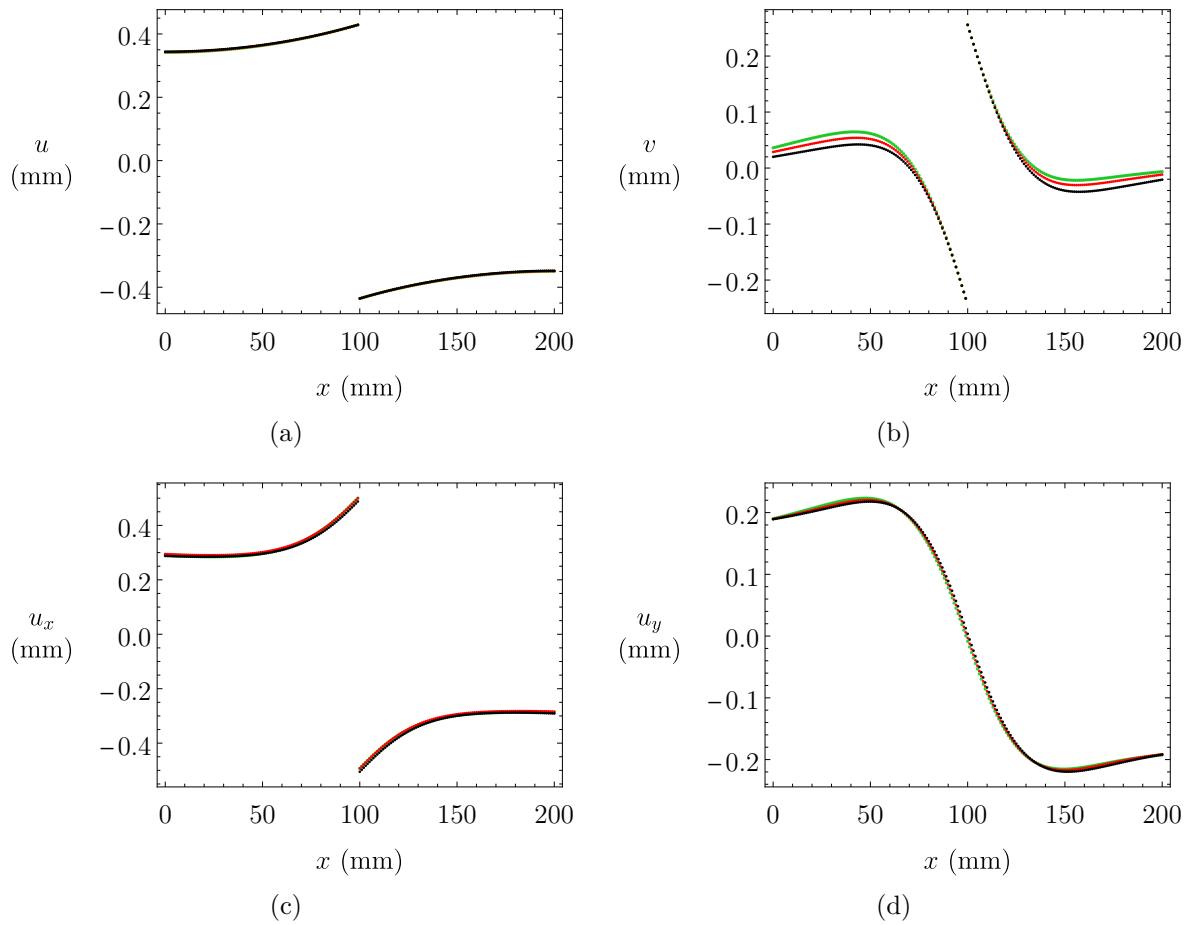
Figure 5.14: $\mu = 0$ (black), $\mu = 0.25$ (red) and $\mu = 0.50$ (green) results in terms of displacements: (a) axial, (b) transversal, (c) parallel to the sliding plane and (d) perpendicular to the sliding plane.
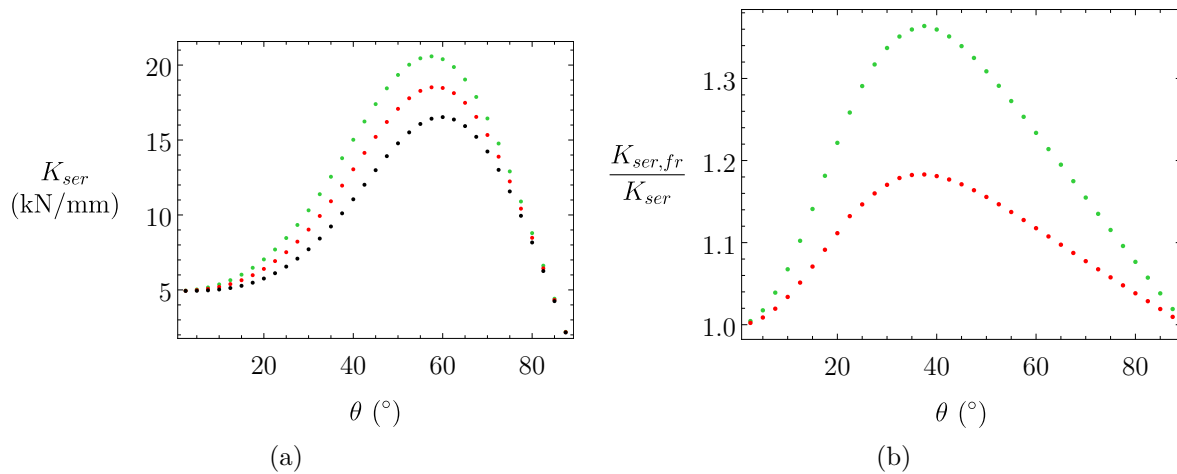
Figure 5.15: $\mu = 0$ (black), $\mu = 0.25$ (red) and $\mu = 0.50$ (green) results in terms of : (a) slip modulus, (b) ratio between slip modulus with and without friction.

5.7   Geometric non-linearity influence

Two different formulation of the problem have been here follow considered. In a small displacement analysis the kinematic equations are linearized and equilibrium is imposed in the undeformed configuration and therefore

geometric non-linearity is neglected. Alternatively the large displacements effects can be considered. In this case the equilibrium is considered in the current configuration using actual nodal coordinates. In the following comparison a friction coefficient of $\mu = 0.5$ has been considered.

The comparison in terms of internal forces and displacement highlighted substantial differences (Fig. 5.16 and 5.17). Accounting for non-linear effects in a configuration with $\theta = 30°$ lead to an high reduction of the axial force while the shear force maintains constant. The displacements in the direction parallel to the sliding plane reduces while the displacements in the direction perpendicular to the sliding plane increases. It is worth noting from Fig. 5.18 that despite the axial force reduction, the slip modulus increases by 40%. The increase in slip modulus is due to the increased friction contribution. In general, a translation to lower inclination angle is observed for the slip modulus-angle curve in the range $\theta \in [0; 60]$ (Fig. 5.18a). The effect of non-linearities is barely appreciable for screw with inclination angle $\theta \geq 45°$ (less than 8%).
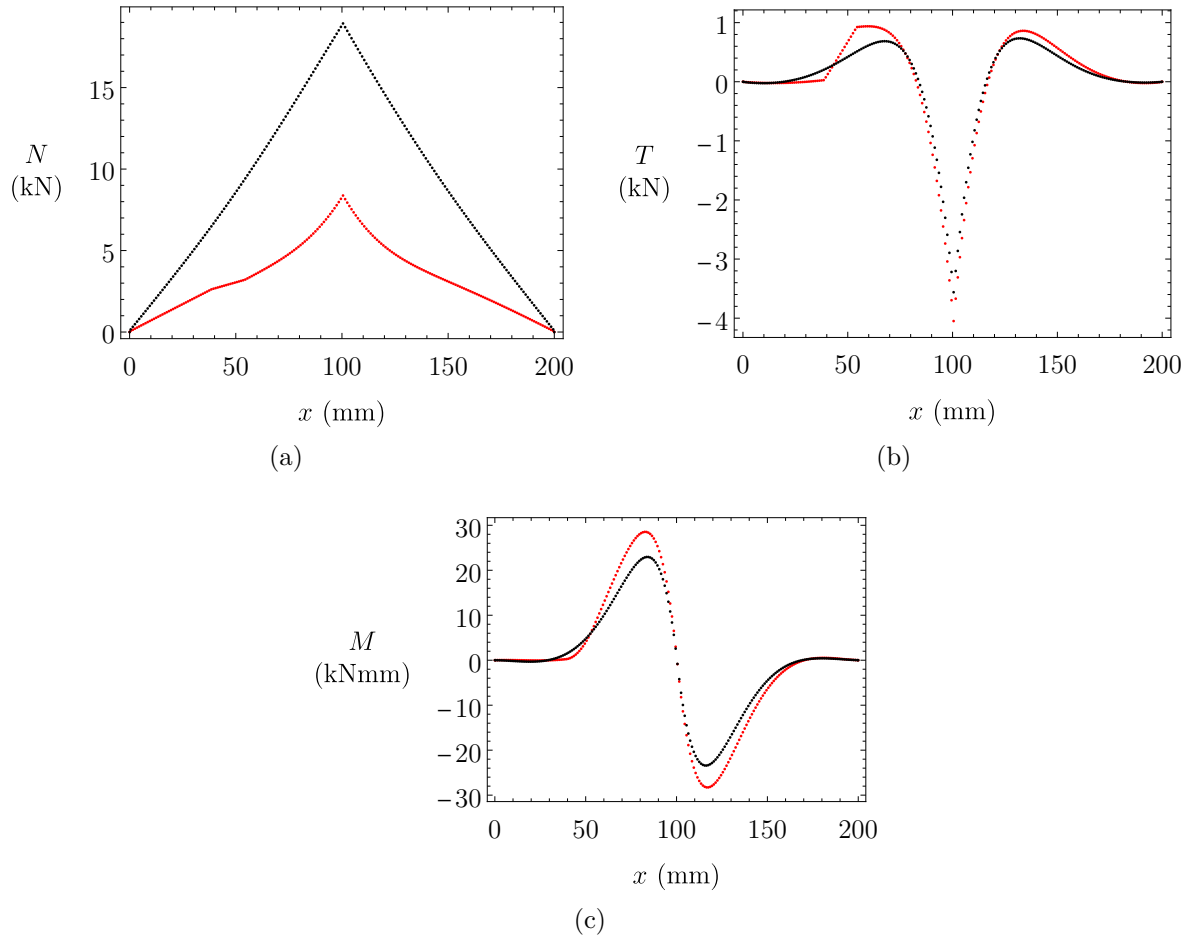
Figure 5.16: Linear (black) and Non-linear (red) model results in terms of internal forces: (a) axial force, (b) shear force, (c) bending moment.
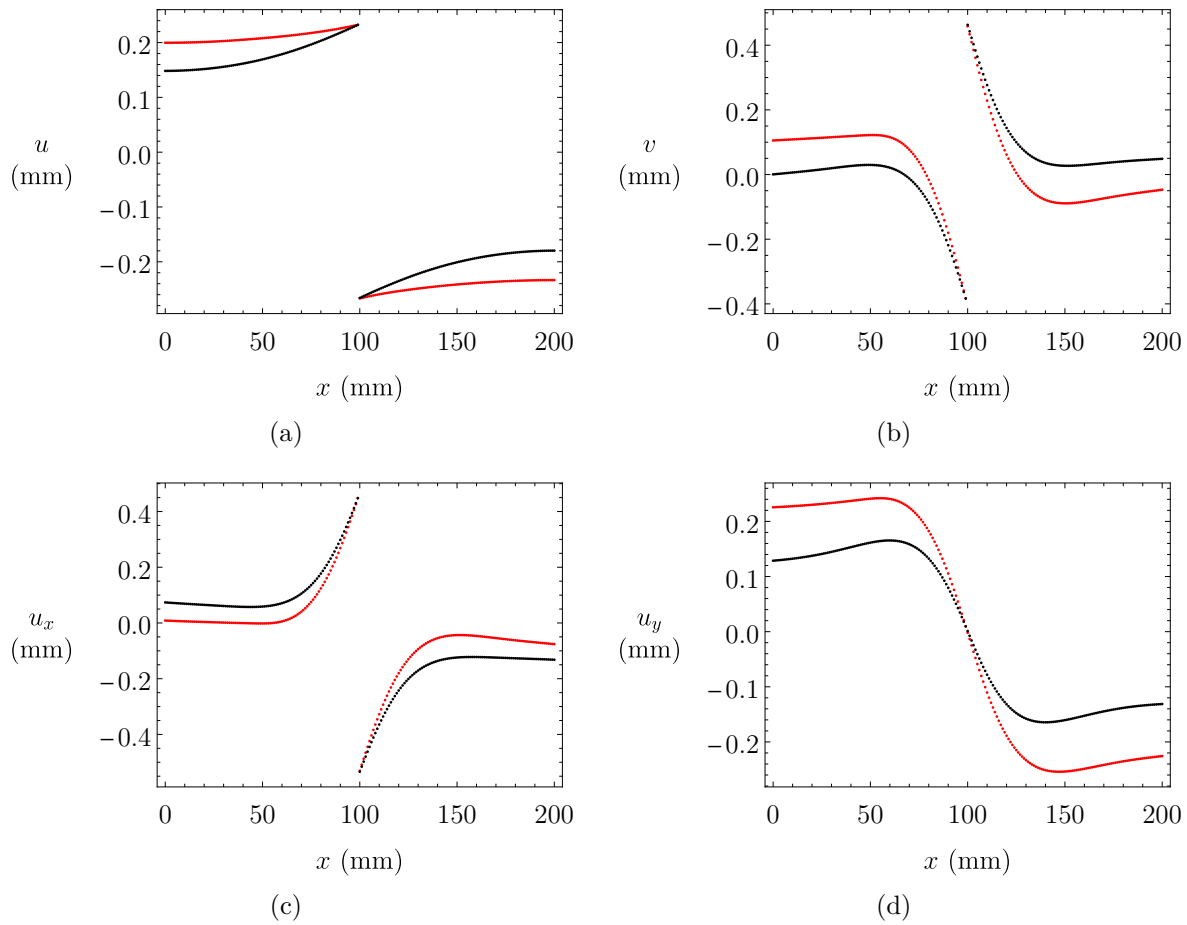
Figure 5.17: Linear (black) and Non-linear (red) model results in terms of displacements: (a) axial, (b) transversal, (c) parallel to the sliding plane and (d) perpendicular to the sliding plane.
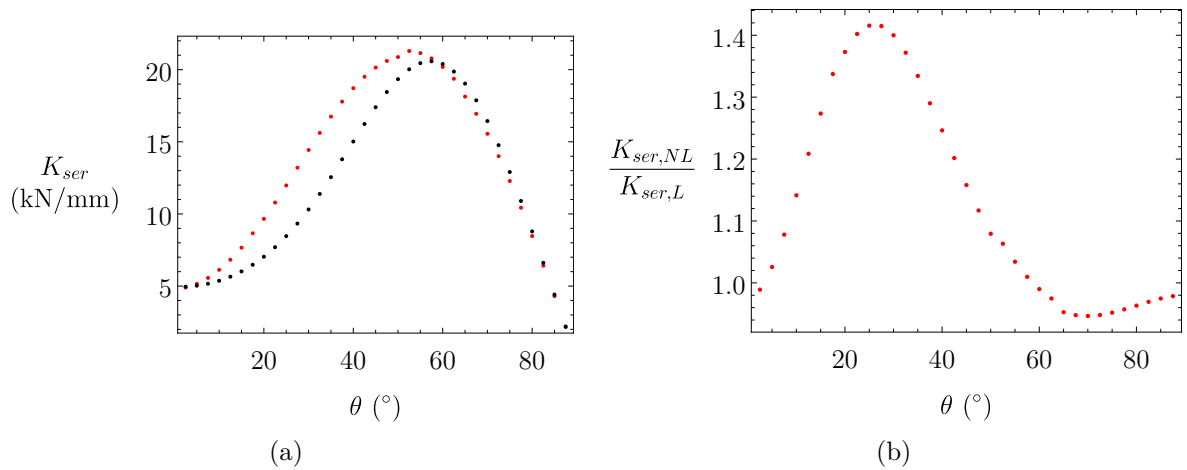
Figure 5.18: Linear (black) and Non-linear (red) model results in terms of : (a) slip modulus, (b) ratio between slip modulus with and without geometric non-linearities.

5.8 Experimental validation

The accuracy of the proposed model was validated on experimental tests from literature. The same test data implied in Sec. 4.9 were used (Tab. 5.2). Since all 50 tests are in push-out configuration, the model with imposed

displacement on external hinges was used. The friction coefficient on the shear plane was set to $\mu = 0.50$ for all the cases except for crossed-screw configurations where $\mu = 0.0$. Differently from the analytical model, the inner thread diameter ϕ_{inn} was used for both the calculation of the axial and bending stiffness, therefore neglecting the thread contribution on the geometrical section properties. The same foundation moduli implied in the analytical model of Sec. 4.9 were used in finite element model. The finite element model resulted more accurate than the analytical one. The coefficients of determination are $R^2 = 0.62$ and $R^2 = 0.71$ for the analytical and FEM respectively (Fig. 5.19). The FEM model exhibited lower maximum percentage scatters and a median value of the scatter closer to zero (Fig. 5.20).

Figure 5.19: Correlation between: experimental results and analytical model predictions (black) and experimental results and finite element model predictions (red).
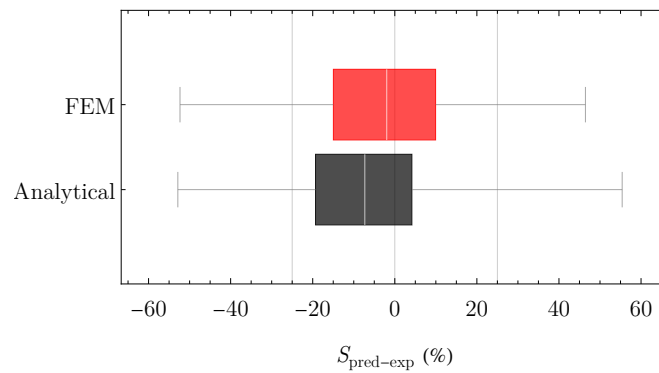
Figure 5.20: Scatters between: experimental results and analytical model predictions (black) and experimental results and finite element model predictions (red).

Reference	Member tip-side	Member head-side	ρ_1 (kg/m^3)	ρ_3 (kg/m^3)	l_1 (mm)	l_3 (mm)	ϕ_{inn} (mm)	ϕ_{out} (mm)	θ (°)	k_{exp} ($\frac{kN}{mm}$)	k_{an} ($\frac{kN}{mm}$)	k_{FEM} ($\frac{kN}{mm}$)
Tomasi 0			426	426	95	95	5,4	8,2	0	2,08	3,24	3,05
Tomasi 15			426	426	95	95	5,4	8,2	15	6,18	3,52	3,97
Tomasi 30	Spruce	Spruce	426	426	110	110	5,4	8,2	30	9,14	6,44	8,03
Tomasi 45	GL24h	GL24h	426	426	110	110	5,4	8,2	45	16,84	11,43	14,12
Tomasi 15 X			426	426	95	95	5,4	8,2	15	7,16	3,52	3,41
Tomasi 30 X			426	426	110	110	5,4	8,2	30	10,54	6,44	5,89
Tomasi 45 X			426	426	110	110	5,4	8,2	45	14,37	11,43	10,65
Schiro PA	Beech LVL	CLT	796	465	69	81	5,2	8,3	45	13,23	12,43	13,33
Schiro PH	Spruce C24	Beech LVL	460	846	91	71	5,2	8,3	45	13,47	12,44	12,55
Schiro PI		CLT	460	465	69	81	5,2	8,3	45	9,77	9,78	12,18
Schiro PM		CLT	460	465	81	81	5,4	8,6	45	7,84	9,37	11,35
Wang 45			560	560	39	61	3,6	5,3	45	3,65	2,83	4,07
Wang 30	Douglas	Douglas	560	560	50	50	3,6	5,3	30	2,46	1,75	2,40
Wang 15	Fir LVL	Fir LVL	560	560	55	45	3,6	5,3	15	1,56	1,18	1,42
Wang 0			560	560	57	43	3,6	5,3	0	0,95	1,12	1,19
Ringhofer 45	Spruce	Spruce	408	408	113	113	5,1	8,0	45	12,10	11,50	13,33
Ringhofer 60	T24	T24	410	408	130	130	5,1	8,0	60	16,20	14,71	17,09
Jacquier S1	Spruce	CLT C24	456	471	75	85	4,0	6,5	45	9,70	9,02	10,59
Jacquier S2	GL32		462	459	75	85	5,4	8,2	45	12,70	10,22	12,80
Blass 1			409	409	113	113	5,1	8,0	45	12,10	11,53	13,36
Blass 2			412	412	130	130	5,1	8,0	60	16,50	14,80	17,18
Blass 3			412	412	113	113	5,1	8,0	45	11,15	11,61	10,12
Blass 4			407	407	130	130	5,1	8,0	60	17,50	14,63	13,94
Blass 6			421	421	130	130	5,1	8,0	60	13,30	15,10	17,47
Blass 8			427	427	130	130	5,1	8,0	60	11,98	15,29	14,45
Blass 9			475	475	113	113	5,1	8,0	45	12,95	13,16	14,99
Blass 10			438	438	130	130	5,1	8,0	60	19,25	15,65	17,98
Blass 11			482	482	113	113	5,1	8,0	45	11,75	13,32	11,40
Blass 12			456	456	130	130	5,1	8,0	60	17,10	16,21	15,15
Blass 15			424	424	85	85	3,8	6,0	45	9,05	8,34	9,64
Blass 16			416	416	85	85	3,8	6,0	45	6,83	8,21	7,15
Blass 17			411	411	141	141	6,4	10,0	45	18,45	15,01	17,35
Blass 18			414	414	141	141	6,4	10,0	45	13,95	15,12	13,13
Blass 21	Spruce	Spruce	426	426	130	130	5,1	8,0	30	7,60	6,68	8,29
Blass 22	T28	T28	424	424	130	130	5,1	8,0	30	7,08	6,66	5,95
Blass 23			433	433	130	130	5,1	8,0	50	17,50	14,89	16,48
Blass 24			429	429	130	130	5,1	8,0	50	11,95	14,77	12,61
Blass 25			428	428	130	130	5,1	8,0	60	24,65	15,33	17,68
Blass 27			426	426	130	130	5,1	8,0	70	22,00	12,26	15,07
Blass 28			430	430	130	130	5,1	8,0	70	26,25	12,37	13,25
Blass 29			442	442	40	40	4,9	8,0	45	6,40	5,64	7,32
Blass 30			417	417	40	40	4,9	8,0	45	5,10	5,32	5,51
Blass 31			420	420	80	80	4,9	8,0	45	10,30	9,28	11,20
Blass 32			434	434	80	80	4,9	8,0	45	10,53	9,58	8,78
Blass 33			443	443	113	113	4,9	8,0	45	12,60	12,39	13,89
Blass 34			455	455	113	113	4,9	8,0	45	13,08	12,69	10,66
Blass 35			413	413	160	160	4,9	8,0	45	14,90	14,17	14,69
Blass 36			427	427	160	160	4,9	8,0	45	11,65	14,56	11,21
Blass 37			433	433	200	200	4,9	8,0	45	14,00	16,10	15,72
Blass 38			446	446	200	200	4,9	8,0	45	14,58	16,44	11,91

Table 5.2: Comparison between experimental mean and analytically and FEM predicted stiffness values.

Both the finite element model and the analytical model exhibited an high correlation with experimental data of the test campaign of Chap. 3 with $R^2 = 0.87$ and $R^2 = 0.91$ respectively (Fig. 5.21). The highest scatters have occurred for configuration with interlayer and are probably due to ignoring the deformability of the interlayer in the direction perpendicular to the sliding plane (Tab. 5.3). It is worth noting that for configuration with screws perpendicular to the sliding plane there are no differences between the analytical and the FEM predictions due to the absence of forces perpendicular to the sliding plane resulting in no-friction (Tab. 5.3).
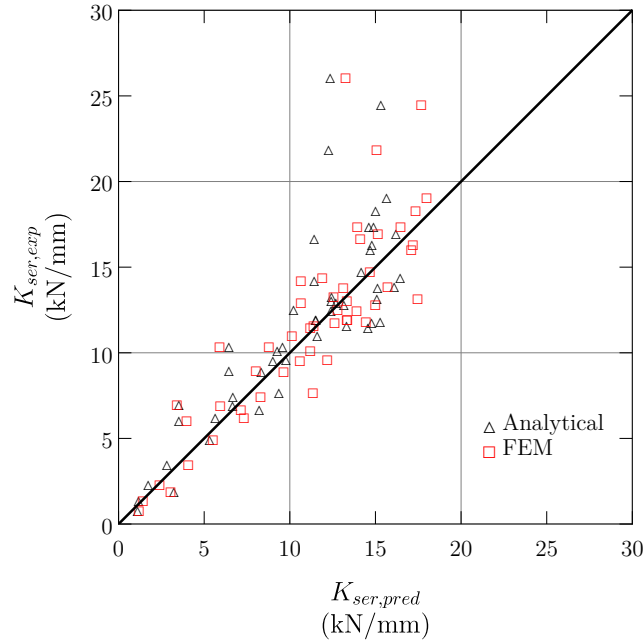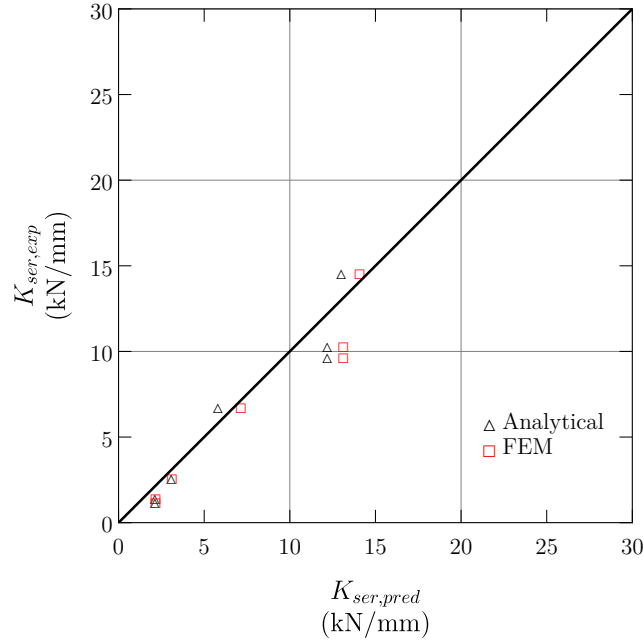

Figure 5.21: Correlation between: experimental results and analytical model predictions (black) and experimental results and finite element model predictions (red).

Reference	Timber member	$\rho_1 = \rho_3$ (kg/m^3)	l_1 (mm)	l_i (mm)	l_3 (mm)	ϕ_{inn} (mm)	ϕ_{out} (mm)	θ (°)	k_{exp} ($\frac{kN}{mm}$)	k_{an} ($\frac{kN}{mm}$)	k_{FEM} ($\frac{kN}{mm}$)
TT 0 8 200 R		440	80	0	120	5,4	8,0	0	2,74	3,09	3,12
TT 0 8 200 S35		440	74	6	120	5,4	8,0	0	1,57	2,13	2,16
TT 0 8 200 S90		440	74	6	120	5,4	8,0	0	1,36	2,13	2,16
TT 45 7 300 R	GL24h	440	130	0	170	4,6	7,0	45	14,73	13,00	14,08
TT 45 7 300 S35		440	122	8	170	4,6	7,0	45	9,79	12,19	13,13
TT 45 7 300 S90		440	122	8	170	4,6	7,0	45	10,47	12,19	13,13
TT 30 7 300 S35		440	155	7	139	4,6	7,0	30	6,86	5,80	7,14

Table 5.3: Comparison between experimental mean and analytically and FEM predicted stiffness values.

5.9 Conclusions

The main results of the numerical investigation can be itemized as follows:

- an accurate estimates of the slip modulus can be obtained by using only 100 elements to discretize the beam;

- shear deformability is negligible even for the squattest screws and consequently Eulero-Bernoulli assumption is reasonable;

- both finite element modelling methods are in excellent agreement with analytical model results;

- for length to diameter ratios in common application ranges the screw can not be regarded as a rigid body;

- friction on the sliding plane can lead to increments of slip modulus up to 40%;

- geometric non-linearity makes the screws behave as if they are more inclined.

Chapter 6

Capacity prediction of timber-to-timber and timber-to-steel screw connections: one-dimensional finite element models

Abstract: The capacity represent an essential parameter in connections design. Johansen theory is extensively used for the capacity prediction of transversely loaded dowel-type fasteners. However, in connections with inclined fasteners, due to the strong coupling between the fastener axial and transversal behavior, the problem of capacity prediction is non-trivial. Moreover, interlayers having poor mechanical properties are often inserted between main connected members to ensure human comfort in the buildings or because it is required by the structural system. The complex interaction between axial and transversal behavior of inclined screws may not be fully considered by some of the simplified models in literature and codes, in this chapter the behavior of timber-to-timber and steel-to-timber connection is reproduced by means of a novel finite element modelling approach. The screw is modelled as a non-linear beam on foundation. The model can reproduce the following mode of failure: timber crushing, screw withdrawal and screw yielding. It was found that even in the case of slender screws, the bending moment component can reduce significantly the capacity of connections due to its interaction with the axial force. A new analytical model for connections with screws in combined loading is proposed and validated based on five-hundred finite element model analysis results.

6.1 Introduction

In this chapter, a beam on foundation model, capable of taking into account of the interaction between moment, shear and normal force which may lead to metal fastener yielding at loads below those predicted by the European yield model is proposed. The model is able to reproduce the following mode of failure: timber crushing, screw withdrawal and screw yielding. The model also accounts for friction on the sliding plane and interlayer. In Sec. 6.2 a paper regarding timber-to-steel connections is included, while in Sec. 6.3 comparisons between the finite element model prediction and experimental outcomes is performed.

6.2 Paper: *Timber-to-steel inclined screws connections with interlayers: experimental investigation, analytical and finite element modelling*
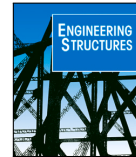
Timber-to-steel inclined screws connections with interlayers: Experimental investigation, analytical and finite element modelling

Yuri De Santis [a],[*], Angelo Aloisio [a], Igor Gavrić [b],[c], Iztok Šušteršič [b],[c], Massimo Fragiacomo [a]

[a] *Department of Civil Engineering, University of L'Aquila, Italy*
[b] *InnoRenew CoE, Livade 6a, 6310 Izola, Slovenia*
[c] *Faculty of Mathematics, Natural Sciences and Information Technologies, University of Primorska, Glagoljaška ulica 8, 6000 Koper, Slovenia*

ARTICLE INFO

Keywords:
Inclined screws
Load-bearing capacity
Timber-to-steel connections
Eurocode 5
Friction
Soundproofing

ABSTRACT

Thanks to the axial resisting contribution, inclined screw connections offer a mechanical advantage over connections with purely transversely loaded fasteners. However, the strong coupling between the axial and the transversal behaviour of the screw makes it challenging to predict the actual connection behaviour. Moreover, the presence of polyurethane interlayers for soundproofing or OSB interlayers of light-frame buildings between main members may increase the bending moment component interacting with the axial force in the screw, thus reducing the connection failure load. This paper experimentally assesses the behaviour of steel-to-timber connections, and a parametric finite element model of Winkler non-linear beam is presented and validated. Finally, a simplified analytical model for capacity prediction is presented. The results of the approach currently provided by the Eurocode 5, of an additive model and the proposed analytical model, are then compared with the results of 500 finite element analysis.

1. Introduction

Self-tapping screws, thanks to the speed and ease of installation and the possibility of arranging them in various geometric configurations, are well suited for use in composite floors and beams [1–3]. Screws can be used for connecting timber with steel members, for instance, the plates used in beam-to-beam and beam-to-pillar joints, the plates used as inter-story connections and the hold downs of cross-laminated timber (CLT) or light-frame timber (LTF) buildings. High slip modulus values characterize connections with inclined self-tapping screws, making its use particularly convenient in composite structures and in non-dissipative connections of tall buildings, reducing the relative slip and the inter-storey drift, respectively [4].

Main connected members can be separated by intermediate layers having different functions. Typical examples of connections with interlayers can be found in composite floors [5,6]. In newly built timber-concrete composite floors, the interlayer is represented by wood-based panels acting as a support for the concrete during the construction phases [7,8]. In retrofitted existing floors, an additional concrete member can be added over the existing joist, and the existing planking is usually left in-between. In addition to Timber Concrete Composite floors (TCC floors) [9], interlayers can also be found in Timber Steel Composite floors (TSC floors) [10–12] and in Timber Timber Composite floors (TTC floors) [13] where a steel beam or a timber plate

element can be used in the upgrading of an existing floor while leaving the existing decking as an intermediate member having negligible structural properties. Joist hanger attached to the shear wall made of wood-based panel and studs, soundproofed hold-down and angle brackets and connection between walls or between walls and floors with soundproofing insulation layers are other examples of connections with intermediate layers [14,15].

Most national standards design methods for strength calculation of dowel type fastener connections are based on the European Yield Model derived from Johansen's work [16]. According to European standards [17], the load-bearing capacity of a screw simultaneously subjected to shear and axial stress, as in the case of inclined screws connections, is given by a quadratic combination of the stress–strengths ratios for transversal and axial directions. This design model highly underestimates the strength of connections with inclined screws in shear-tension [18]. An additive model considering both Johansen's contribution and the withdrawal contribution of the screws was proposed by Bejtka I. and Blaß H.J. in [19] for timber-to-timber connections. However, these simplified models may not fully consider the complex interaction between the axial and transversal behaviour of inclined screws [20]. Moreover, the simplified model for capacity prediction currently provided by Eurocode 5 [17] does not account for the presence of interlayer. De Santis and Fragiacomo have studied

---

* Corresponding author.
E-mail address: yuri.desantis@univaq.it (Y. De Santis).

the influence of the interlayer on the slip modulus in [6], while Blaß and Laskewitz [21] provided capacity prediction formulas for timber-to-timber and timber-to-steel connections with interlayer connected or unconnected to the timber member.

In the last few years, several advanced three-dimensional numerical models have been developed by scholars to study the behaviour of connections made of threaded fasteners embedded in timber. The complex interaction between the screw thread and timber has been modelled using various techniques ranging from reproducing the actual thread geometry [22] to using a fictitious layer that wraps the screw shank and represents the portion of space where damaged timber fibres and screw thread coexist. In conjunction with the fictitious layer, a cohesive contact with damage evolution is often used to reproduce the withdrawal behaviour of inclined fasteners [8,23]. However, three-dimensional models require a complete characterization of the involved materials and a considerable computational cost. Therefore, they are not suitable for parametric analyses. In [24], a hybrid beam-solid elements model is presented. A beam-to-solid coupling is developed to connect the beam elements schematizing the screw to solid elements. Also, empirical models for capturing load-slip behaviour of joints with dowel-type fasteners were derived from non-linear regression of experimental data [25,26]. Some authors tackled the problem by Beam-On-Foundation (BOF) modelling. According to this method, fasteners are numerically modelled as elastoplastic beams on a non-linear foundation representing the interaction with timber. BOF modelling has been used to reproduce timber joints hysteretic behaviour and failure modes [27,28]. Nevertheless, to the author's knowledge, non-linear BOF modelling has been previously used to predict the load-slip behaviour of connections with fasteners perpendicular to the sliding plane only [25].

This paper proposes a BOF model capable of taking into account the interaction between bending moment, shear and normal force, which may lead to metal fastener yielding at loads below those predicted by the European Yielding Model (EYM). The model can reproduce the following mode of failure: embedment, screw withdrawal and screw yielding. The model also accounts for friction on the sliding plane and interlayer. The outcomes of an experimental investigation conducted on various timber-to-steel connection configurations with inclined screws with and without polyurethane soundproofing and OSB interlayers are herein described and discussed. These results have validated two different finite element modelling approaches suitable for describing the in-service and the ultimate conditions, respectively. The validated finite element models have been used to conduct sensitivity studies and extensive comparisons with the capacity model provided by Eurocode 5 and with the model proposed by Bejtka and Blaß extended to the case of timber-to-steel connections with interlayers. A new analytical model for connections with screws in combined loading is proposed and validated based on the results of a five-hundred finite element model analysis.

2. Experimental investigation

2.1. Test configurations

Timber-to-steel connections with screws have been tested in seven configurations, plausibly representing the most common applications of practical interest. The cases of connections with screws perpendicular and inclined with respect to the sliding plane are considered. The central timber elements are made of spruce glued laminated timber GL24h with 40 mm lamellas. The length of the elements is 300 mm, the section height is 360 mm, and the section width is 100 mm (Fig. 1a). The mean density of glue laminated timber member is $\rho_m = 420$ kg/m^3. The side steel elements are made of sections of European standard beam with U profile and a section height of 100 mm (UPN100) (Fig. 1a). The UPN web thickness is 6 mm. Profiles with laser-cut holes in the webs are used for specimens with inclined screws (Fig. 1a and Fig. 6a). The laser-cut

Table 1
Description of tested configurations.

Name	n	θ (°)	d (mm)	d_c (mm)	l (mm)	Interlayer	t (mm)
TS 0 9 140 R	5	0	9,0	5,9	140	–	–
TS 0 9 140 S35	4	0	9,0	5,9	140	XYL35100	6
TS 45 9 240 R	8	45	9,0	5,9	240	–	–
TS 45 9 240 S35	4	45	9,0	5,9	240	XYL35100	6
TS 45 9 240 O	5	45	9,0	5,9	240	OSB	22
TS 45 9 140 RL	6	45	9,0	5,9	140	–	–
TS 45 9 240 DS35	4	45	9,0	5,9	240	Double XYL35100	12

Table 2
Results of timber-to-steel configurations referred to a single screw.

	$k_{i,m}$ (kN/mm)	CoV (%)	$k_{s,m}$ (kN/mm)	CoV (%)	$F_{max,m}$ (kN)	CoV (%)	u_u (mm)	CoV (%)
TS 0 9 140 R	2,40	19	1,97	25	15,17	14	15,00	0
TS 0 9 140 S35	3,20	12	1,96	15	15,98	3	15,00	0
TS 45 9 240 R	9,12	33	10,50	24	33,83	12	6,08	30
TS 45 9 240 S35	9,07	12	8,07	10	30,45	4	5,50	19
TS 45 9 240 O	4,55	51	5,78	42	28,12	12	6,84	50
TS 45 9 140 RL	20,61	32	14,46	48	16,74	10	3,00	39
TS 45 9 240 DS35	1,18	24	1,69	44	25,91	7	15,00	0

hole works as washer housing that grants the mechanical interlocking with the steel member; see Fig. 6. The holes in steel members for perpendicular screws are 1 mm larger than the screw thread outer diameter and are without countersunk. The soundproofing interlayers are made of polyurethane and are 35 shores Rothoblaas XYLOFON [29], 6 mm thick and 100 mm wide. The elastic modulus at 10% compression of the soundproofing layer is 2.74 N/mm^2. OSB interlayers are 22 mm thick. Self-tapping fully threaded VGS 9 × 140 and VGS 9 × 240 screws are from Rothoblaas [30]. VGU washers from Rothoblaas [30] are used in inclined screw configurations, while screws perpendicular to the sliding plane are inserted in the drilled UPN profile. The materials and the geometries of the configurations are summarized in Table 1 and Fig. 1 where n is the number of test repetitions, d is the outer thread diameter, d_c in the inner thread diameter, l is the overall screw length and t is the interlayer thickness.

Other than reference configurations identified by labels TS 0 9 140 R and TS 45 9 240 R, a configuration with soundproofing interlayer is considered for both $\theta = 0°$ and $\theta = 45°$ configurations (TS 0 9 140 S35 and TS 45 9 240 S35 respectively), where θ represents screw orientation angle as shown in Fig. 1a. For $\theta = 45°$ configurations, the cases of OSB interlayer and screw with reduced length are also considered (TS 45 9 240 O and TS 45 9 140 RL respectively). Using a single soundproofing layer, the contact surface between steel and timber is insulated on the sliding surface. However, vibrations can still propagate from one member to another through the screw head and washer. To prevent this, some manufacturers have proposed using a second steel plate and a second soundproofing layer so that the screw head is decoupled from the main steel member [14]. To reproduce this decoupling scheme, a configuration with a double soundproofing interlayer is tested (TS 45 9 240 DS35, Fig. 1b). In all configurations, the screw was inserted without pre-drilling.

2.2. Test methods

The typical test consisted of a standard push-out test. The specimen, made of three members (two steel and one timber member) and, therefore, with two principal shear planes, is brought to failure by pushing the central member using a universal testing machine Zwick with 100 kN capacity (Fig. 2). The relative displacement between the central and side members is measured through an LVDT (Linear Variable Differential Transformer). The measure is indirect as the LVDT measures the relative displacement between the mid-point of the timber member and the mid-point of the retainer restrained to the two side
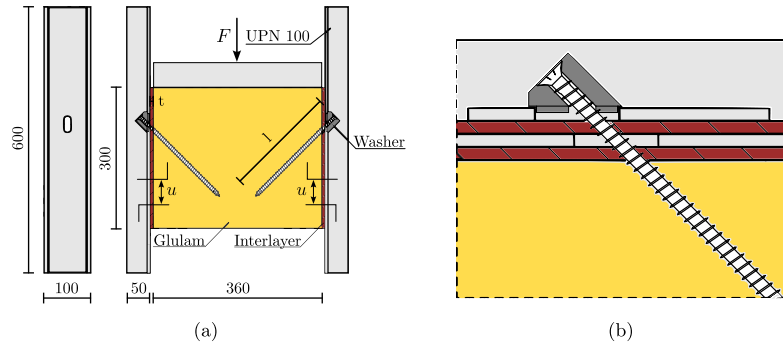
Fig. 1. (a) Test setup and (b) details of double soundproofing interlayer.

Fig. 2. Test setup picture.

steel members (Fig. 2). Due to the eccentricity between the load applied to the central member and the reaction that the test plane exerts on the side members, in the standard configuration for push-out tests, the members tend to separate during the test. For this reason, side members were clamped together using a steel bar unable to induce pre-stress (Fig. 2). The European standard EN-26891 [31] describes the general principles for determining the strength and deformation characteristics of joints made with mechanical fasteners. The procedure requires the knowledge of an estimated maximum load F_{est} to be determined based on calculation or preliminary tests. It should be adjusted if, during the execution of the tests, the mean value of the maximum load of the tests already carried out deviates by more than 20 % from the estimated value. The estimated maximum load for each configuration has been calculated by increasing the characteristic strength declared by the screw producer by 30% to obtain a plausible average value. The chosen loading procedure is divided into the following phases:

1. force controlled loading up to $0.4F_{est}$;
2. force controlled holding at $0.4F_{est}$ for 30 s;
3. force controlled unloading from $0.4F_{est}$ to $0.1F_{est}$;
4. force controlled holding at $0.1F_{est}$ for 30 s;
5. force controlled loading from $0.1F_{est}$ to $0.7F_{est}$;
6. displacement controlled until failure or 15 mm of connection slip.

The speed in the displacement-controlled phase is set equal to 0.058 mm/s and the loading speed in all other phases has been calculated to achieve 15 mm of relative displacement in 11.5 min resulting in a loading speed comprised between 0.03 kN/s and 0.23 kN/s, depending on the estimated maximum load. Each configuration is repeated at least on four different specimens for eight screws tested in the same configuration. Due to the reduced number of specimens for each configuration, it was decided to repeat the test keeping the estimated maximum load constant, even in cases where the maximum experimental load differed by more than 20 % from that initially assumed. In this way, the consistency of the tests was favoured in compliance with the condition imposed by the standard.

2.3. Results and discussion

The load–displacement curves of the tested specimens with two screws are shown in Fig. 3.

The initial slip modulus k_i, the slip modulus k_s, and the maximum load F_{max} and its corresponding displacement u_u are determined as follows. To calculate the stiffness and ultimate displacement values net of displacement components related to local crushing at the member ends, the relative slip LVDT measurements are used instead of the upper crossbar displacement of the press.

The initial slip modulus is determined with the following definition:

$$k_i = \frac{\min(0.4F_{est}, 0.4F_{max})}{v_{04}} \tag{1}$$

Where F_{max} is the maximum force measured up to a relative slip of 15 mm, and v_{04} is the relative slip in the first loading phase corresponding to the considered load in the numerator of Eq. (1). The definition provided by EN-26891 is revised as a consequence of the choice not to update the estimated value of the maximum load F_{est} in the event of a difference between the estimated maximum load F_{est} and the maximum experimental load F_{max} greater than 20 %. Substituting $\min(0.4F_{est}, 0.4F_{max})$ to $0.4F_{est}$, in case of connections with $F_{max} < F_{est}$, the stiffness is still determined in the elastic range.

The slip modulus is determined with the following definition:

$$k_s = \frac{\min(0.4F_{est}, 0.4F_{max}) - 0.1F_{max}}{v_{04} - v_{01}} \tag{2}$$

Where v_{04} and v_{01} are the relative slip in the loading phase corresponding to the considered loads. Substituting $0.1F_{max}$ to $0.1F_{est}$, in case of connections with $F_{max} > F_{est}$, the stiffness is still determined after the initial slip phase.

The initial slip modulus k_i, the slip modulus k_s and the maximum load F_{max} and its corresponding displacement u_u are reported in Table 2 and are referred to a single screw. The same results are also plotted in Fig. 4.

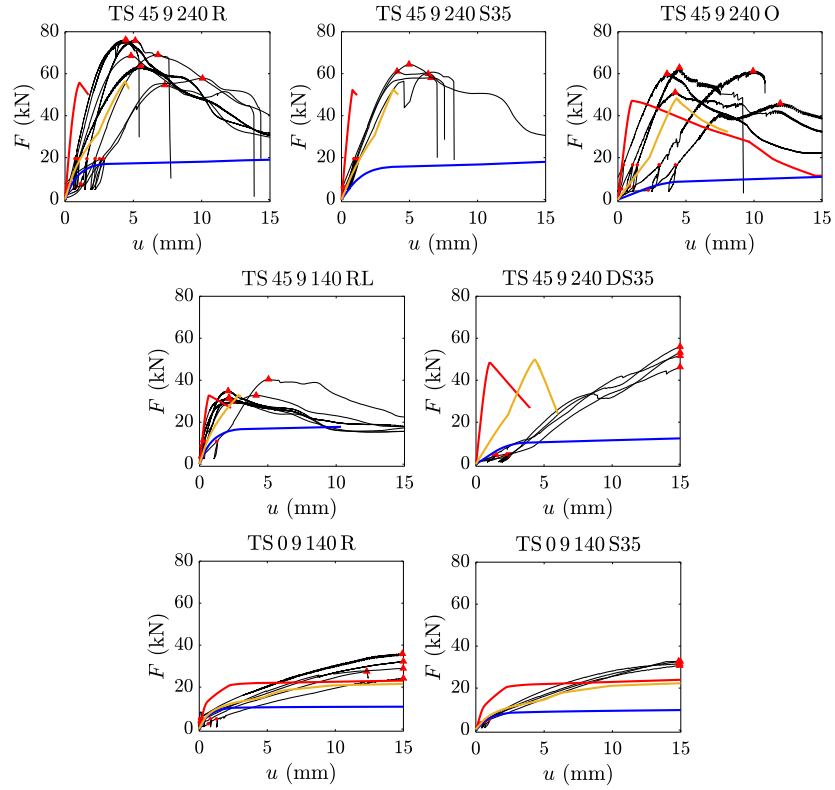**Fig. 3.** Force displacement curves of a specimen with two screws: experimental (black line), finite element model with a free end (blue line), clamped end (red line) and springed end (yellow line). Experimental reference loads for slip modulus calculation (red dots) and experimental failure load (red triangles).
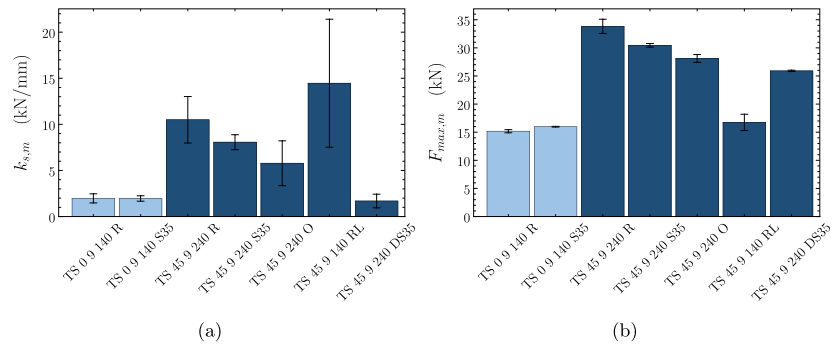

Fig. 4. Experimental results with error bars: (a) slip modulus and (b) failure load.

Table 3
Failure modes of experimental configurations.

Name	Repetitions	Failure mode			
		Embedment and double hinge	Withdrawal and single hinge	Withdrawal	Tensile-bending
	(n°)	(%)	(%)	(%)	(%)
TS 0 9 140 R	5	100			
TS 0 9 140 S35	4	100			
TS 45 9 240 R 8		50		50	
TS 45 9 240 S35	4		25		75
TS 45 9 240 O	5			60	40
TS 45 9 140 RL	6			100	
TS 45 9 240 DS35	4				100

Table 3 specifies, for each configuration, the percentage of specimens that failed due to a specific failure mode.

All the configurations with perpendicular screws showed a failure due to timber embedment and double hinge in the screw (Fig. 5e and f). The reference configuration for screws inclined to 45°, the configuration with single soundproofing interlayer and the configuration with the OSB interlayer showed screw tensile-bending combined failure or screw withdrawal failure (Fig. 5a and b). The configuration with screws inclined to 45° and reduced length showed in all specimens a failure due to the screw withdrawal (Fig. 5c and d). The configuration with screws inclined to 45° and double soundproofing interlayer showed in all specimens a screw failure due to the combined effect of axial force and bending.

Conversely to the other cases, in this latter configuration, the UPN profile was damaged due to contact between the UPN profile itself with the screw shank (Fig. 6a). A visible denting was found in the VGU washers (Fig. 6b).

The insertion of the soundproofing interlayer in the perpendicular screw connection led to a 5% increase in strength. The insertion of the soundproofing interlayer in the configuration with 45° screws led to a reduction of 10%, 17% and 23% in strength in the cases of the soundproofing interlayer, OSB interlayer and double soundproofing interlayer, respectively.

In the case of a perpendicular screw, there is no variation in slip modulus with the interlayer insertion (−1%). In the case of inclined screws, the reduction is significant: 23%, 45% and 84% in the cases of the soundproofing interlayer, OSB interlayer and double interlayer, respectively. The configuration with screws inclined at 45° and reduced length has a slip modulus 38% higher than the reference connection and 51% less strength. It is worth noting that the coefficient of variation of the slip modulus of configurations with OSB interlayer, screw with reduced length and double interlayer is 42% or higher. Therefore the measured values of k_s could not represent the actual configuration behaviour. Part of the scatter can be explained by having only two screws per specimen, making the test samples extremely sensible to installation modes. Another scatter source can be related to using a single LVDT only.

The low sensitivity of the capacity of connections with perpendicular screws to the presence of the interlayer may be related to the clamping effect provided by the steel plate. Even in the presence of an interlayer, the screw is not free of bending in the proximity of the plate due to the end restraint effect. Whilst in the case of inclined screws, the clamped end is further away from the sliding plane due to the washer geometry, thus making the end restraint less effective. When the interlayer is present, the screw is free of bending for a longer part reducing both the slip modulus and the strength appreciably.

3. Finite element model

3.1. Definition

The problem of the determination of the capacity of connections with inclined screws is dimensionally reduced by assuming a beam behaviour of the screw and describing its interaction with timber using 2-node connector elements (Figs. 7 and 8). In the finite element method, a beam is an element in which assumptions are made so that the problem is reduced to one dimension. In this way, the primary solutions are functions of position along the beam axis only. The fundamental assumption in the beam theory is the indeformability of the cross-section. Neglecting the thread, the cross-section of the screw can be regarded as a solid circular section. Circular sections belong to the category of compact sections; therefore, they are not prone to in-plane section deformation, making the fundamental assumption valid. The beam theory can better approximate a three-dimensional continuum when the axial dimension noticeably prevails on the transversal section dimensions. In general, the axial dimension should be interpreted as the distance between significant discontinuities in cross-section or the distance between restraints. Common screw types have negligible section variations over screw length. The small core section increments are usually made in the areas without threads underneath the screw head or between the two threads of double-threaded screws, thus causing a partial compensation of the geometric properties. In determining the section properties, the circular section is assumed to have a diameter equal to 1.1 times the screw core diameter d_c as suggested for transversal capacity calculation in Eurocode 5 [17] to account for the thread roughly.

The beam elements used to model the screw are mono-dimensional and linear, with section properties integrated during the analysis to account for the non-linear behaviour of steel. The elements length l_m is one-hundredth of the overall screw length l. An elastic-perfectly plastic isotropic behaviour is assumed for the screw steel. The adopted Young's elasticity modulus is E_s = 210000 N/mm² and the mean yielding strength is f_y = 1200 N/mm². This value corresponds to typical steel grades of carbon-steel self-tapping screws, hardened after forming the thread geometry [32–35].

The interaction between the screw and the surrounding timber is modelled through discrete connectors. Connector elements in Abaqus/Standard [36] do not eliminate degrees of freedom. The kinematic constraints are enforced with Lagrange multipliers which are additional solution variables. Fig. 8 shows the elementary elements that make the connectors system used to model the complex screw-timber interaction.

The element E_{pa} is an elastic–plastic spring which schematizes the interaction in the grain direction. In the direction perpendicular to the grain, the timber embedment is reproduced via the analogous elastic–plastic spring $E_{pe,2}$ (Fig. 9a and b).

The elastic stiffness of each connector element E_{pa} and $E_{pe,2}$ are assumed as:

$$K_{E_{pa}} = k_h d l_m \cos\theta \tag{3}$$

$$K_{E_{pe,2}} = \beta k_h d l_m \sin\theta \tag{4}$$

where k_h is the stiffness per unit of length of the beam and has been assumed as for the regression formula provided in [6]:

$$k_h = -147.8d + 30.9\rho^{0.46}d^{0.68} \tag{5}$$

Fig. 5. Failure modes: (a) Screw and withdrawal with one hinge (b) Withdrawal with one hinge (c, d) Withdrawal (e, f) Double hinges.
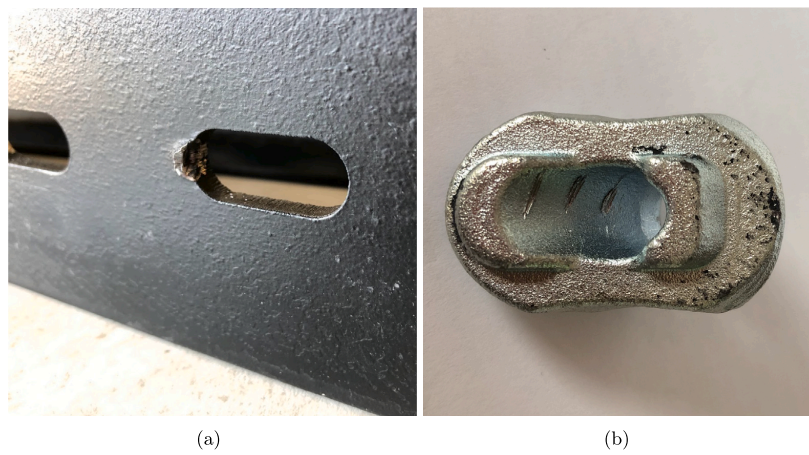
Fig. 6. Damage of the (a) steel member and (b) washer.
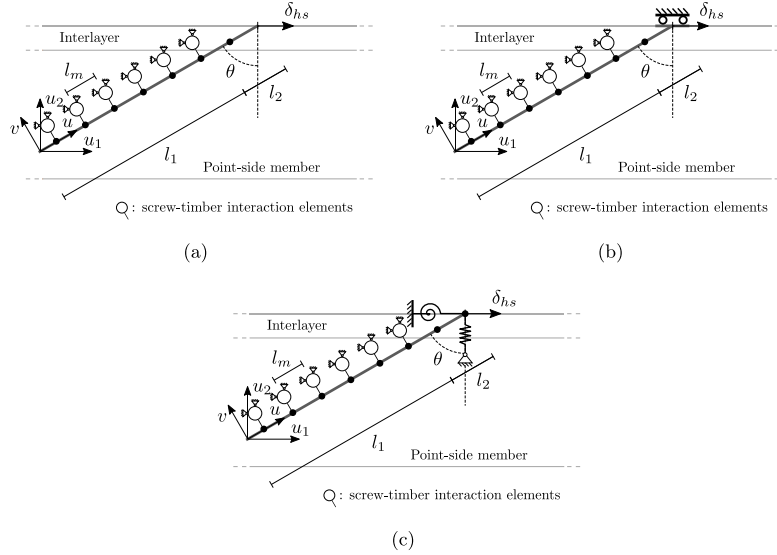
Fig. 7. Finite element models: (a) Free-end and (b) Clamped-end (c) Springed-end.
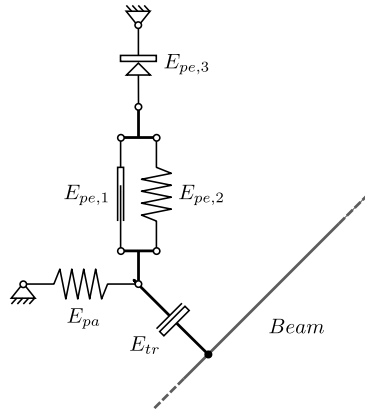
Fig. 8. Scheme of screw-timber interaction modelling.

where $\beta = 0.5$, ρ is the timber density, d is the screw thread outer diameter and l_m the length of the element between two connectors.

In this way, timber is regarded as a fibred medium with non-interacting fibres in the two perpendicular directions. The in-plane shear stiffness in the plane of the screw is neglected, and the projection of the element length l_m over the direction parallel and perpendicular to the sliding plane represents the width of the tributary area of the connector elements, E_{pa} and $E_{pe,2}$ respectively. Coherently with the outcomes of the studies conducted by Schweigler et al. in [37,38] on the load-to-grain angle dependence of the embedment behaviour and the phenomenological modelling of embedment behaviour of dowel-type fasteners, an elastic-perfectly plastic behaviour is assumed for the connectors schematizing parallel to grain behaviour (E_{pa}) while an elastic-hardening behaviour is assumed for connectors schematizing perpendicular to grain behaviour ($E_{pe,2}$). The yielding force of E_{pa} and

$E_{pe,2}$ are assumed as:

$$F_{y,E_{pa}} = f_{h,0} d l_m \cos\theta \tag{6}$$

$$F_{y,E_{pe,2}} = f_{h,90} d l_m \sin\theta \tag{7}$$

and the ultimate force in the direction perpendicular to the grain at a displacement equal to $2d$ is assumed as:

$$F_{u,E_{pe,2}} = \Gamma F_{y,E_{pe,2}} \tag{8}$$

where Γ has been assumed 1.72 as found by Schweigler et al. in [37, 38].

The embedment strength of E_{pa} and $E_{pe,2}$ are assumed as in the Eurocode 5 [17]:

$$f_{h,\alpha} = \frac{f_{h,0}}{k_{90,e} \sin^2\alpha + \cos^2\alpha} \tag{9}$$

where α is the force to the grain angle, $k_{90,e}$ can be assumed as $1.35 + 0.015 d_{ef}$ and $f_{h,0}$ is the embedment strength in the direction parallel to the grain and is given by the following equation:

$$f_{h,0} = 0.082(1 - 0.01 d_{ef})\rho \tag{10}$$

with ρ the mean timber density and d_{ef}, the effective screw diameter that according to Eurocode 5 [17] can be assumed as 1.1 the screw core diameter d_c. The Eq. (10) is currently implemented in the Eurocode 5 and derives from the linear interpolation of the mean embedding strength against mean timber density of an experimental campaign conducted on softwood by Whale and Smith [39].

The bi-linear approach defined for both E_{pa} and $E_{pe,2}$ is plotted in Fig. 9a and b.

The friction on the sliding plane is considered via the combination of $E_{pe,1}$ and $E_{pe,3}$. $E_{pe,1}$ represents a transversely rigid and axially free element (Fig. 9a and b). The role of $E_{pe,1}$ is to transmit forces parallel to the sliding plane between the sliding plane and the screw. $E_{pe,3}$ is a friction element; It provides a reaction parallel to the sliding plane proportional to the force acting perpendicular to it according to the relationship $F_\parallel = \mu F_\perp$ only when it is axially compressed. On the basis of the literature review presented in [40], a coefficient of friction (μ) equal to 0.48 is adopted as a mean value.
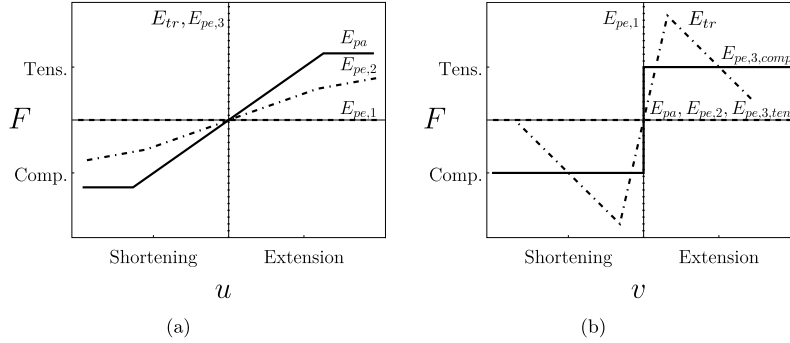
Fig. 9. Constitutive law of elements: (a) axial behaviour; (b) transversal behaviour.
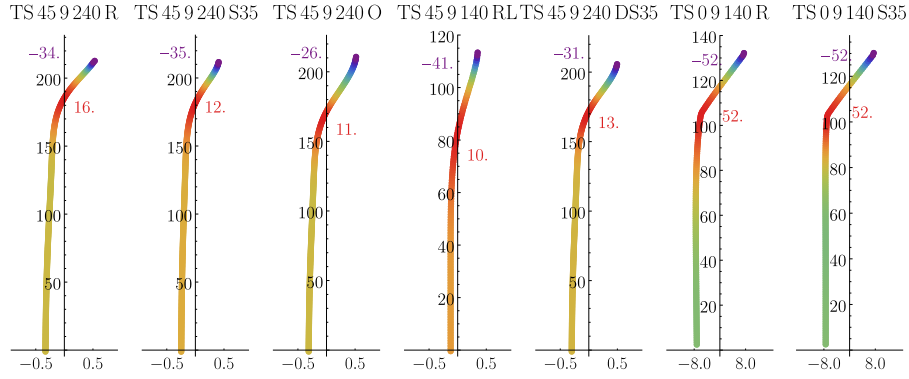
Fig. 10. Finite element clamped-end model predicted deformed shapes and bending moment contour at failure (kN mm).

The withdrawal behaviour is modelled through rigid-plastic connectors E_{tr} whose properties are defined according to the findings of Blaß et al. [41]. According to the formulation proposed by Blaß et al. the withdrawal failure stress can be estimated as follows:

$$f_{w,\alpha} = \frac{f_{w,0}}{k_{90,w} \sin^2 \alpha + \cos^2 \alpha} \tag{11}$$

where $f_{w,0}$ can be estimated according to the following formula (Eq. (12)) descending from a multiple regression analysis of 413 test results conducted on self-tapping screws with $d = 6 \div 12$ without predrilling [41]:

$$f_{w,0} = 0.6 d^{-0.5} l_{ef}^{-0.1} \rho^{0.8} \tag{12}$$

and where d is the screw thread outer diameter, α is the force to the grain angle and $k_{90,w}$ is 1.2. The associated withdrawal failure force per connector is:

$$F_{u,E_{tr}} = f_{w,\alpha} \pi d l_m \tag{13}$$

A linear damage evolution is assigned to E_{tr} to reproduce the withdrawal failure. According to the findings of Bedon et al. [23], based on detailed three-dimensional finite element models, an ultimate displacement of 4 mm is assumed.

Along the portion of the screw inserted in the soundproofing layer, no connectors are considered. Being the soundproofing layer elastic modulus 1/4200 times the timber elastic modulus, the interlayer can be assumed as a pure gap between main connection members.

The connectors are restrained to external hinges capable of blocking translational degrees of freedom only. The slip between the UPN profile

and the timber members is reproduced by an imposed displacement applied to the screw head, parallel to the sliding plane (7a and b). Therefore the typical simulation consisted of a static incremental, displacement-controlled analysis.

Three different boundary conditions are considered for the head-end of the screw. In the first case, the head-end is considered free (Fig. 7a), while in the second case, the translation perpendicular to the sliding plane u_2 and the rotation ϕ_3 are restrained (Fig. 7a). The free-boundary condition describes the initial loading phases where small gaps are present between components. The gap is located between the screw thread and the washer in the case of inclined screw connections and between the screw thread and the hole surface in the steel element in connections with screws perpendicular to the sliding plane. The clamp boundary condition is suitable for describing the restraint given by the washer or by the web of the steel member to the screw head at failure conditions where contact between components is established. This behaviour is testified by Fig. 5f where a plastic hinge under the screw head can be observed. In the third case, the head-end is connected to non-linear translational and rotational springs. A tri-linear hardening behaviour has been defined to describe the evolution of the end restraint from the free-end condition to the full establishment of a clamp restraint. The spring constitutive laws parameters are defined in Table 4. The second constitutive law branch is characterized by a stiffness double the stiffness of the first loading branch, while in the third branch, the clamping constraint is enforced by assigned high stiffness values. The second branch represents the phase during which the screw thread and washer plasticization happen Fig. 6b. The model here described has been implemented in ABAQUS/Standard [36] and parametrized via MATLAB [42].

Fig. 11. Axial stresses at failure load along the screw axis on three section points: centroid (black), circumference point nearest to the shear plane (red) and circumference point nearest to the specimen mid-plane (blue).

Table 4
Tri-linear constitutive law parameters for translational and rotational degree of freedom of Springed-end model.

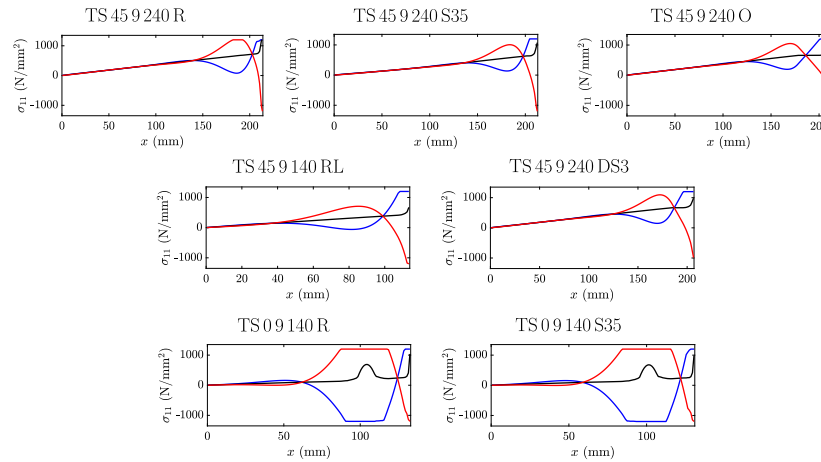| Translational			
u_{lim} (mm)	1.5	3	∞
K_{tr} (N/mm)	2500	5000	∞
Rotational			
ϕ_{lim} (rad)	$\pi/36$	$\pi/18$	∞
K_{rot} (Nmm/rad)	250000	500000	∞

3.2. Validation

Finite element models force–displacement curves are superimposed on experimental results in Fig. 3. The free-end model predicted initial stiffness constitutes a lower limit of the experimental stiffness of inclined screws connections. The model is not able to follow the force–displacement curve beyond approximately 40% of the failure load nor of predicting the failure modes or the failure loads. This model has to be regarded as a model suitable for obtaining a conservative estimate of the slip modulus.

Conversely, the clamped-end model is significantly stiffer compared to the observed experimental behaviour. The FEM-predicted slip modulus is two to seven times the experimental slip modulus as in the first loading phases a gap is present between the screw thread and the washer. This gap prevents the explication of the clamped end restraint at the beginning of the test. The clamped end model tends to underestimate the failure load with an increasing trend for lower inclination angle and longer screws (Table 5). These discrepancies might depend on the indeterminacy of the model input mechanical parameters that have been chosen according to literature instead of direct testing. The scatter between the mean experimental failure loads and finite element model predicted loads is −15% on average.

The springed-end model is able to follow the force–displacement of the connection until failure with reasonable approximation. The slip modulus prediction is more accurate than for previous models, but it is worth noting that strictly speaking, different constitutive laws should have been used for the end restraint springs of configuration with and without washers and with or without interlayers. However, the exact fitting of the connection behaviour for low loads is outside the paper aim.

In the configuration TS 45 9 240 DS35, the connection behaviour is affected by the presence of the large gap between the screw shank and the web of the UPN profile (Fig. 1b) and the conventional ultimate displacement of 15 mm is not enough to enable the screw shank-UPN contact. Consequently, the end-restraint considered in the finite element models is not suitable for describing this particular case.

Despite the differences between the Clamped-end model and the Springed-end model in terms of force–displacement curves, this latter model predicts approximately the same failure load and the same failure modes of the Clamped-end model, being able at the same time of grasping the initial load-slip phase (Table 5). In Fig. 10, the screw bending moment contour-plot is shown on the screw deformed shape at failure. In Fig. 11 the variation of the screw stresses along its axis are reported. The curves represent the axial stresses at failure on three section points of the screw: the centroid and two diametrically opposed points. It is worth noting that in configurations with inclined screws, the axial tensile stress on the section centroid, being representative of the axial force, is prevalent, while in the case of a screw perpendicular to the sliding plane, the axial component is negligible. As proven by the presence of the softening branch in Fig. 3 and by the reaching of the failure stress on all three section points as shown in Fig. 11, configuration TS 45 9 240 R, fails according to the FEM in a combination of withdrawal and screw tensile-bending failure, being coherent with the experimental results expressed in Table 3. Also in the case of configuration TS 45 9 240 S35 the FEM predicted failure mode is in good agreement with the experimental outcomes. In this case, due to the increased bending moment in the part of the screw inserted in the interlayer, a larger portion of the screw is subjected to yielding strength, and the screw failure anticipated the withdrawal. For configuration TS 45 9 240 O a clear withdrawal of the screw is observed. The softening branch accurately follows the experimental behaviour. The screw almost remains in the elastic range. In this case, the reduced effective length of the screw in the main timber member prevails over the effect of the increased bending moment due to interlayer presence. Configuration TS 45 9 140 RL exhibited a clear withdrawal failure in both experimental tests and finite element model, as shown in Fig. 12a.

In both perpendicular screws configuration, TS 0 9 140 R and TS 0 9 140 S35, the finite element model predicts a double-hinge formation (Fig. 10) that is the same experimentally assessed failure mode (Fig. 5f). Significant embedment has been observed in the finite element model (Fig. 12b) as well as on the specimens (Fig. 5e).

Table 5
Finite element models results and comparison with experimental results for different boundary conditions at the head-end of the screw.

Springed end							
	$k_{i,m}$ (kN/mm)	$S_{FEM-exp}$ (%)	$k_{s,m}$ (kN/mm)	$S_{FEM-exp}$ (%)	$F_{max,m}$ (kN)	$S_{FEM-exp}$ (%)	u_u (mm)	$S_{FEM-exp}$ (%)
TS 0 9 140 R	4,13	72%	3,78	92%	11,37	−25%	15,00	0%
TS 0 9 140 S35	2,59	−19%	2,36	20%	11,68	−27%	15,00	0%
TS 45 9 240 R	7,97	−13%	7,36	−30%	28,07	−17%	4,40	−28%
TS 45 9 240 S35	7,59	−16%	7,49	−7%	26,54	−13%	4,08	−26%
TS 45 9 240 O	4,32	−5%	4,31	−26%	24,19	−14%	4,35	−36%
TS 45 9 140 RL	9,18	−55%	8,90	−38%	16,50	−1%	2,85	−5%
TS 45 9 240 DS35	5,08	331%	5,02	198%	24,90	−4%	4,35	−71%

Clamped end							
	$k_{i,m}$ (kN/mm)	$S_{FEM-exp}$ (%)	$k_{s,m}$ (kN/mm)	$S_{FEM-exp}$ (%)	$F_{max,m}$ (kN)	$S_{FEM-exp}$ (%)	u_u (mm)	$S_{FEM-exp}$ (%)
TS 0 9 140 R	13,74	471%	13,68	593%	11,59	−24%	15,00	0%
TS 0 9 140 S35	10,30	222%	10,16	418%	11,98	−25%	15,00	0%
TS 45 9 240 R	38,01	317%	37,98	262%	27,85	−18%	1,06	−83%
TS 45 9 240 S35	36,50	302%	36,50	352%	26,22	−14%	0,81	−85%
TS 45 9 240 O	27,49	504%	27,49	375%	23,57	−16%	1,03	−85%
TS 45 9 140 RL	29,26	42%	29,26	102%	16,37	−2%	0,70	−77%
TS 45 9 240 DS35	29,86	2435%	29,86	1671%	24,15	−7%	0,99	−93%

Free end							
	$k_{i,m}$ (kN/mm)	$S_{FEM-exp}$ (%)	$k_{s,m}$ (kN/mm)	$S_{FEM-exp}$ (%)	$F_{max,m}$ (kN)	$S_{FEM-exp}$ (%)	u_u (mm)	$S_{FEM-exp}$ (%)
TS 0 9 140 R	5,63	134%	5,63	185%	5,36	−65%	15,00	0%
TS 0 9 140 S35	3,31	4%	3,30	69%	4,77	−70%	15,00	0%
TS 45 9 240 R	7,32	−20%	7,24	−31%	9,51	−72%	15,00	147%
TS 45 9 240 S35	4,46	−51%	4,43	−45%	8,99	−70%	15,00	173%
TS 45 9 240 O	1,27	−72%	1,27	−78%	5,43	−81%	15,00	119%
TS 45 9 140 RL	7,16	−65%	7,10	−51%	8,90	−47%	10,35	245%
TS 45 9 240 DS35	2,15	82%	2,14	27%	6,14	−76%	15,00	0%
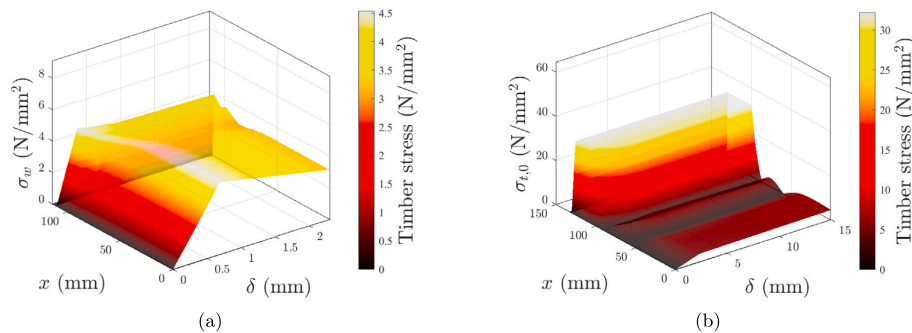
Fig. 12. (a) FEM withdrawal stresses of configuration TS 45 9 140 RL along the screw axis for increasing connection slip and (b) FEM embedment stresses of configuration TS 0 9 140 R along the screw axis for increasing connection slip.

4. Analytical models

In this section the results of five hundred finite element analyses in terms of predicted load are compared with the results of three analytical models namely:

- the analytical model provided by Eurocode 5 [17] based on a quadratic interaction;
- an additive model, similar to the model proposed by Bejtka I. and Blaß H.J. in [19] for the case of timber-to-steel connections;
- a hybrid additive-quadratic interaction model.

The comparison is based on a database of analysis of cases defined by the parameters in the range reported in table Table 6. Being the results in terms of failure modes and failure loads the same between the Springed-end and the Clamped-end model, it was decided to generate the database using the ideal clamping-restraint. In this way, the result

Table 6
The domain boundaries for configurations of practical interest.

Parameter	l_1 (mm)	l_2 (mm)	d (mm)	θ (°)	ρ (kg/m³)	f_y (N/mm²)	μ
Lower Bound	50	0	5	0	400	600	0
Upper Bound	600	50	15	60	800	1800	0.8

is valid for the so-called thick-plate. Plates that are able to rotationally restrain the head of the fastener.

4.1. Eurocode 5 - Quadratic interaction model

The European Yield Model (EYM) is a commonly accepted method to calculate the capacity of connections with laterally loaded dowel-type fasteners. The EYM is adopted in Eurocode 5 [17]. The EYM is

based on Johansen yield theory [16]. According to Johansen's yield theory, it is assumed that steel and timber exhibit a rigid-plastic behaviour. Different failure modes are identified depending on the degree of restraint that the steel plate has on the fastener. According to Johansen theory [16] the transversal strength of a dowel-type fastener connecting a thick plate to a timber member is given by Eq. (14). In the case of a thick plate, it is assumed that the plate is able to restrain the rotation at the end of the fastener. Consequently, the connection may fail due to fastener embedment, due to hinge formation in the proximity of the plate, or the formation of a double hinge. The associated failure loads are:

$$R_{tr} = \min \begin{cases} R_{tr,1} = f_h l_1 d_{ef} & \text{Embedment} \\ R_{tr,2} = f_h l_1 d_{ef} \left(\sqrt{2 + \frac{M_y}{f_h d_{ef} l_1^2}} - 1 \right) & \text{Single hinge} \\ R_{tr,3} = 2\epsilon \sqrt{M_y f_h d_{ef}} & \text{Double hinge} \end{cases} \quad (14)$$

Where coefficient ϵ is assumed 1.15 in the Eurocode 5 to take into consideration the differing partial safety factors and k_{mod} for steel and timber while in the equation associated with single hinge failure mode, this coefficient is incorrectly missing in the code [43]. The Johansen equation has been extended by Blaß and Laskewitz [44] to the case of connection with an interlayer. In the case of a thick plate and interlayer connected to the timber:

$$R_{tr} = \min \begin{cases} R_{tr,1} = f_h l_1 d_{ef} + \delta f_h l_2 d_{ef} & \text{Embedment} \\ R_{tr,2} = 2f_h \left(-l_2 + \sqrt{l_2^2 + \frac{M_y}{f_h d_{ef}} - \frac{\delta l_2^2}{2} + l_1 l_2 + \frac{l_1^2}{2}} \right) d_{ef} \\ \quad - f_h l_1 d_{ef} + \delta f_h l_2 d_{ef} & \text{Single hinge} \\ R_{tr,3} = f_h \left(-l_2 + \sqrt{l_2^2 + \frac{4M_y}{f_h d_{ef}} - \delta l_2^2} \right) d_{ef} + \delta f_h l_2 d_{ef} & \text{Double hinge} \end{cases} \quad (15)$$

with $\delta = f_{h,i}/f_h$, the ratio between the embedment strength of the interlayer and the main timber member. According to Eurocode 5, the yielding moment should be determined according to the following:

$$M_y = 0.3 f_u d_{ef}^{2.6} \quad (16)$$

Moreover, in Eurocode 5 [17] the rope effect is considered. A term equal to μR_{ax} is added to the strength associated with single hinge and double hinge failure modes (Eq. (14)) to account for the friction induced by the force normal to the sliding plane generated by the deformation of the fastener. According to Eurocode 5, this contribution should be limited to 100% of R_{tr}.

In the case of inclined fasteners, two more failure modes exist. Strengths associated with withdrawal failure and tensile failure can be expressed by means of Eq. (17).

$$R_{ax} = \min \begin{cases} R_{ax,1} = f_w l_1 d \min(\frac{d}{8}, 1) & \text{Withdrawal} \\ R_{ax,2} = f_u \pi \frac{d_{ef}^2}{4} & \text{Tensile} \end{cases} \quad (17)$$

According to the current Eurocode 5 [17], a quadratic interaction between transversal and axial capacity should be considered irrespective to the combined failure modes:

$$\left(\frac{F_{tr}}{R_{tr}} \right)^2 + \left(\frac{F_{ax}}{R_{ax}} \right)^2 \leq 1 \quad (18)$$

Substituting in Eq. (18) F_{tr} and F_{ax} as a function of the force parallel to the sliding plane and considering the associated equality which corresponds to a failure condition, the capacity of the connection in the direction parallel to the sliding plane can be rewritten as [18]:

$$R_{v,QI} = \frac{1}{\sqrt{\left(\frac{\cos\theta}{R_{tr}} \right)^2 + \left(\frac{\sin\theta}{R_{ax}} \right)^2}} \quad (19)$$

4.2. Additive model

Alternatively, a purely additive model can be considered. In this case, the capacity of the connection is given by the sum of the components parallel to the sliding plane of the axial and transversal resisting forces and the friction force on the sliding plane generated by the perpendicular components of the resisting forces:

$$R_{v,AD} = \min \begin{cases} R_{v,1} = R_{ax,1} \sin\theta + R_{tr,1} \cos\theta + \mu(R_{ax,1} \cos\theta - R_{tr,1} \sin\theta) \\ R_{v,2} = R_{ax,2} \sin\theta + R_{tr,1} \cos\theta + \mu(R_{ax,2} \cos\theta - R_{tr,1} \sin\theta) \\ R_{v,3} = R_{ax,1} \sin\theta + R_{tr,2} \cos\theta + \mu(R_{ax,1} \cos\theta - R_{tr,2} \sin\theta) \\ R_{v,4} = R_{ax,2} \sin\theta + R_{tr,2} \cos\theta + \mu(R_{ax,2} \cos\theta - R_{tr,2} \sin\theta) \\ R_{v,5} = R_{ax,1} \sin\theta + R_{tr,3} \cos\theta + \mu(R_{ax,1} \cos\theta - R_{tr,3} \sin\theta) \\ R_{v,6} = R_{ax,2} \sin\theta + R_{tr,3} \cos\theta + \mu(R_{ax,2} \cos\theta - R_{tr,3} \sin\theta) \end{cases}$$
$$(20)$$

According to this model, both tensile and bending capacity may be exploited independently of each other.

Blaß and Bejtka in [19] proposed a quasi-additive model for timber-to-timber connections. In the model, the interaction between embedment and withdrawal strength is accounted for by introducing a modified withdrawal parameter while the interaction between tensile and bending stresses in the fastener is neglected. It is worth noting that due to the reduced ultimate displacement of connection with the inclined screw, the reduction in withdrawal parameter caused by the transversal displacement of the fastener is found to be negligible [19].

4.3. Hybrid model

Finite element analysis clearly highlighted that strong coupling between the axial and transversal behaviour of the screw exists. Even in the elastic formulation of an inclined beam on foundation problem, an exact closed-form solution is not available [6]. Therefore, the authors motivated by the striking inaccuracy of the quadratic interaction model provided by the Eurocode 5 and by the lack of a mechanical justification for a purely additive model, formulated a hybrid model. Axial and transversal mechanisms are combined as in Eqs. (21) and (22). When the tensile failure mechanism is combined with plastic hinge formation, a quadratic interaction is considered to account for the interaction between axial force and bending moment, while in other cases the mechanisms are considered purely additive. This model is simple enough to be used by practitioners or to be implemented in codes.

$$R_{v,HY} = \min \begin{cases} \text{Embedment + withdrawal} & \textbf{Additive} \\ \text{Embedment + tensile} & \textbf{Additive} \\ \text{Hinge + withdrawal} & \textbf{Additive} \\ \text{Hinge + tensile} & \textbf{Quadratic interaction} \\ \text{Double hinge + withdrawal} & \textbf{Additive} \\ \text{Double hinge + tensile} & \textbf{Quadratic interaction} \end{cases}$$
$$(21)$$

$$R_{v,HY} = \min \begin{cases} R_{v,1} = R_{ax,1} \sin\theta + R_{tr,1} \cos\theta + \mu(R_{ax,1} \cos\theta - R_{tr,1} \sin\theta) \\ R_{v,2} = R_{ax,2} \sin\theta + R_{tr,1} \cos\theta + \mu(R_{ax,2} \cos\theta - R_{tr,1} \sin\theta) \\ R_{v,3} = R_{ax,1} \sin\theta + R_{tr,2} \cos\theta + \mu(R_{ax,1} \cos\theta - R_{tr,2} \sin\theta) \\ R_{v,4} = \frac{1}{\sqrt{\left(\frac{\cos\theta}{R_{tr,2}} \right)^2 + \left(\frac{\sin\theta}{R_{ax,2}} \right)^2}} \\ R_{v,5} = R_{ax,1} \sin\theta + R_{tr,3} \cos\theta + \mu(R_{ax,1} \cos\theta - R_{tr,3} \sin\theta) \\ R_{v,6} = \frac{1}{\sqrt{\left(\frac{\cos\theta}{R_{tr,3}} \right)^2 + \left(\frac{\sin\theta}{R_{ax,2}} \right)^2}} \end{cases}$$
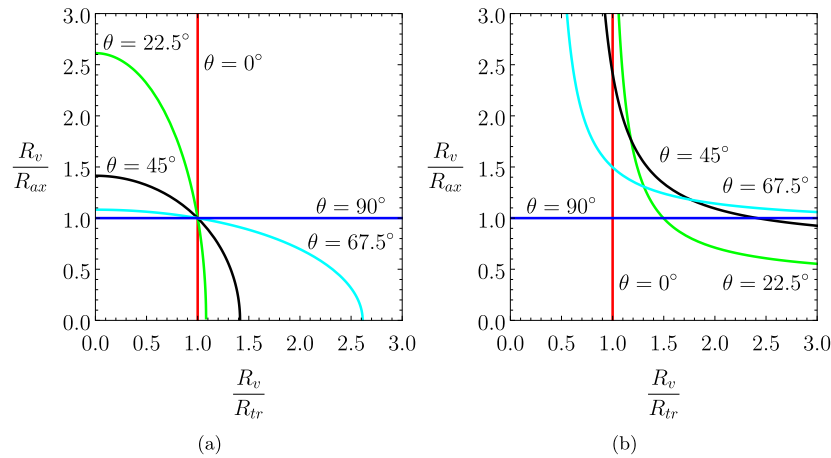$$(22)$$

Fig. 13. Ratios between connection capacity and fastener transversal and axial capacity: (a) quadratic interaction model and (b) additive model with $\mu = 0.0$.

4.4. Comparisons

In a quadratic interaction model, for increasing exploitation of the capacity in one of the fastener reference directions, namely axial or transversal direction, the capacity in the perpendicular direction decreases (Fig. 13a). In an additive model, the decrease of capacity obtained by increasing the exploitation of the resisting mechanism in the perpendicular direction is characterized by an asymptotic behaviour (Fig. 13b).

Figs. 14a and 15a show the correlation between finite element model predicted failure loads and analytically predicted failure loads for connection without and with interlayer respectively, while Figs. 14b and 15b show the distributions of the percentage scatters between models defined as follows:

$$S_{R_v An-FEM} = \frac{R_{v,An} - R_{v,FEM}}{R_{v,FEM}} 100\% \qquad (23)$$

Regarding connections without interlayers, the quadratic interaction model gives conservative estimates of the capacity of the connection in almost all cases. More than 95% of the capacity of the samples is underestimated (Fig. 14b). An opposite behaviour is observed for the additive model. The proposed hybrid model is characterized by the highest correlation ($R^2 = 0.76$) and lowest RMSE (root-mean-square error) (Fig. 14a and Table 7). These results confirm the strong interaction between axial and transversal behaviour of connections without interlayer.

In the case of connections with interlayer, it is assumed $\delta = 0.5$. In this case, the quadratic interaction model is completely unsuitable for describing the effective connection behaviour. The median percentage error is -54%. The hybrid and the additive models show similar correlation with finite element model results (Table 7). The additive model proves to be more overestimating, while the hybrid model is characterized by more dispersed scatters (Fig. 15b). Although less than the additive model, in some cases the hybrid model is still overestimating. This is due to the hypothesis of additivity of withdrawal mechanism with hinges formation mechanisms. Withdrawal of the screw induces high tensile stresses that may significantly affect the screw bending capacity in some cases. However, with the aim of providing an elementary model, the most realistic limit hypothesis is considered.

Table 7
Statistic of the comparison between analytical and finite element model results.

		Quadratic I.	Additive	Hybrid
Without interlayer	RMSE (kN)	16.7	10.4	9.9
	R^2	0.31	0.73	0.76
With interlayer	RMSE (kN)	19.5	9.8	10.0
	R^2	−0.04	0.74	0.73

5. Conclusions

The proposed finite element model represents a valid alternative to complex three-dimensional models for the study of connections with inclined screws as it accurately describes the experimentally assessed behaviour in terms of both failure mode and failure loads (-15% on average). The reduced computational cost, which is associated with the reduced number of degrees of freedom, makes it suitable for carrying out comparisons and analyses for all configurations of practical interest.

The proposed hybrid analytical approach has proven to be more accurate than existing models, accounting, although in an approximate way, for the strong interaction between the axial and transversal behaviour of the screw. The main results of this experimental, numerical and analytical investigation can be itemized as follows:

- the insertion of thin soundproofing interlayer cause negligible reduction of slip modulus and strength in perpendicular screws restrained by a thick plate;
- connection with inclined screws and interlayer exhibit a more pronounced reduction for stiffness (23% to 84%) than for strength (10% to 23%);
- even in the case of slender screws, the bending moment component can reduce significantly the capacity of connections with inclined screws due to its interaction with the axial force;
- The bending moment component increases when an interlayer is inserted between main members due to its reduced mechanical properties compared to timber members.

Further studies on the behaviour of steel-to-timber connection with thin plates are necessary to assess the role of the end restraint on the
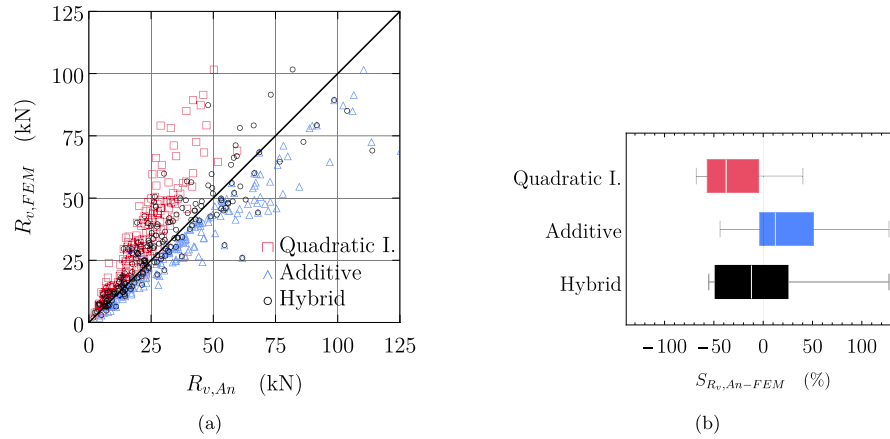
Fig. 14. Connections without interlayer: (a) Correlation plot between analytical and finite element model results (b) Minimum, 5th percentile, median, 95th percentile and a maximum of the percentage error between analytical and finite element model results.
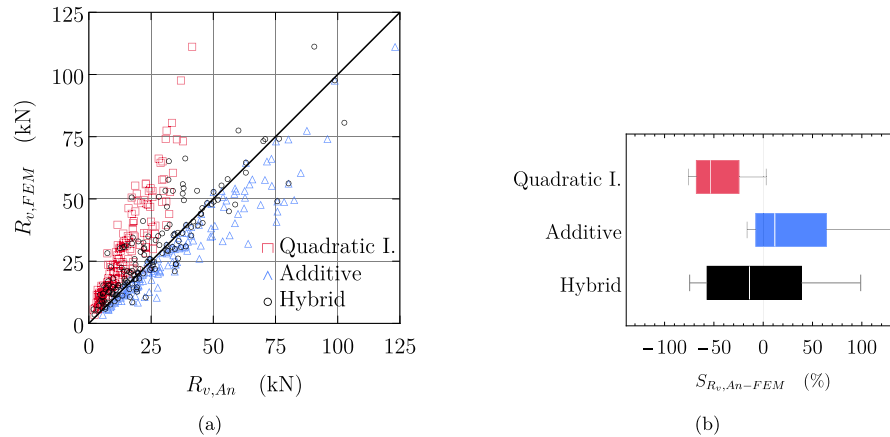
Fig. 15. Connections with interlayer: (a) Correlation plot between analytical and finite element model results (b) Minimum, 5th percentile, median, 95th percentile and a maximum of the percentage error between analytical and finite element model results.

mechanical properties reduction of the connection due to interlayer presence.

CRediT authorship contribution statement

Yuri De Santis: Conceptualization, Data curation, Formal analysis, Investigation, Methodology, Project administration, Resources, Software, Validation, Visualization, Writing – original draft, Writing – review & editing. **Angelo Aloisio:** Conceptualization, Data curation, Formal analysis, Investigation, Methodology, Validation, Visualization, Writing – original draft, Writing – review & editing. **Igor Gavrić:** Resources, Investigation, Writing – review & editing, Supervision. **Iztok Šušteršič:** Resources, Supervision. **Massimo Fragiacomo:** Resources, Supervision.

Declaration of competing interest

The authors declare that they have no known competing financial interests or personal relationships that could have appeared to influence the work reported in this paper.

Data availability

Data will be made available on request.

References

[1] Du H, Hu X, Xie Z, Wang H. Study on shear behavior of inclined cross lag screws for glulam-concrete composite beams. Constr Build Mater 2019;224:132–43.

[2] Chiniforush A, Valipour H, Ataei A. Timber-timber composite (TTC) connections and beams: An experimental and numerical study. Constr Build Mater 2021;303:124493.

[3] Liu Y, Yao Z, Wang F, Huang H, Que Z. Effect of arrangement distances on stiffness of shear-tension mode in timber-to-timber connections with inclined screws. Constr Build Mater 2022;314:125592.

[4] Krauss K, Li M, Lam F. Influence of mixed-angle screw installations in CLT on the cyclic performance of commercial hold-down connections. Constr Build Mater 2023;364:129918.

[5] Mirdad MAH, Chui YH. Stiffness prediction of Mass Timber Panel-Concrete (MTPC) composite connection with inclined screws and a gap. Eng Struct 2020;207(November 2019):110215.

[6] De Santis Y, Fragiacomo M. Timber-to-timber and steel-to-timber screw connections : Derivation of the slip modulus via beam on elastic foundation model. Eng Struct 2021;244(April):112798.

[7] Di Nino S, Gregori A, Fragiacomo M. Experimental and numerical investigations on timber-concrete connections with inclined screws. Eng Struct 2020;209(December 2019):109993.

[8] De Santis Y, Sciomenta M, Spera L, Rinaldi V, Fragiacomo M, Bedon C. Effect of interlayer and inclined screw arrangements on the load-bearing capacity of timber-concrete composite connections. Buildings 2022;12(12).

[9] Marchi L, Scotta R, Pozza L. Experimental and theoretical evaluation of TCC connections with inclined self-tapping screws. Mater Struct/Mater Construct 2017;50(3):1–15.

[10] A. Chiniforush A, Makki Alamdari M, Dackermann U, Valipour HR, Akbarnezhad A. Vibration behaviour of steel-timber composite floors, Part (1): Experimental and numerical investigation. J Construct Steel Res 2019;161:244–57.

[11] Vella N, Gardner L, Buhagiar S. Experimental analysis of cold-formed steel-to-timber connections with inclined screws. Structures 2020;24(December 2019):890–904.

[12] Yang R, Li H, Lorenzo R, Ashraf M, Sun Y, Yuan Q. Mechanical behaviour of steel timber composite shear connections. Constr Build Mater 2020;258:119605.

[13] Nie Y, Karimi-Nobandegani A, Valipour HR. Experimental behaviour and numerical modelling of Timber-Timber Composite (TTC) joints. Constr Build Mater 2021;290:123273.

[14] Kržan M, Azinović B. Cyclic response of insulated steel angle brackets used for cross-laminated timber connections. Eur J Wood Wood Prod 2021;79(3):691–705.

[15] Azinović B, Pazlar T, Kržan M. The influence of flexible sound insulation layers on the seismic performance of cross laminated timber walls. J Build Eng 2021;43(April).

[16] Johansen K. Theory of timber connections. Int Assoc Bridge Struct Eng 1949;9:249-262.

[17] Eurocode-5. Design of timber structures - Part 1-1: General - Common rules and rules for buildings. 2004, CEN.

[18] Tomasi R, Crosatti A, Piazza M. Theoretical and experimental analysis of timber-to-timber joints connected with inclined screws. Constr Build Mater 2010;24(9):1560–71.

[19] I. Bejtka HB. Joints with inclined screws. In: CIB-W18. 2002, p. 35–7–5, Kyoto (Japan).

[20] Blaß HJ, Sandhaas C, Meyer N. Steel-to-timber connections : Failure of laterally loaded dowel-type fasteners. In: Görlacher R, editor. Proceedings of the international network on timber engineering research, inter 2017, meeting 50, Kyoto, Japan, 28th - 31st August 2017. Timber Scientific Publishing; 2017.

[21] Blaß HJ, Laskewitz B. Joints with inclined screws. In: CIB-W18. 2000, p. 33–7–6, Delft (The Netherlands).

[22] Stamatopoulos H, Malo KA. Withdrawal stiffness of threaded rods embedded in timber elements. Constr Build Mater 2016;116:263–72.

[23] Bedon C, Fragiacomo M. Numerical analysis of timber-to-timber joints and composite beams with inclined self-tapping screws. Compos Struct 2019;207:13–28.

[24] Oudjene M, Meghlat EM, Ait-Aider H, Lardeur P, Khelifa M, Batoz JL. Finite element modelling of the nonlinear load-slip behaviour of full-scale timber-to-concrete composite T-shaped beams. Compos Struct 2018;196(March):117–26.

[25] Hassanieh A, Valipour HR, Bradford MA. Load-slip behaviour of steel-cross laminated timber (CLT) composite connections. J Construct Steel Res 2016;122:110–21.

[26] Schweigler M, Bader TK, Hochreiner G, Lemaître R. Parameterization equations for the nonlinear connection slip applied to the anisotropic embedment behavior of wood. Composites B 2018;142(November 2017):142–58.

[27] Izzi M, Rinaldin G, Polastri A, Fragiacomo M. A hysteresis model for timber joints with dowel-type fasteners. Eng Struct 2018;157(July 2017):170–8.

[28] Lemaitre R, Bocquet J-F, Schweigler M, Bader TK. Beam-on-foundation modelling as an alternative design method for timber joints with dowel-type fasteners - Part 1: Strength and stiffness per shear plane of single-fastener joints. Inter / 54-7-8 2019;(1949):1–16.

[29] ETA-23/0061. Flexible interlayer to be used for the reduction of flanking sound transmission and/or vibration transmission in construction works. EOTA; 2023.

[30] ETA-11/0030. Screws and threaded rods for use in timber constructions. EOTA; 2022.

[31] EN-26891. Timber structures - Joints made with mechanical fasteners - General principles for the determination of strength and deformation characteristics. 1991, CEN.

[32] Blaß HJ, Bejtka I, Uibel T. Tragfähigkeit von Verbindungen mit selbstbohrenden Holzschrauben mit Vollgewinde. In: Kalrsruher berichte zum ingenieurholzbau, vol. 4. 2006.

[33] Ringhofer A. Axially Loaded self-tapping screws in solid timber and laminated timber products. Dissertation, 2017.

[34] Ringhofer A, Augustin M, Schickhofer G. Basic steel properties of self-tapping timber screws exposed to cyclic axial loading. Constr Build Mater 2019;211:207–16.

[35] Niebuhr P, Sieder M. High-cycle fatigue behavior of a self-tapping timber screw under axial tensile loading. J Failure Anal Prevent 2020;20:580–9.

[36] Dassault Systèmes. Abaqus.

[37] Schweigler M, Bader TK, Hochreiner G, Unger G, Eberhardsteiner J. Load-to-grain angle dependence of the embedment behavior of dowel-type fasteners in laminated veneer lumber. Constr Build Mater 2016;126:1020–33.

[38] Schweigler M, Bader TK, Bocquet JF, Lemaître R, Sandhaas C. Embedment test analysis and data in the context of phenomenological modeling for dowelled timber joint design. Int Netw Timber Eng Res (INTER) - Meeting Fifty-Two, Tacoma (US) 2019;(INTER / 52 - 07 - 8):1–17.

[39] Whale LRJ, Smith I. The derivation of design clauses for nailed and bolted joints in eurocode 5. In: CIB-W18. 1986, p. 19–7–6, Delft (The Netherlands).

[40] Aurand S, Blaß HJ. Connections with inclined screws and increased shear plane friction. In: Görlacher R, editor. Proceedings - meeting 54 : 16-19 august 2021, online meeting / INTER, international network on timber engineering research. 2021, p. 147–68.

[41] Blaß HJ, Bejtka I, Uibel T. Tragfähigkeit Von Verbindungen Mit Selbstbohrenden Holzschrauben Mit Vollgewinde. In: Kalrsruher berichte zum ingenieurholzbau, vol. 4. 2006.

[42] MathWorks. MATLAB.

[43] Blaß HJ, Sandhaas C. Timber engineering - principles for design. KIT Scientific Publishing; 2017.

[44] Blaß HJ, Laskewitz B. Load-carrying capacity of joint with dowel-type fasteners and interlayers. In: CIB-W18. 2000, p. 33–7–6, Delft (The Netherlands).

6.3   Validation of finite element model for timber-to-timber inclined screws connections with interlayers

The same modelling approach of Sec. 6.2 is herein applied to timber-to-imber connections. In this case the relative displacement between members is reproduced by applying an equal and opposite displacement at hinges as showed in Fig. 6.1.
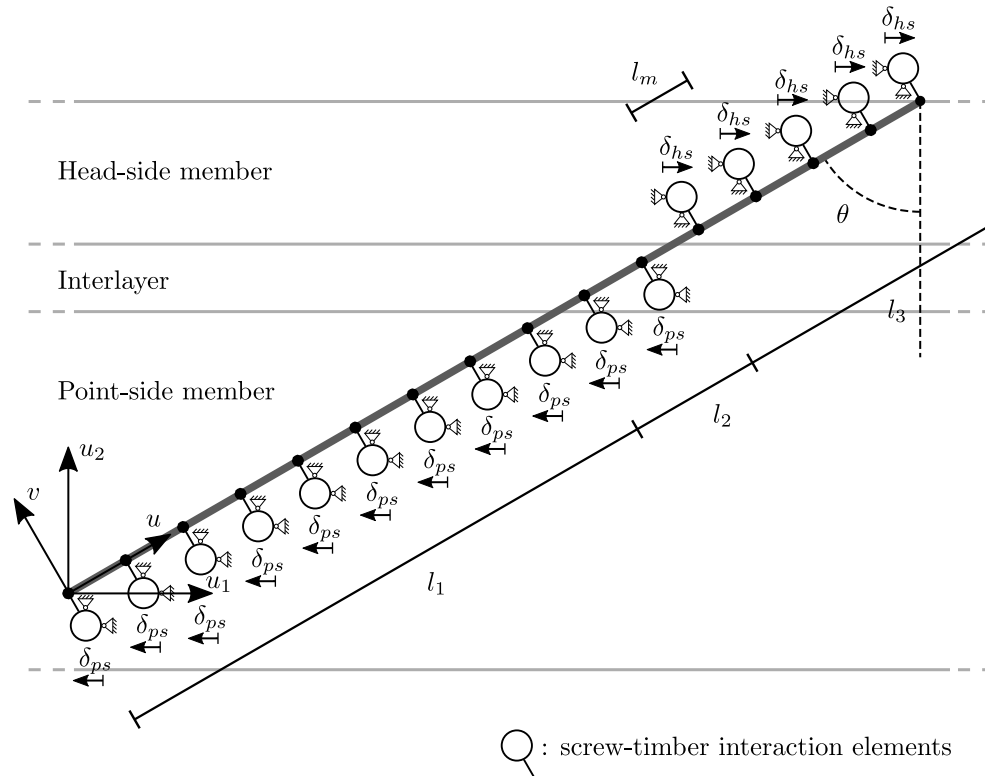
Figure 6.1: Timber-to-timber connection model.

In the following table a comparison between experimental outcomes of the campaign described Chapter 3 and finite element model prediction is showed. Similarly to timber-to-steel connection, the model is slightly underestimating in terms of predicted failure load. The average scatter is -10%. While, the slip modulus k_s is overestimated by a 25% on average. The initial slip modulus k_i is accurately predicted with an average scatter of -2%.

Name	$k_{i,exp}$ (kN/mm)	$k_{i,FEM}$ (kN/mm)	Δ (%)	$k_{s,exp}$ (kN/mm)	$k_{s,FEM}$ (kN/mm)	Δ (%)	$F_{max,exp}$ (kN/mm)	$F_{max,FEM}$ (kN/mm)	Δ (%)
TT 0 8 200 R	5,75	3,55	-38,25	2,74	3,54	29,13	6,62	5,92	-10,61
TT 0 8 200 S35	2,08	2,55	22,69	1,57	2,53	61,00	6,12	5,88	-3,94
TT 0 8 200 S90	2,10	2,55	21,52	1,36	2,53	85,86	5,06	5,88	16,18
TT 45 7 300 R	15,05	13,64	-9,35	14,73	13,64	-7,38	22,57	17,72	-21,47
TT 45 7 300 S35	11,11	13,67	23,08	9,79	13,69	39,79	16,31	13,26	-18,71
TT 45 7 300 S90	13,45	13,67	1,66	10,47	13,69	30,72	15,14	13,26	-12,43
TT 30 7 300 S35	7,31	8,05	10,06	6,86	8,02	16,86	16,45	17,06	3,73
TT 0 8 200 IS	7,37	3,55	-51,83	4,91	3,54	-27,94	7,51	5,92	-21,20
TT 45 7 300 IS	13,24	13,64	3,04	13,42	13,64	1,66	23,11	17,72	-23,31

Table 6.1: Comparison between experimental results (Chap. 3) and finite element model prediction.

Chapter 7

Capacity prediction of timber-to-concrete connections: three-dimensional finite element models

Abstract: Timber-to-concrete composite floors are a well-suited solution for retrofitting existing timber floors or for realizing newly built floors with a classical aesthetic appearance and at the same time characterized by high structural efficiency and human comfort. The concrete layer is poured over the existing planking or on OSB panels and it is mechanically joined to the underlying timber joist by means of steel fasteners. As the stiffness of the connection increases, the composite action increases. A wide-spreading solution consist in using inclined self-tapping screws as fasteners. However, while the mechanical performances of inclined screws connections without interlayer are deeply investigated in literature, comparatively less studies have been carried out regarding connections with interlayers. Lightweight and enhanced thermal and acoustic insulation can be achieved by using rubbercrete instead of traditional concrete. Detailed three-dimensional finite element models are used to investigate the influence of interlayers mechanical properties, of friction, of testing setup and concrete type on the mechanical behavior of connections with inclined screws. Surface interaction between components was found to be the most significant parameter. Both push-out and inclined test configurations introduce additional forces affecting the results. No significant reduction of mechanical performances is registered in connections with rubbercrete.

7.1 Introduction

The results of a numerical investigation are presented in two papers. The paper of Sec. 7.2 is focused on the study of connections with traditional concrete. The influence of interlayers mechanical properties, of friction and of testing setup is assessed. In the paper of Sec. 7.3 the mechanical behavior of a connection with slab made of rubbercrete are compared with the mechanical behavior of a connection with traditional concrete.

7.2 Paper: *Effect of Interlayer and Inclined Screw Arrangements on the Load-Bearing Capacity of Timber-Concrete Composite Connections*

Article

Effect of Interlayer and Inclined Screw Arrangements on the Load-Bearing Capacity of Timber-Concrete Composite Connections

Yuri De Santis [1,*], Martina Sciomenta [1], Luca Spera [1], Vincenzo Rinaldi [1], Massimo Fragiacomo [1] and Chiara Bedon [2]

1   Department of Civil, Architecture and Building and Environmental Engineering, University of L'Aquila, Via Giovanni Gronchi 18, 67100 L'Aquila, Italy
2   Department of Engineering and Architecture, University of Trieste, Via Alfonso Valerio 6/1, 34127 Trieste, Italy
*   Correspondence: yuri.desantis@graduate.univaq.it

Abstract: The solution of timber-to-concrete composite (TCC) floors represents a well-established construction technique, which is consistently used for both the retrofitting of existing timber floors and the realization of new diaphragms. The success of TCC floors relies on the intrinsic effectiveness in increasing both the in-plane (for lateral loads) and the out-of-plane (for gravity loads) performance of existing timber floors. As a widespread retrofit intervention, it is common to use existing floorboards as a permanent formwork for the concrete pouring. Rather few research studies of literature, in this regard, highlighted an overall reduction of load capacity and slip modulus due to the presence of such an interposed interlayer. In this regard, the present paper focuses on the use of screws as efficient mechanical connectors and analyses different configurations and inclination angles for their arrangement. This main goal is achieved by performing parametric Finite Element (FE) numerical analyses, validated on previous experimental tests, in order to specifically investigate the influence of the in-between interlayer, as well as the role of friction phenomena and the influence of the test setup and experimental protocol to achieve the basic mechanical performance indicators.

Keywords: timber-to-concrete composite (TCC) connections; self-tapping screws; inclined screws; interlayers; Finite Element (FE) models; experiments; push-out setup; friction; slip modulus

1. Introduction

Timber-to-concrete composite (TCC) system**s** with screws have become since the 1980s a widespread solution for floor-building and retrofitting, representing an option to the typical "timber plank" additional layer [1].

The framework of a generic TCC floor consists of a thin concrete layer overlapping timber beams mutually joined with steel fasteners (i.e., dowels, plates and screws). These can be fully or partially threaded and can be placed perpendicularly to the floor or inclined at an angle. The high efficiency of this solution compared to traditional floors lies in: (i) increased strength and stiffness, (ii) excellent acoustic/thermal insulation, (iii) improved fire resistance [2–4], (iv) capacity to reduce the sensitivity to vibrations, (v) horizontal diaphragms for structures and (vi) redistribution of more than 50% of a concentrated load to the nearest joists [5]. The overall behaviour of a composite TTC floor is mostly influenced by the interaction between timber, concrete and screws. Timber is installed in the tensile zone, the thin concrete layer in the compression zone, while the screws, which transfer the internal actions between the two members, are mainly subjected to shear stresses. A combination of shear and tensile forces develops into the screws if they are inclined. To guarantee the applicability of the section analysis, no slip should occur at the interface of load-bearing elements, and the shear connectors should be sufficiently stiff. However, a

certain relative slip between concrete and timber is often present, and this phenomenon should be properly taken into account in the design process [6]. Most importantly, for accurate structural design calculations, the partial interaction between members should be accounted for when calculating the equivalent bending stiffness, the maximum stresses in each component and the maximum forces in the fasteners [7]. In most cases, however, the design process is regulated by short-term and long-term deformability checks only. A hybrid multiscale-based material model–standardized structural analysis method could be thus used for the analysis of TCC floor–creep behaviour [8].

The connection system is a fundamental part of TCC structures, and thus different types of connectors have been proposed and studied in recent years. Ceccotti [9] proposed a stiffness classification index by selecting the most common ones. In that study, he emphasized in particular that dowel-type fasteners (i.e., nails, screws and dowels) are less rigid than surface connectors, while the notched elements with connectors are less stiff than those with glued interfaces. Compared to other fasteners, screws have the advantage of being easily available and also easy to install [10].

Long threaded screws have been used for fastening and reinforcement interventions in recent years. Traditionally, screw fasteners have been typically placed perpendicular to the sliding interface plane. In such a configuration, the relative sliding between the timber beam and the concrete slab is mostly contrasted by the bending stiffness of the screw fastener and thus results in a relatively low slip modulus for the TCC system. The configurations with inclined screws, on the other hand, make possible the load transfer to the timber element, even along the axial direction, to take the most advantage of the generally high tensile capacity of screws. However, by reducing the angle between the screw and the shear plane, installation difficulties arise especially for extreme inclination angles, and an inclination of 45° represents a balanced solution between mechanical performance/capacity and ease of application in practice [11]. Overall, under a given geometric and loading condition, TCC floor configurations with inclined screws require a smaller number of connectors compared to those with perpendicular screws.

Several experimental tests and analytical formulations have been thus carried out to assess the load-carrying behaviour of screws for TCC solutions in different configurations. Among others, an interesting comparison has been proposed in terms of single-inclination screws and inclined cross-screws subjected to shear stress forces. Steinberg et al. [12] performed push-out tests with lightweight concrete slabs and different screw configurations, proving that the shear stiffness of inclined cross screws is significantly higher than a single-inclined screw. Kavaliauskas et al. [13] evaluated the possible use of Johansen's yield theory to estimate the ultimate load for TCC floors using self-tapping threaded screws at a given angle to timber-concrete interface. Bedon and Fragiacomo [14] proposed an extended FE numerical model to reconstruct the general mechanical behaviour of notched connections for TCC beams and floor components. The main purpose was to reproduce the failure mechanisms of push-out specimens made of steel, concrete and timber, giving evidence of screw arrangements and their effects on local and global mechanical performances, including damage. Other FE numerical analyses were developed by Sciomenta et al. [15], in order to understand how different concrete types (and especially Rubbercrete instead of ordinary concrete) and inclination angles could modify the connector load-bearing capacity.

In the last years, rather few authors have investigated the influence of the interlayer which is commonly placed between the timber element and the concrete slab, and more precisely its effect on the overall load-bearing capacity. This layout represents the typical structural situation in which timber reinforcing elements are positioned on existing flooring, as for example happens in common practice for most retrofit interventions. Van Der Linden [16], in this regard, investigated the effect of an OSB (Oriented Strand Board) interlayer with screws and observed a decrease of 50% on the slip modulus for the TCC system, compared to the configuration without an interposed OSB interlayer. Jorge et al. [17] carried out a set of experimental tests accounting for the presence of a timber interlayer in a conventional push-out setup, for specimens made of normal-weight concrete (NWC) as

well as of lightweight concrete (LWAC). In the set of specimens made of NWC, for example, it was observed that the interlayer inclusion leads to an average reduction of 30% and 50% for the load-bearing capacity and slip modulus, respectively. In the set of specimens made by LWAC, in contrast, it was found that such a reduction falls to 10% and 30%, respectively.

The effect of a plywood interlayer coupled with self-compacting concrete (SCC) and SFS screws was investigated by Moshiri et al. [18]. Through that experimental campaign, the undesirable effect of interlayer on strength and stiffness was confirmed overall. A significant reduction of both the serviceability and ultimate slip moduli (ranging 20–40%) was also experimentally observed. The influence of an interlayer on mechanical properties of TCC structures using threaded rebars as shear connectors was finally studied in [19], and also in this case the experimental evidences highlighted a modification in shear strength and stiffness of TCC connections. In terms of modelling, a mathematical model capable of estimating the slip modulus of TCC systems was developed in [20], so as to take into account also its dependency upon the screw inclination and the interlayer flooring thickness. In [21], the same mathematical model was further elaborated and extended, confirming the limitation of inclined screws in terms of slip modulus, due to the weakness of the timber interlayer. Recently, two new analytical models have been proposed in [10,22] for the slip modulus prediction of connections with inclined screws in TCC systems. Their main advantage is the capacity of accounting for sound insulation [22] and timber board interlayer [10], respectively. In both cases, it is shown that the concrete thickness has no influence on the connection stiffness, and the interlayer has a negative impact.

In this paper, a set of FE parametric analyses is carried out on TCC connections with inclined screws and an OSB interlayer. A novel approach is proposed to efficiently calibrate the mechanical properties of connection material components, with specific evidence of the cohesive contact between the screw and the surrounding wooden element. Under these working assumptions, a parametric investigation focused on the interlayer influence on TCC load-bearing capacity is thus presented. To this aim, preliminary FE analyses are first validated based on former push-out experimental results [20]. Successively, different screw inclinations, as well as thicknesses and mechanical properties for the interlayer, are taken into account. The influence of interaction type and features on the sliding plane, as well as the test setup (i.e., direct shear, push-out or inclined shear), are also examined and quantified in terms of mechanical performance indicators for the examined TCC connections.

2. Background Experiments

An experimental campaign was carried out to assess and quantify the influence of the in-between interlayer, as well as the role of the screw length, on the basic mechanical performance indicators of inclined screw connections commonly used in TCC floors.

A total of twenty push-out tests were investigated in [20], with specimens divided into two main groups, namely "clc8160" and "clc8240" series, in which the samples differed in geometrical features, as shown in Figure 1. Both the groups were characterized by a symmetric configuration, consisting of an inner glue-laminated timber (glulam) element and two outer concrete slabs. The latter, made of concrete of strength class C25/30 according to Eurocode 2 [23], were connected to the central glulam element, with strength class GL24h according to EN 14080:2013 [24], by two fully threaded screws per side, at an inclination of 45°. Between the timber elements and the concrete ones, an OSB panel was thus interposed, acting as an existing floor panel or a disposable formwork in existing or new buildings, respectively. Regarding the fasteners and interlayers in use in the first group of specimens (clc8160), screws with a diameter d of 8 mm and a length l_p of 160 mm, and OSB panels with a thickness t_i of 22 mm, were taken into account (Figure 1a). In the second group, clc8240, screws with the same diameter (8 mm) and a length of 240 mm, with 44 mm-thick OSB panels, were considered (Figure 1b). The cross-section of concrete slabs of both groups were 50 mm by 500 mm, with a length of 450 mm. The glulam elements were

450 mm in length and 160 mm by 120 mm in cross-section for clc8160 samples, while the cross-section increased to 200 mm by 120 mm for clc8240 specimens.
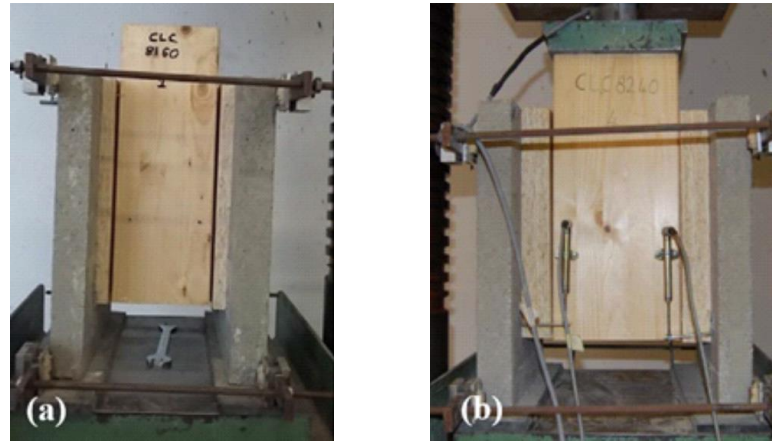
Figure 1. Reference push-out specimens for the experimental tests: (**a**) clc8160 and (**b**) clc8240 series.

All the tests were conducted in accordance with UNI EN 26891:1991 [25], which describes the procedural stages of push-out protocol. After estimating F_{est}, which represents the maximum load expected based on preliminary evaluations, the load was increased to 0.4 F_{est} and maintained for 30 s, then was decreased to 0.1 F_{est} and maintained for the same time period. Subsequently the load was increased further, until the failure of the specimen or a maximum deformation of 15 mm (whichever came first).

The relative slip between concrete and timber was measured with displacement transducers placed on both the interfaces. In addition, two metal rings were adopted in order to prevent the possible separation of the elements due to the load-reaction eccentricity. Finally, all the tests were conducted by load control, and the displacements were recorded versus the total applied load, allowing the typical load-displacement curves to be obtained, as displayed in Figure 2. Relevant specimen data and results are given in Tables 1–3.
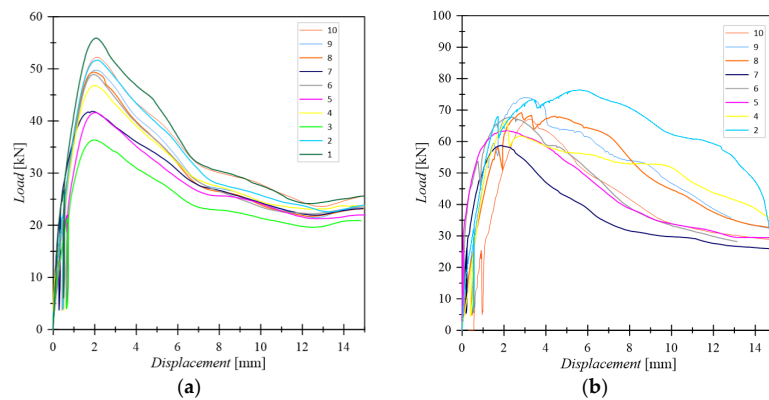
Figure 2. Experimental load-displacement curves for (**a**) clc8160 and (**b**) clc8240 specimens.

Table 1. Specimen geometric data, FE numerical results per screw and corresponding percentage scatters.

	Arrangement						**Mechanical Performance**				
Model	d [mm]	l_p [mm]	t_i [mm]	θ [°]	$F_{u,max}$ [kN]	$S_{FEM-exp}$ [%]	K_s [kN/mm]	$S_{FEM-exp}$ [%]	K_u [kN/mm]	$S_{FEM-exp}$ [%]	**Failure Mode**
E1 (clc8160)	8	128	44	45	11.4	−4	11,3	3	10.0	−9	wt
E2 (clc8240)	8	78	22	45	17.5	3	12,2	−8	10.8	−20	wt

3. FE Numerical Investigation

3.1. Modelling Assumptions

The experimental tests were reproduced by FE numerical models implemented in the ABAQUS software package [26]. With the aim of investigating the influence of previously evidenced selected parameters, such as the interlayer mechanical properties and the interaction of the interlayer with the main load-bearing members, a modelling strategy based on three-dimensional solid brick elements was taken into account. Specifically, the effects of these parameters were investigated in terms of ultimate strength F_u, stiffness K_{ser} and ultimate stiffness K_u for a given TCC connection.

The reference simulation consisted in a static incremental, geometrically linear, displacement-controlled analysis. Two planes of symmetry were taken into account for the experimental setup in Figure 1, and this allowed modelling 1/4th of the nominal geometry for the reference specimen (see Figure 3). More precisely, the glulam member, the concrete member, the interlayer and the screws were described with C3D8R elements, which represent a general-purpose linear brick element type, with reduced integration, and is available in the ABAQUS library.
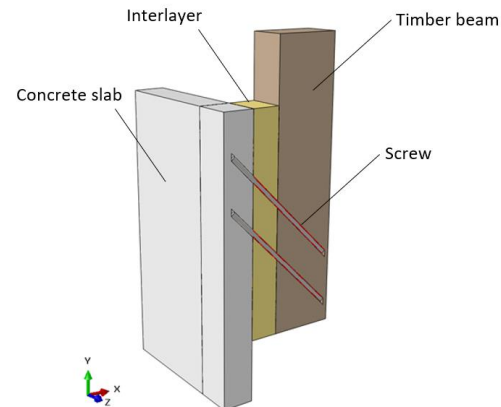
Figure 3. Example of a typical FE assembly of TCC connection (1/4th of the experimental geometry, with hidden mesh).

At the preliminary stage, the complex geometry of the examined TCC systems required numerous mesh sensitivity studies. In order to obtain an accurate and computationally efficient FE model, the spatial domain of each member was divided into several subdomains, in order to allow the definition of transition zones between regions with extremely refined mesh patterns (i.e., close to screws) or with coarser mesh schemes. Overall, sensitivity studies showed that a mesh size of approximately ≈1 mm in proximity of screws and ≈5 mm in the terminal areas of specimens should be taken into account for similar systems. The resulting FE model consisted of a total of 200,000 solid brick elements with an aspect ratio less than 3.

To avoid the separation of TCC members during the loading stage, additional restraints, as in Figure 1, were also taken into account in FE modelling. The effect of these retainers was modelled in the form of an additional translation constraint, which was applied to the concrete member base surface in the x direction (Figure 3). The displacements in the y direction were also constrained on the two base-concrete contact surfaces. Overall, the modelling of 1/4th of the nominal geometry also required the application of constraints for $u_z = u_{r,x} = u_{r,y} = 0$ on the xy symmetry plane and $u_x = u_{r,y} = u_{r,z} = 0$ on the yz symmetry plane, respectively.

3.2. Material Properties and Constitutive Models

The glulam GL24h member was mechanically described as a homogeneous orthotropic elastic-plastic material and its input properties were determined on the basis of product standards, technical specifications of the product and literature data [25,28]. In more detail, the moduli of elasticity parallel and perpendicular to grain were assumed as $E_{0,m} = 11,500$ N/mm^2 and $E_{90,m} = 300$ N/mm^2, respectively. The shear modulus and the rolling shear modulus were also quantified in $G_v = 650$ N/mm^2 and $G_r = 65$ N/mm^2, respectively. Poisson's ratios for the local directions of interest were set to $v = 0.4$, according to the extensive literature research in [27] for softwoods.

To account for damage, an anisotropic yield was defined through Hill's yield criterion. The strength values parallel and perpendicular to grain were assumed to be equal to $f_{0,m} = 37.5$ N/mm^2 and $f_{90,m} = 3.5$ N/mm^2. The shear strength and the rolling shear strength values were defined in $f_v = 3.5$ N/mm^2 and $f_r = 1.2$ N/mm^2, respectively.

The reference OSB panel that was used as interlayer can be described as an OSB/3 class, with a thickness between 18 and 25 mm and $\rho = 600$ kg/m^3 [28,29]. The corresponding mechanical properties were thus used for the definition of an orthotropic material. According to [28], the elastic modulus and the strength in the main and secondary directions were assumed as $E_{0,m} = 3500$ N/mm^2 and $E_{90,m} = 1400$ N/mm^2 and $f_{0,m} = 18$ N/mm^2 and $f_{90,m} = 9$ N/mm^2. According to [29], finally, the shear moduli and shear strength values were defined in $G_v = 1080$ N/mm^2 and $G_r = 50$ N/mm^2, $f_v = 7.0$ N/mm^2 and $f_r = 1.0$ N/mm^2.

The experimental investigation summarized in Section 2, for example, highlighted no significant crack on the concrete side for most specimens. Therefore, the concrete member was modelled as a homogeneous and isotropic elastic material with an elastic modulus defined in accordance with the strength class C25/30 of Eurocode 2 [23], that is $E_{c,m} = 31,476$ N/mm^2 and:

$$f_{cm} = f_{ck} + 8 \tag{1}$$

$$E_{cm} = 22000\left(\frac{f_{cm}}{10}\right)^{0.3} \tag{2}$$

The carbon steel screw was modelled with an elastic-plastic material law, with elastic modulus $E_s = 210,000$ N/mm^2 and yielding stress such as to guarantee the same yield moment declared in the ETA-19/0244 [30], that is $f_y = 1195$ N/mm^2.

Finally, a static friction coefficient of $\mu_{T-O} = 0.5$ and $\mu_{C-O} = 0.62$, respectively, was adopted on the glulam-OSB and concrete-OSB shear planes, in accordance with previous outcomes from Air et al. [31].

3.3. Screw-Members Interaction

Due to the complex geometry of the screw represented by the presence of the thread, as well as due to the state of combined shear and axial force that occurs when the screws are inclined with respect to the shear plane for TCC systems, it is necessary to pay particular attention to the modelling of the screw-member transition area.

An efficient modelling technique herein adopted for the mechanical description of the screw-glulam interaction mechanism was originally developed by Avez et al. [32] and also applied in [33] for the numerical analysis of similar timber-timber connections, as well

as further adapted for localized analysis of bonded-in-rod (BiR) adhesive connections for timber [34]. The technique consists in the use of a fictitious layer of deformable material (herein called "soft-layer") in conjunction with a cohesive surface interaction with damage initiation and propagation criteria. In this way it is possible to take into account:

- the high initial withdrawal stiffness guaranteed by the direct timber-screw interaction through the screw thread;
- the progressive degradation of this interaction due to damage to the interface at the attainment of a limit stress;
- the possibility of separation on the screw-timber interface;
- the actual axial and flexural stiffness of the screw.

According to this recalled approach, the screw is described in the present study by a cylinder with a diameter equal to the inner thread diameter of the screw. In this way, the axial stiffness *EA* and flexural stiffness *EI* of the simplified geometry can be considered to be similar to those of a real fastener.

The gap between the cylinder representative of the screw shank and the surface external to the thread on which withdrawal failure occurs is then modelled by a hollow cylinder of extremely deformable material ("soft-layer"). Therefore, the soft-layer schematizes that area in which the thread and the damaged timber fibres coexist, and consequently this complex medium can only be approximated in a fictitious way by an orthotropic elastic material.

For the present investigation, the mechanical properties of the medium were defined with reference to the main directions of the cylinder (axial, radial and tangential directions in Figure 4) and were assumed to coincide with those of glulam in the direction perpendicular to the fibres ($E_r = E_t = 300 \, \text{N/mm}^2$ and $G_{a-r} = G_{a-t} = G_{r-t} = 650 \, \text{N/mm}^2$). The chosen value of the elastic modulus in the axial direction of cylinder was calibrated in such a manner as not to affect the axial stiffness of the fastener ($E_a = 50 \, \text{N/mm}^2$).
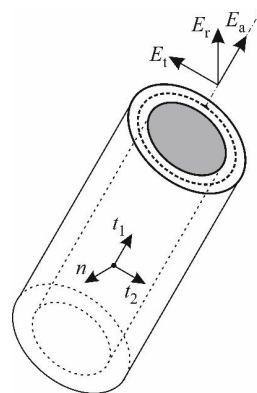
Figure 4. Soft-layer and cohesive contact geometries and reference systems.

A contact interaction with "normal-hard" mechanical behaviour was defined on the outer surface of the soft-layer, which avoids the interpenetration of the nodes of the glulam member and the nodes of the soft-layer without the possibility of transferring tensile stresses in the direction normal to the surface. In defining the cohesive contact, the stiffness and resistance in the normal direction ($K_n = 0 \, \text{N/mm}^3$, $f_n = 0 \, \text{N/mm}^2$) were set to zero, in order to allow free separation of the two surfaces. With these positions and considering a decoupled behaviour, the stiffness matrix of the interaction was hence reduced to:

$$\begin{Bmatrix} \tau_1 \\ \tau_2 \end{Bmatrix} = \begin{bmatrix} K_{s1} & 0 \\ 0 & K_{s2} \end{bmatrix} \begin{Bmatrix} \delta_{s1} \\ \delta_{s2} \end{Bmatrix} \tag{3}$$

with τ_1, τ_2 and δ_{s1}, δ_{s2} being shear stress and displacements in the first (axial) and secondary tangential directions.

The MAXS damage initiation criterion was also reduced to:

$$\max\left\{\frac{\tau_1}{f_{s1}}, \frac{\tau_2}{f_{s2}}\right\} = 1 \tag{4}$$

with f_{s1} and f_{s2} being the shear resistance values for the cohesive contact in the two main directions.

Finally, a linear law for the evolution of damage was used with an ultimate displacement equal to 4 mm [32]. A friction type interaction was added to the tangential interaction of the cohesive type, so that it could be progressively activated with the evolution of cohesive degradation and reproduce the timber-timber sliding after reaching the local breakage by withdrawal of the screw ($\mu_{T-S} = 0.5$). A normal-hard and tangential-penalty type interaction was also assigned to the sliding surface between screw and OSB with ($\mu_{OSB-S} = 0.5$), implicitly assuming a negligible withdrawal resistance in the interlayer and therefore considering the withdrawal prevented by friction between the damaged timber fibres only.

Considering the negligible frequency of withdrawal at concrete side failure in the experimental campaign of Section 2, and with the intention of creating a FE model capable of capturing the average response of those experimental tests, the screw was considered perfectly bound to the concrete slab via a rigid "tie" constraint.

3.4. Model Updating

The use of the soft-layer and cohesive contact makes it possible to consider the screw-timber interaction in a simplified way, but introduces some parameters in the model that are not directly related to the physical characteristics of the modelled object. For the configurations reproduced, a direct dependence of the numerically determined stiffness and strength ($K_{ser,FEM}$ and $F_{u,FEM}$) on the stiffness and resistance of the cohesive contact in the longitudinal direction (K_{s1} and f_{s1}), respectively, was observed. Therefore, considering K_{s1} and f_{s1} as the parameters of the model characterized by greater uncertainty and having fixed all the other parameters as described in the previous paragraph, two independent optimizations were carried out.

With a gradient-based algorithm, an optimization of the average FE-experimental percentage deviation of the stiffness K_{ser} of the two tested configurations (E1 = clc8160 and E2 = clc8240) was carried out. The function $\overline{S_K}$ to minimize as K_{s1} varies can be defined by the following equation:

$$\overline{S_K} = \frac{S_{K,E1} + S_{K,E2}}{2} \tag{5}$$

where

$$S_{K,Ei} = \frac{K_{ser,FEM,Ei} - K_{ser,exp,Ei}}{K_{ser,exp,Ei}} \tag{6}$$

The stiffness of the cohesive contact for the iteration $n+1$ was determined using the following equation:

$$K_{s1,n+1} = K_{s1,n} - \frac{K_{s1,n} - K_{s1,n-1}}{\overline{S_{K,n}} - \overline{S_{K,n-1}}} \; \gamma \; \overline{S_{K,n}} \tag{7}$$

With the same procedure, an optimization of the average FE-experimental percentage deviation of the F_u strength for the two tested TCC configurations was thus performed. The function $\overline{S_F}$ to minimize with f_{s1} variations can be defined by the following equations:

$$\overline{S_F} = \frac{S_{F,E1} + S_{F,E2}}{2} \tag{8}$$

$$S_{F,ci} = \frac{F_{u,FEM,Ei} - F_{u,exp,Ei}}{F_{u,exp,Ei}} \tag{9}$$

$$f_{s1,n+1} = f_{s1,n} - \frac{f_{s1,n} - f_{s1,n-1}}{S_{F,n} - S_{F,n-1}} \, \gamma \, \overline{S_{F,n}} \tag{10}$$

Using as optimization stop criteria such as $\overline{S_K} \leq 0.05$ and $\overline{S_F} \leq 0.05$, and assuming as learning rate $\gamma = 0.5$, the two values able to make the FE models respond like the real systems were thus quantified in $K_{s1} = 22\,\text{N/mm}^3$ and $f_{s1} = 7.5\,\text{N/mm}^2$.

The so calibrated and updated FE models were found to be able to describe well the average experimental response in terms of force displacement curve (see Figure 5) and also in terms of synthetic parameters (Table 1). The failure mode predicted by both the FE models resulted in the screw withdrawal (Figure 6), which is also in line with the most recurrent failure mode of the experimental campaign. Given that the optimization of parameters was performed based on the pre-failure behaviour only, it can be noted that the post-failure force-displacement curves of FE numerical models slightly differ from the experimental measurements. However, it is also important to note that the present analyses were primarily focused on the until-failure behaviour of examined connections, and such an intrinsic limit of FE models was hence considered satisfactory for the purpose of current investigations.
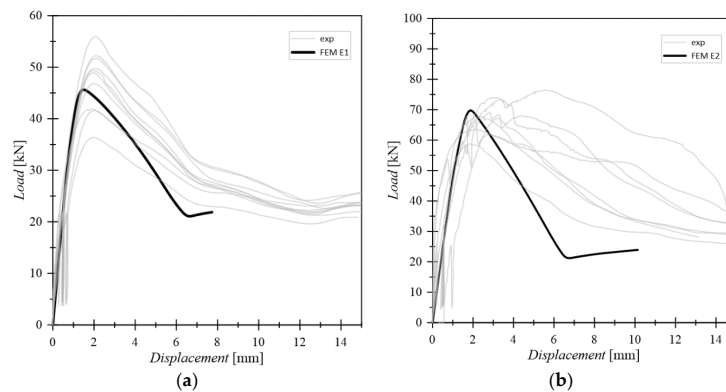
Figure 5. Experimental and FE numerical load-displacement curves for (**a**) clc8160 and (**b**) clc8240 specimens.
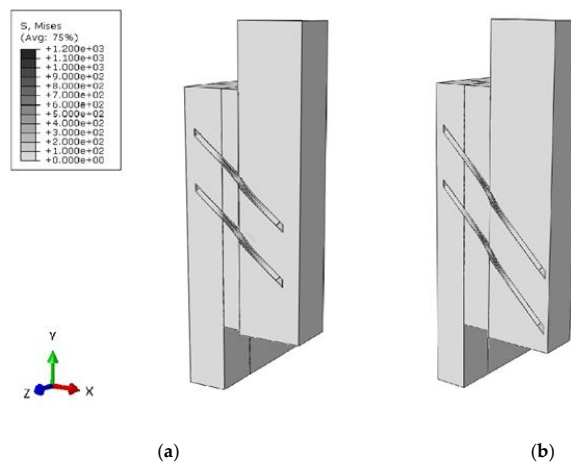
Figure 6. Typical deformed shape and Von Mises stresses for (**a**) E1 (clc8160) and (**b**) E2 (clc8240) tmodels.

4. Elaboration of Push-Out Experimental Results

4.1. Mechanical Performance Indicators

As known, the recorded experimental curves efficiently describe the behaviour of the examined TCC connections and can be used to estimate several parameters, such as K_s and K_u, which are the slip moduli used for design at serviceability limit states and ultimate limit states. In present study, both these parameters were evaluated according to UNI EN 26891:1991 [25] as:

$$K_s = \frac{0.4 \cdot F_{\text{est}}}{v_{\text{i,mod}}} \tag{11}$$

$$K_u = \frac{0.6 \cdot F_{\text{est}}}{v_{0.6} - v_{24} + v_{\text{i,mod}}} \tag{12}$$

$$v_{\text{i,mod}} = \frac{4}{3}(v_{0.4} - v_{0.1}) \tag{13}$$

where $v_{0.1}$, $v_{0.4}$ and $v_{0.6}$ represent the displacements recorded under loads of 0.1 F_{est}, 0.4 F_{est} and 0.6 F_{est}, respectively, whereas v_{24} is the displacement measured under a load of 0.4 F_{est} in the second loading branch.

4.2. Load-Bearing Capacity and Failure Mode

The values of the maximum load and of the slip moduli K_s and K_u with regard to the whole specimens are presented in Tables 2 and 3. The characteristic value $F_{u,k}$ of the maximum load was evaluated by means of the logarithmically normal distribution provided by EN 14358:2016 [35]. With reference to the failure mechanisms, the prevailing failure modes were determined by timber embedment combined with withdrawal of screws from the timber element as indicated in Tables 2 and 3, respectively. Only two specimens of the clc8240 group evinced a different failure mode, characterized by withdrawal of screws from the concrete slabs, and three specimens of the same group showed a partial splitting of the glulam element near the midline of the specimen in addition to the recurring mechanism previously described, as shown in Figure 7.
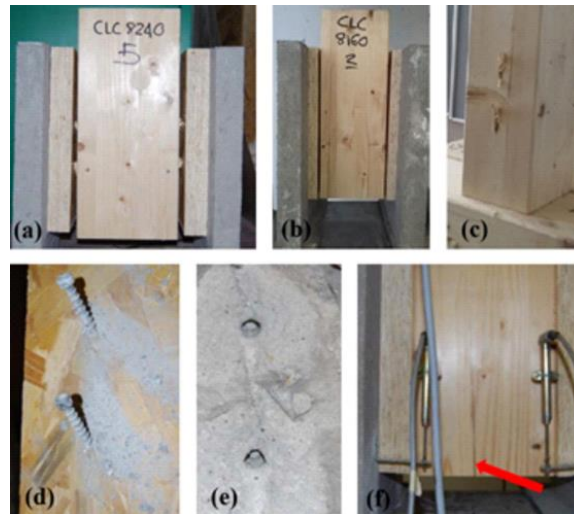
Figure 7. Failure mechanisms for the examined TCC connections in push-out experimental tests: examples of (**a**–**c**) recurring mechanisms or (**d**–**f**) infrequent failure modes. Red arrow: failure.

A significant dispersion of experimental results was found for the tested samples (see Tables 2 and 3). This effect can be caused by the variability of mechanical properties of constituent materials (especially concrete and OSB), but can also be ascribed to additional intrinsic uncertainty in the coupling process of experimental samples.

Table 2. Failure load and stiffness parameters for experimental series clc8160.

Specimen	$F_{u,max}$ [kN]	K_s [kN/mm]	K_u [kN/mm]	Failure Mode
1	55.9	69.6	77.0	c + wt
2	51.7	42.7	43.2	c + wt
3	36.3	28.3	27.2	c + wt
4	46.8	37.2	37.5	c + wt
5	41.6	32.1	32.5	c + wt
6	48.9	38.1	38,6	c + wt
7	41.8	64.8	51.2	c + wt
8	49.4	41.6	41.8	c + wt
9	49.8	43.1	42.0	c + wt
10	52.2	44.9	46.1	c + wt
max	55.9	69.6	77.0	
min	36.3	28.3	27.2	
mean value	47.4	44.2	43.7	
σ_y	0.13 *	13.2	13.5	
$F_{u,k}$	35.9	-	-	

Key: wc = withdrawal at concrete side, wt = withdrawal at timber side, c = timber embedment, s = glulam splitting; (*) = according to EN 14358:2016 [35].

Table 3. Failure load and stiffness parameters for experimental series clc8240.

Specimen	$F_{u,max}$ [kN]	K_s [kN/mm]	K_u [kN/mm]	Failure Mode
1	-	-	-	wc
2	76.3	62.6	73.8	wc
3	-	-	-	c + wt
4	66.7	45.8	48.0	c + wt
5	63.5	-	-	c + wt
6	67.8	-	-	c + wt + s
7	58.7	-	-	c + wt
8	69.1	45.6	45.3	c + wt + s
9	74.0	53.6	54.9	c + wt + s
10	67.2	57.3	46.9	c + wt
max	76.3	62.6	73.8	
min	58.7	45.6	45.3	
mean value	67.9	53.0	53.8	
σ_y	0.08 *	7.4	11.7	
$F_{u,k}$	67.7	-	-	

Key: wc = withdrawal at concrete side, wt = withdrawal at timber side, c = timber embedment, s = glulam splitting; (*) = according to EN 14358:2016 [35].

5. Results of FE Numerical Parametric Study

Parametric studies were carried out using the FE models calibrated towards the experimental configurations, with the aim of identifying the parameters of the system that mostly influence its response in terms of stiffness K_{ser} and K_u and strength F_u. To this aim, typical modifications were taken into account in terms of fastener arrangement and detailing as in Figure 8.
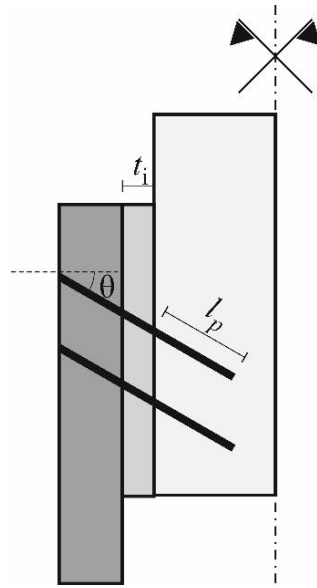
Figure 8. Schematic representation of FE model–influencing parameters (cross-section).

5.1. Screw Inclination and Interlayer Thickness

The first series of parametric studies aimed at investigating the dependence on the inclination of the screw and the thickness of the interlayer while maintaining the length of penetration of the screw into the main member l_p constant (Figure 8). Eight models have been created assuming the experimental configuration E2 as reference model and by varying the thickness of the interlayer (0, 22 mm and 44 mm) and the angle of inclination of screw (30, 45 and 60°), see Table 4.

Table 4. Parametric analysis on screw inclination and interlayer thickness, with evidence of corresponding failure modes.

Model	t_i [mm]	θ [°]	Failure Mode
G1	0	30	phs
G2	22	30	wt
G3	44	30	wt
G4	0	45	wt
G5	22	45	wt
E2 *	44	45	wt
G7	0	60	wt
G8	22	60	c + wt
G9	44	60	c + wt

Key: phs = plastic hinge on shear plane, wt = withdrawal at timber side, c = timber embedment; (*) = experimental configuration as in clc8240.

A modest dependence of the resistance on the investigated parameters was generally observed (see Figure 9a). In this regard, it is worth noting that the G1 configuration was the only one able to manifest a failure mode with the formation of a plastic hinge on the sliding surface.
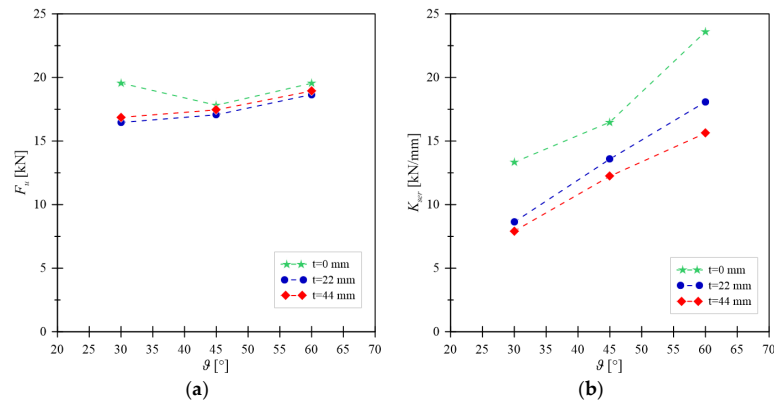
Figure 9. FE numerically predicted trends for (**a**) F_u and (**b**) K_{ser} for different values of inclination angles and interlayer thicknesses.

In this configuration, due to the low inclination angle of screw and the absence of the interlayer, the sharing of forces transferred between the members through the flexural capacity of the screw is generally greater than in the other configurations. Overall, this effect leads to the overcoming of the flexural capacity before withdrawal capacity could be exceeded.

The results in terms of stiffness confirm the results of the analytical model developed by Di Nino et al. [20], see Figure 9b. As shown, by increasing the inclination angle of screw, a significant increase in stiffness can be obtained. The insertion of an interposed interlayer, even of limited thickness, produces a significant reduction in stiffness. By increasing the thickness of the interlayer, finally, the stiffness slightly decreases.

5.2. Interlayer-Timber Member Interaction and Interlayer Mechanical Properties

At a second stage, based on previous outcomes, different types of interaction between the OSB and the glulam member were numerically considered. The two limit cases of frictionless contact and glued contact were taken into account. In addition to the case with the previously recalled friction coefficient from the literature (i.e., model E2), the case with a halved coefficient was also considered, with the aim of evaluating the sensitivity of the overall load-bearing response of TCC system to this parameter. In this regard, the analysed FE model was found to be highly sensitive to the interaction between the members, both in terms of strength and stiffness.

Figure 10, in particular, shows the strength and stiffness modifications for varying the input mechanical properties of the interlayer. In addition to the reference *E*2 configuration reported in Figure 10 (i.e., with OSB/3 interlayer panel), more precisely, additional TCC configurations were defined as:

- "particleboard": interlayer made of particleboard (i.e., structural panels for use in wet areas, as defined in EN 12369-1:2001);
- "glulam": interlayer made of the same material as the main timber member;
- and "gap", that is with an interlayer consisting of a physical gap, but being still capable of keeping the timber and concrete members separated (with appropriate kinematic constraints) in the direction perpendicular to the sliding plane.

In this case as well, the investigated FE models were found to be sensitive to the mechanical properties of the interlayer, especially in terms of TCC connection stiffness. A significant reduction in strength and stiffness was observed for the FE model with "gap", but such an outcome was mostly justified by the absence of friction phenomena (i.e., $\mu = 0$) between the concrete and the glulam members and the interlayer. It can in fact be noted in

Figure 10a,b that the "gap" and the "$\mu = 0$" FE models approximately exhibit the same strength and stiffness capacities.
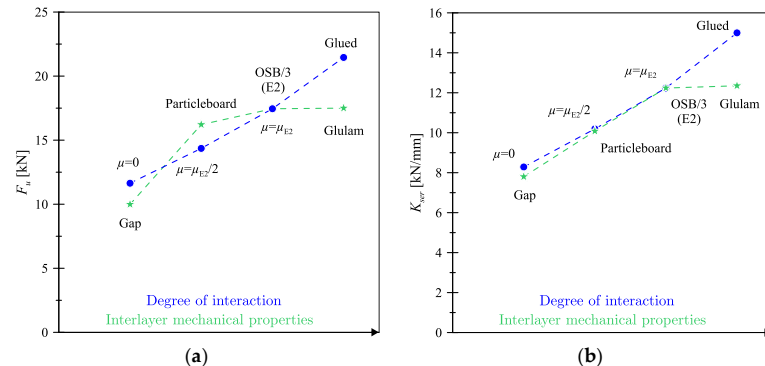

Figure 10. FE numerically predicted trends for (**a**) F_u and (**b**) K_{ser} for different interlayer-to-members interaction and interlayer mechanical properties.

5.3. Friction Contribution and Test Setup

The friction sensitivity study further highlighted the important role of this parameter. For the configurations of Table 4, in more detail, the graph in Figure 11 shows the percentages of F_u which are transferred on the sliding plane through the screw and by friction. It can be noted that:

- the share of force term which is transferred by friction is lower on the interlayer-glulam sliding plane (SL2) with respect to the concrete-interlayer sliding plane (SL1), due to the lower static friction coefficient;
- for the configuration E1, which is similar to the G5 configuration in terms of inclination angle and interlayer thickness but is characterized by a different penetration length $l_{p, E1}/l_{p, G5} = 0.61$, the FE numerical analysis shows a negligible increase in the share of force transferred by friction on the sliding plane SL1. Conversely, on the sliding surface SL2, the share of force transferred by friction slightly decreases;
- as the thickness of the interlayer increases, with constant inclination and length of penetration for the screw into the glulam member, the share of force transferred by friction clearly increases;
- finally, as the angle of inclination of the screw increases with respect to the normal to the sliding plane, for constant thickness of interlayer and length of the screw penetration into the glulam member, the share of force transferred by friction decreases.

The friction force on the sliding plane is proportional, by means of the friction coefficient, to the force perpendicular to it. The force perpendicular to the sliding plane is given by two contributions: the component of the reaction forces to the internal stress of the screw, and the external force necessary to ensure the equilibrium of the entire connection assembly [36].

Figure 12a, in this regard, shows some of the most common experimental test configurations for the mechanical characterization of connection systems. A schematic layout is proposed for direct shear (DS), push-out (PO) and inclined shear (IS), respectively, with evidence of corresponding reaction forces and effects on sliding plane behaviour.

In the direct shear configuration (DS), more precisely, external forces are applied on the sliding plane, thus eliminating any external reaction forces perpendicular to the sliding plane itself. It is clear that such a condition has direct effects on the mechanical performance and load-bearing capacity of main members for TCC systems. In the case of push-out (PO) and inclined shear (IS) test setup conditions, there is evidence of a perpendicular

component $F_\perp$ induced by the geometric configuration of the setup itself. In the case of a push-out test, in more detail, the perpendicular component depends on the lever arm of $F_\parallel$ and $F_\perp$, which is unknown. In the inclined shear case, $F_\perp$ is indeed represented by the component of the external applied force and is therefore a priori known.
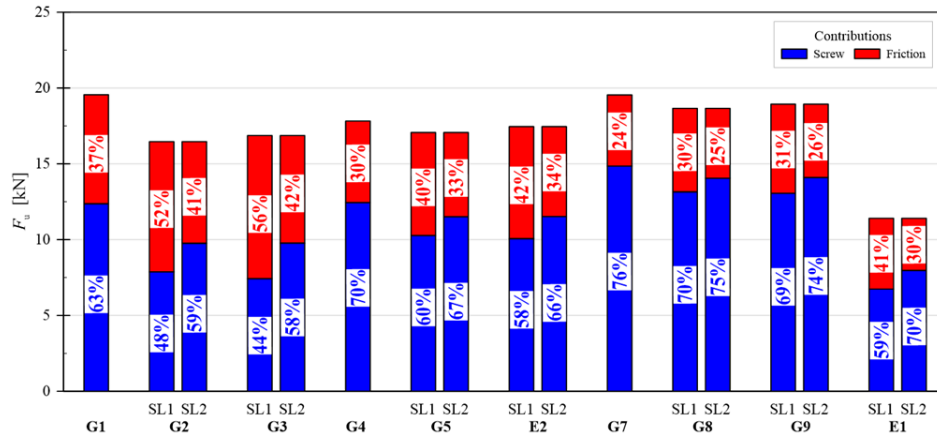

Figure 11. Analysis of F_u percentage transferred on the sliding planes through the screw and by friction. Key: SL1 = sliding plane between the concrete member and the interlayer; SL2 = sliding plane between the glulam member and the interlayer.

To further explore the effect of these setup details on TCC performance, the FE model of the G4 system was used for a sensitivity analysis of synthetic results and TCC performance indicators. The graphical results in Figure 12b, in this regard, show that through the different experimental setup conditions the force transferred between the members by the screw itself does not vary. The frictional force component undergoes an increase of 26% and 20% from the DS configuration to the PO and IS configurations, respectively, causing an overall ultimate force increase of 6% and 5%, respectively. The presence of the $F_\perp$ force term, finally, leads to increases in stiffness between 11% and 13%, respectively. In the selected configuration, a greater force $F_\perp$ was found especially in the case of inclined shear (IS), compared to push-out (with an average ratio equal to $F_{\perp, PO}/F_{\perp, IS} = 0.7$).

5.4. Perfectly Glued Fastener

Finally, the attention of parametric numerical studies was focused on the ideal condition of a perfectly bonded screw. Preventing the screw withdrawal produces an increase of 40%, both in terms of strength and stiffness, and this can be achieved by considering the screw perfectly glued on the timber side. In this case, the failure mode passes from screw withdrawal, to screw and timber plasticization, which consequently leads to a more ductile behaviour of the TCC connection.

Such a limit case was numerically created and investigated starting from the E2 model by applying a rigid "tie" constraint to the interface between the screws and the timber components. In this way, the timber nodes and the screw nodes were rigidly and perfectly bound, thus simulating a typical case in which the glue-side failure mode is prevented.

For all the parametric studies herein discussed, a K_u value between 0.8 K_{ser} and 0.9 K_{ser} was found in the presence of perfectly bonded fasteners. Sensitivity studies, in this regard, showed that the transition to a C45 concrete class could involve relatively small maximum variations in strength and stiffness, in the order of < 1%.
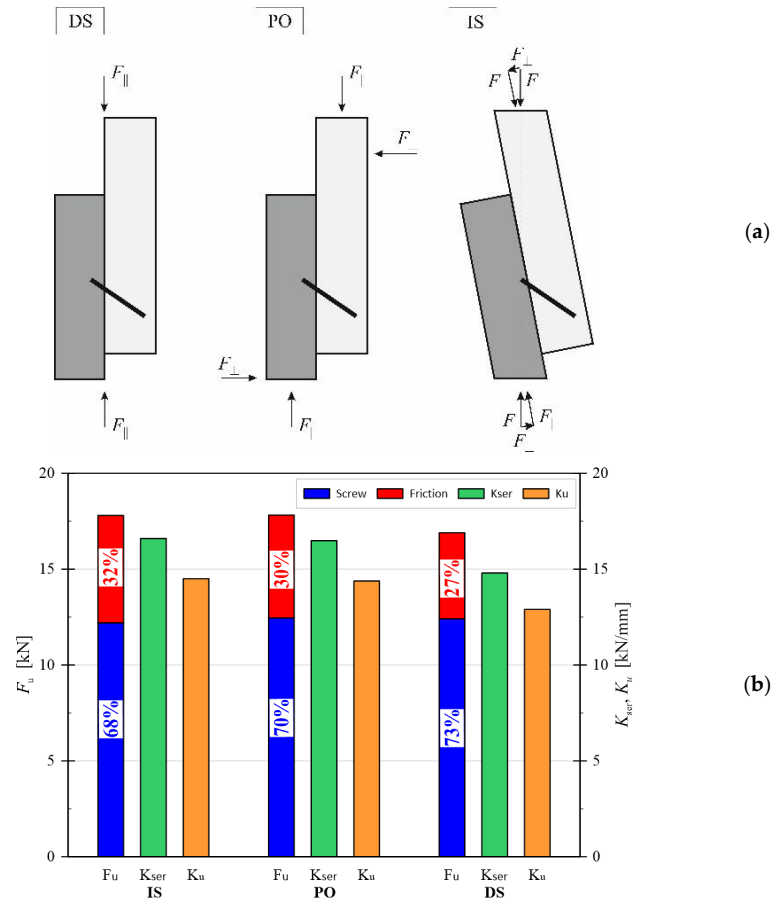
Figure 12. Evidence of (**a**) common test configurations and (**b**) FE numerical estimation of F_u, K_{ser} and K_u performance indicators. Key: DS = Direct shear; PO = Push-out; IS = inclined shear.

6. Discussion

The significant impact that the interlayer has on the load-bearing performance and mechanical parameters of timber-concrete composite connections is generally recognized by literature evidence. However, no distinction is commonly made between the different types of interlayers of typical use in constructions. In this study, the performed FE numerical simulations proved that connections with OSB and glulam interlayers have similar mechanical performance. However, in the case of highly deformable interlayers or particleboards, the strength and stiffness parameters for the examined connections can suffer from significant modifications, compared to previous cases.

Another important aspect is represented by the influence of friction, which is often neglected or minimally considered in a rough way, by simplified analytical models, for the stiffness and strength prediction. In some of the studied configurations herein presented, it was shown that friction can contribute by more than half to the strength of a given connection. Accordingly, further extended studies are needed to define empirical formulations capable of adequately taking into account such a contribution. From a practical point of

view, benefits of friction phenomena could in fact lead to a considerable reduction in the number of fasteners which are commonly used in composite structures.

Finally, the role of the test setup for experimental investigations was properly emphasized by the present outcomes. Significant qualitative and quantitative differences were found between the direct shear (DS) test, the inclined shear (IS) test and the push-out (PO) test configurations. In this context, it is worth noting that all these differences are not minimally considered in current structural design regulations, and it is suggested to extend investigations and future elaborations.

7. Conclusions

In this paper, a Finite Element (FE) model capable of taking into account the main variables of a typical timber-concrete composite (TCC) system with inclined screws and interposed interlayer was developed and discussed in terms of parametric analysis. To this aim, the reference FE model was preliminarily validated based on the push-out experimental results of two different TCC configurations.

Based on discussion of FE parametric numerical results, it was highlighted that:

- the inclination of screw and the thickness of the interlayer have a modest influence on the resistance of a given TCC connection but strongly affect the expected failure mode;
- the insertion of an interlayer, even of limited thickness, produces a significant reduction in stiffness, which slightly increases with its thickness;
- the interlayer type and mechanical capacity is also an important parameter, since it further affects the TCC connection stiffness;
- the type of friction/contact interaction of main load-bearing components on the sliding plane was found to be the most significant parameter. The transition from frictionless ("$\mu = 0$") to bonded ("glued") numerical configurations could lead to increases of 84% and 81% in terms of strength and stiffness, respectively, for TCC systems. A reduction factor of strength and stiffness of 0.66 can be adopted when friction between timber and concrete is not guaranteed, whilst whenever the interlayer is glued a coefficient of 1.25 can be taken into account;
- friction alone contributes between 24% and the 56% to reference mechanical performance parameters, depending on the considered sliding plane and the specific geometric configuration;
- the push-out and inclined test configurations, finally, introduce additional forces perpendicular to the sliding plane, and this phenomenon affects the contribution of friction to the overall ultimate force and stiffness of TCC systems. In this regard, strength and stiffness correction factors equalling 0.95 and 0.90, respectively, are suggested to normalize inclined shear and push-out test results to the direct shear results.

In conclusion, the FE numerical studies herein carried out and discussed highlighted the significant impact of the interlayer and its interaction on the main design parameters for a given TCC connection. In this regard, further experimental and numerical studies are necessary for the development of suitable calculation methods that take these parameters into account.

Institutional Review Board Statement: Not applicable.

Informed Consent Statement: Not applicable.

References

1. Bedon, C.; Sciomenta, M.; Fragiacomo, M. Correlation approach for the Push-Out and full-size bending short-term performances of timber-to-timber slabs with Self-Tapping Screws. *Eng. Struct.* **2021**, *238*, 112232. [CrossRef]
2. Herzog, T.; Natterer, J.; Schweitzer, R.; Volz, M.; Winter, W. *Timber Construction Manual*, 4th ed.; Birkhauser-Publishers for Architecture: Basel, Switzerland, 2004.
3. Fontana, M.; Frangi, A. Fire behaviour of timber-concrete composite slabs using beech. *Bautechnik* **2015**, *92*, 323–329. [CrossRef]
4. Frangi, A.; Fontana, M. A design model for the fire resistance of timber–concrete composite slabs. In Proceedings of the IABSE, International Conference on Innovative Wooden Structures and Bridges, Lahti, Finland, 29–31 August 2001.
5. Monteiro, S.; Dias, A.; Lopes, S. Distribution of Concentrated Loads in Timber-Concrete Composite Floors: Simplified Approach. *Buildings* **2020**, *10*, 32. [CrossRef]
6. Frangi, A.; Knobloch, M.; Fontana, M. Fire Design of Timber-Concrete Composite Slabs with Screwed Connections. *J. Struct. Eng.* **2010**, *136*, 219–228. [CrossRef]
7. Mirdad, M.A.H.; Khan, R.; Chui, Y.H. Analytical Procedure for Timber− Concrete Composite (TCC) System with Mechanical Connectors. *Buildings* **2022**, *12*, 885. [CrossRef]
8. Binder, E.; Derkowski, W.; Bader, T.K. Development of Creep Deformations during Service Life: A Comparison of CLT and TCC Floor Constructions. *Buildings* **2022**, *12*, 239. [CrossRef]
9. Ceccotti, A. Composite concrete-timber structures. *Prog. Struct. Eng. Mater.* **2002**, *4*, 264–275. [CrossRef]
10. Du, H.; Hu, X.; Xie, Z.; Wang, H. Study on shear behavior of inclined cross lag screws for glulam-concrete composite beams. *Constr. Build. Mater.* **2019**, *224*, 132–143. [CrossRef]
11. Marchi, L.; Scotta, R.; Pozza, L. Experimental and theoretical evaluation of TCC connections with inclined self-tapping screws. *Mater. Struct. Constr.* **2017**, *50*, 180. [CrossRef]
12. Steinberg, E.; Selle, R.; Faust, T. Connectors for Timber–Lightweight Concrete Composite Structures. *J. Struct. Eng.* **2003**, *129*, 1538–1545. [CrossRef]
13. Kavaliauskas, S.; Kvedaras, A.K.; Valiūnas, B. Mechanical behaviour of timber-to-concrete connections with inclined screws. *J. Civ. Eng. Manag.* **2007**, *13*, 193–199. [CrossRef]
14. Bedon, C.; Fragiacomo, M. Three-dimensional modelling of notched connections for timber-concrete composite beams. *Struct. Eng. Int.* **2017**, *27*, 184–196. [CrossRef]
15. Sciomenta, M.; de Santis, Y.; Castoro, C.; Spera, L.; Rinaldi, V.; Bedon, C.; Fragiacomo, M.; Gregori, A. Finite elements analyses of timber-concrete and timber rubberized concrete specimens with inclined screws. In Proceedings of the World Conference Timber Engineering (WCTE), Santiago, Chile, 9–12 August 2021.
16. Van Der Linden, M.L.R. Timber-Concrete Composite Floor Systems. Ph.D. Thesis, Technische Universiteit Delft, Delft, The Netherlands, 1999.
17. Jorge, L.F.C.; Lopes, S.M.R.; Cruz, H.M.P. Interlayer Influence on Timber-LWAC Composite Structures with Screw Connections. *J. Struct. Eng.* **2011**, *137*, 618–624. [CrossRef]
18. Moshiri, F.; Shrestha, R.; Crews, K. The Effect of Interlayer on the Structural Behavior of Timber Concrete Composite Utilizing Self-Compacting and Conventional Concretes. *Int. J. Eng. Technol.* **2015**, *7*, 103–109. [CrossRef]
19. Djoubissié Denouwé, D.; Messan, A.; Fournely, E.; Bouchair, A. Influence of Interlayer in Timber-Concrete Composite Structures with Threaded Rebar as Shear Connector-Experimental Study. *Am. J. Civ. Eng. Archit.* **2018**, *6*, 38–45. [CrossRef]
20. Di Nino, S.; Gregori, A.; Fragiacomo, M. Experimental and numerical investigations on timber-concrete connections with inclined screws. *Eng. Struct.* **2020**, *209*, 109993. [CrossRef]
21. De Santis, Y.; Fragiacomo, M. Timber-to-timber and steel-to-timber screw connections: Derivation of the slip modulus via beam on elastic foundation model. *Eng. Struct.* **2021**, *244*, 112798. [CrossRef]
22. Mirdad, M.A.H.; Chui, Y.H. Stiffness Prediction of Mass Timber Panel-Concrete (MTPC) Composite Connection with Inclined Screws and a Gap. *Eng. Struct.* **2020**, *207*, 110215. [CrossRef]
23. *Eurocode 2: Design of Concrete Structures-Part 1-1: General Rules and Rules for Buildings*; EN 1992-1-1; European Committee for Standardization (CEN): Brussels, Belgium, 2004.
24. *Timber Structures-Glued Laminated Timber and Glued Solid Timber–Requirements*; EN 14080; European Committee for Standardization (CEN): Brussels, Belgium, 2013.

25. *Timber Structures. Joints Made with Mechanical Fasteners. General Principles for the Determination of Strength and Deformation Characteristics*; EN 26891; European Committee for Standardization (CEN): Brussels, Belgium, 1991.
26. Abaqus. *Computer Software*; Dassault Systèmes: Providence, RI, USA, 2021.
27. Bartolucci, B.; De Rosa, A.; Bertolin, C.; Berto, F.; Penta, F.; Siani, A.M. Mechanical properties of the most common European woods: A literature review. *Fract. Struct. Integr.* **2020**, *14*, 249–274. [CrossRef]
28. *Oriented Strand Boards (OSB)-Definitions, Classification and Specifications*; EN 300; European Committee for Standardization (CEN): Brussels, Belgium, 2006.
29. *Wood-Based Panels-Characteristic Values for Structural Design-Part 1: OSB, Particleboards and Fibreboards*; EN 12369-1; European Committee for Standardization (CEN): Brussels, Belgium, 2001.
30. European Technical Assessment 19/0244. 2019.
31. Air, J.R.; Arriaga, F.; Iniguez-Gonzalez, G.; Crespo, J. Static and kinetic friction coefficients of scots pine (*Pinus sylvestris* L.), parallel and perpendicular to grain direction. *Mater. Constr.* **2014**, *64*, 2979955. [CrossRef]
32. Avez, C.; Descamps, T.; Serrano, E.; Léoskool, L. Finite element modelling of inclined screwed timber to timber connections with a large gap between the elements. *Eur. J. Wood Wood Prod.* **2016**, *74*, 467–471. [CrossRef]
33. Bedon, C.; Fragiacomo, M. Numerical analysis of timber-to-timber joints and composite beams with inclined self-tapping screws. *Compos. Struct.* **2019**, *207*, 13–28. [CrossRef]
34. Bedon, C.; Rajcic, V.; Barbalic, J.; Perkovic, N. CZM-based FE numerical study on pull-out performance of adhesive bonded-in-rod (BiR) joints for timber structures. *Struct.* **2022**, *46*, 471–491. [CrossRef]
35. *Timber Structures–Calculation and Verification of Characteristic Values*; EN 14358; European Committee for Standardization (CEN): Brussels, Belgium, 2016.
36. Blaß, H.J.; Steige, Y. *Steifigkeit Axial Beanspruchter Vollgewindeschrauben*; KIT Scientific Publishing: Karlsruhe, Germany, 2018. [CrossRef]

7.3   Paper: *Finite elements analyses of timber-concrete and timber rubberised concrete specimens with inclined screws*

FINITE ELEMENTS ANALYSES OF TIMBER-CONCRETE AND TIMBER-RUBBERISED CONCRETE SPECIMENS WITH INCLINDED SCREWS

Martina Sciomenta[1], Yuri de Santis[1], Chiara Castoro[1], Luca Spera[1], Vincenzo Rinaldi[1], Chiara Bedon[2], Massimo Fragiacomo[1], Amedeo Gregori[1]

ABSTRACT:

Timber–concrete composite system represents a diffused solution for floor elements both in new structures as well as for the refurbishment of ancient ones. These two members are linked by a connection elements that, in this case, are inclined lag screws.

This study has the aim to investigate the behaviour of a typical timber-to-concrete composite slab by performing FE simulations. Some previous results coming from push-out tests will be accounted in order to calibrate the numerical model, after this, different screws geometrical features (i.e. inclination,) will be defined in order to establish their influence on the specimens' global behaviour. Then, starting from the previously defined screws configurations, the concrete is replaced with Rubbercrete, which is a concrete in which part of the natural aggregates are replaced with recycled waste tyre rubber. The effect of this substitution will be investigated and highlighted.

KEYWORDS: Composite structures, Timber-to-concrete slab, Rubbercrete, Inclined Lag Screw, FE Model

1 INTRODUCTION

Timber–concrete composite system represents in the last years a diffused solution for floor elements. In these composite slabs, timber element is connected to the concrete cross section by means of special connecting elements. Timber is usually installed in the tensile zone, the thin concrete layer in the compression zone while the connection system is mainly subjected to shear stresses. This solution is an efficient system for the refurbishment of ancient timber floors as well as a convenient way to realize slabs in new buildings, because they combine high seismic resistance and better acoustic and thermal insulation and fire resistance [1 to 3] (up to F30, F60 and F90). In the existing buildings, composite timber-concrete slabs provide an increment of strength and stiffness, reduce the sensitivity to vibrations and simplify the possibility to realize horizontal bracing of the structures. The structural behaviour of timber-concrete composite members is mainly governed by the shear

[1] University of L'Aquila, Department of Civil, Architecture and Building and Environmental Engineering, L'Aquila, Italy,
martina.sciomenta@univaq.it
yuri.desantis@graduate.univaq.it
chiara.castoro@graduate.univaq.it
luca.spera@graduate.univaq.it
vincenzo.rinaldi@univaq.it
massimo.fragiacomo@univaq.it
amedeo.gregori@univaq.it
[2] University of Trieste, Department of Engineering and Architecture, Trieste, Italy,
chiara.bedon@dia.units.it

connection between timber and concrete. Shear connectors should be sufficiently stiff in order to ensure the composite action between timber and concrete elements. If no slip occurs, the composite structure can be considered as a unique member and so the conventional principles of structural analysis can be applied. However, almost all connection systems are flexible, i.e., so they are not able to prevent a relative slip between concrete and timber. Thus, flexible connections develop only partial composite action and therefore the structural analysis requires consideration of interlayer slip between the subcomponents [4].

The connection system is a crucial part of any timber-concrete composite structure, so, in the last years, different types of connectors have been proposed and investigated. Ceccotti [5] sorted the most significant by adopting the stiffness as classification index, highlighting in particular how nails, screws and dowel shaped fasteners are less rigid then elements connected by surface connectors (split rings, toothed or steel punched metal plates), moreover, notched elements with connectors are less stiff than the one with bonded interfaces.

Compared to others fasteners, screws have the advantage of being readily available off-the-shelf and easily installed (Du et al., 2019) [6]. In last years, long threaded screws with have been introduced for fastening and reinforcement purposes. Conventionally, the screw connectors are inserted vertically, in that configuration, the relative slip between the timber beam and concrete slab is primarily resisted by the bending stiffness of the screw connector, and this leads to the low slip modulus.

The inclined configurations with respect to the timber grain, guarantee the load transfer into timber also along the axial direction for an optimal use of high pull-out capacity of the screw. Decreasing the angle between screw and shear plane their withdrawal capacity can be exploited for increase the load-carrying capacities and affordability of connection.

However, installation difficulties arise for excessive angles and an inclination of 45° represents a balanced solution between performance and ease of execution. [7]

The inclined configuration led to a reduction of the number of the screws necessary in a composite floor, with the same geometrical and loading conditions.

Interesting comparison among the single inclined screw subjected to shear–tension forces and the inclined cross screws were highlighted by carrying on experimental tests as well as by analytical formulations. Steinberg et al. [8] conducted push-out tests on this two different inclined screw connectors 'configurations and showed, as test results, that the shear stiffness of the inclined cross screws was higher than that of the single inclined screw. Kavaliauskas et al. [9] adopt the Johansen's yielding theory as a possibility to predict the ultimate load for timber-to-concrete joints using self-tapping threaded connectors screwed at an angle into the wood.

Bedon and Fragiacomo [10] proposed an advanced numerical finite elements (FE) model to reproduce the overall mechanical behaviour of notched connections for timber to concrete (TC) composite beams; the main aim was to reproduce the failure mechanisms of steel, concrete and timber push-out specimen's components.

According to the literature, normal concrete has been used in timber–concrete composite slabs. In this study, a modified concrete is also proposed for the assembly of composite slabs. This modified concrete is obtained substituting part of the natural aggregates with recycled waste tyre rubber, and it is known in literature as rubbercrete.

Some of the many advantages of using recycled rubber in concrete, compared to standard concrete, are a lightweight material, increased ductility, energy absorption, enhanced dynamic properties, increased resistance to cracks, thermal and acoustic insulation, despite a loss in mechanical strength properties [11,12,13,14]. In particular, at high temperature (600°C and above), an improved plastic deformation capacity is observed, with an increasing strain at peak and a flatter softening branch [15].

The purposes of this study are:

i) to propose a FE model able to fit with great accuracy the experimental evidences of normal concrete-to-timber push-out specimens with lag-screw achieved by (Du et al., 2019) [2] and then

ii) to perform a preliminary FE analysis to better understand how the modified concrete (rubbercrete), changes the connector's performance.

2   MATERIALS AND METHODS

2.1   RUBBERCRETE

Rubbercrete exhibits numerous benefits compared to conventional concrete such as lower density, increased ductility, higher impact resistance, lower thermal and acoustic conductivity. Despite such advantages, it is known that rubbercrete mechanical properties decline with an increasing aggregate replacement ratio. This reduction is also in function of the rubber aggregate dimension. In particular, mechanical features decrease more when rubber is used in substitution of coarse aggregates instead of fine ones [3]. The reduction in strength of rubbercrete is expected given the significant difference in density between natural aggregates and rubber aggregates, and it is worsened by the weak bond between the cement matrix and the crumb rubber due to the hydrophobic properties of rubber. In fact, rubber repels water and entraps air causing the formation of micro air pockets between the rubber and the cement, and so thickening the interfacial transition zone.

In the FE models of this work, mechanical features of rubbercrete with different percentages of substitution of fine aggregates at 10%, 20%, and 40% of the total volume have been determined according to the prediction laws for the compressive strength and elastic modulus found in [13].

2.2   FE ANALYSIS METHOD

In this work a series of TC push-out FE simulations are performed. At first, the FE model is calibrated based on the experimental campaign carried out in [2], then, the mechanical features of concrete and the screws' inclination are varied in order to assess their influence on the assembly's global behaviour.

2.2.1   PREVIOUS EXPERIMENTAL EVIDENCES

In their work, Du et al. [2] carried on a total of thirty-six push-out tests to investigate the shear behaviour of the inclined cross lag screws for glulam-concrete composite beams. By varying the concrete strength and the screw's geometrical parameters (diameter, inclination angle from the shear plane, penetration length and arrangement) the most influential features were highlighted. In particular it was clear that the slip modulus was significantly influenced by screw diameter, penetration depth and inclination angle, but not the concrete strength. The shear bearing capacity is mostly influenced by the screw's arrangement that affect the stress state which the screws undergo. The four different configurations provided a: *i)* crossed-positioned screws reacting both to tension and compression (±30, ±45, ±60° inclination angle), *ii)* screws placed perpendicularly to the grain (90° inclination angle), *iii)* screws placed with a +45° inclination angle which experienced shear–tension load, *iv)* screws placed with a +135° inclination angle, which experienced shear–compression load. In this latter arrangement the slip modulus and the screw 'stress state

were the worst. The most working-well configuration was provided by crossed screws.

2.3 FINITE ELEMENT MODELS' FEATURES

The push-out specimens were composed by one central glulam element connected by two inclined screws on each side to two concrete slabs. The member's dimensions (in mm) are specified in Figure 1. Screws have a $\phi 12$ mm diameter, a transverse spacing of 50 mm and a penetration's depth in the concrete slabs of 70 mm.
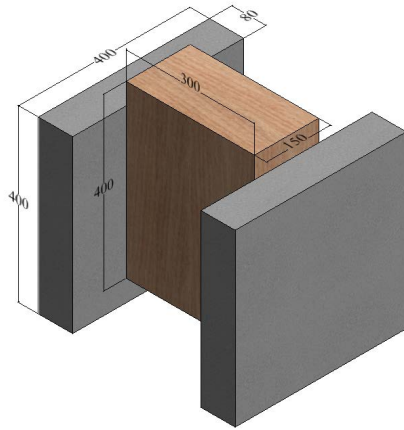

Figure 1. Specimen's assembly

The numerical simulations were carried out employing the ABAQUS/Explicit software package [16], in order to reduce the computational cost of simulations, 1/2th of nominal geometry represented in Figure 1 was adopted for specimens with crossed screws, otherwise a 1/4th of nominal geometry was accounted.

2.4 FE MODEL

Due to the previous considerations, the assigned boundary conditions were: a base hinge of the concrete block (i.e. simply supports) and mechanical conditions on the symmetry planes of the timber element and concrete slab (i.e. to ensure the appropriate symmetry condition).

A quasi-static imposed displacement simulation were conducted on the examined composite systems in order to best reproduce the experimental tests load's conditions. The vertical displacement was applied on the top of the timber member and monotonically increased up to 15 mm.

Based on [17], the screw's geometry and interaction with the surrounding timber was suitably simplified: *i)* the screw was modelled as a cylinder without the head, *ii)* the threated part and the infilled timber is reproduced in the form of an equivalent, circular cross-section with uniform diameter equal to the outer thread size of screws and L the nominal length. This latter 'soft layer', representative of STSs threads and timber fibres, was then interposed at the interface between each screw and the surrounding timber members.

The contact between the concrete and central timber member surfaces was modelled using isotropic Coulomb friction interaction. The software allows to define for this contact model both tangential and normal mechanical behaviour. Tangential behaviour was accounted in order to specify any possible relative sliding among surfaces; the friction coefficient is taken equal to 0.62. Normal behaviour defines the interactions in the direction perpendicular to contact plane; the "hard contact" option was toggled to account for possible detachment of the surfaces after contact. The screw-to-concrete interaction was assessed by a tie constraint.

The external surface of the 'soft layer' and the adjacent timber elements were indeed interrelated via a 'cohesive contact' interaction. The most important parameters necessary to fix in the FE model are the elastic stiffness and the damage input data, the first parameter represents the interface stiffness (radial, longitudinal and normal) prior to damage which were calibrated based on the experimental evidences (in particular, these values were set for model with screws placed with a +45° inclination angle and validated for others). In terms of damage at the 'soft layer'-to-timber interface, a brittle failure was expected to initiate together with the failure propagation in timber. The maximum nominal stress (MAXS) criterion was used. The 'damage initiation criterion' and 'damage evolution criterion' were defined in accordance with [17].

The screw is in steel which is defined as a homogenous, isotropic, linear elastic-plastic material. Glulam timber is an orthotropic media which plasticity was accounted by adopting the Hill plastic criterion; due to the test conditions it was used to specify appropriate compressive stress values along the principal directions of interest for the timber components. Concrete and Rubbercrete are defined as homogenised media having isotropic behaviour.

2.5 CONCRETE

The concrete was considerate in accordance with [2] as C40 (R_{ck}=40.1 MPa) with Poisson ratio equal to $v = 0.3$ and elastic modulus E_{cm} =33,7 GPa.

The concrete damaged plasticity mechanical model was implemented in all the FE models in order to represent the inelastic behavior of concrete and to capture the effects of irreversible damage associated with the failure mechanisms of tensile cracking and compressive crushing. The choice of assuming this model is due to the highlighted experimental concrete failures such as the cone's expulsion upwards the cross inclined screws. The concrete damaged plasticity model assumes softening behavior in tension as opposed to initial hardening followed by softening in compression. Due do the damage associated to the failure mechanisms, both the uniaxial compression and tension responses are characterized by a reduction in the elastic stiffness; this phenomena is described by two degradation variables named d_c and d_t for compression and tension respectively.

The assumed nominal ultimate strain for concrete was $\varepsilon_c=0.0035$ in accordance with [17]. Both the formulation purposed from Eurocode 2 [18] for compression and tension were adopted.

2.5.1 UNIAXIAL COMPRESSIVE BEHAVIOR

The compression stress-strain relation is described by the expression:

$$\frac{\sigma_c}{f_{cm}} = \frac{k\eta - \eta^2}{1 + (k-2)\eta} \qquad (1)$$

Where:

$$\eta = \varepsilon_c / \varepsilon_{c1}$$

$$\varepsilon_{c1} = 0.7 f_{cm}^{0.31} \le 2.8$$

$$k = 1.05 E_{cm} \cdot \frac{|\varepsilon_{c1}|}{f_{cm}}$$

The plastic hardening strain in compression $\tilde{\varepsilon}_c^{pl}$ played a key role in finding the relation between the damage parameters and the compressive strength of concrete, the degradation parameter d_c is defined in [16] as:

$$d_c = 1 - \frac{\sigma_c}{E_{cm}\left(\varepsilon_c - \tilde{\varepsilon}_c^{pl}\right)} \qquad (2)$$

Where

$$\tilde{\varepsilon}_c^{pl} = b_c \cdot \tilde{\varepsilon}_c^{in} = b_c \cdot \left(\varepsilon_c - \frac{\sigma_c}{E_{cm}}\right)$$

With b_c=0.7 in accordance with [17].

2.5.2 UNIAXIAL TENSILE BEHAVIOR

The tensile stress-strain relation in accordance with [13] were transformed into stress-crack opening relations Eq.(3), in which the crack opening w is defined as the total deformation (w_{tot}) minus an elastic part and a part which takes account of non-elastic effects during unloading of the material adjacent to the crack faces. w_c represents the crack opening at which stress no longer can be transferred.

$$\frac{\sigma_t}{f_{ct}} = f(w) - \frac{w}{w_c} f(w_c) \qquad (3)$$

In which:

$$f(w_c) = \left[1 + \left(\frac{C_1 w}{w_c}\right)^3\right] e^{\left(-\frac{C_2 w}{w_c}\right)}$$

C_1= 3 and C_2= 6.93 represent two material constants

$$w_c = 5.14 \frac{G_f}{f_{ct}}$$

$$f_{ct} = 0.7 \cdot f_{cm} = 0.7 \cdot (0.30 \cdot f_{ck})$$

The concrete fracture energy $G_F \approx \frac{G_f}{2.5}$ where $G_f = 0.044$ N/mm from [13].

The tensile damage parameter d_t was evaluated as d_c in Eq. (2) assuming b_t=0.1 in accordance with [17].

2.6 CONCRETE WITH RECYCLED RUBBER AGGREGATES FROM WASTE TYRES

The complex behaviour of rubberized concrete affect also its constitutive stress-strain relationship, in particular, rubber particles replacing a certain percentage of natural aggregates change the concrete mechanical properties and consequently influence the shape of the stress-strain curve, compared to conventional concrete. In the literature, experimental studies conducted to define the compressive stress-strain behaviour of rubbecrete highlight the rubber content and size of the rubber particles as the most influential parameters.

In addition to the compressive strength prediction laws by Gregori et al [13], the constitutive laws proposed by Strukar et al. [16] were adopted to model the entire compressive stress-strain behaviour of rubbercrete, failure mechanism and damage plasticity. This choice was adopted since Strukar et al. operated substitutions of the natural fine aggregates with rubber in the same range of percentages (10%, 20%, 40%) of Gregori et al. and with rubber particles with comparable dimension (0.5-4mm).

2.6.1 UNIAXIAL COMPRESSIVE BEHAVIOR

The stress-strain curve for rubbercrete Eq.(4) can be defined by accounting as input data in the model the peak compressive strenth f_c, the peak strain ε_c and the elastic modulus E_{cm} of normal concrete (NC) which are used to calculate peak compressive strenth f_{rc}, the peak strain ε_{rc} and the elastic modulus E_{rcm} of rubberized concrete (RC).

$$\frac{\sigma}{f_{rc}} = \frac{\rho_m (\varepsilon / \varepsilon_{rc})}{\rho_m - 1 + (\varepsilon / \varepsilon_{rc})^{\rho_m}}; \quad 0 < \varepsilon < \varepsilon_{cu} \qquad (4)$$

Where:

$$f_{rc} = \frac{1}{1 + 2 \cdot \left(\frac{3\lambda \rho_{vr}}{2}\right)^{3/2}} f_c$$

$$\lambda = \begin{cases} 2.43 \rightarrow d_{g,repl} : (0,5) \\ 2.90 \rightarrow d_{g,repl} : (0, d_{g,max}) \\ 2.08 \rightarrow d_{g,repl} : (5, d_{g,max}) \end{cases}$$

$$E_{rcm} = \frac{0.4 f_c}{\varepsilon_{el}} \cdot e^{(-\lambda \rho_{vr})}$$

$$\varepsilon_{rc} = (f_{rc} / E_{rcm})\left(\frac{v}{v-1}\right)$$

Where the coefficient $v = \frac{f_{rc}}{17} + 0.8$

The modified material parameter:

$$\rho_m = \left[1.02 - 1.17\left(E_p / E_{rc}\right)\right]^{-0.74} + (\varphi + \kappa); \quad 0 < \varepsilon < \varepsilon_u$$

With $E_p = f_{rc} / \varepsilon_{rc}$ the secant modulus of elasticity and κ and φ the linear equation's coefficient:

$$\varphi = 35 \cdot (12.4 - 1.66 \cdot 10^{-2} f_{rc})^{-0.9}$$

$$\kappa = 0.75 e^{\left(-\frac{911}{f_c}\right)}$$

2.6.2 UNIAXIAL TENSILE BEHAVIOR

The tensile stress-strain relation is accounted as defined in Eq.(3). The main differences compared with the NC are the values of $f_{ct} = f_{rct}$ and $E_{cm} = E_{rc}$. These latter modifications led to a strong decreasing of concrete features and a stronger degradation. The concrete fracture energy is defined as $G_F \approx \dfrac{G_f}{2.5}$ where $G_f = 0.075$ N/mm from [15].

3 RESULTS

Based on the available experimental results for the selected specimens (Section 2.2.1), the assessment of the obtained FE predictions was first carried out in terms of collapse load F_{max} (Table 1). The shear bearing capacity F_{max} is determined as the maximum shear force during the push-out test before a slip of 15 mm.

Table 1. F_{max} load comparison

Test series	Exper. F_{max} [kN]	FE F_{max} [kN]	Δ [%]
C40-12-110 /± 45°	19,8	18,5	-7%
C40-12-110/ 90°	19,4	13,2	-32%
C40-12-110/ - 45°	24,7	21,4	-13%

Moreover, the stiffness (for each connector) was evaluated and compared with the experimental ones. As summarized in Table 2, the smallest scatter was highlighted for screws having crossed configurations.

Table 2. K_s comparison

Test series	Exper. K_s [kN]	FE K_s [kN]	Δ [%]
C40-12-110 /± 45°	8,4	7,7	-8%
C40-12-110/ 90°	4,7	4,0	-16%
C40-12-110/ - 45°	7,2	9,3	29%

The same failure mechanisms obtained from experimental tests are pointed out from FE simulations, as shown in Fig. 2, 3 and 4. The configuration with inclined screws (45° inclination angle) in tension highlighted the formation of a single plastic hinge at the interface between glulam and concrete side.

For the screw placed with 90° inclination angle, the screws exhibit a double plastic hinges formation, with compression bearing in the bottom part of the hole in glulam member.
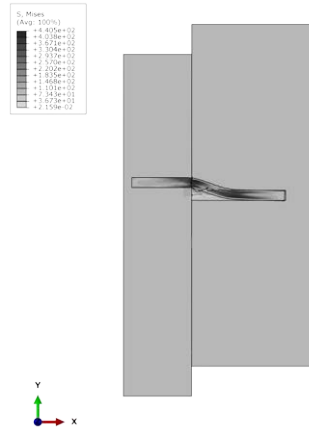
Figure 2. Normal concrete with screw placed perpendicularly to the grain (90° inclination angle) having two plastic hinges

Analyzing the configuration with crossed screws (45° inclination angle), both the screws (the one in tension as well as the compressed one) exhibit a double plastic hinges formation.

Figure 3. Normal concrete with screws having crossed configuration (45° inclination angle) in compression with two plastic hinges: at the interface between concrete and timber and inside the timber member
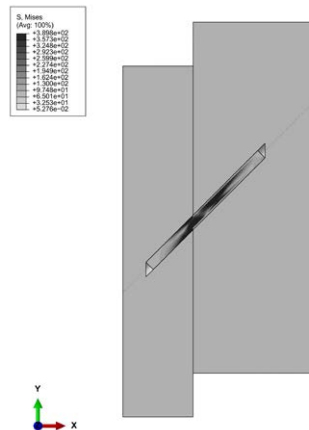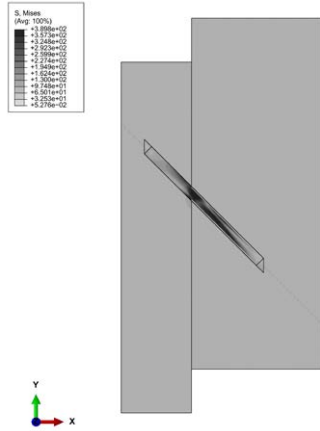
Figure 4. Normal concrete with screws having crossed configuration (45° inclination angle) in tension with two plastic hinges: at the interface between concrete and timber and inside the timber member

The previously described material formulation adopted for the concrete is capable to correctly consider its damage behaviour. In this framework, the crossed screws configuration specimen exhibits experimentally a cone expulsion failure of concrete ahead of the shear-compression loaded screw. This mechanism is reproduced with good accuracy also in FE modelling as described in Figure 5, by analysing the maximum principal stresses in the area around the bottom (compressed) screw.
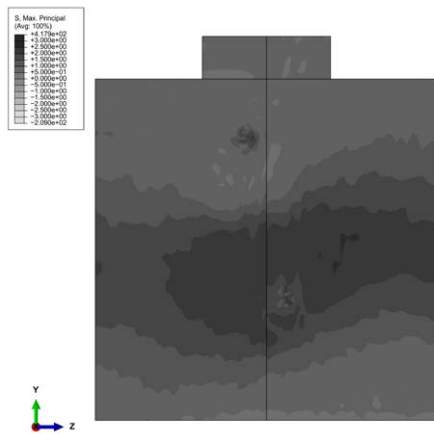
Figure 5. Stress in concrete member in crossed screws configuration

Comparing the FE model with Normal C40 concrete and the Rubbercrete (having the maximum amount of rubber

replacement: 40%) is evident a small scatter in term of both force as well as stiffness (4% for inclined screws and 5% for crossed screws).
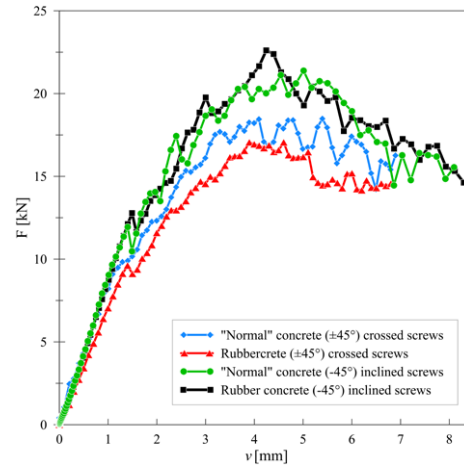
Figure 6. Comparison between load-displacement curves of "Normal" and Rubberised concrete

4 CONCLUSIONS

Rubbercrete slabs obtained with different substitutions of fine aggregates are expected to be lightweight compared to normal concrete, with higher thermal and acoustic insulation properties, suitable for the employment in composite systems like timber-concrete slabs. Moreover, the use of waste tyre rubber aggregate allows to reduce the consumption of the natural resources for the concrete mixtures and allows also to recycle waste tyres. In this framework is important to highlight how the decreasing of mechanical features due to the replacement of normal concrete with rubbercrete doesn't led to a substantial modification in terms of ultimate force as well as in terms of connections stiffness. This latter evidence is an additional benefit and further analysis both experimental and analytical should be carried on to deeply investigate the potential use of Rubbercrete in the timber floor reinforcement field.

REFERENCES

[1] Herzog T, Natterer J, Schweitzer R, Volz M, Winter W Timber construction manual. In: Natterer J (ed) Timber engineering, English translation of the 4th revised German edition. Birkha¨user-Publishers for Architecture, Basel, 2004

[2] Frangi A, Fontana M. A design model for the fire resistance of timber–concrete composite slabs. In: IABSE, ETH Zurich (eds) Proc. of international conference on innovative wooden structures and bridges, Lahti, Finland, Conference Report, 2001.

[3] Fontana M, Frangi A. Fire behaviour of timber–concrete composite slabs. In: Centre Scientifique et Technique du Batiment (CSTB), Av. Jean Jaure`s 84, Champs sur Marne, Marne La Valle´e Cedex 2, France (eds) Proc. of 6th international symposium on fire safety science (IAFSS), ENSMA, University of Poitiers, France. ISBN 0- 925-223-25-5, pp 891–902, 1999.

[4] Frangi A., Knobloch M., Fontana M. Design of Timber-Concrete Composite Slabs with Screwed Connections. Journal of Structural Engineering, 136(2), 2010.

[5] Ceccotti A.,"Composed timber-concrete structures", 1995

[6] Du, H. et al. "Study on shear behavior of inclined cross lag screws for glulam-concrete composite beams." Construction and Building Materials 224 (2019): 132-143.

[7] Marchi, L., Scotta, R. & Pozza, L. Experimental and theoretical evaluation of TCC connections with inclined self-tapping screws. Mater Struct 50, 180 (2017). https://doi.org/10.1617/s11527-017-1047-1

[8] E. Steinberg, R. Selle, T. Faust, Connectors for timber-lightweight concrete composite structures, J. Struct. Eng. 129 (11) 1538–1545, 2003.

[9] S. Kavaliauskas, A. Kazimieras-Kvedaras, B. Valiunas, Mechanical behaviour of timber-to-concrete connections with inclined screws, J. Civ. Eng. Manag 13 (3) (2007) 193–199.

[10] Bedon, Chiara & Fragiacomo, Massimo. FE modelling of notched connections for timber-concrete composite structures. Proceedings of WCTE 2016 - World Conference on Timber Engineering, August 22-25, 2016 - Vienna (Austria).

[11] Eldin N. and Senouci A., Measurement and prediction of the strength of rubberized concrete, Cem. Concr. Compos., 16(4)-287–298, 1994.

[12] Gregori, A., Castoro, C., Marano, G. C., Greco, R. Strength Reduction Factor of Concrete with Recycled Rubber Aggregates from Tires. Journal of Materials in Civil Engineering, 31(8), 2019.

[13] Gregori A., Castoro C., Mercuri M., Angiolilli M., Numerical modelling of the mechanical behaviour of rubbercrete, Computers & Structures, Volume 242, 2021, 106393, ISSN 0045-7949

[14] Gregori, A., Castoro, C., & Venkiteela, G. (2021). Predicting the Compressive Strength of Rubberized Concrete Using Artificial Intelligence Methods. Sustainability, 13(14), 7729.

[15] Bengar, H. A., Shahmansouri, A. A., Sabet, N. A. Z., Kabirifar, K., & Tam, V. W. (2020). Impact of elevated temperatures on the structural performance of recycled rubber concrete: Experimental and mathematical modeling. Construction and Building Materials, 255, 119374.

[16] Simulia. ABAQUS Theory Manual, Version CAE 21, 2021

[17] Bedon C and Fragiacomo M (2019) Numerical analysis of timber-to-timber joints and composite beams with inclined self-tapping screws. *Composite Structures*: 13–28. DOI: 10.1016/j.compstruct.2018.09.008.

[18] CEN. EN 1992-1-1. Eurocode 2: Design of concrete structures: Part 1–1: General rules and rules for buildings. CEN, Brussels, Belgium, 2004.

[19] Cornelissen HAW, Hordijk DA, Reinhardt HW. Experimental determination of crack softening characteristics of normal weight and lightweight concrete. Heron 1986; 31(2): 45–56.

Chapter 8

Empirical model for an hold-down connection: derivation and application

Abstract: Timber-to-steel connections are part of buildings with wall-resisting structure. Timber-to-steel connections are used to join walls on top of each other or to restrain the base wall to the foundation. Hold-downs are commonly used as overturning restraints. They are made of a drilled steel plate and of an housing for a bolt. Nails or screws are used to make the connection between the hold-down and the wall. In modelling the building behavior or the wall behavior, the connection is represented by an equivalent element with a suitable constitutive law. In this way the overall modelling effort decreases. The constitutive law of a connection can be derived by detailed numerical models or by experimental tests. In the following a constitutive law suitable for describing the behavior of an hold-down with nails is derived from experimental test data. Two different connection modelling approaches are proposed. The former is based on a tabular definition of elastic and plastic displacements for different load levels, while the latter uses a combination of a linear and an exponential function. Then, the derived constitutive model in inserted in a finite element model of a wall with openings with the aim of deriving an hybrid elementary model for the rocking capacity prediction.

8.1   Introduction

In global models of buildings is often necessary to condensate the connection behavior into a single finite element. Hold-downs are the most common overturning restraints for cross-laminated timber buildings. In the paper of Sec. 8.2 a suitable constitutive law for describing the non-linear behavior of hold-downs is defined on the basis of experimental data. Two different approaches are presented. A tabular approach and a functional approach. In this latter case the fitting is done by assuming a linear function to model the elastic part and an exponential function to model the plastic part. The same function used in [31, 47, 60] are used for the plastic component. An application of the derived constitutive law is presented.

8.2   Paper: *Rocking capacity model of CLT walls with openings and timber plasticization*

Capacity model of CLT walls with openings and timber plasticization

Yuri De Santis *, Angelo Aloisio, Martina Sciomenta, Massimo Fragiacomo

Department of Civil, Construction-Architectural and Environmental Engineering, University of L'Aquila, Italy

ARTICLE INFO

ABSTRACT

This paper investigates the effect of timber plasticization on the ultimate lateral capacity of rocking Cross-Laminated Timber shear walls with different characteristics. Simplified capacity models predict a CLT wall ultimate capacity by multiplying the hold-down ultimate resistance by its distance to an assumed pivot point, often coincident with the panel edge. However, timber plasticization at the interface with the foundation can significantly reduce the lever arm of the hold down reaction. This paper aims at assessing the effect of timber plasticization and panel characteristics (geometry, width, presence of openings, etc.) on the position of the pivot point, expressed by the dimensionless lever arm τ, namely the ratio between the distance of the hold-down geometrical axis from the compressed timber resultant and the distance between the hold-down geometrical axis and the panel edge. An extended covariance-based sensitivity analysis of several Finite Element (FE) models, representing all the CLT shear wall design variability was carried out. The FE model, developed in Abaqus, has been calibrated on the experimental cyclic response of a CLT wall panel. Among the chosen parameters, the sensitivity analysis proved that the most significant ones affecting τ are two: the ratio between the hold-down reaction and the maximum resistance of the compressed timber, and the width of the opening. Accordingly, the authors estimated an elementary empirical regression equation based on the FE model results for predicting the dimensionless lever arm (τ) in the capacity equation of CLT panels. The use of this elementary formulation allows the designer to estimate with considerable accuracy the lateral capacity of a CLT panel given the panel geometry, the ultimate resistance of the hold-down, the compression strength of timber perpendicular to the grain and the vertical load. Almost all points used for the linear regression fall within the confidence bounds, thus proving the accuracy of the proposed empirical formula for the dimensionless lever arm.

1. Introduction

Since the spreading of Cross-Laminated Timber (CLT) as a valid alternative to engineering wood products and traditional construction materials [1,2], a remarkable number of researchers have investigated the structural performance of CLT shear walls [3–5]. Specifically, a significant amount of research investigated the ultimate lateral capacity of CLT shear walls [6–9]. Experimental and numerical research demonstrated that CLT panels have significant resistance to lateral loads [10–12], making CLT a suitable construction material, especially in earthquake-prone areas [13–16]. The scientific literature presents two approaches for predicting the lateral capacity of CLT panels [17]. The former is entirely analytical and originates from the solution of the equilibrium equations of a CLT panel. The latter one is based on Finite Element modelling and aims at reducing the number of assumptions related to the former approach. Several papers [18] propose novel capacity models or highly-refined FE models. The authors believe that further research is needed for assessing the actual trade-off between computational endeavour required by the use of FE models and model accuracy at this stage. Additionally, practitioners demand elementary but accurate formulations for predicting the lateral capacity of CLT wall panels.

The scientific literature, presenting several models for assessing the strength of Cross-Laminated Timber (CLT) and Light Timber Frame (LTF) shear walls, mirrors this need for analytical and simplified capacity models [19]. Many scholars consider CLT walls as rigid bodies: the capacity of the wall depends on the strength of its anchorage system due to its intrinsic considerable in-plane strength and stiffness [20]. The CLT capacity models merely descend from the equilibrium equations of the wall, while the main differences between them lie on two main points: the inclusion or not of the angle brackets contribution in the tension resisting mechanism and the shape and contribution of the compression zone. Casagrande et al. [21], and Tomasi [22] both neglect the contribution of angle brackets: the first does not make any specific assumptions about the compression stresses distribution and

---

proposes a conventional lever arm equals to $0.9l$ where l in the panel length, the second assumes a rectangular stress block distribution in the compression zone, with size $0.8x$ where x is the compressed zone length. Wallner-Novak et al. [23] proposes a model similar to [24] but with compression zone equals to $0.25l$. Pei et al. [25], Reynolds et al. [26], Gavric and Popovski [27] presented models that include the tensile contribution of angle brackets. Pei et al. [25] assumes an elastic triangular distribution of tensile forces by considering the rigid body rotation around one edge of the shear wall. Reynolds et al. [26] presented three different models, which all include the presence of a compression zone, but differ in the size of that zone and the distribution of tensile forces between angle brackets and hold-down. Gavric and Popovski [27] presents a model similar to [25], but considers the interaction between horizontal and vertical forces on the angle brackets. Aloisio et al. [28] discussed a simplified capacity model that is valid for both LTF and CLT walls based on equilibrium equations. The capacity originates from multiplying the hold-down reaction by a fraction (τ) of the distance between the hold-down geometrical axis and the panel's edge. The experimental data evidenced that τ varies between 0.7 and 0.9.

However, the findings by [28] are entirely based on experimental data. Recently, Sandoli et al. [29] proposed a model to predict the ultimate flexural behaviour of a CLT panel. They investigated the effect of the timber-to-timber contact zone on the capacity of multi-storey walls, by focusing on the role of perpendicular to grain compression strength. However, to the authors' knowledge, no research paper presents an extended sensitivity analysis of the dimensionless lever arm to the design parameters of a CLT shear wall [30].

Therefore, this paper assesses the sensitivity of the dimensionless lever arm (τ) to the design parameters of a CLT shear wall in platform-frame buildings, conceivably representative of all design choices, using a covariance-based sensitivity analysis. The goal is to propose an empirical equation for predicting the dimensionless lever arm given the values of the most sensitive parameters. This investigation leads to a hybrid capacity model. The structure of the capacity equation derives from the panel equilibrium, while the empirical equation of the dimensionless lever arm derives from the linear fitting of the FE results. The authors investigated two limit cases, a CLT wall on a rigid concrete foundation and a CLT wall on a deformable foundation, representative of the timber floor in platform frame buildings, In platform frame buildings CLT panels are prone to rocking, particularly at higher stories, and consequently are subjected to local timber plasticization. Local plasticization of the timber floor panel occurs at the attainment of its low strength in perpendicular to grain direction [31]. Once this strength is exceeded, the base stress distribution changes and the pivot point moves towards the hold-down in tension. Therefore, assessing the effects of timber plasticization is crucial. In addition, the effect of CLT floor on the rocking response of the CLT panel is significant as it affects both the structural capacity [32] and the low-vibration dynamic response [33].

The paper also considers the effects of the openings on the ultimate capacity of CLT walls. In past years, Dujic et al. [34,35] addressed the issue of CLT panels with openings by providing analytical estimates of strength and stiffness reduction related to the openings' aspect ratios, based on non-linear static pushover analyses. Awad et al. [36] carried out experimental tests on CLT walls with openings. Based on FE numerical analyses, the proposed analytical models estimate the lateral capacity and the expected failure mechanism. Also, Shahnewaz et al. [37] carried out sensitivity analysis and proposed analytical estimates of in-plane CLT wall stiffness due to different geometries of the openings. However, to the authors' knowledge, no scholar attempted to estimate the effects of the openings on the dimensionless lever arm to be used in an elementary capacity model of the CLT wall. Recently, Casagrande et al. [38] carried out a numerical and analytical study on the distribution of in-plane internal axial and shear forces in single-storey monolithic CLT shear-walls with cut out openings. The authors
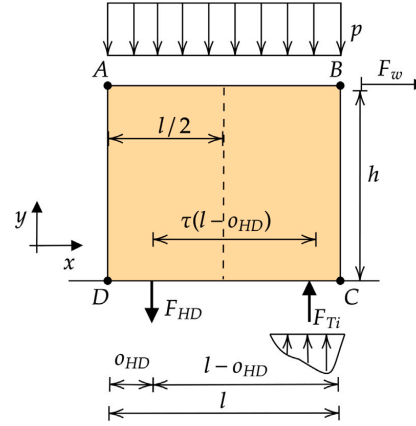

Fig. 1. Mechanical model of the shear wall.

identified the critical zones of maximum axial and shear forces due to in-plane lateral loading of CLT shear-wall with openings and predicted the levels of internal forces for possibly developing design methods for CLT walls with openings. The current research directly addresses the role of openings in the design of CLT panels.

Therefore, the paper proposes a capacity model for the lateral response of CLT walls by highlighting the contributions of opening and timber plasticization (second section). The analyses are based on the FE modelling and calibration of a CLT wall based on the experimental cyclic response of a typical CLT panel with uplift and sliding constraints (third section). An extensive monovariate and multivariate sensitivity analyses [39,40] highlight the most influential parameters affecting the lateral capacity (fifth section). Based on these outcomes, the empirical formula of the dimensionless lever arm is proposed (sixth section). This formula extends the accuracy and applicability of the capacity model proposed by Aloisio et al. [28] to CLT panels with openings.

2. Problem statement

The capacity model presented in this paper is based on equilibrium equations, following [28]. The behaviour of CLT walls is mainly governed by the hold-down connections [28]. As shown in Fig. 1, the wall is assumed to pivot around the position of its neutral axis, characterized by a compression region of a certain extension; no specific assumption is made regarding the shape of the stress distribution in the compression zone. The contribution of angle brackets is neglected. Hereafter the equilibrium equations follows. The equilibrium to the vertical translation of the panel can be written as:

$$\sum_i F_{y,i} = 0 \Rightarrow -pl - F_{HD} + F_{Ti} = 0 \tag{1}$$

where $F_{y,i}$ is the ith horizontal force, p is the vertical load, l and h are the length and height of the panel, F_{HD} is the hold down resisting force, and F_{Ti} is the resultant of the compression stresses. The equilibrium to the rotation around the position of the resultant of the compression stresses can be written as:

$$\sum_i M_{r,i} = 0 \Rightarrow pl \left[o_{HD} + \tau(l - o_{HD}) - \frac{l}{2} \right] - F_W h + F_{HD}\tau(l - o_{HD}) = 0 \tag{2}$$

where F_W is the horizontal force acting on the top of the panel, and o_{HD} is the distance between the hold-down reaction force and the closest edge of the panel, $\tau \cdot (l - o_{HD})$ is the distance between the reaction force of the hold down and the compression force.
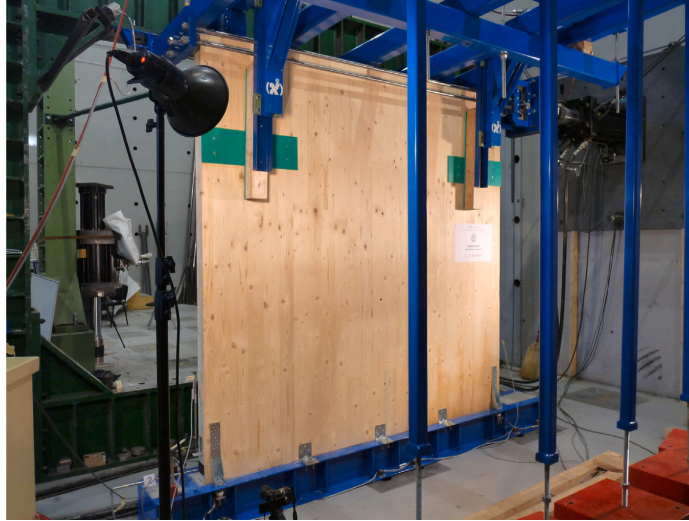
Fig. 2. View of the tested CLT specimen.

By solving Eq. (2), the expression of τ when the hold-down reaches failure ($F_{HD} = R_{HD}$) can be written as shown in Eq. (3):

$$\tau = \frac{-p l o_{HD} + p l^2/2 + R_W h}{(pl + R_{HD})(l - o_{HD})} \tag{3}$$

By solving Eq. (2), the expression of R_W when the hold-down reaches failure can be written as shown in Eq. (4):

$$R_W = \frac{pl}{h} \left[o_{HD} + \tau(l - o_{HD}) - \frac{l}{2} \right] + R_{HD} \frac{\tau(l - o_{HD})}{h} \tag{4}$$

The aim of the paper is to determine the capacity of a rocking CLT panel. If the wall were a rigid panel without holes, the problem would be almost trivial. The position of the neutral axis could be estimated from the equilibrium to the translation, and consequently, the arm of the internal forces. The problem grows in complexity when the in-plane panel stiffness lowers, as occurring in the case of CLT panels with opening, see Fig. 10. Therefore, it is necessary to carry out a Finite Element analysis to assess the contribution of the panel deformability to the lateral capacity of the panel. As anticipated in the previous sections, the paper aims at assessing the effects of the panel stiffness on the lateral capacity of a CLT panel. The study is carried out by simulating a displacement-driven cyclic response of a CLT panel, where the wall capacity is always reached for the hold-down failure and never by complete plasticization of the timber. Given the capacity R_W, the geometry of the wall (length l and height h, the offset of the hold-down o_{HD}), the resistance of the hold-down R_{HD} and the vertical load p, from the equilibrium equation to rotation, it is possible to estimate τ (Eq. (3)), which is the non-dimensional arm of the forces with respect to the maximum lever arm if there pivot point corresponded to the panel's edge ($l - o_{HD}$). The authors will repeat the analyses for several structural configurations and then interpolate the results and find a simple expression for τ so that practitioners can derive the capacity of the wall by a simple equilibrium to rotation (Eq. (4)).

3. Materials and methods

3.1. Experimental tests

The results presented in this paper descend from the experimental data on CLT shear wall tests performed at the University of Trento [41].

Table 1
Characteristics of the considered CLT shear wall after [28].

Specimen CLT	NA620
Sliding restraint	Angle brackets
n_{sr}°	3
Fastener type	Ringed shank nail
$n_{n,sr}^\circ$	30
ø [mm]	4
l [mm]	60
Uplift restraint	WHT620
n_{ur}°	2
Fastener type	Ringed shank nail
$n_{n,ur}^\circ$	52
ø [mm]	4
l [mm]	60

The test set-up, shown in Fig. 2, follows the EN 12512 (UNI, 2001) protocol. In this research, the cyclic response of a single CLT panel, labelled NA620 [28], has been selected. The CLT shear wall has the following characteristics: three layers (thickness 30–30–30 mm) of C24 boards, and dimensions 2.5 × 2.5 m. The sliding and uplift restraints consist in 3 angle brackets and 2 hold downs bolted to the underlying steel beams respectively. The same type of ringed shank nail has been used to connect angle brackets and hold downs to the CLT panel. The nail diameter and length are: ø = 4 mm and l = 60 mm. The sliding restraint nail number $n_{n,sr}^\circ$ is 30 and the uplift restraint nail number $n_{n,ur}^\circ$ is 52 (Table 1). Further details on the experimental setup are fully reported in [28,42]. The horizontal displacement, following the EN 12512 (UNI, 2001) protocol, was imposed on the top edge of the panel. The experimental setup includes force and displacement transducers to measure the resisting forces and displacements of the two hold-downs and the panel. As demonstrated in [28], more than 88% of the horizontal displacement the panel can be attributed to the rocking, while 12% to both the sliding and in plane deformation of the panel. Therefore, the selected specimen can be considered a good case study to investigate the rocking response of CLT panels.
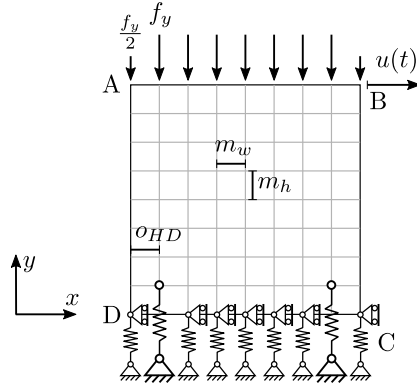
Fig. 3. Finite element model representation.

3.2. FE models: Hold-down calibration and validation

The rocking behaviour of the CLT wall has been schematized through a 2D model consisting of an assembly of two-dimensional elements representing the CLT panel and elastic–plastic springs representing the uplift restraints and the panel-underlying structure interaction (Fig. 3).

The CLT panel is modelled via S4R 4-node general-purpose shell elements (ABAQUS/Standard library), with elastic orthotropic behaviour. The shell thickness is assumed equal to the actual panel thickness t_p and the in-plane elasticity modules were calculated according to the well-known approach from the literature [43]:

$$E_x = \frac{\sum_{i=1}^{n_{lx}} E_0 t_{x,i} + \sum_{i=1}^{n_{ly}} E_{90} t_{y,i}}{t_p} \tag{5}$$

$$E_y = \frac{\sum_{i=1}^{n_{ly}} E_0 t_{y,i} + \sum_{i=1}^{n_{lx}} E_{90} t_{x,i}}{t_p} \tag{6}$$

where E_x and E_y are the equivalent elastic modules referred respectively to the x and y global direction (Fig. 3), E_0 and E_{90} are the parallel and perpendicular elastic modules of the planks of the panel, t_x and t_y are the thickness of the layers oriented along x and y direction respectively and n_{lx} and n_{ly} are the number of the layers oriented along x and y direction respectively. The in-plane shear module for CLT-elements without lateral gluing interfaces at the narrow faces can be calculated according to the formula given by [44]:

$$G_{xy} = \frac{G_{0,90}}{1 + 6\alpha(t_m/w_l)^2} \tag{7}$$

where $G_{0,90}$ is the shear modulus of the planks, t_m is the average layer thickness, w_l is the plank width and $\alpha = r(t_m/w_l)^{-0.79}$ with r equal to 0.53, 0.43 and 0.39 in the cases of 3, 5 and 7 layers CLT respectively.

The panel has been discretized by means of square elements. The mesh dimension $m_w = m_h = 50$ mm has been chosen on the basis of the outcome of a preliminary mesh sensitivity study (halving m_w and m_h the wall capacity R_w decreases of 0.3%).

With the aim of reproducing the experimentally assessed behaviour of quasi-pure rocking behaviour, the base nodes translation in x direction were restrained ($u_x = 0$ on CD, Fig. 3).

The typical simulation consisted in a static incremental, geometrical linear, displacement-controlled analysis divided in two steps. In the first step, the vertical imposed load was applied in the form of vertical, concentrated forces applied to the upper nodes of the wall ($f_y = pm_w$ on AB, Fig. 3). The second step was carried-out on the pre-compressed FE-model, and a monotonic or cyclic history of horizontal displacements was imposed at the node B(($u_x = u(t)$ on B, Fig. 3).

Regarding the wall-panel-base interaction both the case of a wall on a rigid base and the case of a wall on CLT floor were considered.

In the first case the interaction was modelled by means of compression-only rigid-plastic springs representing the rigid behaviour of the base and the plastic behaviour of the wall. A finite stiffness value of $k_{s,r} = 31$ N/mm^3 was chosen to avoid convergence problem. The value was determined by means of a sensitive study (doubling $k_{s,r}$ the wall capacity R_w increases of 0.03%). The springs yield stress f_s was determined assuming y oriented layers only as resistant and considering their compression strength parallel to grain (EN338:2016):

$$f_s = f_w = \frac{n_{ly}}{n_l} f_{c,0,m} \approx \frac{n_{ly}}{n_l} \frac{f_{c,0,k}}{0.9} = 15.5 \text{ N/mm}^2 \quad (C24) \tag{8}$$

where f_w is the resulting wall compression strength in y direction and $f_{c,0,m}$ is the mean compression strength parallel to grain of the y oriented layers. In the second case the interaction was modelled by means of compression-only elastic–plastic springs representing the behaviour of the underlying CLT panel. The yield stress was assumed equal to the compression strength of the floor panel perpendicular to grain. $f_s = f_f = 2.5$ N/mm^2 according to EN338:2016 and to the test of [31] consisting of line loads applied close to the specimen edge. The springs stiffness k_s was calculated:

$$k_s = k_f = \frac{E_{f,90}}{t_f} = 2.5 \text{ N/mm}^3 \quad (C24, \quad 5 \quad layers) \tag{9}$$

where $E_{f,90}$ is the mean modulus of elasticity perpendicular to grain direction according to EN338 (UNI, 2016) and t_f is the floor CLT panel thickness.

Careful consideration was given to the mechanical characterization of the uplift restraints. The hold-down behaviour including its interaction with the panel through the nailed connection is modelled via CONN3D2, a two nodes connector element with elastic–plastic behaviour. Two experimentally fitted constitutive relationships have been considered and in both cases the hold-down was reduced to two springs placed in series, accounting for the elastic and plastic displacements components respectively.

The cyclic test allows the separation of the elastic and plastic displacements for different levels of forces. Naming $F_{HD,max,i}$ the maximum hold down force for each cycle and fixing a reference force of $0.2F_{HD,max,i} = F_{HD,lo,i} = F_{HD,un,i}$ (Fig. 4a), the plastic displacement corresponding to $F_{HD,max,i}$ is given by the difference between the displacement corresponding to the reference force in the loading phase and the displacement corresponding to the same reference force during the unloading phase (Eq. (10) for $i = 1, 2, 3, 6, 9, 12$, i.e. considering only the first load cycle of each amplitude).

$$u_{HD,pl}(F_{HD,max,i}) = u_{HD}(F_{HD,un,i}) - u_{HD}(F_{HD,lo,i}) \tag{10}$$

The elastic displacement component is derived by the difference between the total displacement and the plastic displacement (Eq. (11) for $i = 1, 2, 3, 6, 9, 12$).

$$u_{HD,el}(F_{HD,max,i}) = u_{HD}(F_{HD,max,i}) - u_{HD,pl}(F_{HD,max,i}) \tag{11}$$

The tabular constitutive law thus obtained was validated with an incremental static FEM simulation of the connector only with the experimentally recorded displacement time history (Fig. 4a, b).

With the aim of deriving a constitutive law in analytic form, the points of constitutive law in tabular form (Fig. 5a) has been interpolated with the following functions:

$$F_{HD}(u_{el}) = K_0 u_{el} \tag{12}$$

$$F_{HD}(u_{pl}) = F_{HD,0} + a(1 - e^{-bu_{pl}}) \tag{13}$$

A linear law was chosen to interpolate the elastic component ($K_0 = 21.8$ kN/mm, coefficient of determination $R^2 = 0.93$, Root Mean Square
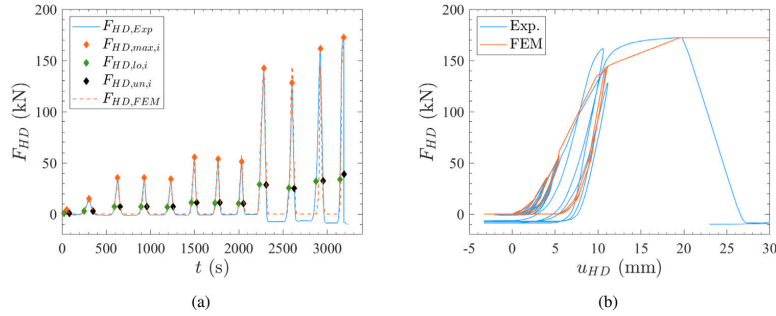
Fig. 4. (a) Hold-down force time history and reference forces (b) Hold-down force–displacement curve: experimental and FEM with fitted tabular constitutive law.
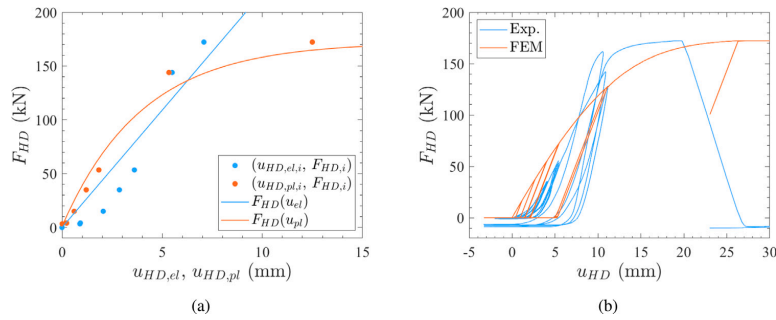

Fig. 5. (a) Hold down force as a function of elastic and plastic displacement components (b) Hold-down force–displacement curve: experimental and FEM with fitted analytic constitutive law.

Error $RMSE$ = 21.5 kN) and an exponential law was chosen to interpolate the plastic component ($F_{HD,0}$ = 1.0 kN, a = 171.3 kN, b = 0.25, coefficient of determination R^2 = 0.98, Root Mean Square Error $RMSE$ = 10.1 kN). It is worth nothing that the linear function chosen for the elastic component did not allow to account for the initial connection slip resulting in an underestimate of the overall connection stiffness (Fig. 5b and Table 2).

Both the tabular and analytical constitutive law accurately describe the failure behaviour of the uplift restraint in terms of strength and displacement (Table 2). The force peaks of the first load cycle for each amplitude predicted by the tabular constitutive law coincides with the experimentally assessed force peaks (Fig. 4a). Although the analytic constitutive law is not able to accurately predict the initial stiffness of the uplift constraint, K_{HD} turns out to be one of the irrelevant parameters for the purpose of evaluating the ultimate strength of the wall and the associated equivalent arm (Fig. 7). In both constitutive law post failure behaviour has been neglected.

The wall on rigid base FEM model with the tabular and analytical hold-down constitutive law was validated on the basis of the experimental results in terms of force–displacement response (Fig. 6a and b). In both cases the model overestimate the experimentally assessed wall capacity ($R_{W,FEM,tab}/R_{W,exp}$ = 1.21 and $R_{W,FEM,an}/R_{W,exp}$ = 1.22). According to Aloisio et al. [28] the sliding fraction of the FEM reproduced experimental configuration is equal to 7.7% of the imposed displacement and this could explain the overestimation of the strength, since the FEM model completely neglects the sliding. Evaluating the wall force at a corrected imposed displacement net of the contribution of the sliding: $R_{W,FEM,tab}/R_{W,exp}$ = 1.10 and $R_{W,FEM,an}/R_{W,exp}$ = 1.15. No appreciable difference was found between the two constitutive laws in terms of wall capacity and therefore in terms of extension of compressed zone at the base of the panel, so from now on the analytical constitutive law will be used in all analysis.

Table 2
Comparison between experimental, tabular and analytical constitutive law for uplift restraint.

	$F_{HD,u}$ (kN)	$u_{HD,u}$ (mm)	$k_{HD,i}$ (kN/mm)	$k_{HD,s}$ (kN/mm)	$k_{HD,u}$ (kN/mm)
Experimental	172.3	19.6	10.7	14.2	15.1
Tabular	172.3	19.6	11.7	16.1	14.8
Analytic	172.3	18.9[a]	13.1	12.7	10.9

[a] Due to the asymptotic behaviour $u_{HD,u} = u_{HD}(0.95F_{HD,u})$.

Compared to the wall on rigid base model, the wall on CLT base model showed reduced capacity ($R_{W,FEM,CLT}/R_{W,FEM,RB}$ = 0.88) due to the extensive CLT floor base plasticization (Fig. 6c).

4. Sensitivity analysis

4.1. OAT sensitivity analysis

The models of wall on rigid base and wall on CLT base were both analysed by an OAT (One-at-a-time) sensitivity analysis observing the response of the models in terms of dimensionless equivalent arm τ (Eq. (3)). Nine of the parameters describing the basic experimental configuration (Fig. 8) have been individually varied: panel length l, panel height h, opening length ratio l_d/l for a centered door opening with h_d = 2 m, opening length ratio l_w/l for a centered window opening with h_w = 1 m, wall CLT class (all softwood classes of EN 338:2016), number of layers of the wall panel n_l, hold-down secant stiffness K_{HD}, hold-down strength R_{HD} and uniformly distributed load at wall top base p.
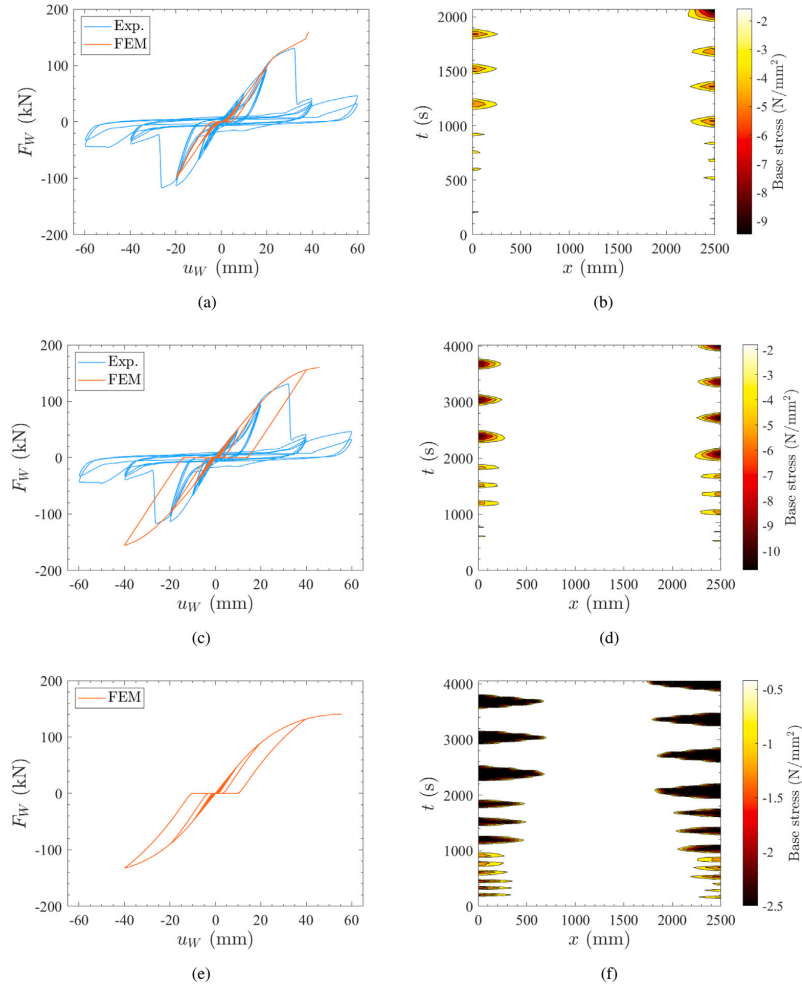
Fig. 6. Wall force–displacement curve (left) and base stresses (right): (a, b) Tabular constitutive hold-down law and rigid base, (c, d) Analytical constitutive hold-down law and rigid base and (e, f) Analytical constitutive hold-down law and CLT base.

The equivalent dimensionless arm τ of the wall model on a rigid base tends to the value 0.98 and is substantially insensitive to all the parameters investigated (Fig. 7 blue dots). Only for shorter panels, not very resistant or subject to high vertical loads, τ slightly decreases due to the plasticization of an area of limited extension of the compressed end of the panel.

Due to the limited compressive strength in the direction perpendicular to the fibres of the CLT base, in order to grant the equilibrium of the panel, a larger compressed area of the panel base is required compared to the case of the wall on rigid base (see Eq. (1)), which correspond to lower τ values (Fig. 7 orange dots).

Fig. 7 shows the results of the parametric analysis. The main results could be itemized as follows:

- The dimensionless lever arm in CLT panel on a rigid foundation is not very sensitive to the considered modelling parameters. Conversely, the presence of the CLT floor leads to a significant variation of τ due to local plasticization of timber.

- In case of CLT panels on CLT floors, the base length l, the openings size l_d/l, the hold-down resistance R_{HD}, the vertical load p and the number of layer n_l play the most significant role.
- In case of CLT panels on CLT floors, if the panel base is shorter than approximately 3 m, the lever arm is lower than 0.9, reaching 0.6 for a 1 m base length. As the length of the wall increases, the base zone in the elastic field prevails over that in the plastic field consequently moving the resultant F_{Ti} towards the compressed edge of the panel
- In case of CLT panels on CLT floors, if the ratio between the door opening and panel size exceeds 0.4, the dimensionless arms drops to values between 0.8 to 0.7. The drop of τ value occurs when the compressed area of the panel extends beyond the opening. Assuming complete plasticization up to the edge of the centered door ($F_{Ti} = f_f n_l t_l (l - l_d)/2$) and $p = 0$, from Eq.(1) the critical value of the opening ratio is $l_d/l = 1 - 2R_{HD}/(f_f n_l t_l l) = 0.38$ (see Fig. 8) and for greater values also the left part start plasticizing (see Fig. 10)
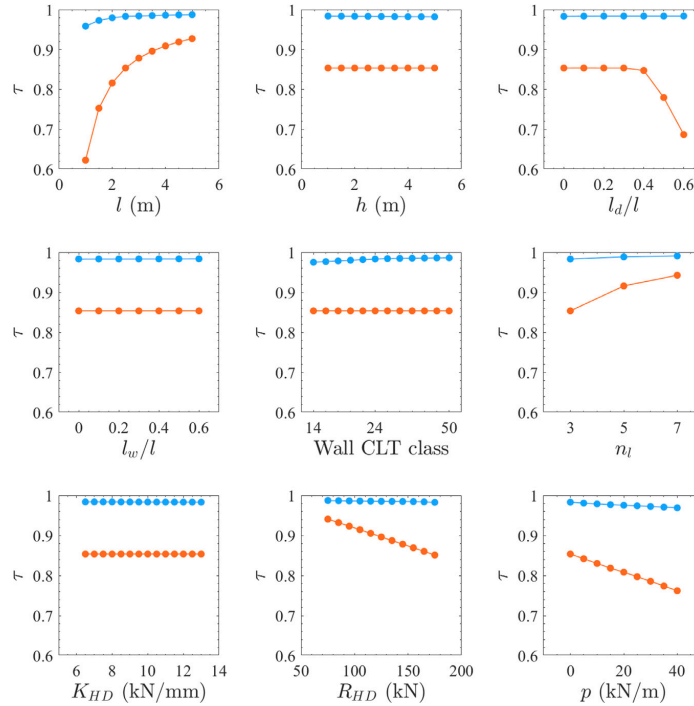
Fig. 7. Parametric study of the FEM derived dimensionless equivalent arm τ (Blue dots: wall on rigid base, Orange dots: wall on CLT floor)..

- In case of CLT panels on CLT floors, an increment of the number of wall panel layers causes an almost asymptotic increase of τ. The main effect of increasing n_l is the base contact area increase resulting in a progressive reduction of the length of plastic zone
- In case of CLT panels on CLT floors, an increment of the hold-down resistance causes an almost linear reduction of τ. As the resistance of the hold-down increases, due to the negligible dimensions of the elastic zone compared to those of the plastic zone, the extension of the timber plastic zone at hold-down failure must increase linearly to grant equilibrium, therefore τ must decrease linearly.
- In case of CLT panels on CLT floors, analogously, an increment of the vertical load causes an almost linear reduction of τ. In a similar way to what happens by increasing the hold down resistance, also in this case the negligibility of the base area of the panel in the elastic field makes the relationship between τ and p linear with a good approximation.

In conclusion, the presence of a deformable foundation may lead to a significant shift of the pivot point of the panel. Therefore, a proper calibration of the dimensionless arm is needed if an elementary capacity model based on the equilibrium equations is used.

4.2. Multivariate variance-based sensitivity analysis

A Multivariate variance-based Sensitivity analysis aimed at assessing the role and mutual dependence of each parameter in the lateral capacity of the CLT panel. The variance-based sensitivity analysis of the correlation function allows discerning the effects of the uncertainties of the modelling parameters. Specifically, the Sobol method by [39] decomposes the variance of the output of the model or system into fractions which can be attributed to inputs or sets of inputs. The so-called

Sobol indicators measure sensitivity across the whole input space, they can deal with nonlinear responses, and they can measure the effect of interactions in non-additive systems. The computation of Sobol integrals, is performed through a Monte Carlo simulation. Latin hypercube sampling generates a near-random sample of parameter values from a multidimensional distribution to speed up the convergence [45]: in the first step, a matrix of N randomly sampled input combinations is built, each one made up of M components, where M is the number of model inputs. Both the Sobol index S_1 and the total sensitivity index S_T are computed in this paper. While S_1 measures the effect of varying a single parameter alone, S_T measures the contribution to the output variance of the selected parameter, including all variance caused by its interactions. In short, the more different the ranking generated by the two indices, the more complex the interaction between the parameters [46–48].

An extended covariance-based sensitivity analysis plausibly representing all the CLT shear wall design variability of several Finite Element (FE) models has been carried out with $N = 1000$, $M = 9$ and parameter domains in Table 3.

The objective functions chosen for the sensitivity analysis are the ultimate resistance of the wall R_W corresponding to the hold down failure and the stiffness of the shear-wall K_W evaluated as:

$$K_W = \frac{0.4R_W - 0.1R_W}{u_{x,B,0.4} - u_{x,B,0.1}} \tag{14}$$

The limits of the domain of the parameters l, length of the wall and h, height of the wall have been chosen in order to consider panels with slenderness λ between 0.5 and 5. The openings were always considered centered in the length of the wall and placed at a distance of $0.2h$ from the wall top. The ratios between the length of the opening and the length of the wall l_{op}/l and that between the height of the

Table 3
VBSA parameters domain.

	l (m)	h (m)	l_{op}/l	h_{op}/h	CLT class	n_l	K_{HD} (kN/mm)	R_{HD} (kN)	p (kN/m)
Lower	1	2.5	0	0	C14	3	6.5	75	0
Upper	5	5	0.6	0.8	C50	7	13	175	40

Table 4
First order (S_1) and total-order (S_T) sensitivity indices.

Parameter	Rigid base				CLT floor base			
	K_W		R_W		K_W		R_W	
	S_1 (%)	S_T (%)	S_1 (%)	S_T (%)	S_1 (%)	S_T (%)	S_1 (%)	S_T (%)
l	56	80	77	80	62	73	76	75
h	14	20	10	37	22	19	13	37
l_{op}/l	12	37	−1	32	11	29	−1	30
h_{op}/h	5	30	−2	33	7	25	−2	31
$CLT class$	8	22	−1	32	12	19	−1	30
n_l	6	30	−1	33	11	28	−2	32
K_{HD}	5	27	−1	32	8	24	−1	30
R_{HD}	7	23	7	42	10	21	7	41
p	9	22	2	34	14	22	1	32
Sum	123	292	88	356	157	261	90	339

opening and the wall height h_{op}/h have been varied between 0 and 0.6 and 0.8 respectively in order to also consider the cases of intact panel and door openings. It should be noted that it was necessary to round off the values of the descriptive parameters of the wall geometry obtained from the continuous random sampling in order to make it compatible with the chosen discretization (i.e. mesh dimensions). With a similar methodology it was possible to associate to two fictitious continuous variables, the commercially available CLT classes described in EN338:2016 and the number of plank layers n_l of a chosen thickness $t_l = 30$ mm. Known K_{HD} and R_{HD} from the sampling, having the analytical form of the constitutive bond and setting the parameters $F_{HD,0}$ and b it was possible to obtain the values of the remaining parameters of Eqs.(12) and (13) (K_0 and a). The distributed load domain p has been chosen in order to reproduce the most common real case scenarios.

Both the case of a ground floor wall panel (panel on a rigid base) and the case of an upper floor wall panel (panel on CLT base) have been considered.

In both cases of rigid base and CLT base, Table 4 proves that the most significant parameters affecting the lateral stiffness of the panels are the size of the panels and the openings. Conversely, the sole size of the panel, the hold down strength and the distributed load affects the lateral capacity in the considered ranges of interest, shown in Table 3. The discrepancy between the first-order (S_1) and total order indicators (S_T), proves that the effects of the parameters are highly correlated.

5. Empirical formulation of the dimensionless equivalent arm (τ)

The OAT and VBSA analysis highlighted the dependence of the non-dimensional equivalent arm τ on the extension of the plastic area at the base of the panel. The reduction of τ is particularly significant in the case of walls on CLT floor base. It has been observed that the factors that determine an increase in the base stresses at hold-down failure, such as the distributed load on the top of the wall p, the resistance of the hold-down itself R_{HD} or the decrease in the length of the wall l, cause a decrease of τ. On the contrary, the variables that increase the resistant area of the base of the panel with a consequent decrease in terms of base stresses, such as the number of layers n_l or the decrease in the length of the door-type openings l_d determine an increase of τ.

Defining $F_{HD,lim}$ as the hold-down reaction force at complete plasticization of the underlying CLT floor panel (Eq. (16)) (Fig. 8), Eq. (15) has been chosen as trial function for the fitting.

$$\tau = c_0 + c_1 \frac{R_{HD}}{F_{HD,lim}} + c_2 \frac{l_d}{l} \quad (15)$$
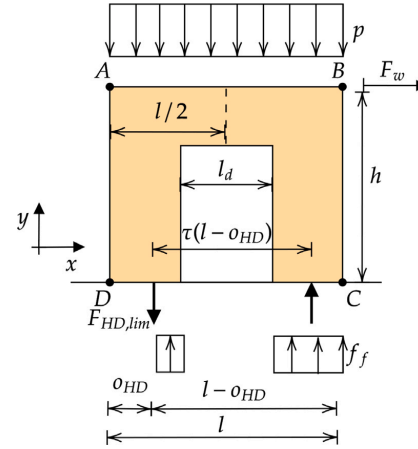

Fig. 8. Equilibrium at complete floor panel plasticization.

$$F_{HD,lim} = f_f n_l t_l (l - l_d - o_{HD}) - pl \quad (16)$$

A multidimensional dataset of significant input parameters uniformly distributed in the domain of practical interest (Table 5) was generated (2625 configurations) and the corresponding solution in terms of non-dimensional equivalent arm τ was calculated by Eq. (3) with the FEM derived wall capacity R_W.

Best fit coefficient has been determined ($c_0 = 1$, $c_1 = -0.5$, $c_2 = 0.14$ with coefficient of determination $R^2 = 0.75$ and Root Mean Square Error $RMSE = 0.04$) (Fig. 9) and a cross-validation was carried out on two datasets of uniformly distributed pseudo-random inputs parameters falling within the same domain used for the VBSA analysis (Table 3) (Fig. 9b).

It is worth noting that the interpolating function found (Eq. (15)) coincides, for $l_d = 0$ (i.e. panel without door opening), with the one that we would find analytically for a rigid panel (planarity of base section) on rigid-plastic compression only base springs (complete plasticization of the compressed portion of the section).

The validation performed on the dataset of configurations with window openings confirmed that despite the opening, the panel can
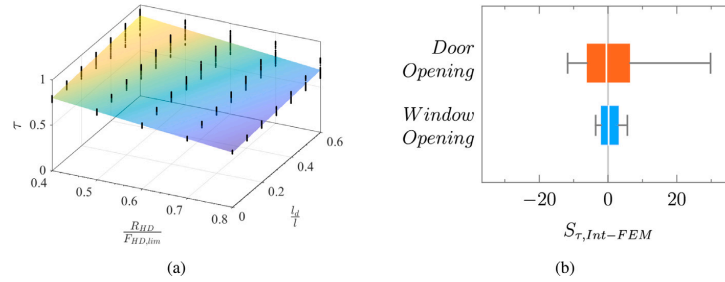
Fig. 9. (a) Interpolation of FEM derived dimensionless equivalent arm τ and (b) Maximum, 95th percentiles, median, 5th percentiles and minimum values of the percent deviations between interpolating formula and exact solution for 1000 configurations.
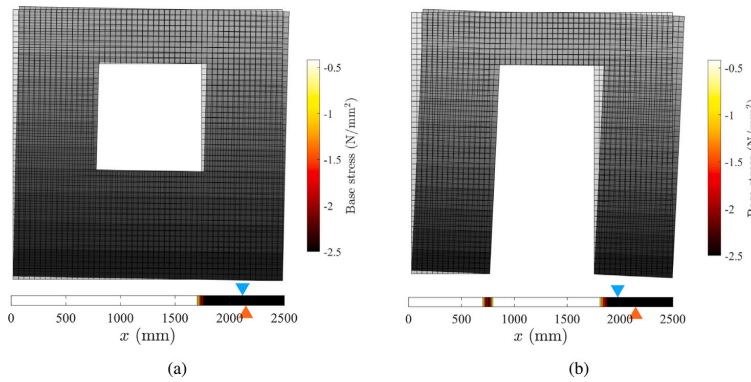

Fig. 10. Deformed shape of wall on CLT floor at hold-down failure and base force reaction resultant position (orange markers-FEM derived, blue markers-Interpolating function derived): (a) window opening and (b) door opening.

Table 5
Interpolation parameters domain.

	l (m)	h (m)	l_d/l	CLT Wall class	nl	K_{HD} (kN/mm)	$R_{HD}/F_{HD,lim}$	p (kN/m)
Lower	1		0		3		0.4	0
Upper	5	2.5	0.6	C24	7	10	0.8	40

actually be considered with an excellent approximation as in-plane rigid (Fig. 10a). For 90% of the configurations, the percent deviation between τ determined with the interpolation law and the FEM derived τ is between -2.08% and $+3.13\%$ (Fig. 9b).

Looking at Eq. (15) used for the fitting we can consider how neglecting the third term, the simplified equation coincides with the one that we would find analytically for a rigid panel on rigid-plastic compression only base springs with a door opening centered in the compression area. Due to the in-plane deformability of the panels with door opening (Fig. 10b) and due to the actual positioning of door opening (centered in the wall) of the interpolated dataset, a correction factor proportional to l_d/l was added. For 90% of the configurations of the validation dataset, the percent deviation between τ determined with the interpolation law and the FEM derived τ is between -6.23% and $+6.38\%$ (Fig. 9b).

The simplified expression for the dimensionless equivalent arm τ (Eq. (15)), together with Eq. (4), represents a predictive closed-form expression of the wall capacity. The predicted wall capacity grows almost linearly with the hold-down strength R_{HD} only when $F_{HD,lim} \gg R_{HD}$. $F_{HD,lim}$ rapidly decrease with the length of the door opening l_d/l reducing the resulting capacity of the wall R_W as can be seen from Fig. 11.
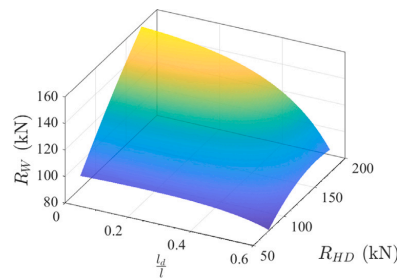

Fig. 11. Wall capacity (Eq. (4)) with τ from Eq. (15) as a function of R_{HD} and l_d/l.

6. Conclusions

The extended sensitivity analysis of the Finite Element (FE) model calibrated on the experimental cyclic response have shown that:

- for CLT shear walls on rigid base the plasticization of the wall occurs on a very limited area of the base of the wall panel and

consequently the value of τ is almost constant as the configuration analysed varies and it is close to unity.

- for CLT shear walls on CLT base the reduced strength of the floor panel in the direction perpendicular to the grain determines a greater extension of the plastic area below the wall panel with consequent reduction of τ.
- for CLT shear walls on CLT base without openings, or with window-type openings with $l_w/l \leq 0.6$, the behaviour of the wall can be assimilated to that of a rigid body on rigid-plastic springs. The derived simplified formula for the calculation of τ found by interpolation of the FEM results coincides with the analytical one associated with the aforementioned hypotheses.
- for CLT shear walls on CLT base with door opening the panel can no longer be considered rigid in its plane and the amount of τ reduction depends not only on the door length but also on its position. A simplified expression has been derived for the case of centered door openings.
- for CLT shear walls on CLT base the extension of the plastic area at the base of the wall panel and, consequently, the dimensionless lever arm ratio τ depend on the ratio between the hold-down strength and the strength of compressed timber between the hold-down and the panel edge. When $R_{HD}/F_{HD,lim} \rightarrow 1$ the wall capacity is limited on the timber side and an increase in the hold-down strength R_{HD} does not produce an appreciable increase of the wall capacity F_W.
- for CLT shear walls on CLT base the extension of door openings was found to be the most influencing parameter for the wall capacity F_W.

An elementary empirical regression equation based on the FE model results for predicting the dimensionless lever arm τ in the capacity equation of CLT panels has been derived and has proven to be accurate for the configurations of practical interest. The simplified expression for τ, together with equilibrium equations of the wall, represents a predictive closed-form expression of the wall capacity.

CRediT authorship contribution statement

Yuri De Santis: Conceptualization, Data curation, Formal analysis, Investigation, Methodology, Resources, Software, Validation, Visualization, Writing – original draft, Writing – review & editing. **Angelo Aloisio:** Conceptualization, Data curation, Formal analysis, Investigation, Methodology, Resources, Software, Validation, Visualization, Writing – original draft, Writing – review & editing. **Martina Sciomenta:** Supervision. **Massimo Fragiacomo:** Supervision.

Declaration of competing interest

The authors declare that they have no known competing financial interests or personal relationships that could have appeared to influence the work reported in this paper.

Acknowledgements

The authors acknowledge prof. Roberto Tomasi and Dr. Francesco Boggian for sharing the experimental data.

References

[1] Brandner R, Flatscher G, Ringhofer A, Schickhofer G, Thiel A. Cross laminated timber (CLT): overview and development. Euro J Wood Wood Prod 2016;74(3):331–51.

[2] Shahnewaz M, Pan Y, Shahria Alam M, Tannert T. Seismic fragility estimates for cross-laminated timber platform building. J Struct Eng 2020;146(12):04020256.

[3] Li Z, Wang X, He M. Experimental and analytical investigations into lateral performance of cross-laminated timber (CLT) shear walls with different construction methods. J Earthq Eng 2020;1–23.

[4] Aloisio A, Pasca D, Tomasi R, Fragiacomo M. Dynamic identification and model updating of an eight-storey CLT building. Eng Struct 2020;213:110593.

[5] Casagrande D, Doudak G, Vettori M, Fanti R. Proposal for an equivalent frame model for the analysis of multi-storey monolithic CLT shearwalls. Eng Struct 2021;245:112894.

[6] Izzi M, Casagrande D, Bezzi S, Pasca D, Follesa M, Tomasi R. Seismic behaviour of cross-laminated timber structures: A state-of-the-art review. Eng Struct 2018;170:42–52.

[7] Trutalli D, Marchi L, Scotta R, Pozza L. Capacity design of traditional and innovative ductile connections for earthquake-resistant CLT structures. Bull Earthq Eng 2019;17(4):2115–36.

[8] Aloisio A, Alaggio R, Fragiacomo M. Fragility functions and behavior factors estimation of multi-story cross-laminated timber structures characterized by an energy-dependent hysteretic model. Earthq Spectra 2021;37(1):134–59.

[9] Aloisio A, Fragiacomo M. Reliability-based overstrength factors of cross-laminated timber shear walls for seismic design. Eng Struct 2021;228:111547.

[10] van de Lindt JW, Furley J, Amini MO, Pei S, Tamagnone G, Barbosa AR, et al. Experimental seismic behavior of a two-story CLT platform building. Eng Struct 2019;183:408–22.

[11] Shahnewaz M, Dickof C, Tannert T. Seismic behavior of balloon frame CLT shear walls with different ledgers. J Struct Eng 2021;147(9):04021137.

[12] Zhang X, Isoda H, Sumida K, Araki Y, Nakashima S, Nakagawa T, et al. Seismic performance of three-story cross-laminated timber structures in Japan. J Struct Eng 2021;147(2):04020319.

[13] Sandoli A, D'Ambra C, Ceraldi C, Calderoni B, Prota A. Sustainable cross-laminated timber structures in a seismic area: Overview and future trends. Appl Sci 2021;11(5):2078.

[14] Pozza L, Trutalli D. An analytical formulation of q-factor for mid-rise CLT buildings based on parametric numerical analyses. Bull Earthq Eng 2017;15(5):2015–33.

[15] Aloisio A, Boggian F, Tomasi R, Fragiacomo M. Reliability-based assessment of LTF and CLT shear walls under in-plane seismic loading using a modified Bouc-Wen hysteresis model. ASCE-ASME J Risk Uncertain Eng Syst A 2021;7(4):04021065.

[16] Aloisio A, Alaggio R, Fragiacomo M. Equivalent viscous damping of cross-laminated timber structural archetypes. J Struct Eng 2021;147(4):04021012.

[17] Franco L, Pozza L, Saetta A, Savoia M, Talledo D. Strategies for structural modelling of CLT panels under cyclic loading conditions. Eng Struct 2019;198:109476.

[18] Christovasilis I, Riparbelli L, Rinaldin G, Tamagnone G. Methods for practice-oriented linear analysis in seismic design of cross laminated timber buildings. Soil Dyn Earthq Eng 2020;128:105869.

[19] Casagrande D, Doudak G, Mauro L, Polastri A. Analytical approach to establishing the elastic behavior of multipanel CLT shear walls subjected to lateral loads. J Struct Eng 2018;144(2):04017193.

[20] Lukacs I, Björnfot A, Tomasi R. Strength and stiffness of cross-laminated timber (CLT) shear walls: State-of-the-art of analytical approaches. Eng Struct 2019;178:136–47.

[21] Casagrande D, Rossi S, Sartori T, Tomasi R. Proposal of an analytical procedure and a simplified numerical model for elastic response of single-storey timber shear-walls. Constr Build Mater 2016;102:1101–12.

[22] Tomasi R, Sartori T. Mechanical behaviour of connections between wood framed shear walls and foundations under monotonic and cyclic load. Constr Build Mater 2013;44:682–90.

[23] Wallner-Novak M, Koppelhuber J, Pock K. Brettsperrholz Bemessung Grundlagen Für Statik Und Konstruktion Nach Eurocode. proHolz Austria; 2013.

[24] Pei S, Lindt J, Popovski M. Enhance mechanical properties of timber, engineered wood products and timber structures. 2014, CLT Course At FPS COST Action FP1004. CLT Training School.

[25] Pei S, Lindt J, Popovski M. Approximate R-factor for cross-laminated timber walls in multistory buildings. J Archit Eng 2013;19:245–55.

[26] Reynolds T, Foster RM, Bregulla J, shao Chang W, Harris R, Ramage M. Lateral load resistance of cross-laminated timber shear walls. J Struct Eng-Asce 2017;143:06017006.

[27] Gavric I, Popovski M. Design models for CLT shearwalls and assemblies based on connection properties. In: Proceedings of international network on timber engineering research, INTER/47-15-4. 2014, http://dx.doi.org/10.13140/RG.2.1.3845.0728.

[28] Aloisio A, Boggian F, Tomasi R, Fragiacomo M. The role of the hold-down in the capacity model of LTF and CLT shear walls based on the experimental lateral response. Constr Build Mater 2021;289:123046.

[29] Sandoli A, D'Ambra C, Ceraldi C, Calderoni B, Prota A. Role of perpendicular to grain compression properties on the seismic behaviour of CLT walls. J Build Eng 2021;34:101889.

[30] Tamagnone G, Rinaldin G, Fragiacomo M. A novel method for non-linear design of CLT wall systems. Eng Struct 2018;167:760–71.

[31] Serrano E, Enquist B. Compression strength perpendicular to grain in cross-laminated timber (CLT). In: 11th World conference on timber engineering 2010. Trees and Timber Institute, National Research Council; 2010, World Conference on Timber Engineering, 2010, WCTE 2010 ; Conference date: 20-06-2010 Through 24-06-2010.

[32] Popovski M, Gavric I, Schneider J. Performance of two-storey CLT house subjected to lateral loads. FP Innovations Research Rep. FPIPRODUCT-1-6896, 2014, Vancouver, BC, Canada.

[33] Kurent B, Brank B, Ao WK. Model updating of seven-storey cross-laminated timber building designed on frequency-response-functions-based modal testing. Struct Infrastruct Eng 2021;1–19.

[34] Dujic B, Klobcar S, Zarnic R. Influence of openings on shear capacity of wooden walls. 40th CIB-W18 Meeting, Bled, Slovenia. tech. rep., Paper 40-15-6; 2007.

[35] Dujic B, Klobcar S, Zarnic R. Shear capacity of cross-laminated wooden walls. In: Proceedings of the 10th world conference on timber engineering, Miyazaki, Japan. 2008.

[36] Awad V, Giresini L, Koshihara M, Puppio ML, Sassu M. Experimental analyses and numerical models of CLT shear walls under cyclic loading. Wood Civ Eng 2017;223.

[37] Shahnewaz I, Tannert T, Shahria Alam M, Popovski M. In-plane stiffness of cross-laminated timber panels with openings. Struct Eng Int 2017;27(2):217–23.

[38] Casagrande D, Fanti R, Greco M, Gavric I, Polastri A. On the distribution of internal forces in single-storey CLT symmetric shear-walls with openings. In: Structures. 33, Elsevier; 2021, p. 4718–42.

[39] Sobol IM. Sensitivity estimates for nonlinear mathematical models. Math Model Comput Exp 1993;1(4):407–14.

[40] Aloisio A, Fragiacomo M. Assessment of the seismic response of CLT shear walls using the EEGBW, a Bouc–Wen class predictive model. Infrastructures 2021;6(4):55.

[41] Endrizzi P. I sistemi di connessione di base del pannello xlam compensato di tavole indagine sperimentale in scala reale e modellazione numerica della capacità portante globale di parete ottenuta con l'impiego di una nuova tipologia di angolare a taglio. University of Trento; 2011.

[42] Grossi P, Sartori T, Tomasi R. Tests on timber frame walls under in-plane forces: part 2. Proc Inst Civ Eng-Struct Build 2015;168(11):840–52.

[43] Brandner R, Dietsch P, Dröscher J, Schulte-Wrede M, Kreuzinger H, Sieder M. Cross laminated timber (CLT) diaphragms under shear: Test configuration, properties and design. Constr Build Mater 2017;147:312–27. http://dx.doi.org/10.1016/j.conbuildmat.2017.04.153.

[44] Bogensperger T, Moosbrugger T, Silly G. Verification of CLT-plates under loads in plane. In: World conference on timber engineering. 2010, p. 1–9, 11th World Conference on Timber Engineering, WCTE 2010 ; Conference date: 20-06-2010 Through 24-06-2010.

[45] Iman RL, Conover WJ. The use of the rank transform in regression. Technometrics 1979;21(4):499–509.

[46] Ma F, Zhang H, Bockstedte A, Foliente GC, Paevere P. Parameter analysis of the differential model of hysteresis. J Appl Mech 2004;71(3):342–9.

[47] Aloisio A, Di Battista L, Alaggio R, Fragiacomo M. Sensitivity analysis of subspace-based damage indicators under changes in ambient excitation covariance, severity and location of damage. Eng Struct 2020;208:110235. http://dx.doi.org/10.1016/j.engstruct.2020.110235.

[48] Pasca DP, Aloisio A, Fragiacomo M, Tomasi R. Dynamic characterization of timber floor subassemblies: Sensitivity analysis and modeling issues. J Struct Eng 2021;147(12):05021008.

Chapter 9

Appendix - Analytical model for withdrawal behavior of axially deformable screws

Abstract: The definition of the withdrawal parameter of the EN 1382 is discussed. An analytical model of a rod on elastic foundation is used to study the influence of screw axial deformability. A threshold for the ratio between the screw axial stiffness and foundation modulus is found. Under the threshold value the assumption of axially rigid behavior lead to an inaccurate evaluation of withdrawal stiffness and capacity.

9.1 Introduction

In standards and in research screws are often implicitly considered as axially rigid. The EN 1382 [20] define a length independent parameter called withdrawal parameter, often named f_{ax} and defined as in Eq. 2.14. The definition suggest that is possible to test an arbitrary length screw to derive an f_{ax} that allows for the calculation of the withdrawal capacity of a screw with a generic length. However, due to their slenderness the screw axial stiffness may be too law to satisfy the assumption of a screw axially rigid behavior. The limits of this assumption are analyzed in the following by means of an analytical model of a rod on elastic foundation. Although the proposed model is linear and elastic, it can be used, with reasonable approximation, to study the withdrawal behavior of axially loaded screws that exhibit an almost linear behavior until failure.

9.2 Derivation of the field equations

The field equations are derived below by referring to a beam segment of infinitesimal length dx.
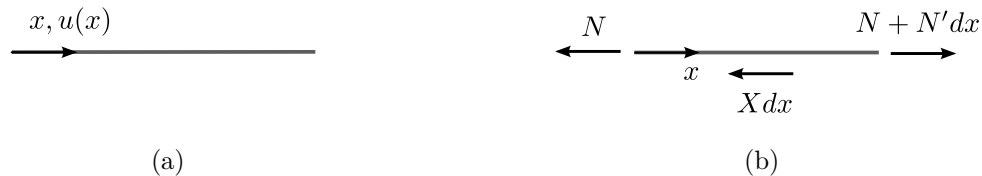

Figure 9.1: Scheme of beam on elastic foundation model: (a) Kinematic; (b) Equilibrium.

Naming $u(x)$ the axial displacements respectively (Fig.9.1a), under the hypothesis of small displacements and small deformations the linear kinematic equations are the following:

$$\epsilon = u' \tag{9.1}$$

where ϵ is the beam axial elongation.

Naming E the Young's modulus, k_{ax} the stiffness of the distributed springs per unit of length in the axial direction and A the area the constitutive law equations are:

$$N = EA\epsilon$$
$$X = k_{ax}u \tag{9.2}$$

where N is the axial force and X are the distributed springs reaction forces.

The equilibrium of the forces and of the moments on the segment of infinitesimal dimensions can be written starting from the forces indicated in Fig.9.1b.

$$\sum F_x = 0 \quad -N + N + N'dx - Xdx = 0 \tag{9.3}$$

Simplifying equilibrium:

$$N' - X = 0 \tag{9.4}$$

Substituting kinematic Eqs. 9.1 in constitutive Eqs. 9.2

$$N = EAu'$$
$$X = k_{ax}u \tag{9.5}$$

Substituting Eqs. 9.5 in equilibrium

$$EAu'' - k_{ax}u = 0 \tag{9.6}$$

The general solution of Eq. 9.6 can be written as:

$$u(x) = c_1 e^{\sqrt{\frac{k_{ax}}{EA}}x} + c_2 e^{-\sqrt{\frac{k_{ax}}{EA}}x} \tag{9.7}$$

9.3 Withdrawal stiffness

In the cases analyzed below, the part of the screw inserted in the timber member of length l can be modeled as a beam on elastic foundation, free on the tip side ($x = 0$).

The stiffness of the system is determined by assigning an imposed displacement at an external constraint located on the timber surface and determining the axial internal force associated with it. The stiffness or slip modules can be determined as the ratio between the force and the imposed displacement. Alternatively, it is possible to assign a force to the boundary of a domain and determine the corresponding displacement.
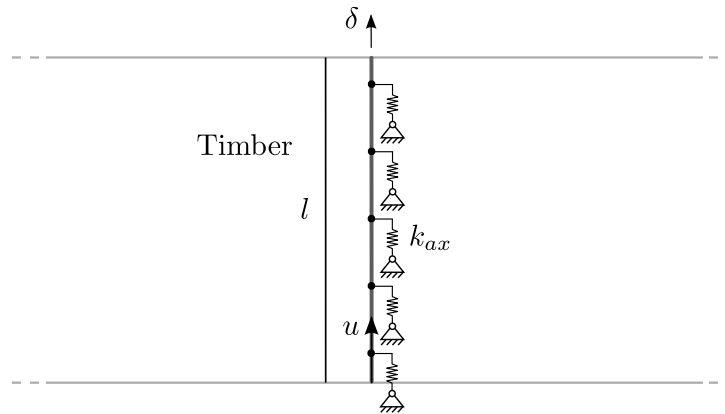

Figure 9.2: Withdrawal model.

$$EAu'(0) = 0$$
$$\tag{9.8}$$
$$u(l) = \delta$$

The solution of Eqs. 9.6 and 9.8 when $\delta = 1$ can be written as:

$$u(x) = \frac{\left(e^{\sqrt{\frac{k_{ax}}{EA}}2x} + 1\right)e^{\sqrt{\frac{k_{ax}}{EA}}l - \sqrt{\frac{k_{ax}}{EA}}x}}{e^{\sqrt{\frac{k_{ax}}{EA}}2l} + 1} \tag{9.9}$$

The associated force in $x = l$ which is the stiffness:

$$K_{ax} = \sqrt{EAk_{ax}} \tanh\left(\sqrt{\frac{k_{ax}}{EA}}l\right) \tag{9.10}$$

Defining the ratio between the withdrawal stiffness of the finite stiffness screw and the withdrawal stiffness of the infinite stiffness screw and assuming ψ as the square root of the ratio between the axial stiffness of the screw and the total stiffness of the springs:

$$\zeta = \frac{K_{ax}}{k_{ax}l}$$
$$\psi = \frac{1}{l}\sqrt{\frac{EA}{k_{ax}}} \tag{9.11}$$

ζ can be rewritten as:

$$\zeta = \psi \tanh\left(\frac{1}{\psi}\right) \tag{9.12}$$

From the plot in Fig. 9.3, $\zeta = 0.99$ for $\psi = 5.74$ and $\zeta = 0.95$ for $\psi = 2.50$.
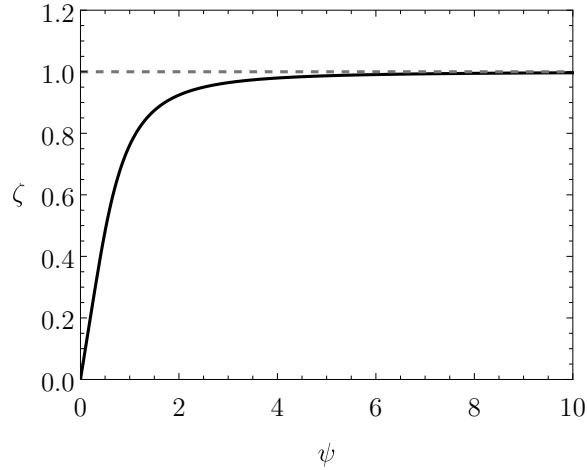

Figure 9.3: Ratio between the withdrawal stiffness of the finite stiffness screw and the withdrawal stiffness of the infinite stiffness screw as a function of the square root of the ratio between the axial stiffness of the screw and the total stiffness of the springs

In dimensional form Eq. 9.12 becomes:

$$K_{ax} = k_{ax}l\psi \tanh\left(\frac{1}{\psi}\right) \tag{9.13}$$
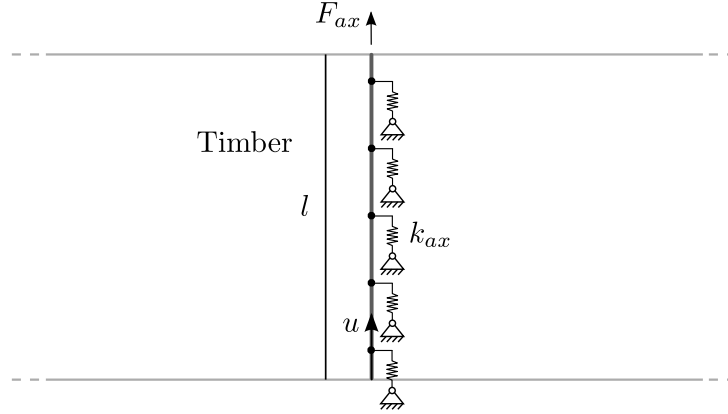
9.4 Withdrawal strength

Figure 9.4: Withdrawal model.

$$EAu'(0) = 0$$

$$EAu'(l) = F_{ax}$$

(9.14)

The solution of Eqs. 9.6 and 9.14 when $\delta = 1$ can be written as:

$$u(x) = \frac{\left(e^{\sqrt{\frac{k_{ax}}{EA}}2x} + 1\right) e^{\sqrt{\frac{k_{ax}}{EA}}l - \sqrt{\frac{k_{ax}}{EA}}x}}{\sqrt{EAk_{ax}}\left(e^{\sqrt{\frac{k_{ax}}{EA}}2l} - 1\right)} F_{ax}$$

(9.15)

From Eq. 9.15 substituting in Eq. 9.5 and assuming the dimensionless axial force and the dimensionless abscissa respectively as:

$$\Lambda = \frac{N}{F_{ax}}$$
$$\xi = \frac{x}{l}$$

(9.16)

The dimensionless axial force:

$$\Lambda = \frac{1}{2}e^{-\frac{\xi-1}{\psi}}\left(e^{\frac{2\xi}{\psi}} - 1\right)\left(\coth\left(\frac{1}{\psi}\right) - 1\right)$$
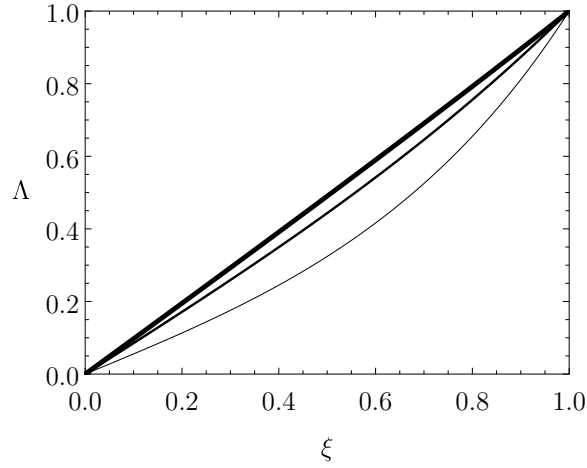
(9.17)

Figure 9.5: Dimensionless axial force as a function of dimensionless abscissa for varying square root of the ratio between the axial stiffness of the screw and the total stiffness of the springs: 2.5 thicker line, 1.0 intermediate line and 0.5 thinner line.

Assuming Γ_{ax} as the ratio between the distributed spring reactions per unit length of the finite stiffness screw and the distributed spring reactions per unit length of the infinite stiffness screw:

$$\Gamma_{ax} = \frac{X}{p_{ax}}$$
$$p_{ax} = \frac{F_{ax}}{l}$$

(9.18)

Γ_{ax} can be expressed as a function of ψ and ξ substituting Eq. 9.15 in Eq. 9.2:

$$\Gamma_{ax} = \frac{e^{-\frac{\xi-1}{\psi}}\left(e^{\frac{2\xi}{\psi}}+1\right)\left(\coth\left(\frac{1}{\psi}\right)-1\right)}{2\psi}$$

(9.19)
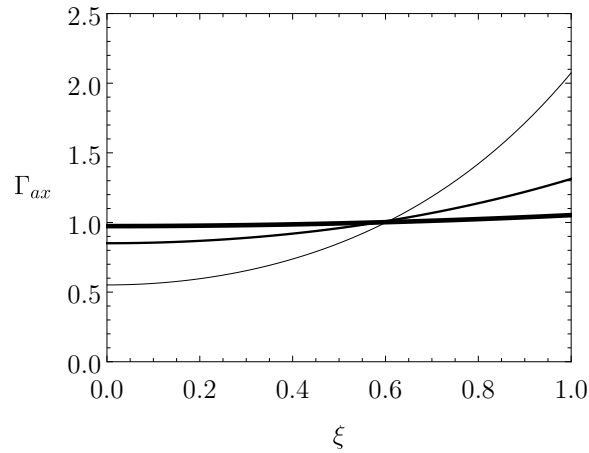
Figure 9.6: Dimensionless distributed spring reaction as a function of dimensionless abscissa for varying square root of the ratio between the axial stiffness of the screw and the total stiffness of the springs: 2.5 thicker line, 1.0 intermediate line and 0.5 thinner line.

The maximum uniformly distributed spring reactions per unit length verifies in $\xi = 1$.

$$\Gamma_{ax,max} = \frac{1}{\psi}\coth\left(\frac{1}{\psi}\right)$$

(9.20)

From the plot in Fig. 9.7, $\Gamma_{ax,max} = 1/0.99$ for $\psi = 5.74$ and $\Gamma_{ax,max} = 1/0.95$ for $\psi = 2.50$.
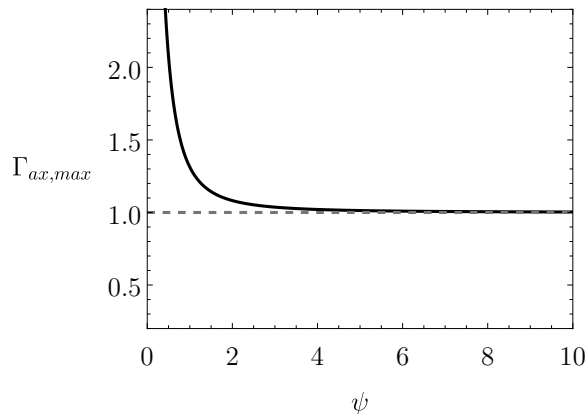
Figure 9.7: Ratio between the maximum distributed spring reactions per unit length of the finite stiffness screw and the distributed spring reactions per unit length of the infinite stiffness screw as a function of the square root of the ratio between the axial stiffness of the screw and the total stiffness of the springs

9.5 Conclusions

An elementary model of a rod in elastic foundation is used to model the withdrawal behavior of self-tapping screws. The assumption of rigid-axial behavior is analyzed. The dimensionless studies demonstrated that when the screw axial stiffness EA/l is 33 times the stiffness of an analogous connection with an axially rigid fastener that is $k_{ax}l$, the rigid-axial assumption is reasonable.

Bibliography

[1] ASTM F 1575. Standard Test Method for Determining Bending Yield Moment of Nails. *ASTM*, 2017.

[2] Elif Appavuravther, Bram Vandoren, and Jose Henriques. Behaviour of screw connections in timber-concrete composites using low strength lightweight concrete. *Construction and Building Materials*, 286:122973, 2021. ISSN 0950-0618. doi: https://doi.org/10.1016/j.conbuildmat.2021.122973. URL https://www.sciencedirect.com/science/article/pii/S0950061821007339.

[3] ASTM-D5764. Standard Test Method for Evaluating Dowel-Bearing Strength of Wood and Wood-Based Products. *ASTM International*, 2007.

[4] Simon Aurand and Hans Joachim Blaß. Connections with inclined screws and increased shear plane friction. In *Proceedings - meeting 54 : 16-19 August 2021, online meeting / INTER, International Network on Timber Engineering Research. Ed.: R. Görlacher*, pages 147–168, 2021.

[5] Boris Azinović, Tomaž Pazlar, and Meta Kržan. The influence of flexible sound insulation layers on the seismic performance of cross laminated timber walls. *Journal of Building Engineering*, 43(April), 2021. ISSN 23527102. doi: 10.1016/j.jobe.2021.103183.

[6] Chiara Bedon and Massimo Fragiacomo. Three-dimensional modelling of notched connections for timber-concrete composite beams. *Structural Engineering International*, 27(2):184–196, 2017. ISSN 16830350. doi: 10.2749/101686617X14881932435295.

[7] Chiara Bedon and Massimo Fragiacomo. Numerical analysis of timber-to-timber joints and composite beams with inclined self-tapping screws. *Composite Structures*, 207:13–28, 2019. ISSN 02638223. doi: 10.1016/j.compstruct.2018.09.008. URL https://doi.org/10.1016/j.compstruct.2018.09.008.

[8] Ireneusz Bejtka. *Verstärkung von Bauteilen aus Holz mit Vollgewindeschrauben*. Number 2. 2005. ISBN 3937300546.

[9] Hans Joachim Blaß and Yvonne Steige. *Steifigkeit axial beanspruchter Vollgewindeschrauben*, volume 34 of *Karlsruher Berichte zum Ingenieurholzbau / Karlsruher Institut für Technologie, Holzbau und Baukonstruktionen*. KIT Scientific Publishing, 2018. ISBN 978-3-7315-0826-7. doi: 10.5445/KSP/1000085040.

[10] Hans Joachim Blaß, Ireneusz Bejtka, and Thomas Uibel. *Tragfähigkeit von Verbindungen mit selbstbohrenden Holzschrauben mit Vollgewinde*, volume 4. 2006. ISBN 3-86644-034-0.

[11] Reinhard Brandner, Andreas Ringhofer, and Tobias Reichinger. Performance of axially-loaded self-tapping screws in hardwood: Properties and design. *Engineering Structures*, 188: 677–699, 2019. ISSN 0141-0296. doi: https://doi.org/10.1016/j.engstruct.2019.03.018. URL https://www.sciencedirect.com/science/article/pii/S0141029618329377.

[12] A.A. Chiniforush, H.R. Valipour, and A. Ataei. Timber-timber composite (ttc) connections and beams: An experimental and numerical study. *Construction and Building Materials*, 303: 124493, 2021. ISSN 0950-0618. doi: https://doi.org/10.1016/j.conbuildmat.2021.124493. URL https://www.sciencedirect.com/science/article/pii/S0950061821022492.

[13] Timo Claus, Werner Seim, and Johannes Küllmer. Force distribution in self-tapping screws: experimental investigations with fibre bragg grating measurement screws. *European Journal of Wood and Wood Products*, 80:183–197, 2 2022. ISSN 1436736X. doi: 10.1007/S00107-021-01740-Z/FIGURES/13. URL https://link.springer.com/article/10.1007/s00107-021-01740-z.

[14] S. Di Nino, A. Gregori, and M. Fragiacomo. Experimental and numerical investigations on timber-concrete connections with inclined screws. *Engineering Structures*, 209(December 2019):109993, 2020. ISSN 18737323. doi: 10.1016/j.engstruct.2019.109993. URL https://doi.org/10.1016/j.engstruct.2019.109993.

[15] DIN-1052. Entwurf Berechnung und Bemessung von Holzbauwerken - Allgemeine Bemessungsregeln und Bemessungsregeln fuer den Hochbau. 2008.

[16] Hao Du, Xiamin Hu, Zhong Xie, and Hanchen Wang. Study on shear behavior of inclined cross lag screws for glulam-concrete composite beams. *Construction and Building Materials*, 224:132–143, 2019. ISSN 09500618. doi: 10.1016/j.conbuildmat.2019.07.035. URL https://doi.org/10.1016/j.conbuildmat.2019.07.035.

[17] 130118-01-0603 EAD. Screws and threaded rods for use in timber construction. 2019.

[18] J. Ehlbeck and H.J. Larsen. Eurocode 5 - design of timber structures: Joints. In *International Workshop on Wood Connectors*, pages 9–23, United States, 1993. Forest Products Society. ISBN 0935018565. null ; Conference date: 19-05-2010.

[19] Juergen Ehlbeck. Softwood and hardwood embedding strength for dowel-type fasteners. In *Proceedings of the CIB-W18 meetings*, 1992.

[20] EN-1382. Timber Structures - Test methods - Withdrawal capacity of timber fasteners. *BSi*, 2014.

[21] EN-1383. Timber structures - Test methods - Pull-through resistance of timber fasteners. *BSi*, 1999.

[22] EN-14592. Timber structures - Dowel-type fasteners - Requirements. *BSi*, 2008.

[23] EN-26891. Timber structures - Joints made with mechanical fasteners - General principles for the determination of strength and deformation characteristics. *CEN*, 1991.

[24] EN-383. Timber structures - Test methods - Determination of embedment strength and foundation values for dowel type fasteners. *BSi*, 2007.

[25] EN 383. Timber structures - test methods - determination of embedment strength and foundation values for dowel type fasteners. *British Standards Institute*, 3(2007):pp. 1–18, 2007.

[26] EN-409. Timber structures - Test methods - Determination of the yield moment of dowel type fasteners. *BSi*, 2009.

[27] ETA-11/0190. *Self-tapping screws for use in timber constructions. European Technical Approval.* 2018.

[28] ETA-12/0063. *SFS intec AG: SFS self-tapping screws WT, European Technical Approval, OIB.* 2013.

[29] Eurocode-5. Design of timber structures - Part 1-1: General - Common rules and rules for buildings. *CEN*, 2004.

[30] Eurocode-5/A2. Design of timber structures - Part 1-1: General - Common rules and rules for buildings. *CEN*, 2014.

[31] R. Foschi. Load-slip characteristic of nails. *Wood Science*, (7), 1974.

[32] M. Frese and H.J. Blaß. Models for the calculation of the withdrawal capacity of self-tapping screws. In *CIB-W18*, pages 42–7–3, 2009. Dübendorf (Switzerland).

[33] Matthias Frese, Peter Fellmoser, and Hans Joachim Blass. Modelle für die berechnung der ausziehtragfähigkeit von selbstbohrenden holzschrauben. *European Journal of Wood and Wood Products*, 68, 2009. doi: 10.1007/s00107-009-0378-1Ã¯. URL https://hal.archives-ouvertes.fr/hal-00568255.

[34] Ivan Giongo, Maurizio Piazza, and Roberto Tomasi. Investigation on the self tapping screws capability to induce internal stress in timber elements. *Advanced Materials Research*, 778:604–611, 2013. ISSN 10226680. doi: 10.4028/www.scientific.net/AMR.778.604.

[35] Ivan Giongo, Gianni Schiro, and Daniele Riccadonna. Innovative pre-stressing and cambering of timber-to-timber composite beams. *Composite Structures*, 226(July):111195, 2019. ISSN 02638223. doi: 10.1016/j.compstruct.2019.111195. URL https://doi.org/10.1016/j.compstruct.2019.111195.

[36] Ulf Arne Girhammar, Nicolas Jacquier, and Bo Källsner. Stiffness model for inclined screws in shear-tension mode in timber-to-timber joints. *Engineering Structures*, 136:580–595, 2017. ISSN 18737323. doi: 10.1016/j.engstruct.2017.01.022. URL http://dx.doi.org/10.1016/j.engstruct.2017.01.022.

[37] Hankinson. Investigation of crushing strength of spruce at varying angles of grain. *Air service information circular*, Material section report No. 130, 1921.

[38] A. Hassanieh, H. R. Valipour, and M. A. Bradford. Load-slip behaviour of steel-cross laminated timber (CLT) composite connections. *Journal of Constructional Steel Research*, 122:110–121, 2016. ISSN 0143974X. doi: 10.1016/j.jcsr.2016.03.008. URL http://dx.doi.org/10.1016/j.jcsr.2016.03.008.

[39] B: Laskewitz H.J. Blaß. Load-carrying capacity of joint with dowel-type fasteners and interlayers. In *CIB-W18*, pages 33–7–6, 2000. Delft (The Netherlands).

[40] G. Hochreiner, T. K. Bader, De Borst, and J. Eberhardsteiner. Stiftformige Verbindungsmittel im EC5 und baustatische Model/bi/dung mittels kommerzieller Statiksoftware. Bauingenieur. *Bauingenieur, Band*, (88): 275–289, 2013.

[41] Kevin Hoelz, Lukas Kleinhans, and Sven Matthiesen. Wood screw design: influence of thread parameters on the withdrawal capacity. *European Journal of Wood and Wood Products*, 79(4):773–784, Jul 2021. ISSN 1436-736X. doi: 10.1007/s00107-021-01668-4. URL https://doi.org/10.1007/s00107-021-01668-4.

[42] U. Hubner. Withdrawal strength of self-tapping screws in hardwoods. In *CIB-W18*, pages 46–7–4, 2013. Vancouver (Canada).

[43] H.J. Blaß I. Bejtka. Joints with inclined screws. In *CIB-W18*, pages 35–7–5, 2002. Kyoto (Japan).

[44] ISO-10984-2. Timber structures - Dowel-type fasteners - Part 2: Determination of embedding strength. *ISO*, 2009.

[45] Matteo Izzi, Giovanni Rinaldin, Andrea Polastri, and Massimo Fragiacomo. A hysteresis model for timber joints with dowel-type fasteners. *Engineering Structures*, 157(July 2017):170–178, 2018. ISSN 18737323. doi: 10.1016/j.engstruct.2017.12.011. URL https://doi.org/10.1016/j.engstruct.2017.12.011.

[46] Nicolas Jacquier and Ulf Arne Girhammar. Tests on glulam-CLT shear connections with double-sided punched metal plate fasteners and inclined screws. *Construction and Building Materials*, 72:444–457, 2014. ISSN 09500618. doi: 10.1016/j.conbuildmat.2014.08.095. URL http://dx.doi.org/10.1016/j.conbuildmat.2014.08.095.

[47] Gunnar Jansson. *Effect of nail characteristics on the load-carrying capacity of a nailed joint*. PhD thesis, 1955.

[48] Jørgen L Jensen, Makoto Nakatani, Pierre Quenneville, and Bryan Walford. A simple unified model for withdrawal of lag screws and glued-in rods. *Eur. J. Wood Prod*, 69:537–544, 2011. doi: 10.1007/s00107-010-0478-y.

[49] K.W. Johansen. Theory of timber connections. *International Association of Bridge and Structural Engineering*, 9:249-262, 1949. doi: http://doi.org/10.5169/seals-9703.

[50] Ari Kevarinmaki. Joints with inclined screws. In *International Council for Research and Innovation in Building and Construction, Working Commission W18 - Timber Structures, Meeting*, pages 35–7–3. ., 2002. International Council for Research and Innovation in Building and Construction, Working Commission W18 - Timber Structures, Meeting ; Conference date: September 2002; Kyoto.

[51] Kilian Krauss, Minghao Li, and Frank Lam. Influence of mixed-angle screw installations in clt on the cyclic performance of commercial hold-down connections. *Construction and Building Materials*, 364:129918, 2023. ISSN 0950-0618. doi: https://doi.org/10.1016/j.conbuildmat.2022.129918. URL https://www.sciencedirect.com/science/article/pii/S0950061822035747.

[52] Meta Kržan and Boris Azinović. Cyclic response of insulated steel angle brackets used for cross-laminated timber connections. *European Journal of Wood and Wood Products*, 79(3):691–705, 2021. ISSN 1436736X. doi: 10.1007/s00107-020-01643-5. URL https://doi.org/10.1007/s00107-020-01643-5.

[53] Romain Lemaitre, Jean-Francois Bocquet, Michael Schweigler, and Thomas K. Bader. Beam-on-foundation modelling as an alternative design method for timber joints with dowel-type fasteners - Part 1: Strength and stiffness per shear plane of single-fastener joints. *Inter / 54-7-8*, (1949):1–16, 2019. URL `http://urn.kb.se/resolve?urn=urn:nbn:se:lnu:diva-89340`.

[54] Romain Lemaitre, Jean-Francois Bocquet, Michael Schweigler, and Thomas K. Bader. Beam on Foundation Modeling as an Alternative Design Method for Timber Joints with Dowel-Type Fasteners - Part 3: Second Order Theory Effects for Considering the Rope Effect. pages 1–16, 2019. URL `http://urn.kb.se/resolve?urn=urn:nbn:se:lnu:diva-89340`.

[55] Romain Lemaitre, Jean-Francois Bocquet, Michael Schweigler, and Thomas K. Bader. Beam-on-Foundation Modelling as an Alternative Design Method for Timber Joints with Dowel-Type Fasteners : Part 2: Modelling Techniques for Multiple Fastener Connections. (2018):175–189, 2019. URL `http://urn.kb.se/resolve?urn=urn:nbn:se:lnu:diva-89340`.

[56] Yifan Liu, Ziyin Yao, Feibin Wang, Hui Huang, and Zeli Que. Effect of arrangement distances on stiffness of shear-tension mode in timber-to-timber connections with inclined screws. *Construction and Building Materials*, 314:125592, 2022. ISSN 0950-0618. doi: https://doi.org/10.1016/j.conbuildmat.2021.125592. URL `https://www.sciencedirect.com/science/article/pii/S0950061821033298`.

[57] Luca Marchi, Roberto Scotta, and Luca Pozza. Experimental and theoretical evaluation of TCC connections with inclined self-tapping screws. *Materials and Structures/Materiaux et Constructions*, 50(3):1–15, 2017. ISSN 13595997. doi: 10.1617/s11527-017-1047-1.

[58] Md Abdul Hamid Mirdad, Arman Jucutan, Rafid Khan, Jan Niederwestberg, and Ying Hei Chui. Embedment and withdrawal stiffness predictions of self-tapping screws in timber. *Construction and Building Materials*, 345:128394, 2022. ISSN 0950-0618. doi: https://doi.org/10.1016/j.conbuildmat.2022.128394. URL `https://www.sciencedirect.com/science/article/pii/S0950061822020542`.

[59] P. Niebuhr and M. Sieder. High-cycle fatigue behavior of a self-tapping timber screw under axial tensile loading. *Journal of Failure Analysis and Prevention*, 20:580–589, 4 2020. ISSN 18641245. doi: 10.1007/S11668-020-00863-4/TABLES/5. URL `https://link.springer.com/article/10.1007/s11668-020-00863-4`.

[60] Bengt Noren. Nailed joints: a contribution to the theoretical analysis of yield and strength. *Swedish For. Prod. Res. Laboratory Report*, (123B), 1962.

[61] M. Oudjene, E. M. Meghlat, H. Ait-Aider, P. Lardeur, M. Khelifa, and J. L. Batoz. Finite element modelling of the nonlinear load-slip behaviour of full-scale timber-to-concrete composite T-shaped beams. *Composite Structures*, 196(March):117–126, 2018. ISSN 02638223. doi: 10.1016/j.compstruct.2018.04.079. URL `https://doi.org/10.1016/j.compstruct.2018.04.079`.

[62] Francesca Pianosi, Fanny Sarrazin, and Thorsten Wagener. A Matlab toolbox for Global Sensitivity Analysis. *Environmental Modelling and Software*, 70:80–85, 2015. ISSN 13648152. doi: 10.1016/j.envsoft.2015.04.009. URL `http://dx.doi.org/10.1016/j.envsoft.2015.04.009`.

[63] Francesca Pianosi, Keith Beven, Jim Freer, Jim W. Hall, Jonathan Rougier, David B. Stephenson, and Thorsten Wagener. Sensitivity analysis of environmental models: A systematic review with practical workflow. *Environmental Modelling and Software*, 79:214–232, 2016. ISSN 13648152. doi: 10.1016/j.envsoft.2016.02.008. URL `http://dx.doi.org/10.1016/j.envsoft.2016.02.008`.

[64] Gernot Pirnbacher. Base parameters of self-tapping screws. In *CIB-W18*, pages 42–7–1, 2009. Dübendorf (Switzerland).

[65] A. Frangi R. Jockwer, R. Steiger. Design model for inclined screws under varying load to grain angles. In *INTER*, pages 47–7–5, Bath, United Kingdom, 2014. null ; Conference date: September 2014.

[66] Douglas R. Rammer and Samuel L. Zelinka. Method and apparatus for determining the surface area of a threaded fastener.

[67] Thomas Reynolds, Richard Harris, and Wen Shao Chang. Viscoelastic embedment behaviour of dowels and screws in timber under in-service vibration. *European Journal of Wood and Wood Products*, 71(5):623–634, 2013. ISSN 00183768. doi: 10.1007/s00107-013-0720-5.

[68] A. Ringhofer, M. Augustin, and G. Schickhofer. Basic steel properties of self-tapping timber screws exposed to cyclic axial loading. *Construction and Building Materials*, 211: 207–216, 2019. ISSN 0950-0618. doi: https://doi.org/10.1016/j.conbuildmat.2019.03.200. URL `https://www.sciencedirect.com/science/article/pii/S0950061819306907`.

[69] Andreas Ringhofer. *Axially Loaded Self-Tapping Screws in Solid Timber and Laminated Timber Products*. 2017. ISBN 9783851255553. URL `https://diglib.tugraz.at/axially-loaded-self-tapping-screws-in-solid-timber-and-laminated-timber-products-2017-volume-5`.

[70] Andreas Ringhofer. *Axially Loaded Self-Tapping Screws in Solid Timber and Laminated Timber Products*. 2017. ISBN 9783851255553. URL `https://diglib.tugraz.at/axially-loaded-self-tapping-screws-in-solid-timber-and-laminated-timber-products-2017-volume-5`.

[71] Andreas Ringhofer, Reinhard Brandner, and Gerhard Schickhofer. A Universal Approach for Withdrawal Properties of Self-Tapping Screws in Solid Timber and Laminated Timber Products. *INTER 2015- International Network on Timber Engineering Research*, (i):paper 48 − 07 − 01, 2015.

[72] Carmen Sandhaas, Ani Khaloian Sarnaghi, and Jan-Willem van de Kuilen. Numerical modelling of timber and timber joints: computational aspects. *Wood science and technology*, 54(1):31–61, 2020. ISSN 0043-7719, 1432-5225. doi: 10.1007/s00226-019-01142-8.

[73] Hans Joachim Sandhaas, C. Blaß. Head pull-through properties of self-tapping screws. *INTER conference*, pages 55 − 7 − 1, Aug 2022.

[74] C. L. Santos, A. M.P. De Jesus, J. J.L. Morais, and J. L.P.C. Lousada. A comparison between the en 383 and ASTM D5764 test methods for dowel-bearing strength assessment of wood: Experimental and numerical investigations. *Strain*, 46(2):159–174, 2010. ISSN 00392103. doi: 10.1111/j.1475-1305.2008.00570.x.

[75] Gianni Schiro, Ivan Giongo, Wendel Sebastian, Daniele Riccadonna, and Maurizio Piazza. Testing of timber-to-timber screw-connections in hybrid configurations. *Construction and Building Materials*, 171:170–186, 2018. ISSN 09500618. doi: 10.1016/j.conbuildmat.2018.03.078. URL `https://doi.org/10.1016/j.conbuildmat.2018.03.078`.

[76] Michael Schweigler, Thomas K. Bader, Georg Hochreiner, Gerhard Unger, and Josef Eberhardsteiner. Load-to-grain angle dependence of the embedment behavior of dowel-type fasteners in laminated veneer lumber. *Construction and Building Materials*, 126:1020–1033, 2016. ISSN 09500618. doi: 10.1016/j.conbuildmat.2016.09.051. URL `http://dx.doi.org/10.1016/j.conbuildmat.2016.09.051`.

[77] Michael Schweigler, Thomas K. Bader, Georg Hochreiner, and Romain Lemaître. Parameterization equations for the nonlinear connection slip applied to the anisotropic embedment behavior of wood. *Composites Part B: Engineering*, 142(November 2017):142–158, 2018. ISSN 13598368. doi: 10.1016/j.compositesb.2018.01.003. URL `https://doi.org/10.1016/j.compositesb.2018.01.003`.

[78] Michael Schweigler, Thomas K. Bader, Jean François Bocquet, Romain Lemaître, and Carmen Sandhaas. Embedment test analysis and data in the context of phenomenological modeling for dowelled timber joint design. *International Network on Timber Engineering Research (INTER) - Meeting fifty-two, Tacoma (US)*, (INTER / 52 - 07 - 8):1–17, 2019.

[79] S. Shaw. Encyclopedia of Vibration. *Encyclopedia of Vibration*, 2001.

[80] SIA-265. Timber Structures. 2003.

[81] Ilya Meyerovich Sobol. Sensitivity Estimates for Nonlinear Mathematical Models. *Mathematical Modelling and Computational Experiments*, (4):407–414, 1993.

[82] Haris Stamatopoulos and Kjell Arne Malo. Withdrawal stiffness of threaded rods embedded in timber elements. *Construction and Building Materials*, 116:263–272, 2016. ISSN 09500618. doi: 10.1016/j.conbuildmat.2016.04.144. URL `http://dx.doi.org/10.1016/j.conbuildmat.2016.04.144`.

[83] Haris Stamatopoulos and Kjell Arne Malo. On strength and stiffness of screwed-in threaded rods embedded in softwood. *Construction and Building Materials*, 261:119999, 2020. ISSN 09500618. doi: 10.1016/j.conbuildmat.2020.119999. URL `https://doi.org/10.1016/j.conbuildmat.2020.119999`.

[84] D. Symons, R. Persaud, and H. Stanislaus. Slip modulus of inclined screws in timber-concrete floors. *Proceedings of the Institution of Civil Engineers: Structures and Buildings*, 163(4):245–255, 2010. ISSN 17517702. doi: 10.1680/stbu.2010.163.4.245.

[85] Roberto Tomasi, Alessandro Crosatti, and Maurizio Piazza. Theoretical and experimental analysis of timber-to-timber joints connected with inclined screws. *Construction and Building Materials*, 24(9):1560–1571, 2010. ISSN 09500618. doi: 10.1016/j.conbuildmat.2010.03.007. URL `http://dx.doi.org/10.1016/j.conbuildmat.2010.03.007`.

[86] Feibin Wang, Xinmeng Wang, Weizhen Cai, Cheng Chang, and Zeli Que. Effect of inclined self-tapping screws connecting laminated veneer lumber on the shear resistance. *BioResources*, 14(2):4006–4021, 2019. ISSN 19302126. doi: 10.15376/biores.14.2.4006-4021.

[87] Emil Winkler. Die Lehre von der Elastizitat und Festigkeit. *Domonicus, Prague*, 1867.

List of publications

- De Santis Y, Fragiacomo M. Timber-to-timber and steel-to-timber screw connections: Derivation of the slip modulus via beam on elastic foundation model. Eng Struct 2021; 244:112798. https://doi.org/10.1016/j.engstruct.2021.112798.

- De Santis Y, Fragiacomo M. Slip Modulus Formulas for Timber-to-Timber Inclined Screw Connections - Comparison with other Simplified Models. INTER - International Network on Timber Engineering Research. 16th-19th August 2021.

- De Santis Y, Aloisio A, Gavrić I, Šušteršič I, Fragiacomo M. Timber-to-steel inclined screws connections with interlayers: Experimental investigation, analytical and finite element modelling. Eng Struct 2023; 292:116504. https://doi.org/10.1016/j.engstruct.2023.116504.

- De Santis Y, Sciomenta M, Spera L, Rinaldi V, Fragiacomo M, Bedon, C. Effect of Interlayer and Inclined Screw Arrangements on the Load-Bearing Capacity of Timber-Concrete Composite Connections. Building 2022; 12. https://doi.org/10.3390/buildings12122076.

- Sciomenta M, De Santis Y, Castoro C, Spera L, Rinaldi V, Bedon C, Fragiacomo M, Gregori A. Finite elements analyses of timber-concrete and timber- rubberized concrete specimens with inclined screws. WCTE - World Conference on Timber Engineering. Santiago, Chile, 9-12 August 2021.

- De Santis Y, Aloisio A, Sciomenta M, Fragiacomo M. Capacity model of CLT walls with openings and timber plasticization. Eng Struct 2022; 264:114411. https://doi.org/10.1016/j.engstruct.2022.114411.